EFFECT OF SATURATION ON ACOUSTICS OF CARBONATE ROCKS

BY

MURTADA ABDEIN ALI ELHAJ

A Thesis Presented to the

DEANSHIP OF GRADUATE STUDIES

KING FAHD UNIVERSITY OF PETROLEUM & MINERALS

DHAHRAN, SAUDI ARABIA

In Partial Fulfillment of the
Requirements for the Degree of

MASTER OF SCIENCE

In

PETROLEUM ENGINEERING

December 2012

KING FAHD UNIVERSITY OF PETROLEUM & MINERALS

DHAHRAN- 31261, SAUDI ARABIA

DEANSHIP OF GRADUATE STUDIES

This thesis, written by **Murtada Abdein Ali** under the direction his thesis advisor and approved by his thesis committee, has been presented and accepted by the Dean of Graduate Studies, in partial fulfillment of the requirements for the degree of **MASTER OF SCIENCE IN PETROLEUM ENGINEERING.**

Dr. Abdulazeez Abdulraheem
(Advisor)

Dr. Abdullah S. Sultan
Department Chairman

Dr. Abdullah S. Sultan
(Member)

Dr. Salam A. Zummo
Dean of Graduate Studies

Dr. Osman M. Abdullatif
(Member)

1/1/13

Date

Dedicated to my beloved Parents

And

All family members

Whose Prayers and Perseverance led to this accomplishment

ACKNOWLEDGMENTS

All praises and glory is to **Allah**, our God, the most beneficent, the most compassionate, and the most merciful who has given me the strength and patience to accomplish this degree.

I express my profound gratitude to my thesis committee, Dr. Abdulazeez Abdulraheem, Dr. Abdullah S. Sultan, and Dr. Osman M. Abdullatif for their guidance and endless effort to make this work successful.

I also would like to extend my appreciation to The Center for Petroleum & Mineral in The Research Institute at KFUPM for giving me the opportunity to conduct the experimental work of this work in their labs.

Finally, I express my deep gratitude to my parents for their infinite support and advice all through my life. Gratitude extended to all my family members and friends for their prayers.

TABLE OF CONTENTS

LIST OF TABLES

LIST OF FIGURES

LIST OF ABBREVIATIONS

NPHI:	Neutron Porosity
RHOB:	Bulk Density
AVO:	Amplitude Variation with Offset
RCA:	Routine Core Analysis
RAE:	Relative Absolute Error
E.C.P:	Effective Confining Pressure

ABSTRACT

Full Name : Murtada Abdein Ali Elhaj

Thesis Title : Effect of Saturation on Acoustic of Carbonate Rocks

Major Field : Petroleum Engineering

Date of Degree : December 2012

This study was carried out to analyze more than eighty outcrop samples from the carbonate Dam Formation in Al-Lidam area in the Eastern Province – Saudi Arabia for texture, mineralogy, and to investigate the influence of confining pressure on compressional and shear-wave velocities at room temperature. The methods used in this study included field investigations, facies analysis, petrographic analysis, petrophysical analysis, and acoustic data analysis.

The laboratory investigations revealed that Dam Formation in Al-Lidam area has four facies types including, mudstone, packstone, wackestone and grainstone. The measured porosity values range between 25% and 55% with an average value 38% and permeability values from 0.39 mD to 18 D, with an average of 3 D.

The results show that P-wave and S-waves velocities increase with the increase in confining pressure for dry samples. The P-wave velocity increased and the S-wave velocity decreased with confining pressure under saturated condition. This increase is non-linear with confining pressure. A regression equation of the form $V = A \times P^2 + B \times P + \mathrm{C}$ gives a good fit to the measured velocity when compared with equations suggested by other studies.

ملخص الرسالة

الاسم الكامل: مرتضى عابدين على الحاج

عنوان الرسالة: تأثير التشبع فى سرعة الموجات الصوتية فى الصخور الكربونية

التخصص: هندسة البترول

تاريخ الدرجة العلمية: ديسمبر 2012

أُجريت هذه الدراسة على تحليل أكثر من ثمانين عينة من منكشف صخرى من حقبة الميوسين الكربونية من مكون الدام الواقع فى منطقة اللدام شرقى المملكة العربية السعودية. الدراسة أُجريت لفحص النسيج الصخرى، المكزنات المعدنية وتأثير الضغط على سرعة كل من الموجات الإنضغاطية والقصية فى درجة الحرارة المعيارية. طرق الدراسة فى هذا البحث شملت الفحوصات الحقلية، تحليل وتحديد السحنات الصخرية، تحليل الخواص الجيوفيزيائية، و تحليل بيانات سرعة الموجات الصوتية.

كشفت الفحوصات المعملية أنّ طبقة الدام فى منطقة اللدام لها أربعة أنواع من السحنات الصخرية تشمل سحنة طينية، سحنة حجر جيرى مرصوص، سحنة حجر جيرى واكى وسحنة حبيبية. قيم المسامية المقاسة تتراوح بين ٢٥% إلى ٥٥% بقيمة متوسطة ٣٥% وقيم النفاذية من ٠.٣٩ مليدارسى الى ١٨ دارسى بقيمة متوسطة ٣ دارسى. النتائج أظهرت بان السرعة الانضغاطية القصية تزيد بزيادة الضغط المسلط على عينات الصخور الجافة. سرعة الموجة الانضغاطية تزيد وسرعة الموجة القصية تنقص مع الضغط المسلط على العينات المشبعة كليا. الزيادة فى السرعات هى زيادة بعلاقة غير خطية مع الضغط. معادلة فى الشكل $V = AP^2 + BP + C$ تعطى أفضل تمثيل للقيم المقاسة للسرعة عند مقارنها مع المعادلات المقترحة من قبل دراسات أخرى.

CHAPTER 1

INTRODUCTION

1.1 Overview

Acoustics is the interdisciplinary science that deals with the study of all mechanical waves in gases, liquids, and solids including vibration, sound, ultrasound and infrasound. Although reservoir characterization and simulation have made significant advances toward integrating all available reservoir information, in order to decrease uncertainties in characterizing reservoirs between wells, acoustic data are integrated with rock properties obtained from well logging and laboratory measurements.

Acoustic logging is an important part of formation evaluation. This type of logging uses the propagation of acoustic waves within and around the borehole. Acoustic properties measured in well logging are compressional- and shear – wave velocity, compressional – and shear- wave attenuation, and amplitude of reflection wave. The measurement of wave velocity can be used to evaluate formation porosity, lithology, and both bulk and pore compressibilities. Cement bond quality determination and fracture zone identification are based on measurements of wave attenuation. It is also used to locate vugs and fractures, to determine fracture orientation, and to inspect casing the measurements of reflected wave amplitude. This study will focus on studying one of these three properties measured in well, i.e., compressional and shear wave velocities.

The velocity waves in rocks depend on many properties of rock, for example, density, porosity, saturation, and the amount of fracturing. Consequently, using acoustic has proved to be quite valuable. Unfortunately, the same properties that make the transition of wave sound possible give rise to extremely complex wave-forms when transmitter and receiver are placed in a borehole that penetrates material with varying properties. With confidence we can say that, the acoustic "sonic" logging is almost unique among logging methods because more information is available than can be interpreted.

Because of the increasing value of oil, the growing complexity of recently discovered oil fields, and the growing realization that geologic properties of reservoirs and conditions affecting hydrocarbon fluid recovery are more heterogeneous than assumed in the past, a major shift in the use of seismic methods has taken place during the recent past. One of the central aspects of this shift involves the need to establish and understand the relation between the seismic properties of reservoir and reservoir related rocks and their production properties (porosity and permeability) and state (mineralogy, saturation, pore pressure, etc.).

Seismic inversion, i.e., converting seismic amplitudes and velocities to reservoir properties, requires valid rock physics relationships. Rock physics models of clastic reservoirs, mainly sandstones, have been the focus of many studies Nur, Walls et al. (1980) [1], Thierry Bourbie (1985) [2], Murphy (1982) [3], and Bourbie (1987) [4]. Although 50% of the world's hydrocarbon reserves are found in carbonate rocks, unfortunately they have not received the same attention as clastic reservoirs, probably due to the heterogeneity of the carbonate reservoirs at all scales which makes them extremely difficult to characterize. Recently, carbonate reservoirs have become the focus

of several rock physics studies. A special section on carbonates published in The Leading Edge, presents some of this recent work (Sayers, 2008).

1.2 Significance of the Research

The petroleum industry faces several challenges in different areas and need more research to develop and improve understanding of the petroleum reservoirs. One of the most difficult challenges associated with seismology is the study of acoustic waves in carbonate rocks that have received little attention so far. By studying this type of rocks the outcome is expected to enhance the exploration efforts. It will also lead to better reservoir characterization, and integration of geological, geophysical, and engineering data. In particular, the results will impact reserves calculation, 4-D seismic interpretation, super-k evaluation, attribute analysis, and reservoir simulation studies.

1.3 Description of the Problem

Reservoir rocks are always saturated with a fluid. The influence of these fluids on the acoustic properties is an essential factor to be considered for modeling. Pore structure controls the distribution of these fluids within the rock frame. The combined effects of the fluids and the pore structure should be modeled together.

Detailed investigations are therefore needed to determine the acoustic properties of rock, especially the wave velocities as functions of variables such as saturating fluid and confining pressure, which a rock is subjected to during the producing life of a reservoir.

These properties have to be established from a systematic laboratory program and then related to the rock pore structure to obtain rock physics models.

1.4 Research Objectives

The general objective of this research is to develop empirical relationships between acoustics (compressional velocity V_p, and shear-wave velocity V_s) at two different fluid saturations and porosity for carbonate reservoir rocks.

The Miocene carbonate rock of Dam formation in the Al-Lidam area has been taken as reservoir outcrops equivalent to subsurface carbonate reservoir.

The specific objectives of this study are as follows:

1. Capture petrophysical parameters (macro-porosity, porosity types, and mineralogy) from thin sections of the rock samples and provide full petrographic description;
2. Determine the porosity, permeability, and density of rock samples at ambient condition.
3. Measure porosity and permeability as a function of confining pressure.
4. Determine pore size distribution, pore surface area, and the mean distance between pores.
5. Determine the compressional and shear velocities in dry and fully saturated samples as a function of confining pressure.
6. Develop empirical relationships between acoustic velocities and porosity.

CHAPTER 2

LITERATURE REVIEW

A significant amount of work has been done on rock physics models for petroleum reservoirs, mainly sandstones. Almost 50% of the world's oil reserves are found in carbonate rocks. Regrettably, they have not received enough attention as sandstone.

Gassmann (1951) [5] studied elastic wave through a packing of spheres and developed theory of porous solids by considering the porous solid as homogenous elastic solid if the porous are assumed sufficiently small, also, he assumed all pores are connected. The velocities of propagation of elastic waves have been calculated for evacuated interspaces and for interspaces filled with a liquid or gas. He proposed model that can be used to predict wave velocities from confining pressure as shown below

$$V_P = A_P * P^{B_P} \quad (2.1)$$

$$V_S = A_S * P^{B_S} \quad (2.2)$$

Wyllie, Malcolm [6] investigated wave velocities for aggregates of uniform spheres of different diameters both dry and saturated with water, brine, organic liquids, and plastics. He also measured wave velocities through natural sedimentary rocks under brine-oil and brine-gas saturation. In addition, he presented experimental relationships between wave velocity, porosity, pore content, and matrix nature of sedimentary rocks.

Measurements of compressional ,V_p, and shear ,V_s, waves velocities and their attenuation in dry, partial, and fully saturated clay-bearing sandstone at different temperatures and confining pressures were recorded by Nur, Walls et al. (1980) [1]. They observed that as water saturation increases the shear wave velocity decreases, whereas compressional wave velocity decreases from dry to partial saturation, and pointedly increases for fully saturated case (Figure 2.1). All Figures at the end of this chapter.

Raymer, Jone et. al (1980) [7] studied acoustic well logging and noticed some deficiencies in the transit time to porosity transform. At the porosity extremes, 0 and 100%, the transit time varied than predicted. Therefore, a new empirical transform based on extensive field observations of transit time versus porosity, was proposed. It permits the determination of porosity in low velocity sandstone without the need for any correction factor.

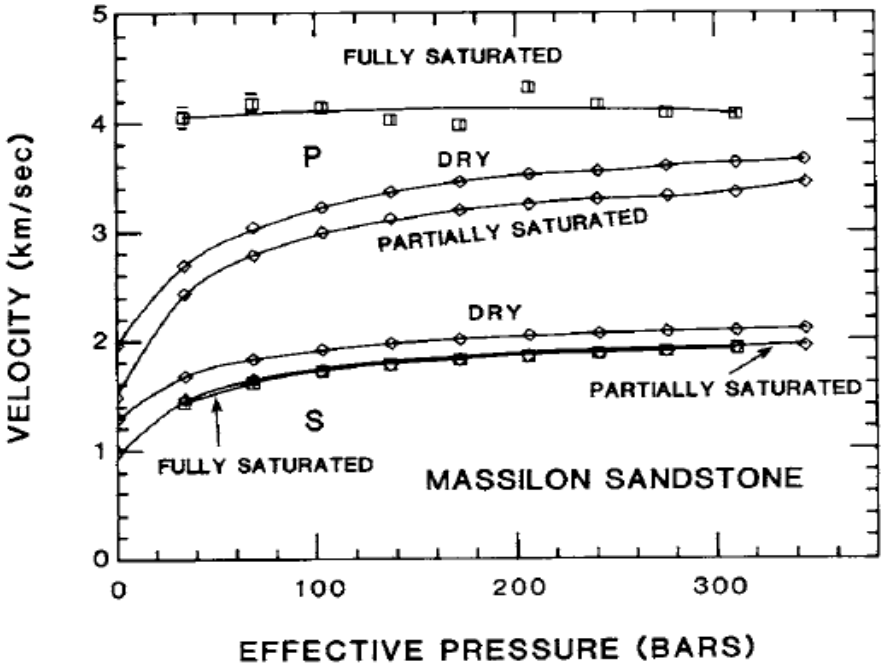

Figure 2.1 Wave velocity vs. Effective Pressure (Nur. 1980)

Seventy five samples of sandstone rock under different pressure up to 50 MPa, and porosity range from 2 to 30% with varying clay contests were studied by De- hua and Nur (1986) [8]. Both V_p and V_s were found to correlate linearly with porosity and clay content in sandstone as shown below:

$$V_p\left(\frac{km}{s}\right) = 5.59 - 6.93\emptyset - 2.18C \quad (2.3)$$

$$V_s\left(\frac{km}{s}\right) = 3.52 - 4.91\emptyset - 1.89C \quad (2.4)$$

Asnelmetti et. al (1993) [9] studied 210 samples of carbonates from different areas. The variation in velocities for a given effective pressure mainly was effected by variation in value and type of porosity. The variation in the mineralogy had no significant effect on the velocities. Generally, the measured velocities were observed to be inversely proportional with porosity and directly proportional to density. Carbonates located in the shallow water generally have a higher average velocity than those in deeper shelf. The age of rocks had on velocity.

Simon, Timothy et. al. (1997) [10] studies nine sandstone samples with a big range of permeability and porosity were used for P-wave and S-wave velocity measurements with a wide range of confining pressures and water saturations. Confining pressure on those samples ranged from 5MPa to 60MPa. The effects of progressive micro-crack closure were observed between 5MPa and 30MPa for all measured seismic parameters. Above 30MPa, micro-cracks were largely closed. At these pressures, P-wave velocity showed a decrease at intermediate saturation, whereas S-wave velocity and $\frac{V_p}{V_s}$ ratio increased and decreases with decrease in saturation, respectively.

Anselmettin et.al (1997) [9] compared P- and S-wave velocities with experimental data from XRD and thin section analyses for 50 carbonate samples. They observed that velocity is mainly controlled by porosity and primary pore type, quartz content, and dolomite content. In general, high-porosity rocks have lower velocities than low-porosity rocks with pressure. Pore type can also affect the velocity. Overall, as the percentage of dolomite increases in carbonate rocks velocities increase.

Khaksar et. al (1999) [11] investigated the influence of confining pressure on compressional and shear wave velocities for sandstone samples. They proposed empirical equations between velocities and confining pressure, they found the best fit for the measured velocities with improved prediction of velocities at high confining pressure presented by

$$V_P = A_P - B_P * e^{-PC_P} \quad (2.5)$$

$$V_s = A_s - B_s * e^{-PC_s} \quad (2.6)$$

Assefa, Solomon (1999) [12] studied ultrasonic compressional- and shear-wave attenuation for 40 limestone samples saturated with water and oil. They had two main aims of their work: (i) to relate textural/mineralogical properties and the petrophysical properties (saturation, permeability, and porosity) with seismic attenuation in limestone and; (ii) compare this relationship with that for sandstones. The results show that when the limestone is full with the fluid the attenuation increases with increase in both porosity and permeability. The mineralogical change had no significant effect on attenuation. P-wave and S-wave quality factors decrease with the increase in oolitic grain content. Replacement of water with oil as the pore fluid caused an overall increase in the

compressional- and shear-wave attenuation. Within the squirt-flow mechanism, frequency, *f*, and viscosity, μ, occur together as a product ($f * \mu$) and hence the increased viscosity of the oil used as the pore fluid is equivalent to measurement at an increased frequency.

Shear wave velocity from sonic logs using compressional wave velocity was predicted by Eskandri (2003) [13]. Using their model shear wave can be predicted by knowing the density, porosity and compressional velocity. Neutron Porosity (NPHI), bulk density (RHOB), and V_p are very important variables that have significant part in their statistical model.

$$V_s = -17.0885 + 0.4068 * Vp - 2.1907 * NPHI^2 - 1.1794 * NPHI - 3.2747 * RHOB^2 + 15.3587 * RHOB \qquad (2.7)$$

Ravi, Manika et. al (2006) [14] discussed the applicability of Gassmann's model for carbonates. Gassmann's model needs to be tested on more rigorous grounds. In their study, they had used Gassmann's equation to calculate saturated velocities for predicting fluid effects on a wide range of carbonate rocks with different textures and porosities ranging from at an effective pressure of 50 MPa. The velocities and modulus calculated using the Gassmann's equation underestimate the saturated velocities and modulus, especially for formations with low porosity where there is no variation of shear modulus after saturation. Gassmann's equation for high porosity formation overestimates the value of *Vp* and Vs. The theory was successful in modeling the variation in the *Vp/Vs* ratio for the effect of porosity and fluid as it is known to do for clastics and also to lay checks for proposed Amplitude Variation with Offset (AVO) study of an area.

Adam, Ludmila (2006) [15]studied the variation in P-wave and S-wave velocities for9 carbonate samples at ultrasonic (0.8 MHz) and seismic (3–3000 Hz) frequencies. Dry samples as well as saturated with liquid butane and brine were used in that study. Gassmann's theory on dolomite and limestone rocks in the context of shear- and bulk-modulus dispersion was applied on the measurements obtained from those samples. They observed that there is sensitivity in the rock shear modulus when it is saturated with brine, especially at seismic frequencies. At ultrasonic frequencies the bulk modulus had significant dispersion affecting the application of Gassmann's fluid-substitution theory. The use of brine with different salinities and temperatures to enhance production can cause variation in the module of the rocks resulting from the change of the solid frame.

Klaas, Verwer (2008) [16] had analyzed more than 250 carbonate plugs from outcrops and three nearby boreholes in an undisturbed reef of Miocene (Tortonian) for texture, mineralogy, and acoustic properties. P and S-waves velocities were measured under dry and brine-saturated condition at 10 MPa effective confining pressure. Regarding acoustic properties, they concluded that only a small increase in velocity is observed with the increase in effective pressure. Figure 2.2 shows the difference between the two velocities as representative by continues and dash curves for different rock types.

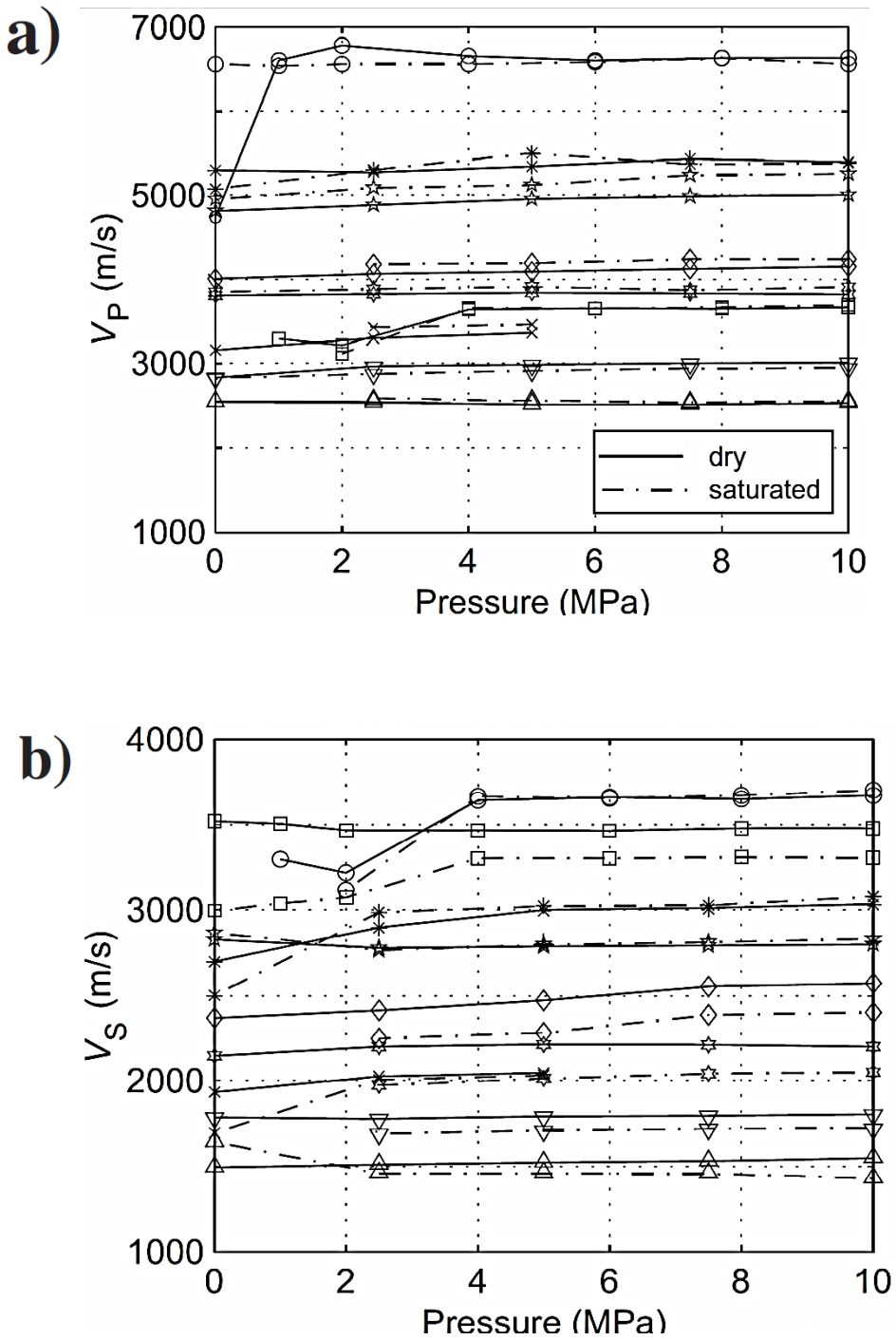

Figure 2.2 Velocities versus Effective Pressure for different rock samples (Klaas 2008)

CHAPTER 3

STUDY AREA

3.1 Introduction

The name Dam formation was introduced in 1935 by Steineke and Koch for the Miocene succession. The Dam formation is a mixed carbonate/siliciclastic unit of Middle Miocenein age.

During the field study, representative stratigraphic section of the Dam formation in Al-Lidam Area (Figures 3.1 and 3.2) was studied and approximately ninety three samples collected representing different cycles depending on change in lithology. Using these samples, thirty one stratigraphically oriented standard thin-sections were prepared for the petrographic studies.

3.2 Location of the Study Area

The largest distribution of Miocene rocks in the Arabian Peninsula is located East and North East part of Saudi Arabia (Figure 3.3). The Lidam area is about 70 Km from Dhahran city along the west–bound side on the Dammam-Riyadh highway. Lidam area named after Jabal Al-Lidam (26°21’42” N, 49°27’42”E).

The Dam Formation is about 41 m thick and consists of pink, white, and gray marls, and red, green, and olive clays, and limestone with minor amount of sandstones.

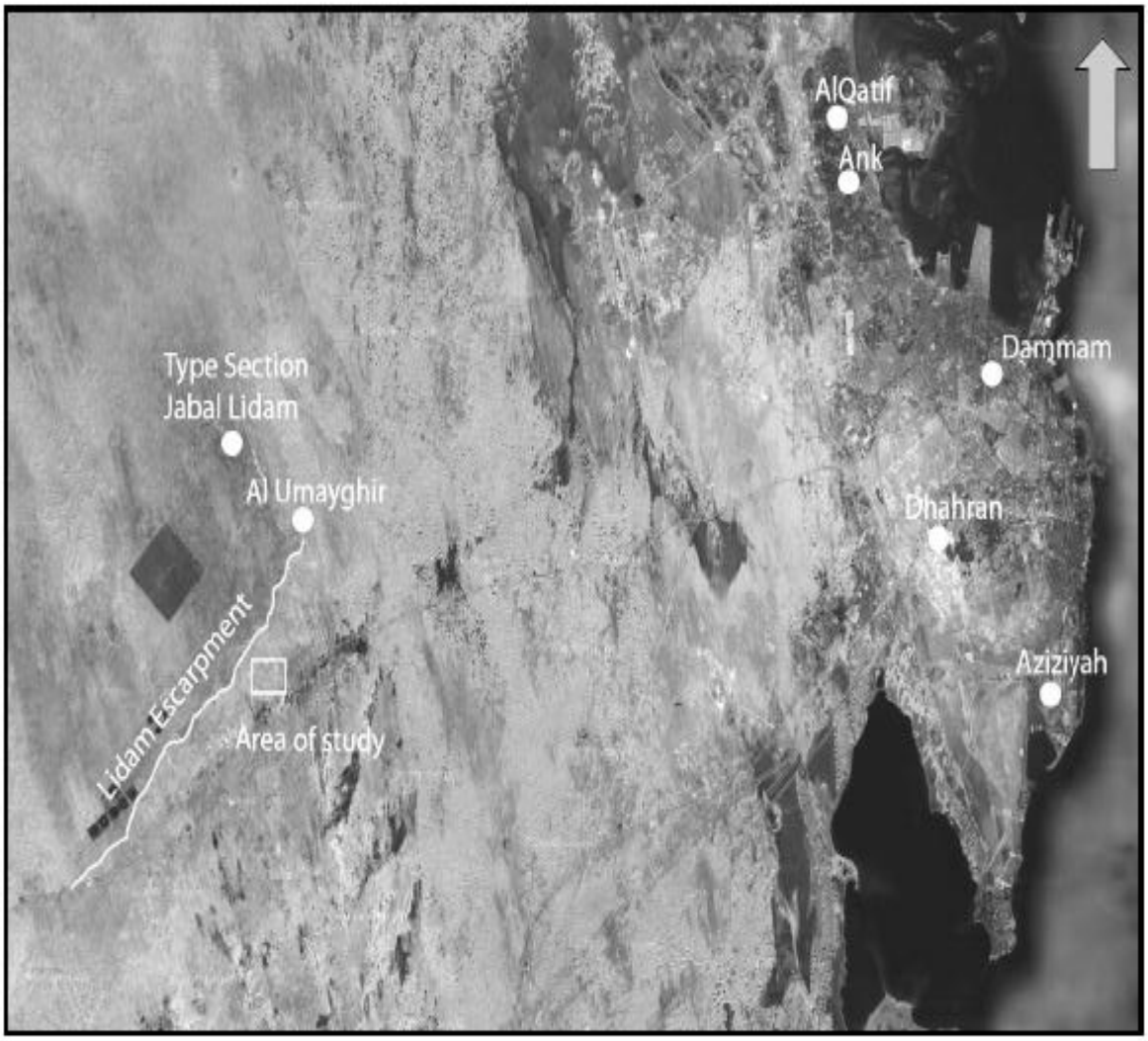

Figure 3.1 Outcrop Location for Lidam Formation

Figure 3.2 Part of Jabal Al-Lidam

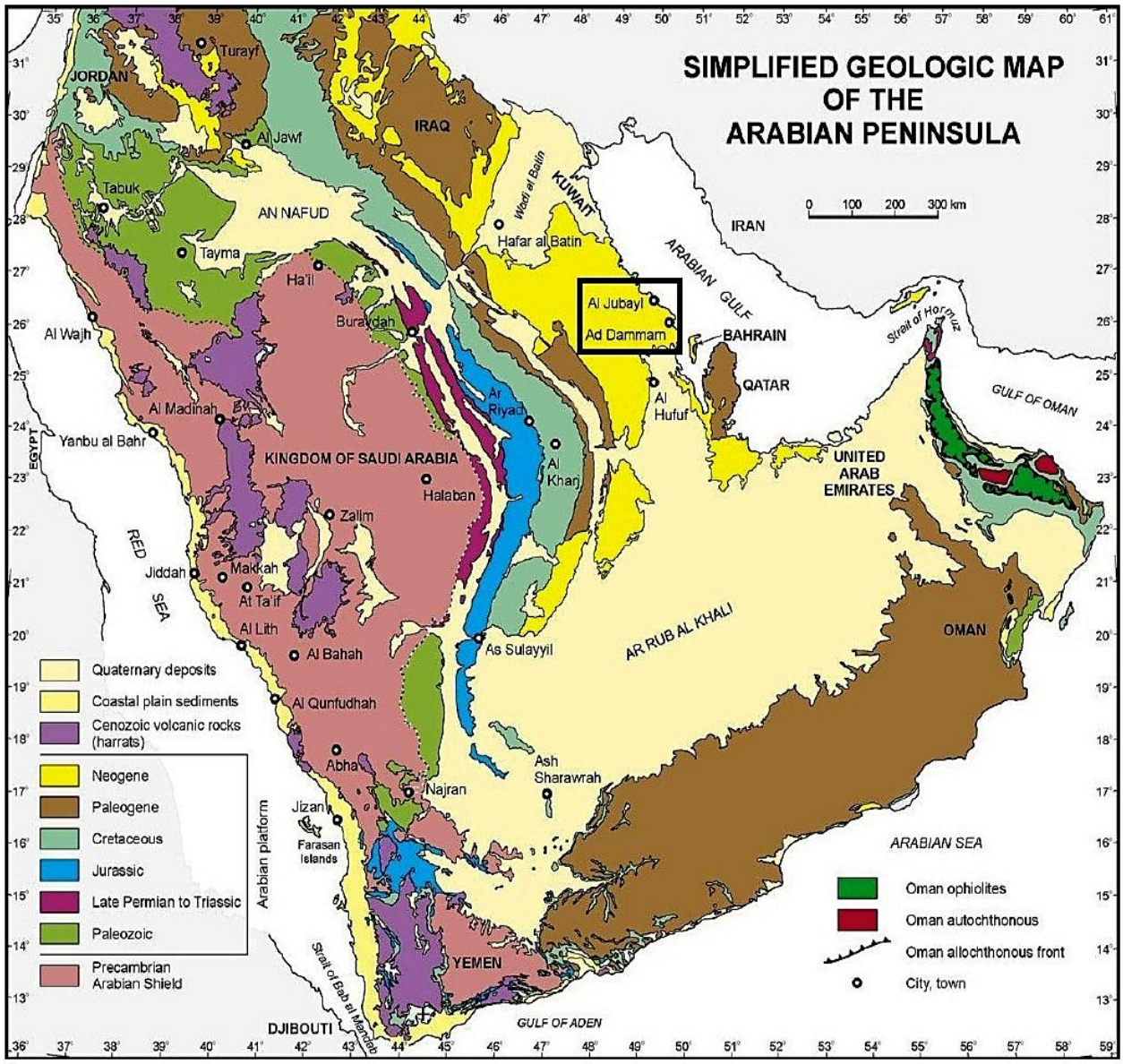

Figure 3.3 Simplified geologic Map of Arabian Peninsula. Note the distribution of Miocene rocks in the Eastern Part of Saudi Arabia. The Area of study is shown box

3.3 Previous work

Dam formation exists in Iran, Qatar, Kuwait, and Saudi Arabia. This review will focus only to that related to Saudi Arabia. Steineke (1935) [17] first introduced the name Dam Formation for the Miocene succession. Thralls (1956) [18] published a paper on Dam formation. The age of Dam formation has been classified as middle Miocene by identifying many fossils in rock samples from Dam formation studied by Powers (1966) [19]. Irtem (1986) [20] studied the dam formation in Al-Lidam area and recognize three upward-deepening cycles. A typical cycle begins at the bottom with supratidal gypsierous claystone grading upward into itertidal sandstone and shallow subtidal to lower interidal limestone and thin bedded oolitic grainstone (Figures 3.4, 3.5 and 3.6). Tleel (1973) [21] presented a detailed measured section of the Dam Formation at Jabal Midra Al-Janubi. This location has been removed due to recent urban development. A comparative study between the microbio components of the coastal regime of the Arabian Gulf in Saudi Arabia, and those of the Middle Miocene Dam Formation in Jabal Midra Al-Janubi has been done byAl-Enezi (2006) [22]. Alkhaldi (2009) [23] defined the spectrum of carbonate and siliciclastic facies in Dam Formation, depositional environments, and platform models within a high-resolution cycle-and-sequence stratigraphic framework.

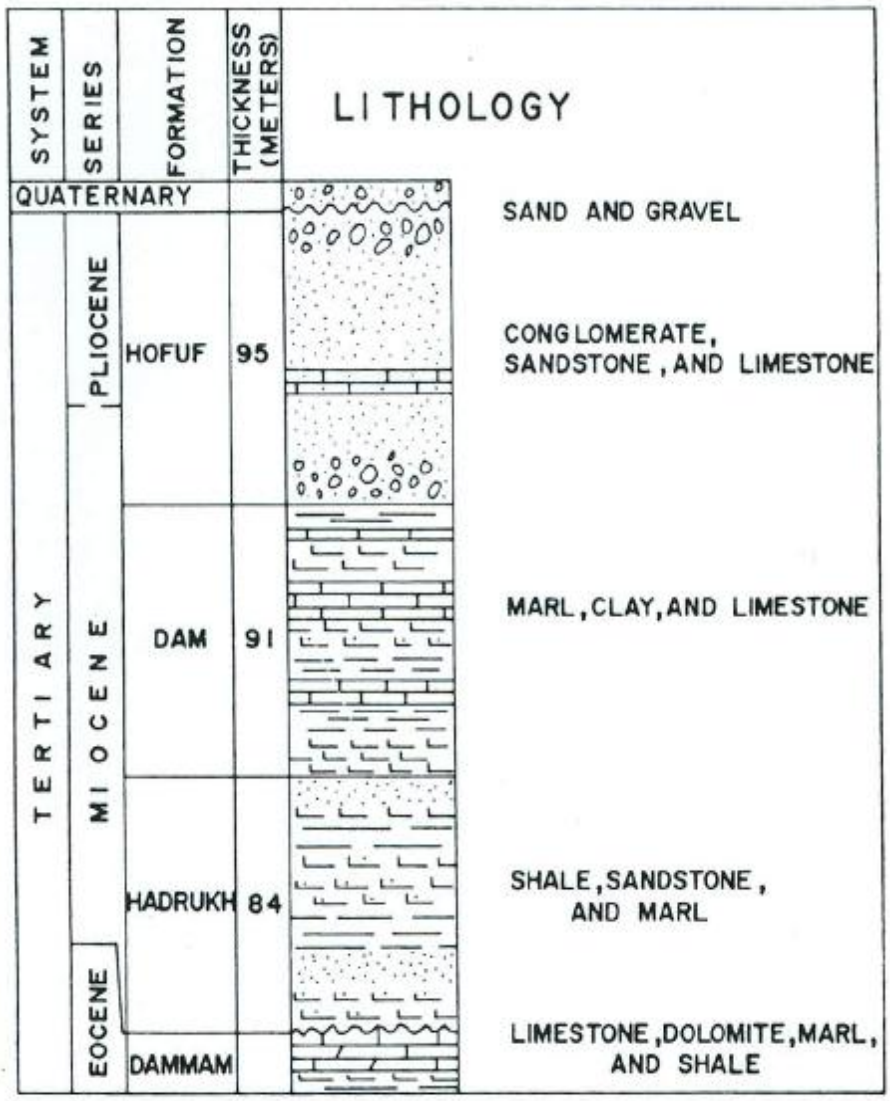

Figure 3.4 General Statgraphic Column of Rocks Cropping out in Al- Lidam Area
(Modified from Powers and Others, 1966)

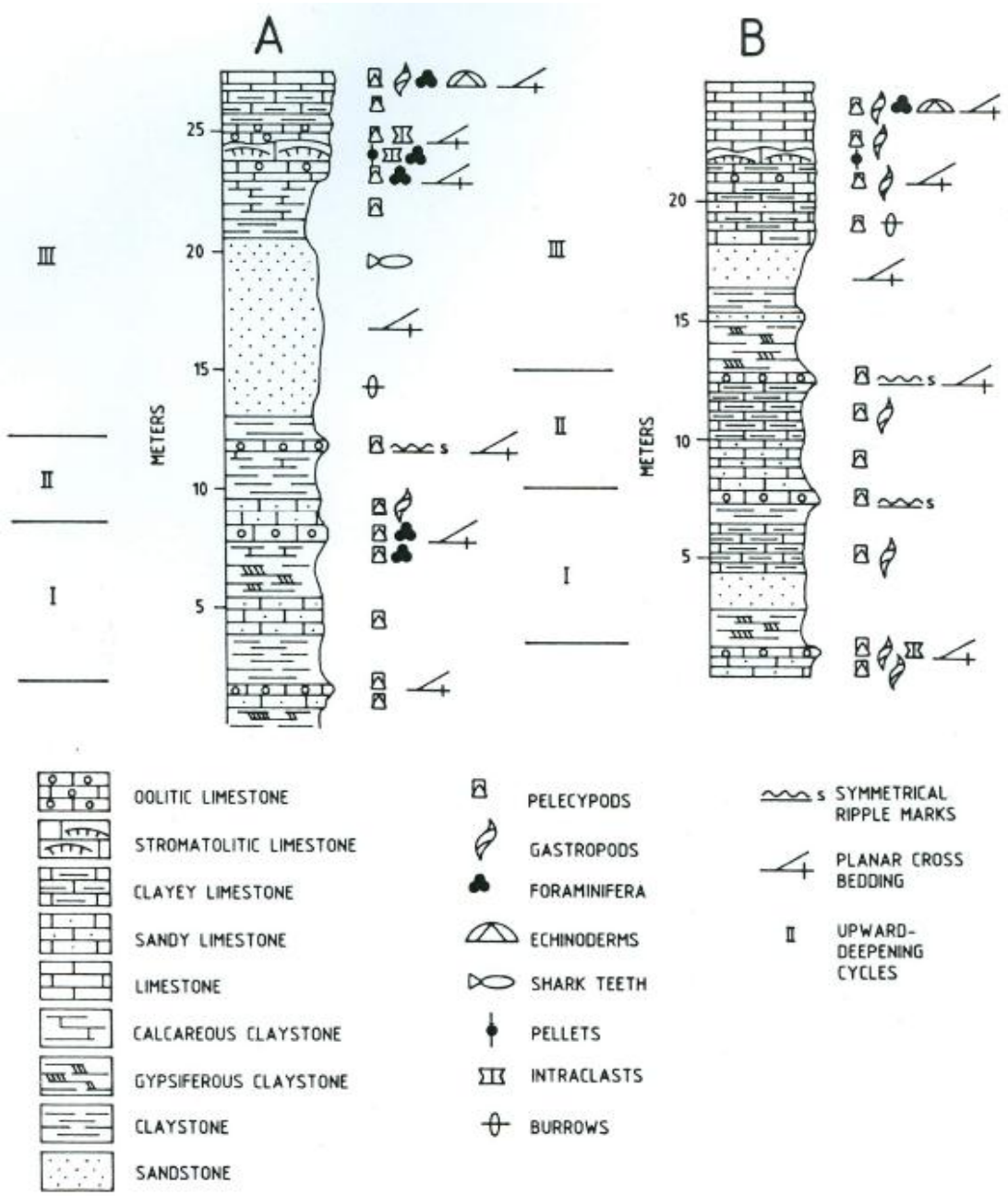

Figure 3.5 Two Representative Sections of Lower Part of Dam Formation Illustrating cycles in Al-Lidam area

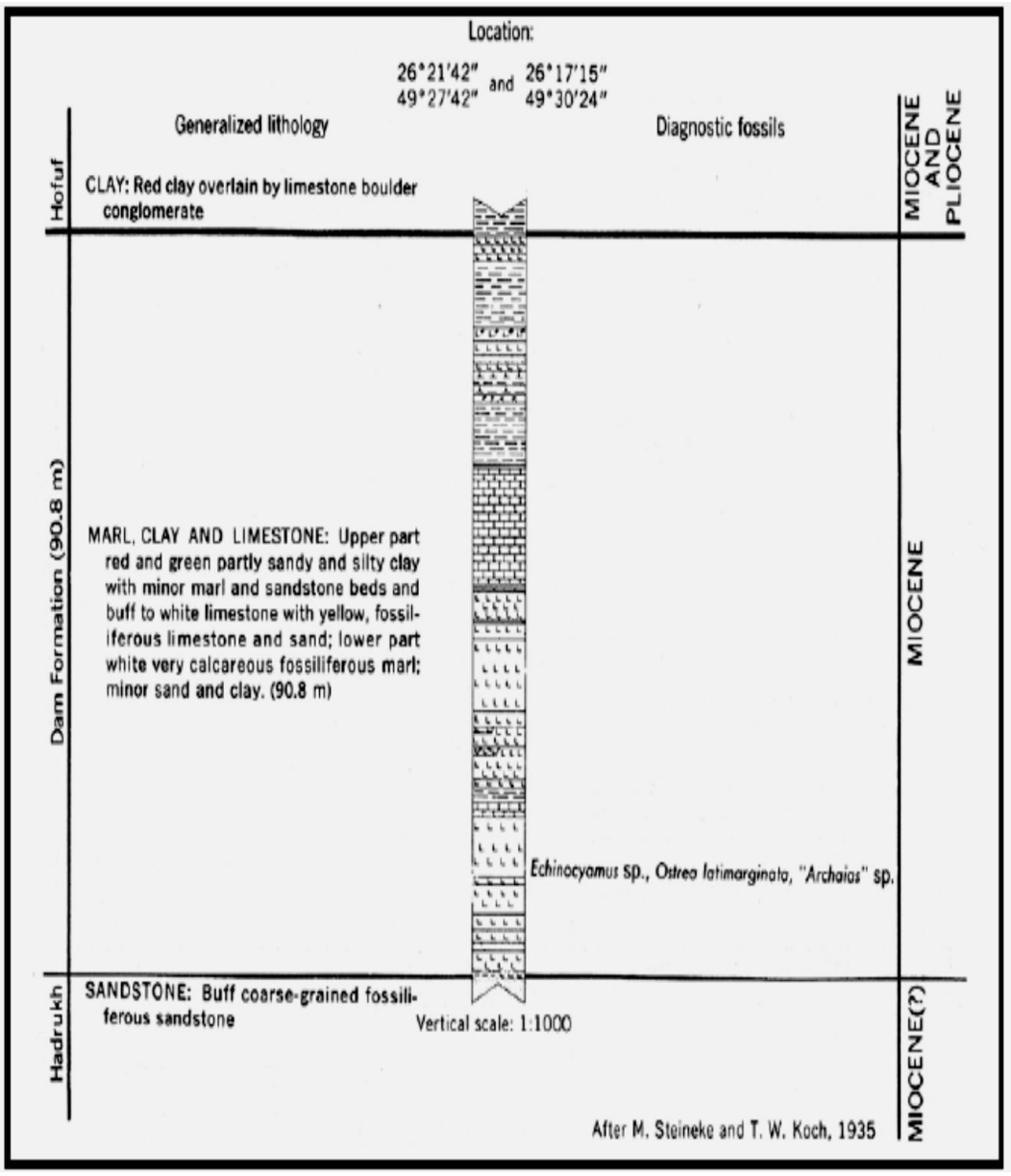

Figure3.6 Type section of Dam Formation as defined by Steineke and Koch (1935)

CHAPTER 4

PETROGRAPHIC ANALYSIS

4.1 Introduction

This chapter discusses the results obtained from laboratory measurements and observations. The petrographic analysis includes thin section petrography and carbonate classification conducted on 30 selected samples.

4.2 Petrographic Analysis

The main objective of petrographic description is to determine the composition and classify the rock types for purpose of revealing information about environment, source area, paleoclimate and inferring the depositional history of area Tucker (2005) [24]. For carbonates facies from Dam formation in Al-Lidam, the petrographic analysis will focus only on the composition of samples.

A field trip to Al-Lidam area was conducted to collect the rocks required for this study. Sixty-one specimens of 1.5 inch (38 mm) and 32 specimens of 1 inch (25 mm) diameter were drilled from cores ranging from 5 in. to 8 in. size blocks. Total of 93 samples were used in this study. To maximize the number of specimens from a single core and to study the anisotropic properties of rocks, cores were drilled both along the longitudinal axis and

perpendicular on it and marked as vertical (V) and horizontal (H), respectively, as shown in Figure 4.1. The coring machine is shown in Figure 4.2. The drilled specimens were then cut into 0.9 to 3.5 in (20±2 to 87±2 mm) long pieces using a high speed rotary saw shown in Figure 4.3. The end faces of the specimens were grinded using an End-Face Grinder, shown in Figure 4.4. The end-faces were checked for evenness and their perpendicularity with respect to the length axis of the specimen using a V-block and a dial gauge Figure 4.5. Each of the 93 samples was photographed before it had undergone cutting, trimming and testing. Typical photo for samples are shown in Figure 4.6.appendix A shows the orientation and dimensions of all the samples used in this study. Then during the plug preparation sample chips were collected from which impregnated thin sections were prepared. The thin sections were described with a binocular microscope and photographed.

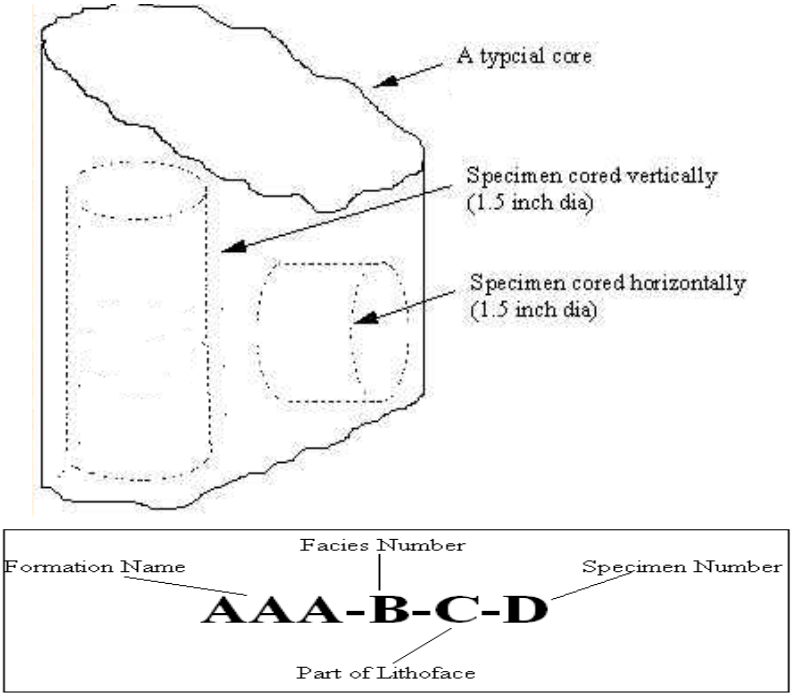

Figure 4.1 Cored specimen orientations and notation for cored specimens

Figure 4.2 Coring machine

Figure 4.3 High speed rotary saw for cutting rock specimens

Figure 4.4 End-Face Grinder

Figure 4.5 Dial gage and V-block for checking evenness and perpendicularity of the end-faces

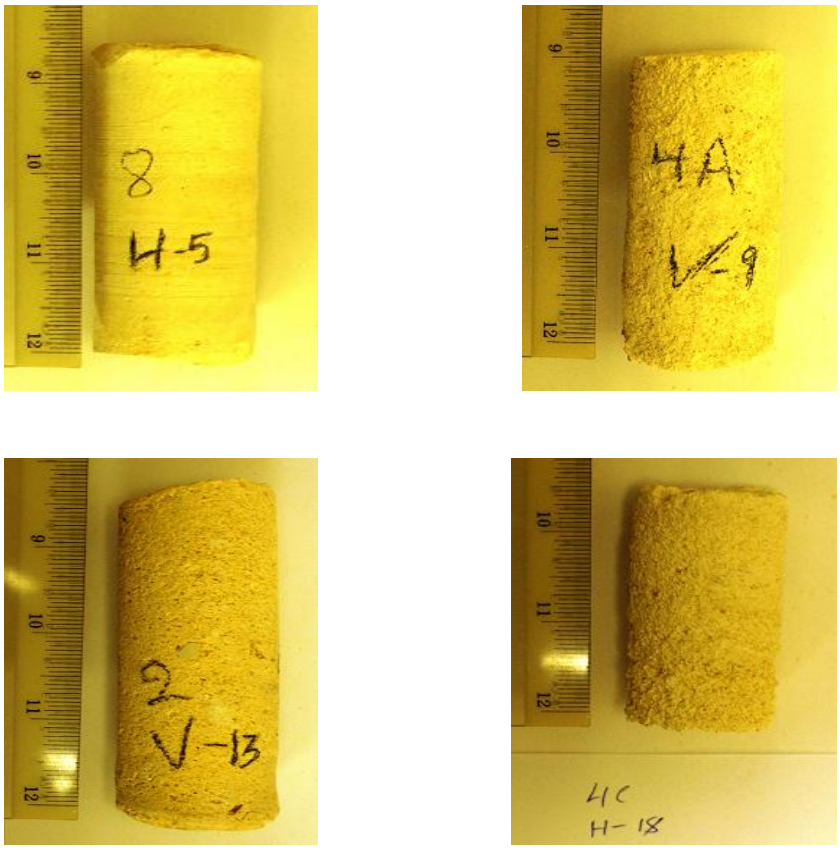

Figure 4.6 Photos of a few selected samples from Dam Formation

4.2.1 Texture Classification

The texture classifications of the samples were based on grain support and grain type to siliciclastic, carbonate (grain supported, and mud supported). The grain supported rocks are skeletal and non-skeletal rocks. These classifications were further enhanced based on Dunham's texture classification (Dunham 1962) [25].

Dunham's classification (1962) has become the most widely used classification for carbonate rocks in the Oil industry. The presence or virtual absence of an interpreted very fine-grained carbonate lime mud matrix has been used as a principle of Dunham's classification (Figure 4.7).

Based on preliminary survey of outcrop, hand-specimens, and core plugs, eight facies have been found as shown in Appendix A. However the thin section description and Dunham's classification lead to the identifications four facies only. The rest of this work is based on these four facies. Out of these classifications a general texture distribution map was constructed in Figure 4.8.

Figure 4.7 Amplification of Original Dunham (1962) Classification of Limestone According to Depositional Texture by Embry and Klovan (1971)

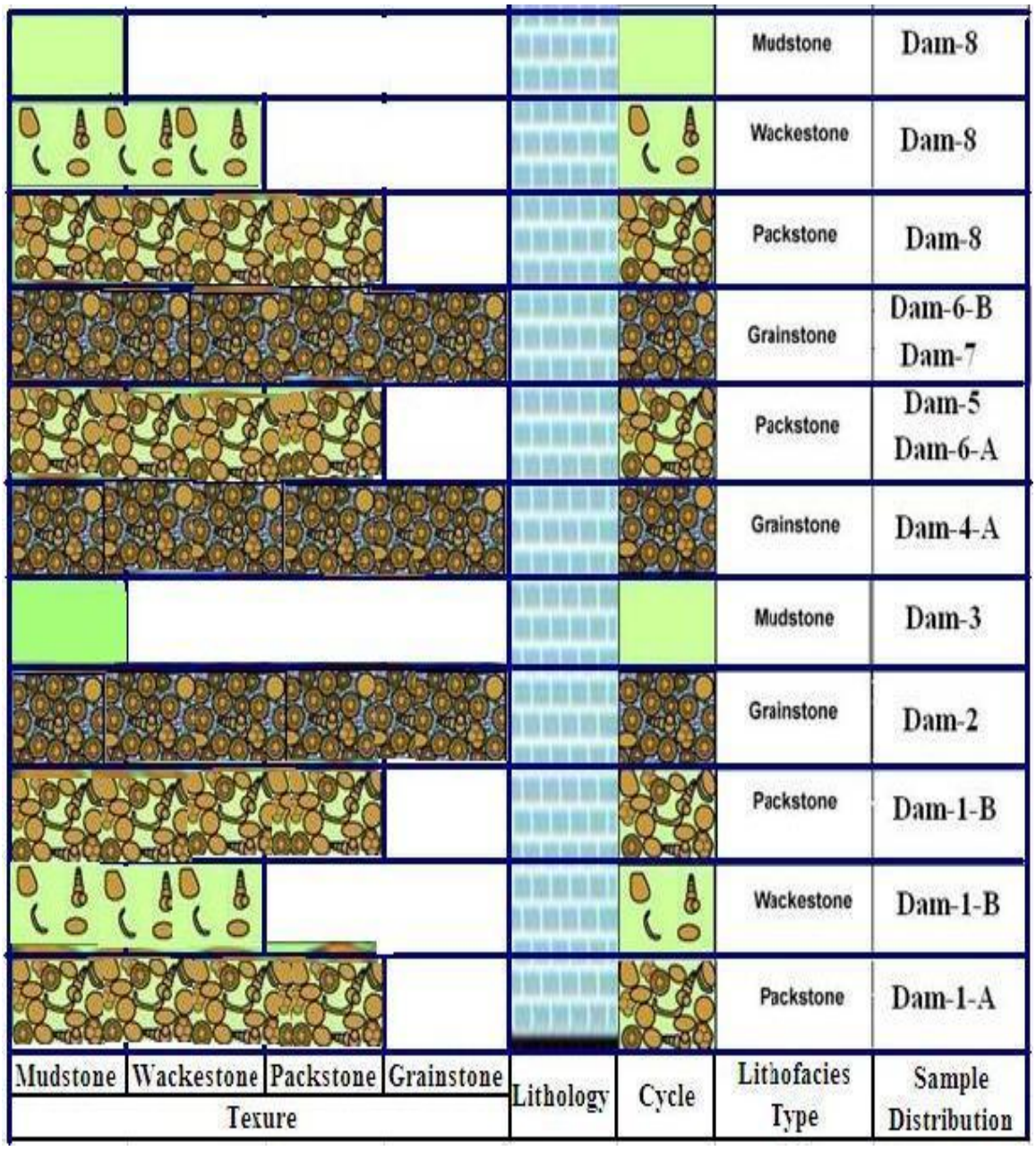

Figure 4.8 Texture distribution map from bottom to top of facies types in Dam Formation

4.2.2 Thin Section

A total of thirty-one thin sections were prepared from the rock samples collected from Al-Lidam area. Three to sixteen samples were studies for each one of the four textures that have been identified in Al-Lidam area as discussed earlier (Table 4.1). Figure 4.9 shows histogram and pie-chart diagram for the number of the thin sections in the four facies. The detailed petrographic studies consist of description of primary carbonate particles, the depositional and diagenetic fabrics, and porosity types.

The thin sections show that the rock samples are mostly limestones, in particular peloidaloolitic skeletal lime grainstones. Muddy limestone lithologies ranging from packstone to mudstone were also observed. The studied samples are almost pure limestones with scattered detrital quartz grains (1 to 5%) in some of them. However few samples are sandy limestones and contain 10 to 20 % detrital quartz grains. The non-skeletal grains are composed of oolites, peloids, and intraclasts. Bivalves, gastropods and forams make up the skeletal grains.

Oolitic lime grainstones are well sorted, well rounded and have good porosities up to 40%. Main porosity type is interparticle; however, moderate amounts of moldic and interparticle porosities are also observed. Occasionally interparticle pores are filled up partially by blocky calcite cement and finely bladed isopachous calcite rim cement.

The detailed petrographic studycovers the description of primary carbonate particles, the depositional and diagenetic fabrics, and porosity types as discussed in the following sub-section.

Table 4.1 Thirty one samples represent all facies

Sample No.	Sample Name	Direction	Length (in)	Diameter (in)	Dunham
5	Dam-1-B-5	V	2.8	1	Wackestone
6	Dam-1-B-6	V	2.5	1	
79	Dam-8-79	V	1.6	1	
16	Dam-3-16	H	2.8	1.5	Mudstone
17	Dam-3-17	H	2.3	1.5	
18	Dam-3-18	V	3.1	1.5	
20	Dam-3-20	V	3.2	1.5	
80	Dam-8-80	V	1.6	1	
9	Dam-2-9	H	2.5	1.5	Grainstone
10	Dam-2-10	H	1.8	1.5	
11	Dam-2-11	H	2.6	1.5	
13	Dam-2-13	V	3.8	1.5	
21	Dam-4-A-21	V	2.7	1.5	
26	Dam-4-A-26	H	2.2	1.5	
27	Dam-4-A-27	H	1.9	1.5	
29	Dam-4-A-29	H	2.3	1.5	
50	Dam-6-A-50	V	2.4	1.5	
55	Dam-6-B-55	V	3	1.5	
56	Dam-6-B-56	H	3.5	1.5	
64	Dam-6-B-64	H	2.9	1	
66	Dam-7-66	V	3	1.5	
67	Dam-7-67	V	2.1	1.5	
68	Dam-7-68	V	1.6	1.5	
69	Dam-7-69	V	1	1.5	
3	Dam-1-A-3	V	3.3	1.5	Packstone
8	Dam-1-B-8	V	2.2	1	
46	Dam-5-46	H	1.9	1	
47	Dam-5-47	H	1.7	1	
48	Dam-5-48	H	1.2	1	
70	Dam-8-70	V	2.6	1.5	
87	Dam-8-87	V	0.9	1	Corrupted

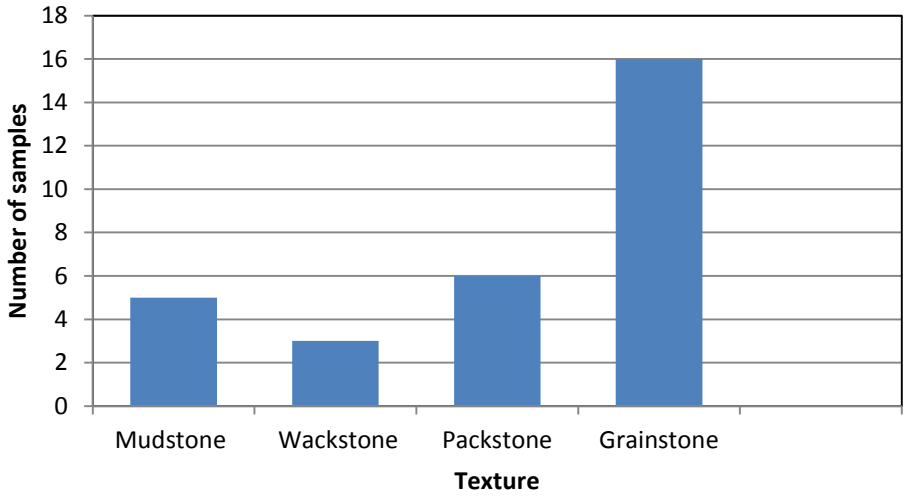

Figure 4.9 Histogram diagram for the number of thin sections for all four facies

4.2.3 Petrographic Description for each facies

4.2.3.1 Mudstone

Five samples 16, 17, 18, 20, and 80 were represented this texture. The thin section photomicrographs for these samples are given in Appendix A. These five textures, viz., sandy lime mudstone, lime mudstone, sandy lime mudstone, sandy lime mudstone, and peloidal lime mudstone. These samples show the presence of peloids, unidentified fossils, moldic porosities, intraclasts, mainly burrow fill, burrowed, minor amounts of fracture. Porosity ranges from 7 to 15% (5-7% moldic, 2-8 burrow fill, and 1-0% fracture), pore size 50-400 micron, calcite 90-100%, and quartz 5-10%. (Figure 4.10 and Figures B-9, B-10, B-11, B-12, and B-30).

Porosity	7 – 15 %
Pore Size	50 – 200 microns
Calcite	90 – 100 %
Quartz	5 – 10 %

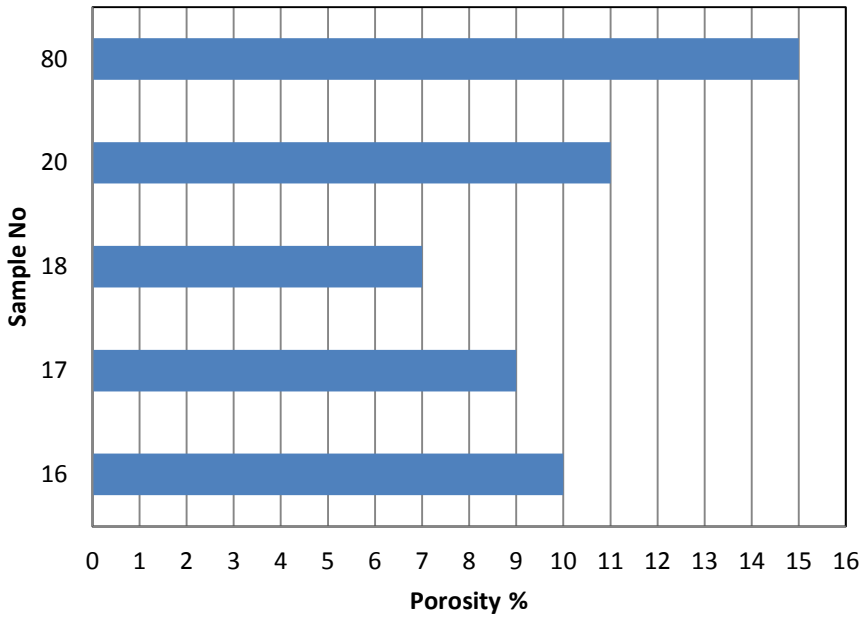

Figure 4.10 Porosity distribution for Mudstone facies

4.2.3.2 Wackestone

Three samples represent this texture (5, 6, and 79).Sample 6 was corrupted during preparation process. Samples 5 and 79 show the presence of peloidal lime wackestone and peloidal skeletal lime wackestone: peloids, forams, pellets, unidentified fossils, burrowed, bivalves, mainly moldic porosities, minor amounts of burrow fill, and intraparticle porosities, echinoids. Porosity ranges from 25 to 27 % (17-20% moldic, 5-6%burrow fill, 1-2% intreaparticle), pore size 50 – 200 microns, calcite 97 – 98%, and quartz 2 – 3% (Figure 4.11, and Figures B-2, and B-29).

Porosity	25– 27 %
Pore Size	50 – 200 microns
Calcite	97 – 98 %
Quartz	2 – 3 %

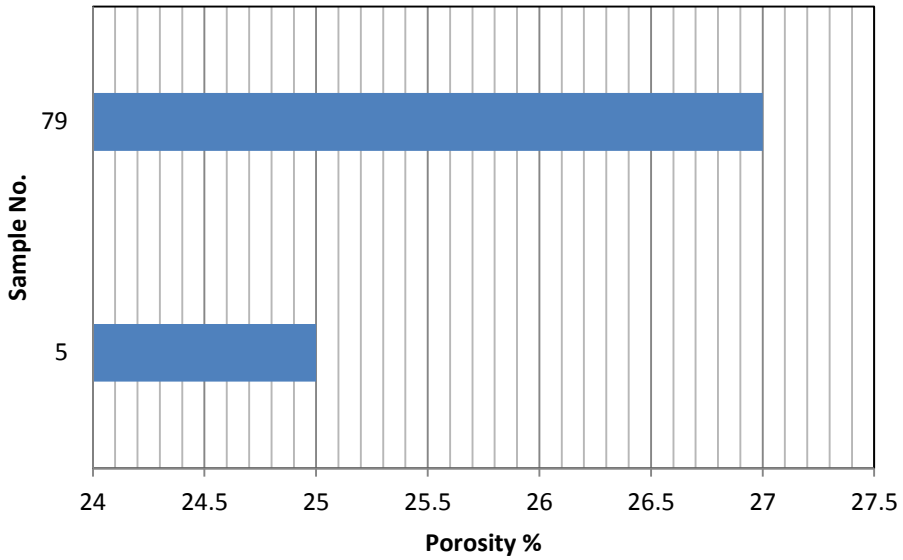

Figure 4.11Porosity distribution for Wackestone facies

4.2.3.3 Packstone

Six samples represent this texture (3, 8, 46, 47, 48, and 70). Sandy peloidal, intraclastic, skeletal lime packstone and peloidal skeletal lime packstone/grain dominated lime packstone. The samples show the presence of fine to medium-grained (125-250 micron), peloids, intraclasts, forams, unidentified fossils, and mainlymoldic porosities, minor amounts of intraparticle porosities, bivalves, unidentified fossils, pellets, fracture, leached dolomite and moldic porosities. The porosities 25 – 34% (20 – 30% moldic and 4 -5%

intraparticle), pore size 50 -300 microns, quartz 2 -20%, calcite 85 – 98% (Figure 4.12 and Figures B-1, B -4, B -17, B -18, B -19, and B -28).

Porosity	25– 34%
Pore Size	50 – 300 microns
Calcite	85– 98 %
Quartz	2 – 20 %

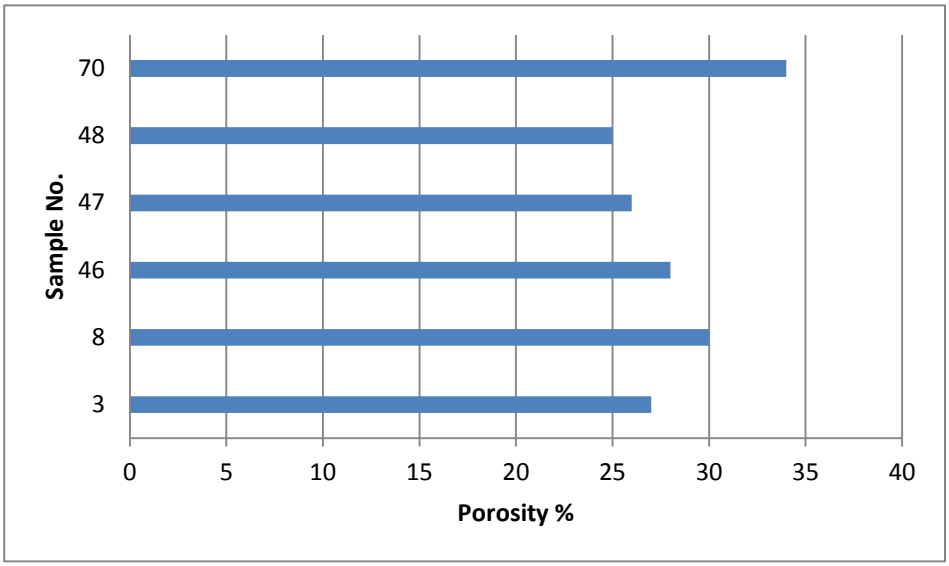

Figure 4.12 Porosity distribution for Packstone facies

4.2.3.4 Grainstone

The rest of the samples represent grainstonetexture. Calcite cemented peloidaloolitic bivalve gastropod lime grainstone, peloidalintraclastic skeletal lime grainstone, sandy peloidal skeletal lime grainstone, ooliticintraclasticpeloidal lime grainstone. The samples show the presence of medium to coarse-grained (250-1000 micron), peloids, oolites, bivalves, gastropods, forams, well sorted, rounded, interparticle, moldic and intraparticle

porosities, interparticle pores reduced by blocky calcite cement and finely bladed isopachous calcite rim cement, intraclasts, moldic, subrounded mainly reduced interparticle porosities. Porosity ranges from 22 to 40 % (7 – 14 % interparticle, 7 – 13 % moldic and 7 – 15% intraparticle), pore size 50 – 800 microns, quartz 1- 10%, calcite 90 – 99% (Figure 4.13, and Figures B -5, B-6, B-7, B-8, B-13, B-14, B-15, B-16, B-20, B-21, B-22, B-23, B-24, B-25, and B-27).

Porosity	22– 40%
Pore Size	50 – 800 microns
Calcite	90– 99 %
Quartz	1 – 10 %

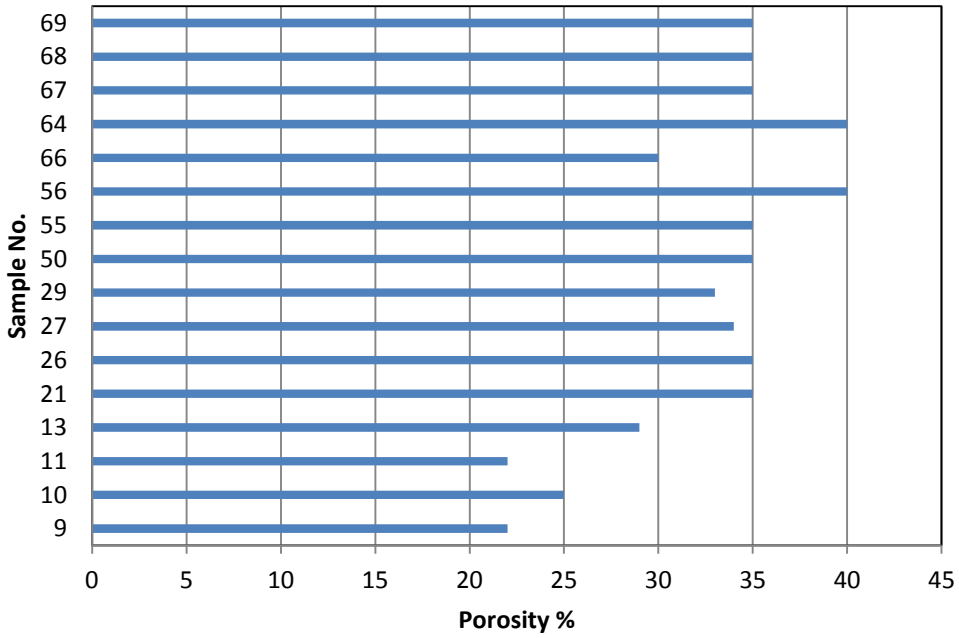

Figure 4.13 Porosity distribution for Grainstone facies

4.2.3.5 Summary for Petrographic Description

Dam formation shows different values of porosity range between 7 to 40% as can be seen in Figure 4.14. From Figure 4.15 it can be observed that Grainstone have the highest average values for porosity compare to Packstone, Wackestone and Mudstone. The largest size of pore in the all samples is 800 microns in Grainstone samples as can be notice from Table 4.2. Summary is shown in Table 4.3.

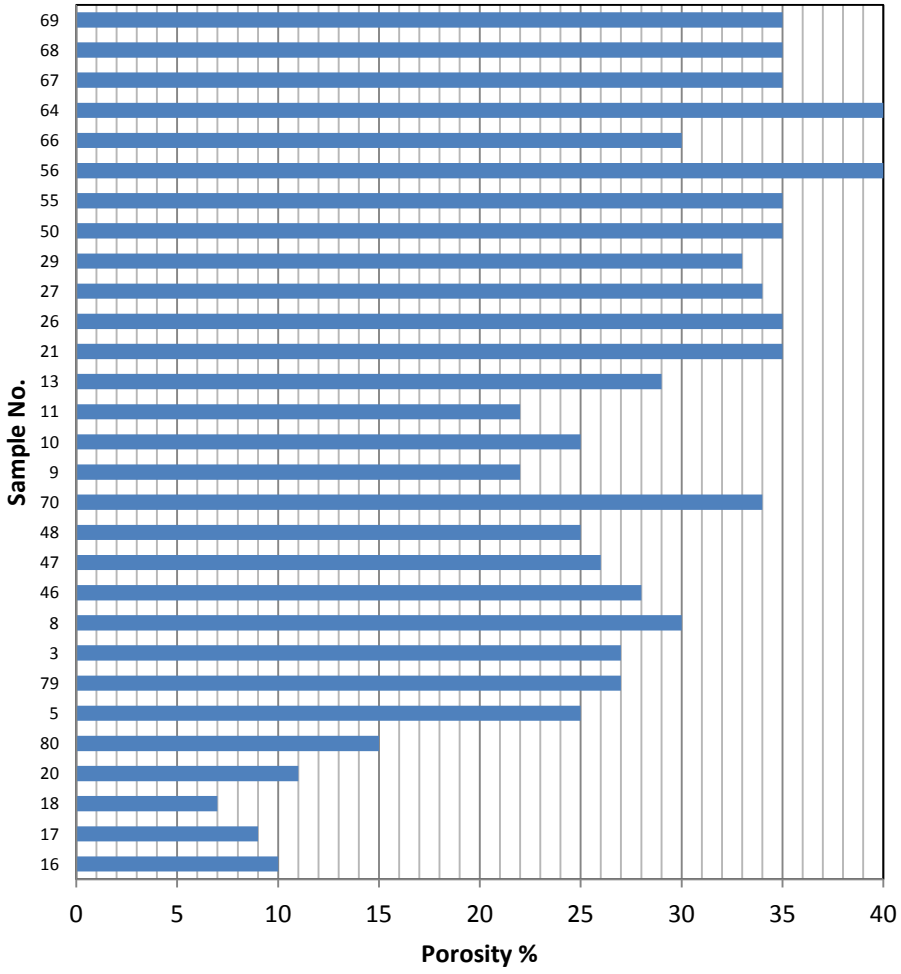

Figure 4.14 Porosity distribution for all Textures

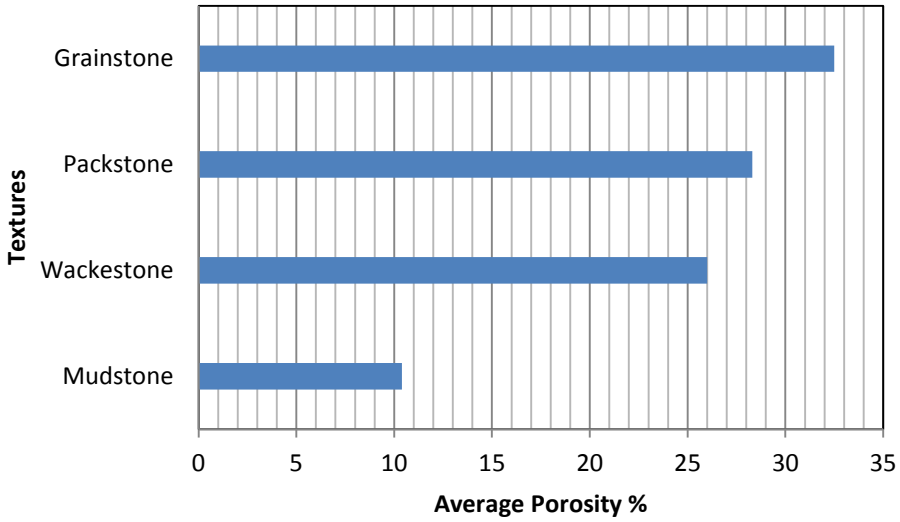

Figure 4.15 Average Porosity vs. Texture

Table 4.2 Pore size, Calcite and Quartz for All Texture

Texture	Porosity				Pores Size microns	Calcite %	Quartz %
	Max.	Min.	Median	Avg.			
Mudstone	15	7	10	10.4	50 – 200	90 – 100	5 – 10
Wackestone	27	25	26	26	50 – 200	97 – 98	2 – 3
Packstone	34	25	27.5	28.3	50 – 300	85– 98	2 – 20
Grainstone	40	22	35	32.5	50 – 800	90– 99	1 – 10

Table 4.3 Summary of Samples from All Texture

Porosity	7 – 40 %
Max. Porosity	40%
Min. Porosity	7%
Avg. Porosity	27.37931
Median Porosity	29
Pore size	50 – 800 microns
Calcite	85 – 100%
Quartz	1 – 20%

CHAPTER 5

PETROPHYSICAL ANALYSIS

5.1 Introduction

Porosity and permeability are important parameters in carbonate reservoirs. Their magnitude, pattern, and variability significantly influence the migration and distribution of the fluids and gas in the reservoir. Therefore, the production of fluids and gases from the reservoir depends on both porosity and permeability (Pryor 1973) [26].

This chapter discusses the relationship between porosity and permeability and relates it to the texture and mineral composition in Dam formation. For this purpose, porosity and permeability were measured in laboratory using Helium Porosimeter, AP-608 Automated Porosimeter-Permeameter and thin section. The porosity and permeability of the 83 samples were measured as a function of confining pressure.

5.2 Porosity

For quality control purpose, the measurement of porosity was conducted using two devices: Helium Porosimeter (Figure 5.1) and AP-608 Automated Porosimeter-Permeameter (Figure 5.2).

Figure 5.1 Helium Porosimeter for measuring porosity

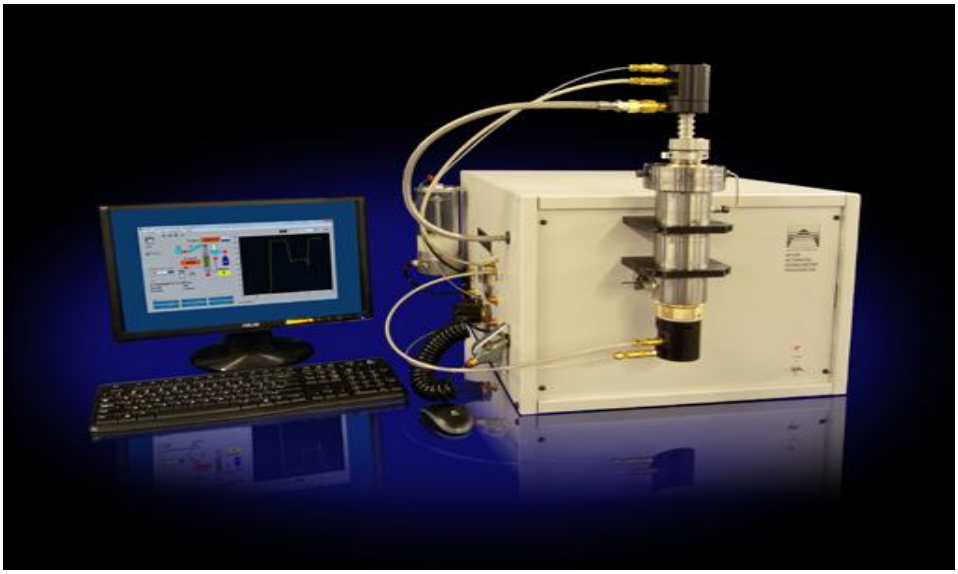

Figure 5.2 AP-608 Automated Porosimeter-Permeameter for measuring porosity

Porosity of these samples was estimated using thin section analysis as well. The measured porosity values using Helium Porosimeter range from24.36% to 54.22% and with an average value of 37.87%. The measured porosity values using AP-608 Automated Porosimeter-Permeameter range from24.97 % to 55.73 % with an average value of 38.5%. Figure 5.3 shows the comparison between the values for porosities obtained from the two devices. The difference between the two measurements was found to be less than 3 %.

The histogram in Figure 5.4 and Figure 5.5 show that the most frequent values are in range between 26% to 45% as obtained from both AP-608 Automated Porosimeter-Permeameter and Helium Porosimeter.

From the two histograms high porosity have been observed and they are out of standard range according to McWorter (1977) [27]. The porosity values expected by Alkhaldi (2009) [23] also fall below the extreme values (47%) as observed in this study. These high values could be due to human error, sample preparations, as well as equipment error. The porosity value of 47% is considered as the highest value for this study.

Porosity Distribution in Facies

Table 5.1 shows porosity values obtained from the three methods: Helium Porosimeter, AP-608 Automated Porosimeter-Permeameter and thin section analysis. It has been observed from Table 5.1 and Figure 5.6that the porosity estimated from thin section analysis is slightly different from the other methods. The difference can be due to several

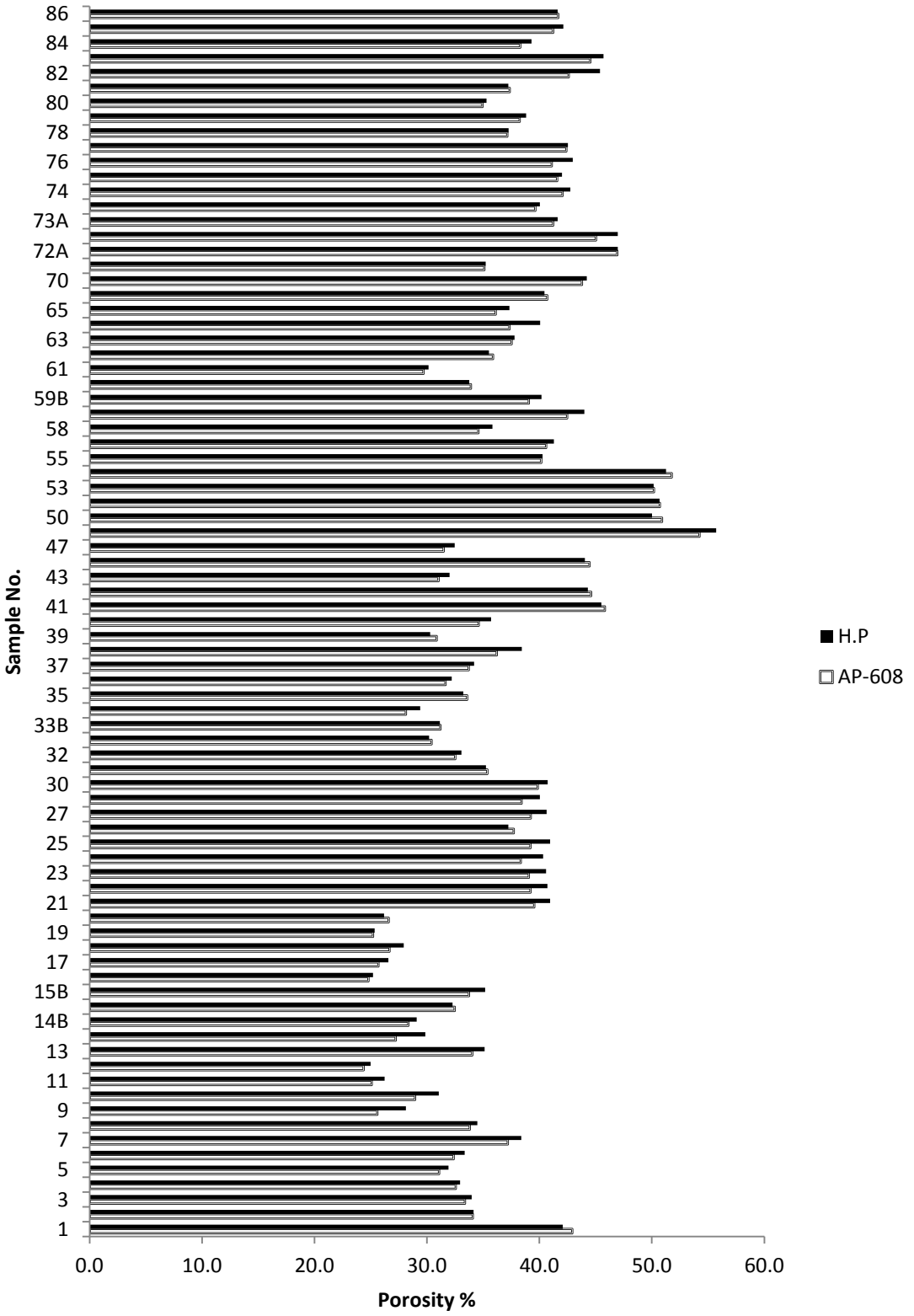

Figure 5.3 Distributions values for porosities obtained from two devices

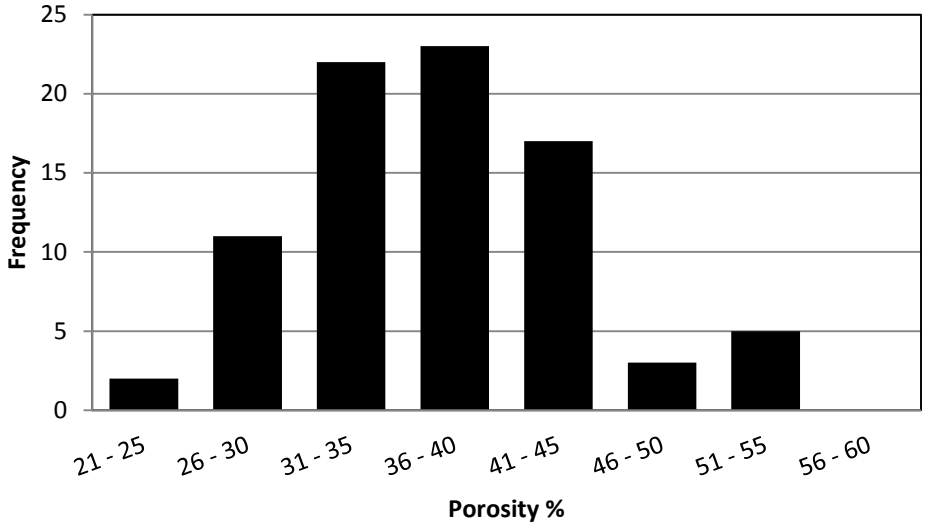

Figure 5.4 Histogram of porosity values from AP-608 Automated Porosimeter-Permeameter

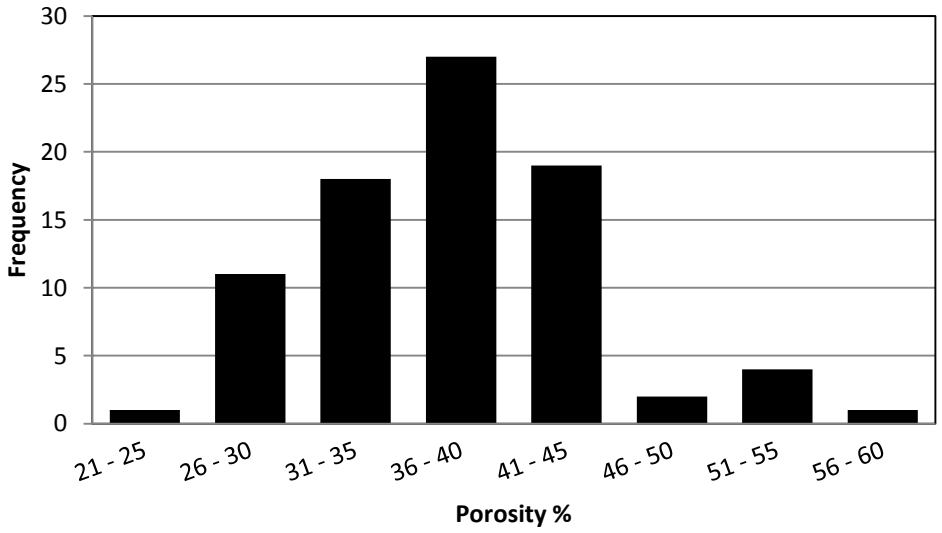

Figure 5.5 Histogram of porosity values from Helium Porosimeter

Table 5.1 Porosities Values from Three Methods

sample	porosity		
	AP-608	H. P	Thin Section
3	33.382	33.964	27
5	31.07	31.916	25
8	33.812	34.468	30
9	25.576	28.128	22
10	28.947	31.053	25
11	25.07	26.241	22
13	34.028	35.133	29
16	24.794	25.192	10
17	25.681	26.577	9
18	26.655	27.929	7
20	26.581	26.174	11
21	39.543	40.949	35
26	37.714	37.236	35
27	39.215	40.645	34
47	31.489	32.473	26
50	50.893	50.007	35
55	40.167	40.283	35
64	37.329	40.074	40
66	40.697	40.455	30
70	43.79	44.204	34
79	38.236	38.81	27
80	34.93	35.286	15

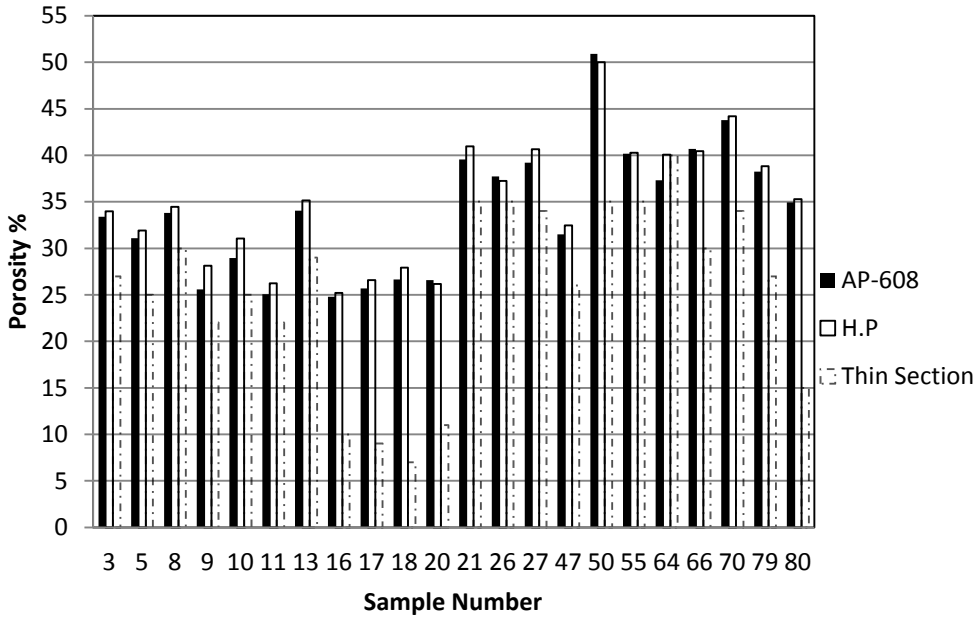

Figure 5.6 Distributions values for porosities obtained from three methods

reasons such as: (i) Errors during thin section preparation; (ii) Lack of representation of the 3 D rock structure in thin section sample; and (iii) Errors due to human judgment in defining pore boundaries. Table 5.2 and Figure 5.7 show summary for values of porosity obtained from each method for each texture.

5.3 Permeability

The Dam formation outcrop samples reflected wide range of permeability values ranging from 0.39 mD to 18748 mD, with an average of 3375 mD. The permeability depends on effective porosity (Tiab, 2004) [28]. The histogram in Figure 5.8 shows that the permeability for the most of the samples under this study ranges from 0.39 mD to 1 D.

This histogram for permeability also shows unexpected values due to reasons mentioned earlier. 11 D will be considered as the highest value for permeability in this study.

Table 5.2 Summary for Values of Porosity in Textures

Texture	Porosity			Method
	Max.	Min.	Avg.	
Mudstone	34.9	24.8	27.7	AP-608
	35.3	25.2	28.2	H. P
	15.0	7.0	10.4	Thin S.
Wackestone	38.2	31.1	34.7	AP-608
	38.8	31.9	34.7	H. P
	27.0	25.0	26.0	Thin S.
Packstone	33.8	31.5	35.6	AP-608
	44.2	32.5	33.6	H. P
	15.0	7.0	29.3	Thin S.
Grainstone	50.9	25.1	36.3	AP-608
	50.0	26.2	37.3	H. P
	40.0	22.0	31.1	Thin S.

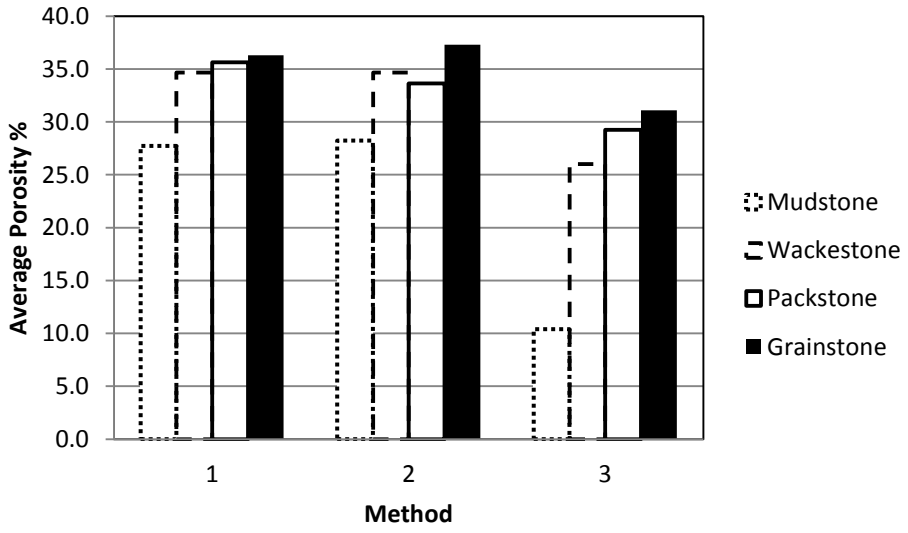

Figure 5.7 Average Porosity for Each Texture Measured With Three Methods

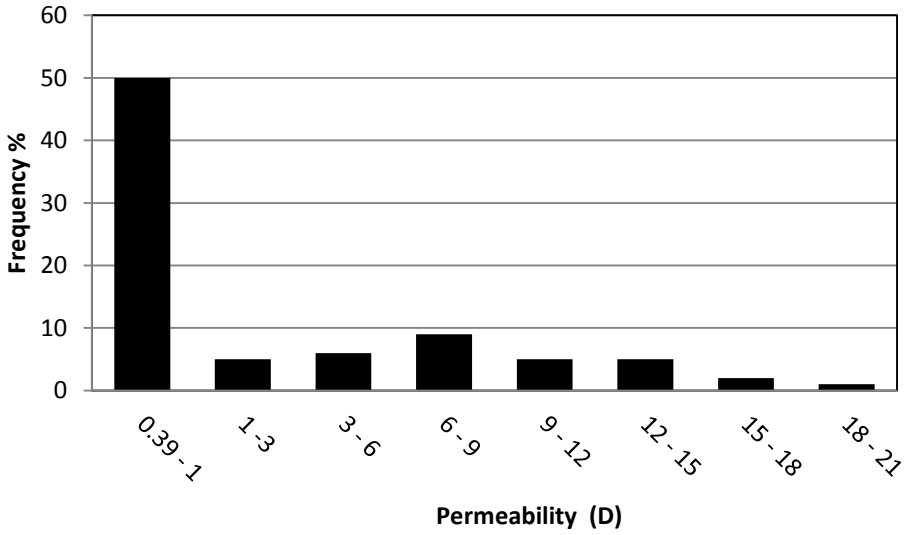

Figure 5.8 Histogram of Permeability Values

5.4 Porosity-Permeability Relationship

It is well known that there is no universal permeability-porosity relationship which is valid in all porous media and in particular for carbonate reservoirs. Porosity is invariant under a homothetic transformation (e.g., uniform, isotropic stretching) of the pore space whereas permeability is not. All pores are not effective in conducting fluid flow (Bernabe, 2003) [29]. Most carbonate reservoirs exhibit a poor relationship between porosity and permeability and Dam formation, consisting of carbonate rock is no exception (Figure 5.9). Figure 5.10 through 5.13 show porosity-permeability relationship for each texture. These figures indicate that Mudstone has less average porosity and permeability because its pore size ranges from 50 to 200 microns.

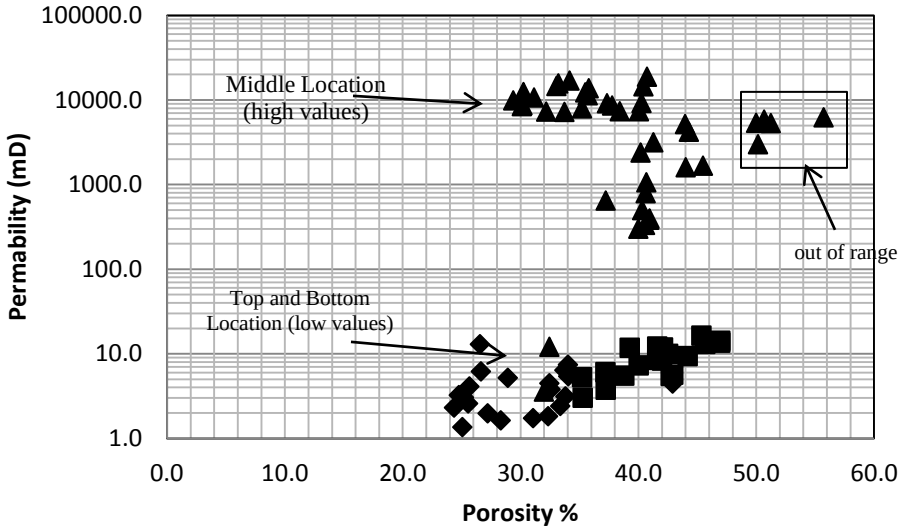

Figure 5.9 Porosity-Permeability Distribution of Samples

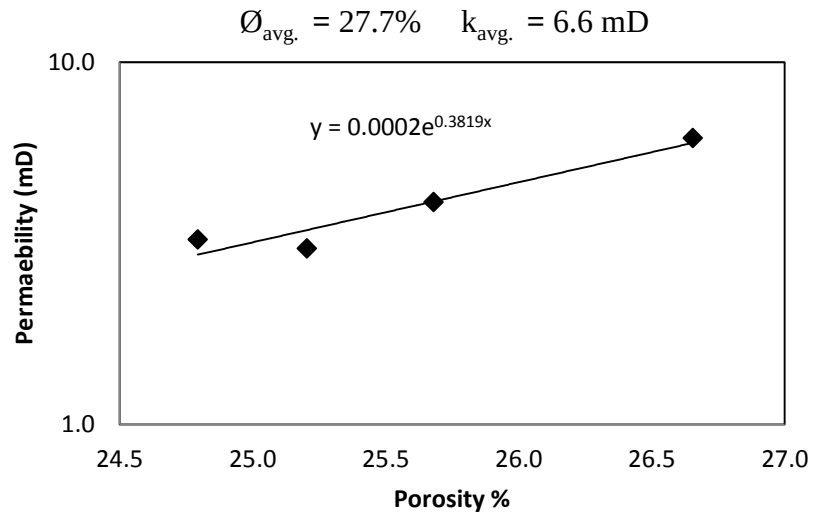

Figure 5.10 Semilog Plot of Permeability versus Porosity for Mudstone

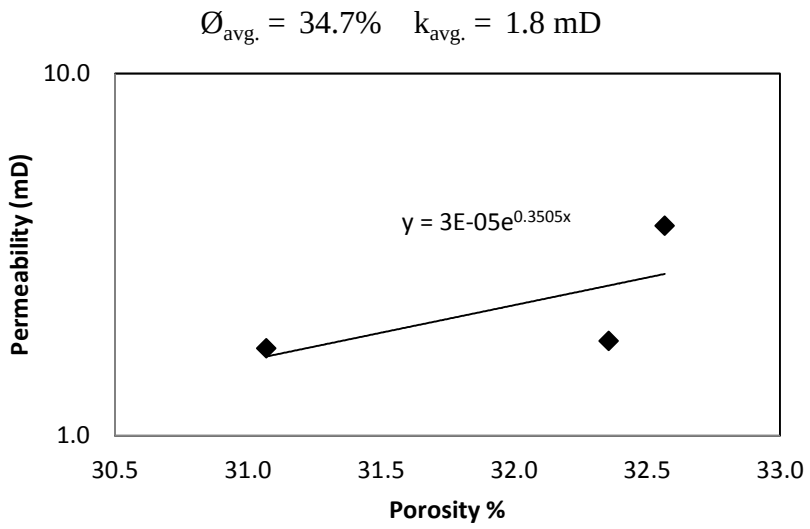

Figure 5.11 Semilog Plot of Permeability versus Porosity for Wackestone

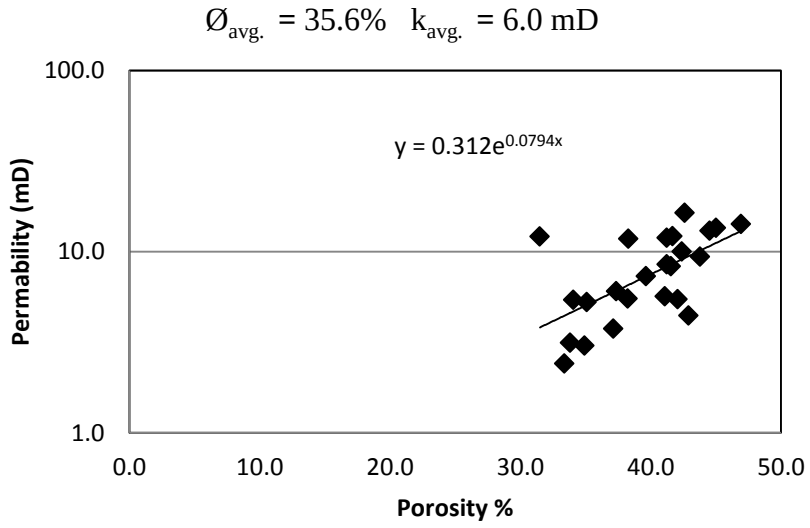

Figure 5.12 Semilog Plot of Permeability versus Porosity for Packstone

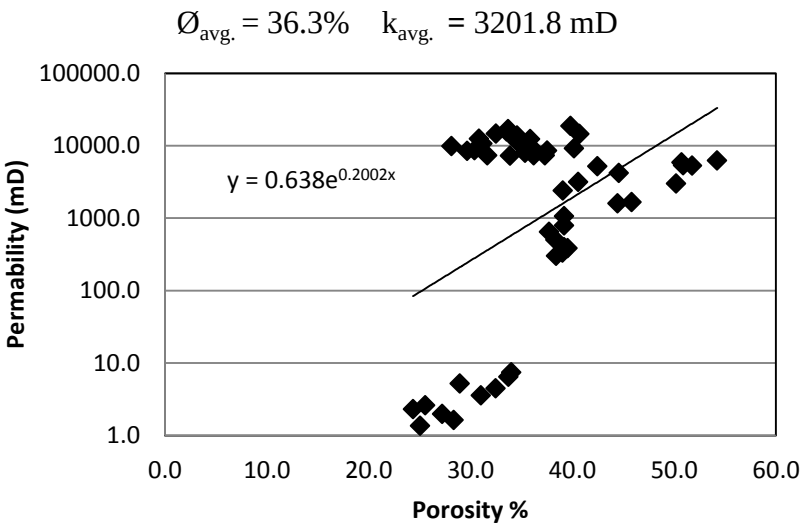

Figure 5.13 Semilog Plot of Permeability versus Porosity for Grainstone

CHAPTER 6

GEOMETRY MODEL FOR PORE NETWORK OF SEDIMENTARY ROCKS

6.1 Introduction

A model for estimation of the mean distance between pores in a permeable sedimentary rock from the measured hydraulic and electric transport properties was introduced for sandstones by Korvin, (1989) [30] and Perez-Rosales, (1982) [31]. It was modified by Korvin, (1999) [32] for carbonates. The model has four geometric parameters, viz., average coordination number of the pores, *Z*, average pore radius, *r*, average distance between nearest pores, *d*, average throat radius,δ, (Figure 6.1), These parameters can be directly determined from the measured porosity ϕ, hydraulic permeability *k*, and cementation exponent *m* of the rock via simple analytic expressions.

The purpose of this chapter is to predict the network structure and distribution in carbonate rock as proposed by Korvin (1999) using porosity, permeability and cementation exponent, m, of Archie's second law. The cementation exponent is assumed to be 1.9 for the carbonate samples used in this study.

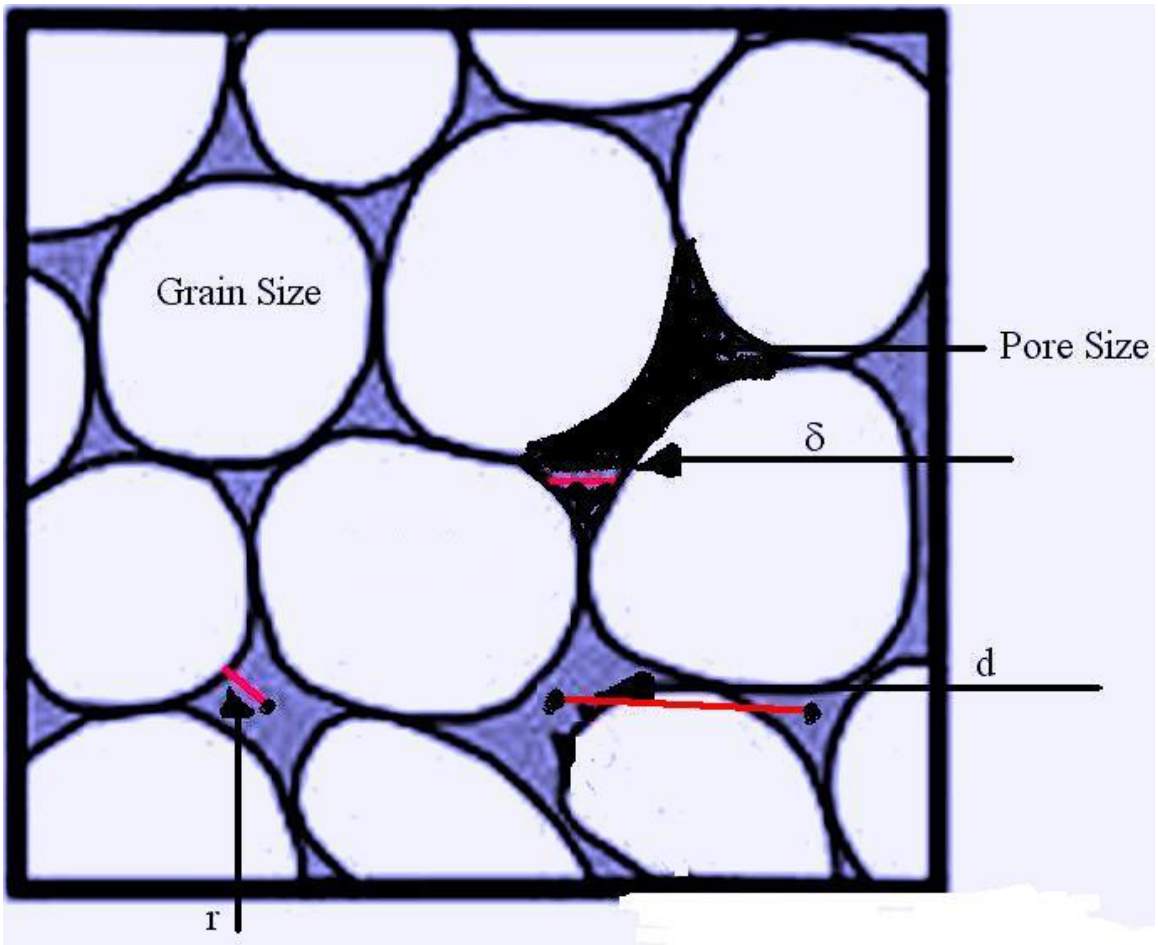

Figure 6.1 Average pore radius r, average distance between nearest pores d, and average throat radius δ.

6.2 The Equivalent Rock Model

As the detailed pore geometries of any two cuttings from the same rock body are obviously different, there exist infinitely many "equivalent pore structures" which would lead, through computer simulation or laboratory measurement, to the same set of macroproperties. Among all different microstructures which would result in the same petrophysical macroproperties, there must exist a simple effective pore-space model corresponding to that set of macroproperties. The search for this simple effective rock model had been the key idea of this chapter. The geometric rock model which was proposed by Korvin (1999) to fit macroscopic properties is a simplified version of Doyen's model (Doyen, 1987) [33].

The prediction of the interior structure of sedimentary rocks from measured bulk physical properties is a nonlinear inverse problem where the number of unknowns is much larger than the number of measurements. Such problems allow an infinite number of solutions, out of which solutions with small variance can be obtained by the Tikhonov Regularization method (Lamm, 1997) [34]. The solutions which are most likely to occur in nature are given by the Maximum Entropy Method (MEM) (Lifshitz, 1980) [35]. The first application of MEM to rock-physical inversion was due Doyen (1987) [36] who determined the statistical crack geometry in igneous rocks from measured hydraulic conductivity and/or D_c electric conductivity values at a series of confining pressures. His rock model consisted of a random distribution of spherical pores connected with nearby pores by tubes (throats).

Assume that the porosity, Φ, permeability, k, and cementation exponent, m, are measured for some sedimentary rock at a reference pressure P. Korvin et. al (1999) constructed an equivalent rock model which has the same measured Φ, k, m values. The model consists of a connected system of pores and throats distributed within a homogeneous rock matrix. Pores are spheres of radius r, and they are distributed in the rock matrix in such a way that the Euclidian distance between two nearest pores is d. A pore is connected on the average by Z neighboring pores with tortuous cylindrical pipes (throats) of radius δ. The parameters of the rock model, r, d, Z, δ can be uniquely determined as functions of Φ, k, and, m, using these equations:

$$r = 10^{-4}\sqrt[3]{\frac{3(\emptyset-\emptyset^m)}{4\pi}} * \frac{2\pi*\sqrt{2k}}{\emptyset^m*\sqrt{10\emptyset}}.\left[2*\left\{\frac{3(\emptyset-\emptyset^m)}{4\pi}\right\}^{\frac{2}{3}}+\sqrt{\frac{1}{\pi}*\frac{m}{m-1}*\emptyset}\right] \quad (6.1)$$

$$\delta = 10^{-4}\sqrt{\frac{m-1}{m}*\frac{\emptyset^{2m-1}}{\pi}} * \frac{2\pi*\sqrt{2k}}{\emptyset^m*\sqrt{10\emptyset}}.\left[2*\left\{\frac{3(\emptyset-\emptyset^m)}{4\pi}\right\}^{\frac{2}{3}}+\sqrt{\frac{1}{\pi}*\frac{m}{m-1}*\emptyset}\right] \quad (6.2)$$

$$d = 10^{-4} * \frac{2\pi*\sqrt{2k}}{\emptyset^m*\sqrt{10\emptyset}}.\left[2*\left\{\frac{3(\emptyset-\emptyset^m)}{4\pi}\right\}^{\frac{2}{3}}+\sqrt{\frac{1}{\pi}*\frac{m}{m-1}*\emptyset}\right] \quad (6.3)$$

Where $\emptyset$is the porosity in percentage, m, is the cementation exponent, and k is permeability in milliDarcy.

6.3 Computation of the geometrical parameters from the Rock Model

The porosity and permeability data obtained from Routine Core Analysis (RCA) were used in Equations 6.1 through 6.3 to obtain r, δ, and d. The results are shown in Table 6.1. The values correspond to an equivalent network structure of pores and pore throat sizes of the rock samples.

Note that if k is in mD in these equations, r, δ, d will be obtained in mm. For convenience, however, in Table 6.1 these values are shown in microns.

To compare the values of $r, \delta,$ and d as presented by model with the real network or pores, the micrographs of 30 outcrop carbonate samples were analyzed. Visual inspection shows that the computed values $r, \delta, d$are reasonably close, i.e., with an order of magnitude.

Also from the results it was observed that the distance between pores is directly proportional to permeability and inversely proportional to porosity.

Table 6.1 Geometric Parameters Obtained from Korvin's Model

Sample No.	Sample Name	Porosity	Permeability	m	r	δ	d
		Fraction	mD		μ	μ	μ
3	Dam-1-A-3	0.33	2.4	1.9	1.67	0.4	4.5
5	Dam-1-B-5	0.31	1.7	1.9	1.61	0.3	4.4
8	Dam-1-B-8	0.34	3.1	1.9	1.86	0.4	5.0
9	Dam-2-9	0.26	2.6	1.9	2.76	0.5	7.9
10	Dam-2-10	0.29	5.2	1.9	3.16	0.6	8.8
11	Dam-2-11	0.25	1.4	1.9	2.07	0.3	5.9
13	Dam-2-13	0.34	7.4	1.9	2.82	0.7	7.6
16	Dam-3-16	0.25	3.2	1.9	3.26	0.5	9.4
17	Dam-3-17	0.26	4.1	1.9	3.46	0.6	9.8
18	Dam-3-18	0.27	6.2	1.9	3.97	0.7	11.2
20	Dam-3-20	0.27	12.9	1.9	5.78	1.0	16.3
21	Dam-4-A-21	0.40	383.0	1.9	15.35	4.3	40.7
26	Dam-4-A-26	0.38	645.3	1.9	21.78	5.8	58.1
27	Dam-4-A-27	0.39	789.0	1.9	22.38	6.2	59.5
47	Dam-5-47	0.31	12.1	1.9	4.15	0.9	11.4
50	Dam-6-A-50	0.47	5351.4	1.9	40.88	14.5	107.3
55	Dam-6-B-55	0.40	9180.6	1.9	72.92	20.9	193.3
64	Dam-6-B-64	0.37	7336.9	1.9	74.86	19.6	200.1
66	Dam-7-66	0.41	14419.4	1.9	89.12	26.0	235.9
70	Dam-8-70	0.44	9.4	1.9	1.97	0.6	5.2
79	Dam-8-79	0.38	1.8	1.9	1.13	0.3	3.0
80	Dam-8-80	0.35	3.0	1.9	1.72	0.4	4.6

CHAPTER 7

ACOUSTIC DATA ANALYSIS

7.1 Introduction

The earliest systematic measurements of variation in the acoustic properties of rocks appeared in the 1950/1960s. Work to investigate on the velocity of acoustic waves in porous media as a function of porosity, saturation, and pressure have been done by many researchers, including Taylor (1950) [37] and Wyllie (1956) [6].

The objective of this chapter is to develop relationships between acoustic and reservoir rock properties. The theory of Gassmann can be used to calculate the effect of different saturation on P-wave and S-wave velocities in a porous rock.

7.2 Measurements of Velocities

The ultrasonic velocity measurement system used in this study is shown in Figures 7.1 through 7.4 which are capable of measuring high quality compressional and shears waves through rock specimens as a function confining and pore pressures. The system has the following basic components:

1. Ultrasonic transducer assembly.
2. The pore and confining pressure system connected to pressure vessel through appropriate plumbing.
3. Data acquisition system.

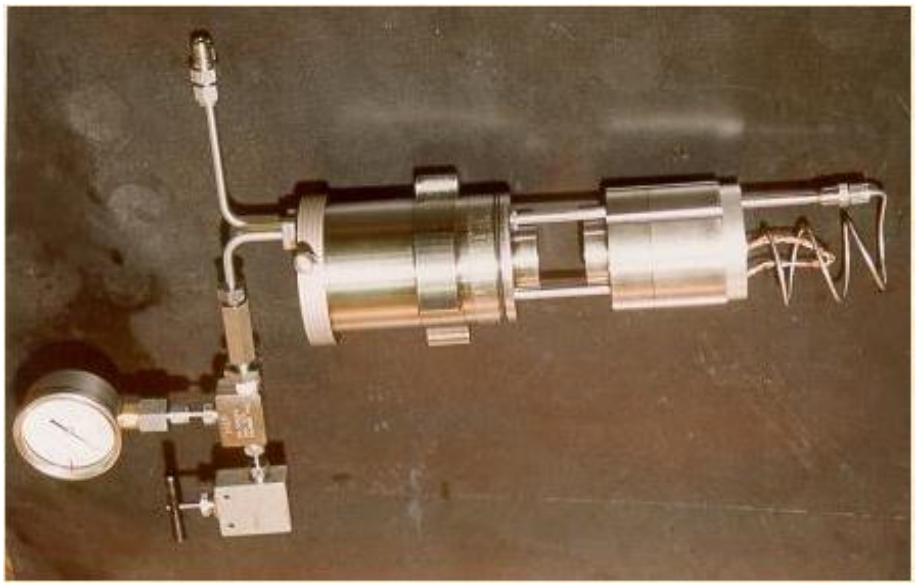

Figure 7.1 Ultrasonic Transducer Assembly without A Rock Sample

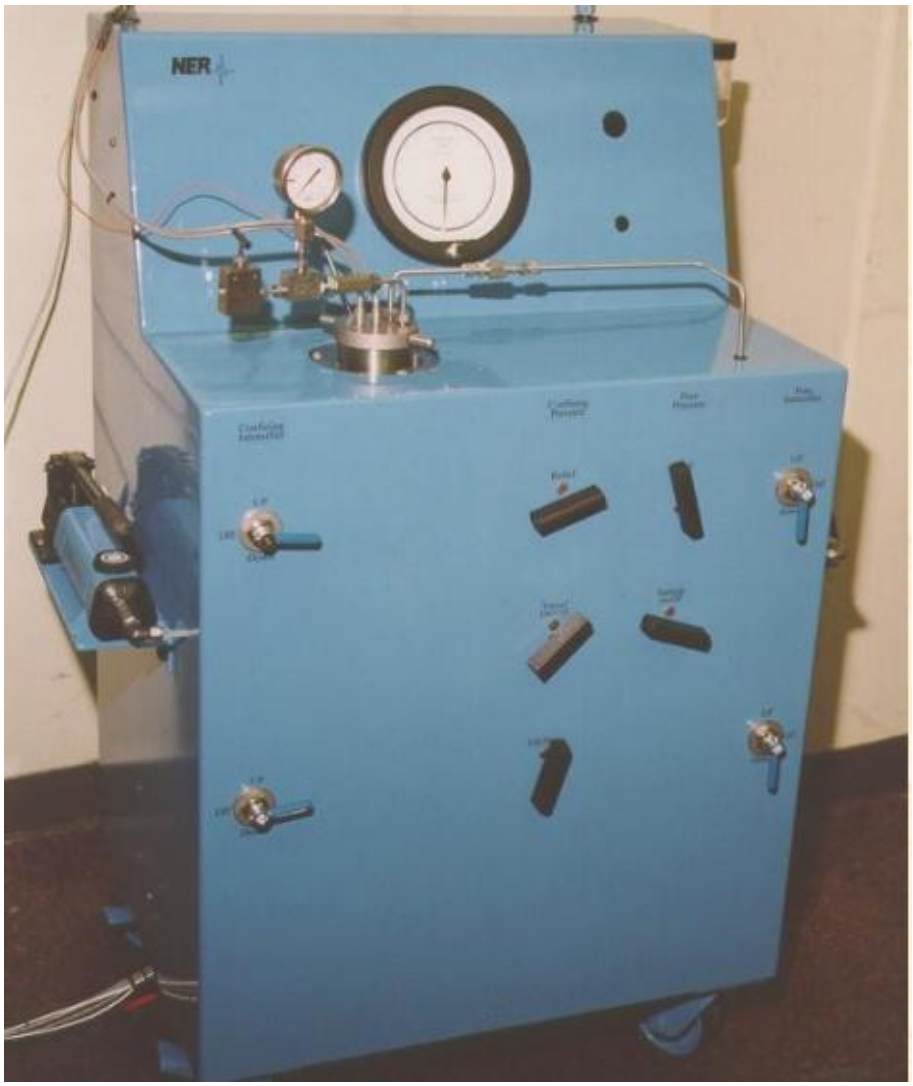

Figure 7.2 Safety Enclosure with Pressurization System

Figure 7.3 Data Acquisition System

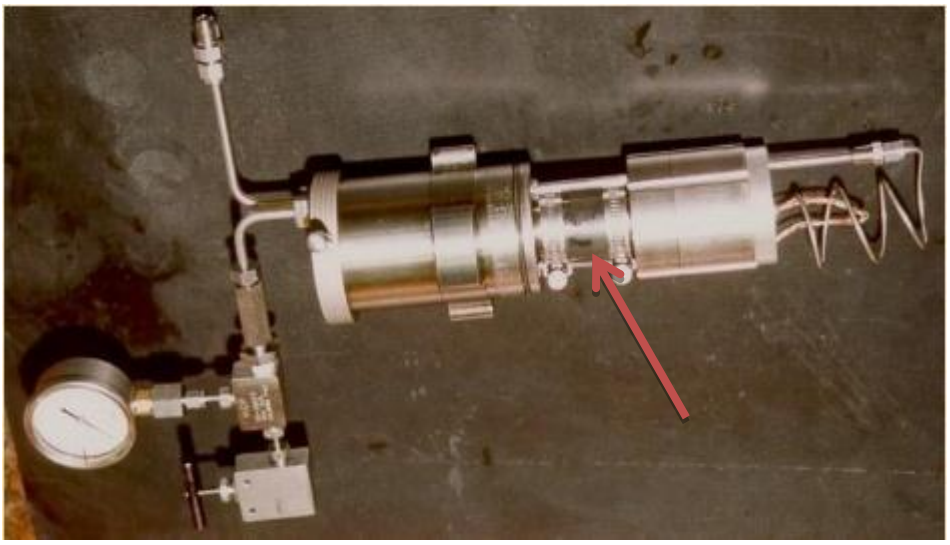

Figure 7.4 Ultrasonic Transducer Assembly with The Rock Sample

The first two components are stored in a safety enclosure. Samples can be tested under dry, saturated, and partially saturated conditions. The ultrasonic transducer assembly Figure 7.1 is composed of a set of transducers for transmitting and receiving a compressional (P) wave and two polarized shear waves (S1 and S2).The transducers are rated to a confining pressure of 100MPa.

The rock specimen is placed inside a pressure vessel and the vessel is filled by the confining fluid. The pore and confining pressures are generated with the help of intensifiers. Manually operated hand pumps are fixed on both sides of the safety enclosure (Figure 7.2). The data acquisition system (Figure 7.3) consists mainly of a microcomputer and an electronic console. The electronic console transmits and receives the compressional waves and two polarized shear waves. The wave data after necessary conversions is stored in the microcomputer.

7.2.1 Velocity Measurement under Dry Conditions

Twenty six rock samples each of 1.5 in diameter and 2.0 in length were chosen for measuring P-wave and S-wave velocities (Table 7.1). Under dry condition, the density of specimen was measured. The specimen was then slipped into a rubber sleeve. The rubber sleeve along with the specimen was placed between the platens of the transducer assembly such that the platens were in good contact with the specimen's faces. Both ends of the rubber sleeve were tightly clamped against the platens with the help of steel clamps (Figure 7.4). The transducer assembly was then placed inside the pressure vessel mounted in the safety enclosure of the ultrasonic velocity measurement assembly (Figure 7.2).

Table 7.1 A list of samples tested for velocities (Wet & Dry)

Sample	Avg Length	Avg Diameter	Volume	Dry Weight	Wet Weight	Dry Density	Saturated Density
#	(mm)	(mm)	(cc)	(gms)	(gms)	(gm/cc)	(gm/cc)
1	0	37.986	61.17	98.816	120.5	1.615	1.970
12	52.542	38.022	59.66	121.312	145	2.033	2.431
13	54.342	37.724	60.74	105.1	130	1.730	2.140
14	51.828	37.896	58.46	110.486	135	1.890	2.309
15	51.996	37.792	58.33	99.614	121	1.708	2.075
19	53.188	37.878	59.93	92.636	111	1.546	1.852
21	52.914	37.94	59.82	98.052	125.05	1.639	2.090
22	51.524	37.552	57.06	91.709	116.68	1.607	2.045
23	51.044	37.944	57.72	92.248	119.8	1.598	2.076
24	51.704	37.758	57.89	97.135	125.4	1.678	2.166
25	50.492	37.878	56.90	93.109	115.7	1.636	2.034
38	50.604	37.936	57.20	94.665	119.3	1.655	2.086
54	51.7944	37.744	57.95	75.462	Destroyed	1.302	Destroyed
55	52.358	37.98	59.32	88.495	Destroyed	1.492	Destroyed
58	52.522	37.606	58.34	88.417	109.6	1.516	1.879
61	52.328	37.964	59.23	100.568	120.8	1.698	2.039
62	51.708	37.942	58.46	91.744	116.3	1.569	1.989
66	50.972	37.846	57.34	84.646	104.68	1.476	1.826
71	52.828	37.804	59.30	100.882	128.7	1.701	2.170
72	52.424	37.894	59.12	88.767	118.7	1.501	2.008
73	51.552	37.82	57.91	95.281	122.5	1.645	2.115
74	49.256	38.058	56.03	89.313	115.2	1.594	2.056
75	49.324	37.826	55.43	87.159	112.3	1.572	2.026
76	52.064	37.798	58.42	92.912	123.6	1.590	2.116
77	52.498	37.956	59.40	93.953	124.7	1.582	2.099
81	56.116	37.946	63.46	102.055	132.57	1.608	2.089

Light oil was filled into the pressure vessel as a confining fluid by a hand pump attached to the side of the safety enclosure. The same pump was then used to pressurize the confining fluid. The transmitting and receiving transducers in the transducer assembly were then connected to the computer through a data acquisition system. With the help of software, P and S-waves were triggered and the transmitted waves were captured and stored in the computer at desired confining pressure levels. Readings were taken at confining pressures of 5MPa through 25MPa with increments of 5MPa.

7.2.2 Velocity Measurement under Saturated Conditions

In case of testing under saturated condition, brine was used as the saturating fluid with these properties: NaCl, 100,000 ppm, and 1.06 grams/cc density.

After applying the confining pressure, saturating fluid (brine) was made to flow through the sample to ensure that the sample was fully saturated. A valve and a pressure gauge attached to the downstream side were used to control the flow through the specimen and pressure at the downstream. Upstream pressure is sensed and recorded by an electronic transducer. Data was acquired at confining pressure levels from 10MPa through 25MPa with increments of 5MPa. Throughout the testing, pore pressure was maintained around 5MPa.

7.3 Data Analysis

7.3.1 Velocity with Pressure

Results for four samples tested under dry and saturated conditions are provided in Figures 7.5 through 7.8.The results for the remaining samples are given in Appendix E. From these Figures, following observations can be made:

1- Both velocities, P-wave and S-waves, increase with increase in confining pressure under dry condition.
2- The rate of increase in P-wave velocity with confining pressure under dry condition is more than that for the saturated case.
3- The P-wave velocity increase and the S-waves velocities decreased with confining pressure under saturated condition

# ID	C.P.	Dry			Saturated		
		Vp	Vs1	Vs2	Vp	Vs1	Vs2
1	5	2066	1504	1508			
	10	2077	1543	1550	2579	1247	1257
	15	2091	1569	1579	2597	1266	1276
	20	2174	1683	1678	2675	1384	1379
	25	2309	1707	1698	2709	1409	1392

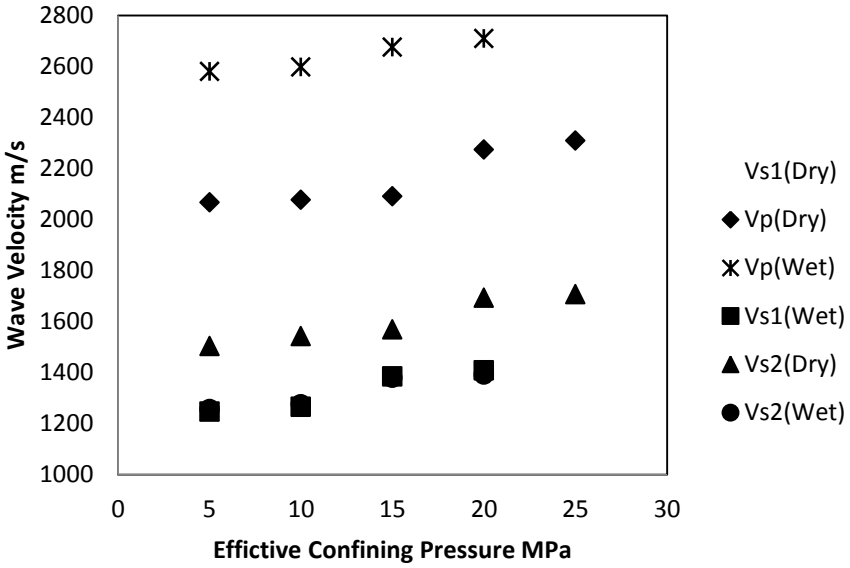

Figure 7.5 Velocities vs. Confining Pressure for Wet and Dry Sample No. 1

# ID	P	Dry			Saturated		
	MPa	Vp	Vs1	Vs2	Vp	Vs1	Vs2
12	5	3903	2153	2211			
	10	3977	2239	2239	4065	2063	2016
	15	4008	2240	2225	4151	2127	2075
	20	4054	2267	2251	4175	2167	2111
	25	4070	2276	2266	4178	2199	2140

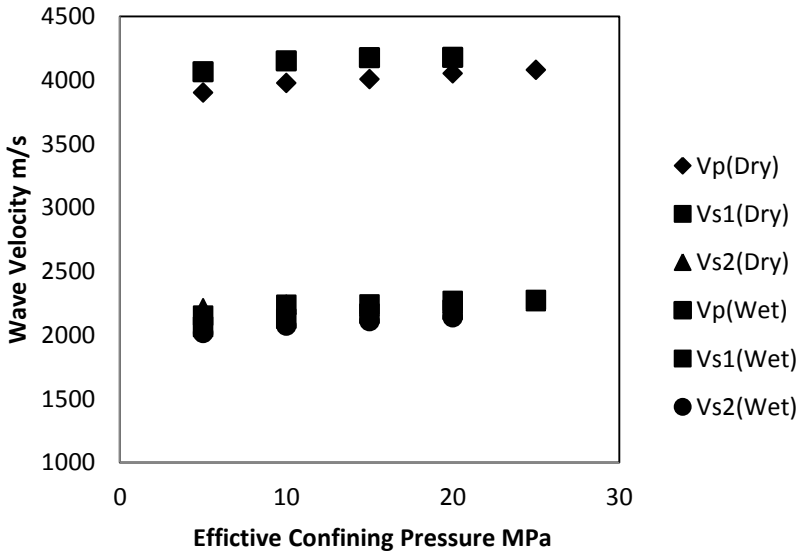

Figure 7.6 Velocities vs. Confining Pressure for Wet and Dry Sample No. 12

# ID	P	Dry			Saturated		
	MPa	Vp	Vs1	Vs2	Vp	Vs1	Vs2
13	5	2286	1704	1715			
	10	2643	1875	1887	3355	1519	1521
	15	2874	1899	1899	3418	1647	1652
	20	2920	1946	1937	3422	1683	1683
	25	3134	1975	1692	3444	1698	1703

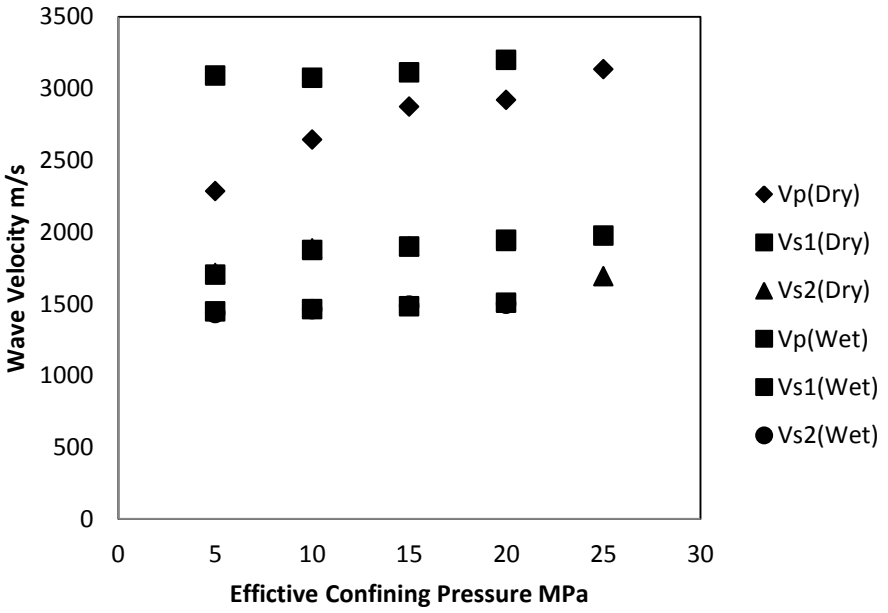

Figure 7.7 Velocities vs. Confining Pressure for Wet and Dry Sample No. 13

# ID	P	Dry			Saturated		
	MPa	Vp	Vs1	Vs2	Vp	Vs1	Vs2
14	5	2755	1585	1514			
	10	3050	1625	1629	3355	1519	1521
	15	3053	1727	1707	3418	1647	1652
	20	3099	1759	1757	3422	1683	1683
	25	3159	1790	1682	3444	1698	1703

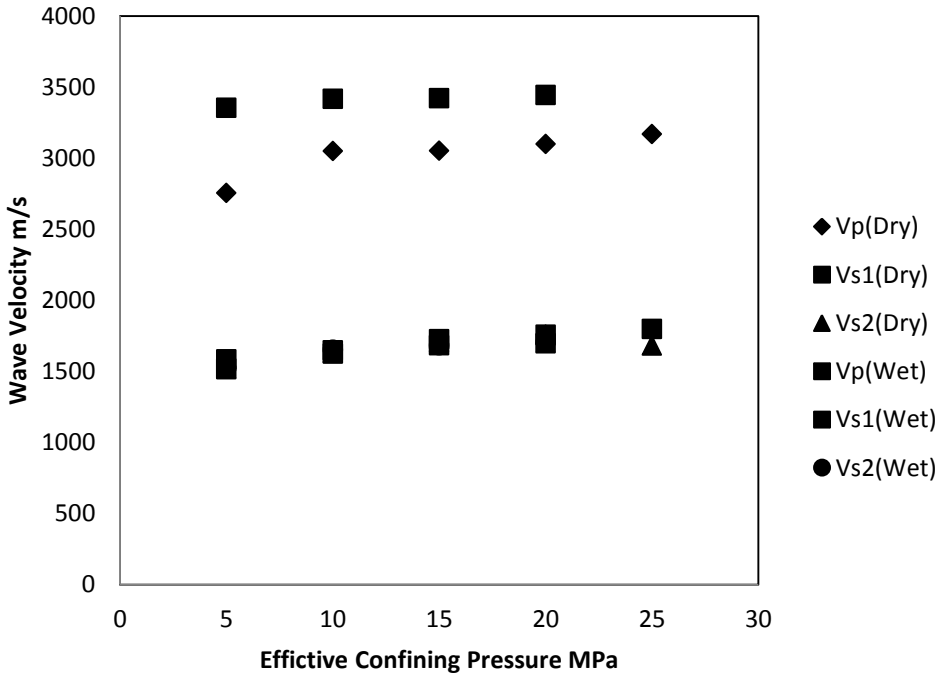

Figure 7.8 Velocities vs. Confining Pressure for Wet and Dry Sample No. 14

7.3.1.1 Gassmann's Equations

The increasing in wave velocities with confining pressure is confirmed by Gassmann (1951) [5] for sandstone. Gassmann's theory will be tested for carbonate in this study by using Dam formation data in his equation and see if it could fit or not. According to this theory the velocity can be expressed as:

$$V_P = A_P * P^{B_P} \quad (7.1)$$

$$V_S = A_S * P^{B_S} \quad (7.2)$$

Where:

V_P = P-wave velocity, V_S = S-wave velocity, A_P, B_P are coefficients for P-wave velocity, and A_S,B_S are coefficients for S-wave velocity.

Tables 7.2,7.4 and Tables 7.3, 7.5 display the values of the coefficients A_p ,B_p, A_s, B_s, values of velocities P-wave and S-wave using this method for the dry and saturated samples, respectively. According to Gassmann's theory, the value of B_p and B_s for dry sandstones lies between 0.10 and 0.26. For carbonates, the values of B_p and B_s are very small. This is because the velocities vs. confining pressure curves are much flatter than for sandstones.

Table 7.2 Regression Coefficients for Gassmann's Equation - Dry Samples

# ID	P-wave		S-wave	
	A_p	B_p	A_s	B_s
1	1803.1	0.0705	1297.1	0.082
12	3733.7	0.0272	2052.2	0.0332
13	1698.4	0.1885	1488	0.0913
14	2460.4	0.0801	1366.9	0.0852
15	1644.4	0.1797	1445.9	0.089
19	2536.5	0.0107	1415	0.0159
21	2610.6	0.0119	1437.9	0.0275
22	2076.4	0.0647	1062.7	0.1652
23	2260.1	0.0268	1519.7	0.0152
24	2424.7	0.0181	1453	0.0213
25	2598.7	0.0109	1334.5	0.084
38	2677.7	0.0252	1654.8	0.0203
54	1666.1	0.0526	1050.6	0.0888
55	2653.3	0.0193	1594.2	0.0164
58	3024.1	0.0343	1838	0.0302
61	3147.1	0.0281	1984.6	0.0058
62	2894.5	0.0149	1848.7	0.0166
66	1912	0.014	1404	0.0303
71	2384.5	0.0395	1496.9	0.031
72	2503.2	0.0096	1271.6	0.0217
73	2424.3	0.0289	1748.5	0.0228
74	2582.7	0.0058	1528.5	0.0289
75	2582.9	0.0049	1491.8	0.0143
76	2449	0.0146	1488.7	0.0153
77	2499.4	0.006	1513.5	0.0107
81	2685.9	0.0097	1719.7	0.0131

Table 7.3 Values of P-wave and S-wave for Gassmann's Equation - Dry Samples

# ID	For 5MPa		For 10MPa		For 15MPa		For 20MPa		For 25MPa	
	V_p	V_s	V_p	V_s	V_p	V_s	V_p	V_s	V_p	V_s
1	2019.75	1480.09	2120.9	1566.66	2182.4	1619.62	2227.11	1658.28	2262.43	1688.9
12	3900.78	2164.84	3975.02	2215.23	4019.1	2245.26	4050.68	2266.8	4075.34	2283.66
13	2300.36	1723.53	2621.44	1836.13	2829.65	1905.37	2987.34	1956.08	3115.67	1996.34
14	2798.94	1567.79	2958.73	1663.17	3056.4	1721.63	3127.65	1764.35	3184.06	1798.21
15	2195.9	1668.58	2487.18	1774.75	2675.17	1839.97	2817.1	1887.69	2932.36	1925.55
19	2580.56	1451.68	2599.77	1467.76	2611.07	1477.26	2619.12	1484.03	2625.38	1489.31
21	2661.08	1502.97	2683.12	1531.89	2696.1	1549.07	2705.34	1561.37	2712.54	1570.98
22	2304.28	1386.37	2409.97	1554.57	2474.03	1662.27	2520.51	1743.17	2557.16	1808.63
23	2359.72	1557.34	2403.96	1573.83	2430.23	1583.56	2449.04	1590.5	2463.73	1595.9
24	2496.37	1503.67	2527.89	1526.04	2546.51	1539.28	2559.8	1548.74	2570.16	1556.12
25	2644.69	1527.68	2664.75	1619.27	2676.55	1675.37	2684.96	1716.35	2691.5	1748.82
38	2788.53	1709.76	2837.67	1733.99	2866.81	1748.32	2887.67	1758.56	2903.96	1766.54
54	1813.29	1212.01	1880.62	1288.95	1921.16	1336.21	1950.45	1370.78	1973.48	1398.22
55	2737.01	1636.84	2773.87	1655.55	2795.66	1666.6	2811.23	1674.48	2823.36	1680.62
58	3195.74	1929.54	3272.62	1970.36	3318.46	1994.64	3351.36	2012.04	3377.11	2025.64
61	3292.7	2003.21	3357.46	2011.28	3395.93	2016.02	3423.49	2019.38	3445.03	2022
62	2964.75	1898.76	2995.53	1920.73	3013.68	1933.7	3026.63	1942.96	3036.71	1950.17
66	1955.57	1474.16	1974.64	1505.45	1985.88	1524.06	1993.9	1537.41	2000.13	1547.84
71	2541.01	1573.48	2611.54	1607.65	2653.71	1627.99	2684.03	1642.57	2707.8	1653.97
72	2542.18	1316.79	2559.15	1336.75	2569.13	1348.56	2576.23	1357.01	2581.76	1363.6
73	2539.72	1813.85	2591.11	1842.75	2621.65	1859.86	2643.54	1872.1	2660.64	1881.65
74	2606.92	1601.27	2617.42	1633.67	2623.59	1652.93	2627.97	1666.73	2631.37	1677.51
75	2603.35	1526.53	2612.21	1541.74	2617.4	1550.7	2621.09	1557.1	2623.96	1562.07
76	2507.23	1525.81	2532.73	1542.08	2547.77	1551.68	2558.49	1558.52	2566.84	1563.85
77	2523.65	1539.79	2534.17	1551.25	2540.34	1558	2544.73	1562.8	2548.14	1566.54
81	2728.16	1756.34	2746.56	1772.36	2757.39	1781.8	2765.09	1788.53	2771.09	1793.77

Table 7.4 Regression Coefficients for Gassmann's Equation - Saturated Samples

# ID	P-wave		S-wave	
	A_p	B_p	A_s	B_s
1	2418.1	0.0364	1055.5	0.0945
12	3942.8	0.0205	1915.5	0.0458
13	2961.5	0.0215	1379.1	0.0279
14	3264.4	0.0181	1342.6	0.082
15	2711.3	0.0691	1178.7	0.0645
19	2758.3	0.0123	1297.1	0.0061
21	2695.2	0.0011	1505.8	0.0099
22	2225.9	0.0463	1340.5	0.0541
23	2382.9	0.0098	1564.9	0.005
24	2519.07	0.0669	1109	0.059
25	2882.9	0.0153	1094.4	0.0603
38	3522.1	0.0204	1254.9	0.0798
58	3453	0.0227	1720	0.0179
61	3612.6	0.0109	1481.5	0.0197
62	3194.9	0.0153	1782.2	0.0119
66	2053.8	0.028	1342.4	0.0257
71	2791.9	0.0235	1440.7	0.0257
72	2570.2	0.0324	1209.1	0.0143
73	2902.3	0.0178	1612.8	0.0132
74	2865.2	0.0078	1361.4	0.0272
75	2533.5	0.0166	1320.3	0.0102
76	2658	0.0141	1304.6	0.0152
77	2604.5	0.0062	1428.6	0.0089
81	2925.1	0.005	1548.9	0.0094

Table 7.5 Values of P-wave and S-wave for Gassmann's Equation - Saturated Samples

# ID	For 5MPa		For 10MPa		For 15MPa		For 20MPa	
	V_p	V_s	V_p	V_s	V_p	V_s	V_p	V_s
1	2563.993	1228.884	2629.507	1312.074	2668.603	1363.323	2696.694	1400.895
12	4075.056	2062.03	4133.374	2128.542	4167.874	2168.439	4192.527	2197.199
13	3065.77	1442.438	3111.8	1470.604	3139.046	1487.335	3158.522	1499.321
14	3360.893	1532.012	3403.325	1621.611	3428.393	1676.433	3446.292	1716.45
15	3030.236	1307.636	3178.905	1367.424	3269.23	1403.658	3334.869	1429.946
19	2813.448	1309.897	2837.537	1315.447	2851.724	1318.705	2861.832	1321.021
21	2699.976	1529.985	2702.035	1540.52	2703.241	1546.716	2704.096	1551.127
22	2398.104	1462.45	2476.314	1518.332	2523.241	1552.006	2557.074	1576.35
23	2420.782	1577.544	2437.282	1583.021	2446.986	1586.233	2453.895	1588.517
24	2805.439	1219.469	2938.595	1270.374	3019.397	1301.131	3078.071	1323.404
25	2954.771	1205.935	2986.273	1257.408	3004.857	1288.53	3018.112	1311.077
38	3639.659	1426.878	3691.49	1508.027	3722.151	1557.619	3744.059	1593.791
58	3581.486	1770.272	3638.284	1792.373	3671.925	1805.429	3695.983	1814.75
61	3676.535	1529.225	3704.417	1550.25	3720.825	1562.682	3732.511	1571.564
62	3274.549	1816.662	3309.461	1831.709	3330.055	1840.568	3344.745	1846.88
66	2148.47	1399.089	2190.575	1424.236	2215.586	1439.155	2233.505	1449.834
71	2899.517	1501.541	2947.134	1528.529	2975.35	1544.54	2995.533	1556.002
72	2707.781	1237.25	2769.28	1249.575	2805.901	1256.841	2832.176	1262.022
73	2986.648	1647.43	3023.725	1662.572	3045.627	1671.494	3061.263	1677.854
74	2901.395	1422.321	2917.124	1449.392	2926.365	1465.465	2932.939	1476.977
75	2602.099	1342.153	2632.212	1351.676	2649.989	1357.278	2662.674	1361.266
76	2719.008	1336.909	2745.712	1351.069	2761.454	1359.421	2772.678	1365.378
77	2630.619	1449.211	2641.949	1458.178	2648.598	1463.45	2653.327	1467.202
81	2948.734	1572.511	2958.971	1582.79	2964.976	1588.834	2969.244	1593.137

7.3.1.2 Khaksar's Equations

An empirical equation was proposed Khaksar and his co-workers which fits the data better than Gassmann's equation. According to them, the P and S-wave velocities should be described in terms of an exponential function rather than a power-function as in Equations 7.3 and 7.4. The equations proposed by Khaksar are:

$$V_P = A_P - B_P * e^{-PC_P} \quad (7.3)$$

$$V_s = A_s - B_s * e^{-PC_s} \quad (7.4)$$

Where:

A_P,B_P,C_P are coefficients for P-wave velocity, and A_s,B_s, C_s are coefficients for S-wave velocity.

Tables 7.6 and 7.7 show these coefficients for dry samples along with the values of P-wave velocity using this empirical equation. Tables 7.8 and 7.9 show the same for S-wave velocity.

Table 7.6 Regression Coefficients for Khaksar's Equation - Dry Samples

Velocity # ID	P-wave			S-wave		
	A_p	B_p	C_p	A_s	B_s	C_s
12	4159.42	338.729	0.057529	2271.39	322.122	0.203011
13	3290.71	1493.11	0.080971	1982.99	605.56	0.157436
14	3128.39	1296.7	0.251034	2021.96	537.608	0.037078
15	3110.53	1352.32	0.077607	2478.72	883.57	0.020218
21	2724.11	194.002	0.185924	1560.78	91.0085	0.105219
22	2479.69	437.386	0.193372	1911.93	2726.73	0.362141
23	2451.7	314.786	0.225232	1600.59	71.8059	0.099689
24	2649.18	177.014	0.034424	1618	137.2	0.067294
25	2693.48	92.0255	0.120926	1778.42	413.615	0.096993
38	2931.73	582.061	0.308089	1760	67.5	0.081093
55	2815.33	83.1515	0.048232	1698	81	0.081093
58	3390.5	180.719	0.102138	2049.28	177.787	0.079756
61	3445.19	307.915	0.134146	2323.04	320.086	0.001911
62	3044.13	101.392	0.085489	2000.46	119.404	0.036843
66	2007.29	208.286	0.300815	1651.32	199.369	0.028139
71	2791.19	354.297	0.081769	1698.24	160.2	0.053721
72	2648.7	117.576	0.024276	1371.35	86.3577	0.090827
73	2702.96	227.048	0.068272	1879.03	150.645	0.154882
74	2642.4	72.9	0.162186	1674.67	95.2381	0.071335
75	2842.55	237.577	0.001713	1565.8	67.1461	0.104138
77	2582.78	66.4033	0.028177	1588.22	58.3406	0.042099
81	2781.71	79.1442	0.080375	1798.48	70.2336	0.099963

Table 7.7 Values of P-wave and S-wave for Khaksar's Equation - Dry Samples

E.C.P	For 5MPa		For 10MPa		For 15MPa		For 20MPa		For 25MPa	
# ID	V_p	V_s	V_p	V_s	V_p	V_s	V_p	V_s	V_p	V_s
12	3905.3	2154.65	3968.8	2229.08	4016.50	2256.	4052.22	2265.83	4079.0	2269.37
13	2294.6	1707.38	2626.29	1857.55	2847.49	1925.	2995.05	1957.00	3093.4	1971.16
14	2758.7	1575.32	3023.04	1650.90	3098.36	1713.	3119.83	1765.85	3125.5	1809.19
15	2193.	1680.10	2488.17	1756.88	2688.33	1826.	2824.11	1889.0	2916.2	1945.71
21	2647.5	1507.00	2693.88	1529.00	2712.18	1542	2719.40	1549.68	2722.2	1554.223
22	2313.36	1466.00	2416.44	1839.00	2455.63	1900	2470.54	1909.98	2476.2	1911.61
23	2349.62	1556.97	2418.59	1574.09	2440.96	1584.	2448.21	1590.81	2450.5	1594.65
24	2500.15	1520	2523.72	1548	2543.55	1568	2560.25	1582.28	2574.3	1592.49
25	2643.20	1523.7	2666.01	1621.61	2678.47	1681.9	2685.28	1718.97	2689.0	1741.81
38	2807	1715	2905.00	1730	2926.00	1740	2930.50	1746.66	2931.4	1751.11
55	2749.99	1644	2763.99	1662	2774.99	1674	2783.64	1682	2790.4	1687.33
58	3282.05	1929.96	3325.42	1969.2	3351.44	1995.	3367.06	2013.21	3376.4	2025.07
61	3287.7	2005.997	3364.68	2009.01	3404.02	2012	3424.14	2014.95	3434.4	2017.88
62	2978.0	1901.14	3001.00	1917.85	3016.00	1931.	3025.78	1943.31	3032.1	1952.92
66	1961.0	1478.1	1997.	1500.85	2005.0	1520.6	2006.7	1537.7	2007.1	1552.66
71	2555.78	1575.77	2634.7	1604.62	2687.272	1626.7	2722.145	1643.532	2745.3	1656.41
72	2544.56	1316.51	2556.46	1336.52	2567.00	1349.	2576.34	1357.30	2584.6	1362.43
73	2541.57	1809.58	2588.24	1847.01	2621.42	1864.	2645.00	1872.22	2661.7	1875.89
74	2610	1608.00	2628	1628.00	2636	1642	2639.55	1651.80	2641.1	1658.66
75	2606.99	1525.90	2609.00	1542.1	2610.99	1551.	2612.97	1557.43	2614.9	1560.83
77	2525.10	1540.95	2532.68	1549.92	2539.26	1557.	2544.98	1563.08	2549.9	1567.85
81	2728.75	1755.87	2746.28	1772.63	2758.00	1782.	2765.85	1788.96	2771.0	1792.71

Table 7.8 Regression Coefficients for Khaksar's Equation - Saturated Samples

Velocity	P-Wave			S-Wave		
ID	A_p	B_p	C_p	A_p	B_p	C_p
12	-150.1	-4143	-0.00264	-1802	-3799	-0.002807
13	3081	-0.3264	-0.2953	1387	-47.81	-0.046
14	-3504	-6839	-0.00085	-7121	-8526	-0.001998
15	3019	-25.79	-0.1358	1028	254.5	-0.02456
19	2501	-299.6	-0.0099	1317	4.406	0.1507
22	2419	-1.937	-0.23	1442	-19.8	-0.1041
23	2416	-5.645	-0.1025	579.5	-994.3	-0.0007731
24	-6531	-9151	-0.00272	-3544	-4732	-0.001509
25	2959	-2.515	-0.1697	-3413	-4588	-0.001563
38	3440	-180.6	-0.02822	-3240	-4561	-0.003218
58	-2718	-6211	-0.00181	-3239	-4993	-0.0006509
61	3686	-0.9508	-0.2213	-795.9	-2312	-0.001253
62	3269	-8.042	-0.1213	1800	-14.31	-0.06413
66	2158	-1.092	-0.2294	-1829	-3213	-0.001083
71	-691.9	-3559	-0.00191	-4832	-6306	-0.0007058
72	-3684	-6317	-0.00173	344.9	-885.1	-0.001899
73	-547.6	-3498	-0.00171	-1660	-3297	-0.0006525
74	2820	-74.63	-0.02239	1417	-6.962	-0.1166
75	2555	-40	-0.054	-1521	-2856	-0.0004981
76	2333	-372.4	-0.00893	1322	-12.38	-0.06754
77	2626	-4.757	-0.09548	827.9	-616.5	-0.001924
81	2946	-2.885	-0.1134	-1623	-3188	-0.0004614

Table 7.9 Values of P-wave and S-wave for Khaksar's Equation - Saturated Samples

E.C.P	For 5MPa		For 10MPa		For 15MPa		For 20MPa	
ID	V_p	V_s	V_p	V_s	V_p	V_s	V_p	V_s
12	4047.887	2050.695	4103.604	2105.149	4160.061	2160.372	4217.266	2216.376
13	3082.429	1447.174	3087.255	1462.735	3108.382	1482.32	3200.865	1506.969
14	3364.296	1490.602	3393.717	1577.063	3423.265	1664.392	3452.939	1752.598
15	3069.855	740.2475	3119.282	702.6502	3216.747	660.1406	3408.938	612.0767
19	2815.805	1314.926	2831.782	1316.024	2848.569	1316.54	2866.208	1316.784
22	2425.117	1475.321	2438.32	1498.075	2480.016	1536.366	2611.701	1600.806
23	2425.424	1577.651	2431.733	1581.517	2442.266	1585.398	2459.85	1589.293
24	2745.304	1223.838	2872.323	1259.947	3001.082	1296.33	3131.604	1332.989
25	2964.875	1210.996	2972.726	1247.274	2991.065	1283.837	3033.909	1320.686
38	3647.968	1394.98	3679.484	1470.16	3715.775	1546.56	3757.566	1624.198
58	3549.465	1770.276	3606.443	1786.605	3663.939	1802.988	3721.957	1819.424
61	3688.875	1530.63	3694.693	1545.252	3712.286	1559.965	3765.483	1574.771
62	3283.749	1819.72	3296.05	1827.174	3318.609	1837.446	3359.983	1851.602
66	2161.438	1401.446	2168.827	1418.986	2192.09	1436.621	2265.341	1454.353
71	2901.323	1496.293	2935.875	1518.665	2970.76	1541.116	3005.98	1563.647
72	2688.006	1238.444	2743.492	1246.969	2799.461	1255.575	2855.917	1264.263
73	2980.507	1647.774	3010.872	1658.583	3041.5	1669.428	3072.39	1680.308
74	2903.47	1429.472	2913.358	1439.342	2924.417	1457.024	2936.786	1488.698
75	2607.399	1342.122	2623.64	1349.261	2644.916	1356.419	2672.787	1363.594
76	2722.403	1339.353	2740.181	1346.324	2758.772	1356.096	2778.211	1369.793
77	2633.668	1450.359	2638.359	1456.376	2645.922	1462.451	2658.112	1468.585
81	2951.086	1572.363	2954.967	1579.743	2961.808	1587.141	2973.869	1594.555

7.3.1.3 Proposed Equations for P- and S-wave Velocities

Statistical analysis was performed on the measured data to develop a new velocity–pressure relationship. Gassmann and Khaksar's equation and several authors demonstrated that the velocity–pressure relationship could be expressed by an empirical equation consisting of a constant, an exponential part and a linear part (Eberhart-Phillips D. (1989) [38]; Freund (1992) [39]; Jones (1995) [40]). In this study polynomial equations were used because they show satisfactory results. The equations are:

$$V_P = A_P * P^2 + B_P * P + C_P \qquad (7.5)$$

$$V_S = A_S * P^2 + B_S * P + C_S \qquad (7.6)$$

Where A_P, B_P, C_P, A_S, B_S, C_S are coefficients for P-wave velocity and S-wave velocity, respectively.

Tables 7.10 and7.11 show these coefficients for dry and saturated rock samples, respectively.

Equations 7.5 and 7.6 were used initially to find the best fit for the 26 samples studied here. It was found that the variations of both V_p and V_s with confining pressure are describe well by these equations. It seems that, although Equations 7.5 and 7.6 give a good fit for the interpolation between the measured data, it is not applicable for extrapolating beyond the experimental limit (P >25MPa), because as the pressure increases the error in predicted velocity also increase.

Table 7.10 Regression Coefficients for the Proposed Equations- Dry Samples

# ID	P-wave			S-wave		
	A_p	B_p	C_p	A_s	B_s	C_s
1	0.62	-4.94	2067	0.1371	0.70057	1460.4
12	-0.231	15.56	3834.6	-0.3657	16.451	2088
13	-1.3457	79.831	1944	-0.8029	36.746	1553.4
14	-1.1629	52.426	2558.6	-0.2571	19.354	1483.4
15	-1.2971	74.594	1859.8	-0.1743	18.489	1590.2
19	0.0343	1.2914	2578.8	-0.0429	3.1457	1438.6
21	-0.5286	17.797	2570	3E-14	3.48	1491
22	0.1857	7.5286	2289.6	1.2229	12.086	1480.4
23	-0.3343	14.809	2291.4	-0.0657	3.8314	1540.8
24	-0.0543	5.3286	2475.4	0.1086	-0.4171	1511
25	-0.1229	5.9057	2617.6	-0.5771	27.914	1397.6
38	0.2657	-0.1631	2808.4	0.0543	1.3514	1708.2
54	0.8943	-17.329	1922.8	-0.44	22.16	1110
55	0.2	-1.28	2752.8	0.062	0.4743	1638.6
58	-0.4857	23.131	3089.4	-0.1886	10.337	1883.4
61	-0.18	12.74	3241.4	-0.0429	-0.2657	2006.6
62	0.229	-2.6857	2986.6	-0.0486	4.0371	1882.2
66	0.0257	1.5686	1951.4	-0.0514	5.2629	1453.2
71	-0.0029	8.6257	2511.2	-0.1143	7.4286	1541.4
72	-0.0229	2.6857	2531.8	-0.0886	4.9171	1295
73	-0.2029	12.026	2487	-0.2314	10.083	1766.2
74	0.0257	0.5286	2606.9	0.0486	2.5229	1595.2
75	0.0657	-0.8314	2609.8	-0.0886	4.371	1506.6
76	0.08	0.08	2508.8	0.0257	1.2086	1523.2
77	-0.0171	1.7543	2516.8	-0.0257	2.114	1531.2
81	0.06	3.9	2712	-0.0886	4.314	1736.6

Table 7.11 Regression Coefficients for Proposed Equations for Saturated Samples

# ID	P-wave Velocity			S-wave Velocity		
	A_p	B_p	C_p	A_s	B_s	C_s
1	0.16	5.36	2543	0.06	10.58	1183
12	-0.83	28.01	3947.8	-0.32	16.96	1987
13	1.03	-18.41	3156.3	0.09	1.73	1436.3
14	-0.41	15.6	3290.8	-1.13	39.71	1352.3
15	1.38	-12.18	3097.5	0.11	5.79	1284.3
19	0.02	2.86	2801.5	-0.21	5.83	1282.8
21	-0.69	16.87	2620.8	-0.13	4.59	1509.3
22	1.18	-17.46	2486	0.44	-2.72	1479
23	0.07	0.55	2419.8	-0.05	1.95	1568.8
24	-1.6	57.46	2546	-0.05	8.31	1184.3
25	0.28	-2.44	2969	-0.09	9.35	1165.8
38	0.11	4.55	3622.3	-0.93	33.71	1274.8
58	-0.62	22.86	3477.5	-0.17	7.15	1738.3
61	0.8	-15.52	3752.5	-0.05	4.11	1511.3
62	0.26	-1.46	3284.5	0.06	0.62	1815
66	0.77	12.67	2211.3	-0.04	4.44	1380
71	-0.14	9.9	2857	-0.18	8.06	1465.5
72	-0.29	15.67	2637.3	-0.02	2.18	1228
73	-0.2	9.92	2942.5	-0.19	6.65	1617.3
74	0.03	1.47	2895.8	0.2	-1.08	1429.5
75	0.15	0.59	2601.3	-0.08	3.24	1327.5
76	0.02	3.22	2705.5	0.07	0.27	1336
77	0.07	-0.13	2632.3	-0.02	1.7	1442
81	0.09	-0.75	2953.3	-0.07	3.09	1558.8

For example, in case of sample 15, the errors in V_p is 0.84%, 2.33%, and 2.55% at pressure of 5, 10and 15 MPa, respectively. More values are shown in Table 7.12.

Table 7.12 RAE in the three empirical correlation for dry samples

Effective Confining Pressure 5MPa

Sample No	12		13		14		15	
Method	Vp	Vs	Vp	Vs	Vp	Vs	Vp	Vs
Gassmann	0.06	0.55	0.63	0.15	1.59	1.09	0.51	1.79
Khaksar	0.06	0.08	0.38	0.20	0.14	0.61	0.64	1.11
Proposed	0.09	0.38	1.03	0.77	1.33	0.71	0.84	1.22

Effective Confining Pressure 10MPa

Sample No	12		13		14		15	
Method	Vp	Vs	Vp	Vs	Vp	Vs	Vp	Vs
Gassmann	28.85	14.90	7.06	1.62	0.21	5.95	5.53	7.66
Khaksar	0.99	0.76	7.74	2.71	1.59	5.46	6.05	6.86
Proposed	0.25	1.03	1.33	1.84	2.74	1.61	2.33	2.85

Effective Confining Pressure 15MPa

Sample No	12		13		14		15	
Method	Vp	Vs	Vp	Vs	Vp	Vs	Vp	Vs
Gassmann	0.82	1.11	8.79	3.31	3.09	3.70	5.07	4.07
Khaksar	0.98	0.49	8.62	2.18	0.98	4.41	5.03	5.03
Proposed	0.20	0.56	1.23	1.31	0.99	0.64	2.55	1.17

Data from four samples (No. 12, 13, 15 and 22) were selected to show the fit using Gassmann, Khaksar and the Proposed Equations as shown in Figures 7.9 through 7.12. Figures for the remaining samples are shown in Appendices F and G.

From Table 7.12 and Figures 7.9 through7.12 it can be stated that the new empirical correlation gives better fit. At the same time, it has the least Relative Absolute Error (RAE).

It is also observed that Gassmann, Khaksar and Proposed equations are almost closed to each other for dry samples.

However, for saturated samples, Gassmann's equation does not quite fit the data because they have the largest value for RAE as can be observed from Table 7.12. The proposed Equations 7.5 and 7.6 give a satisfactory fit for the data.

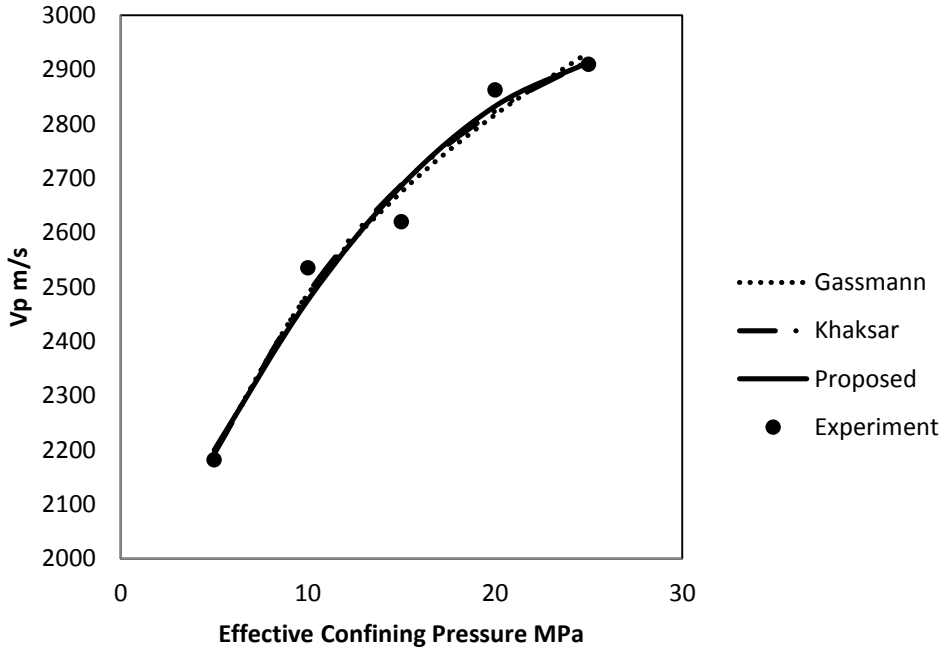

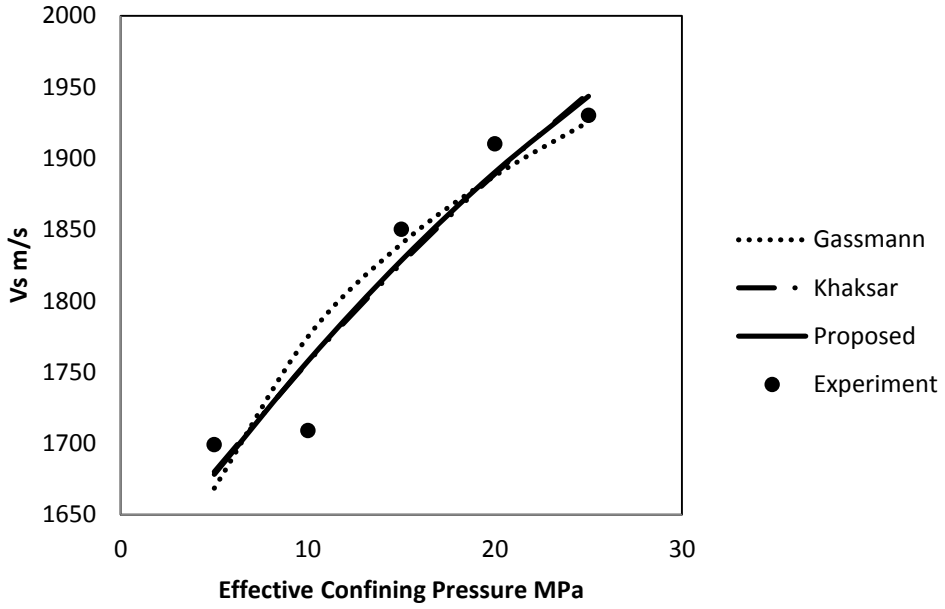

Figure 7.9 P-wave Velocity and S-wave vs. Effective Confining Pressure - Curve Fits for a Typical Dry Sample No. 12

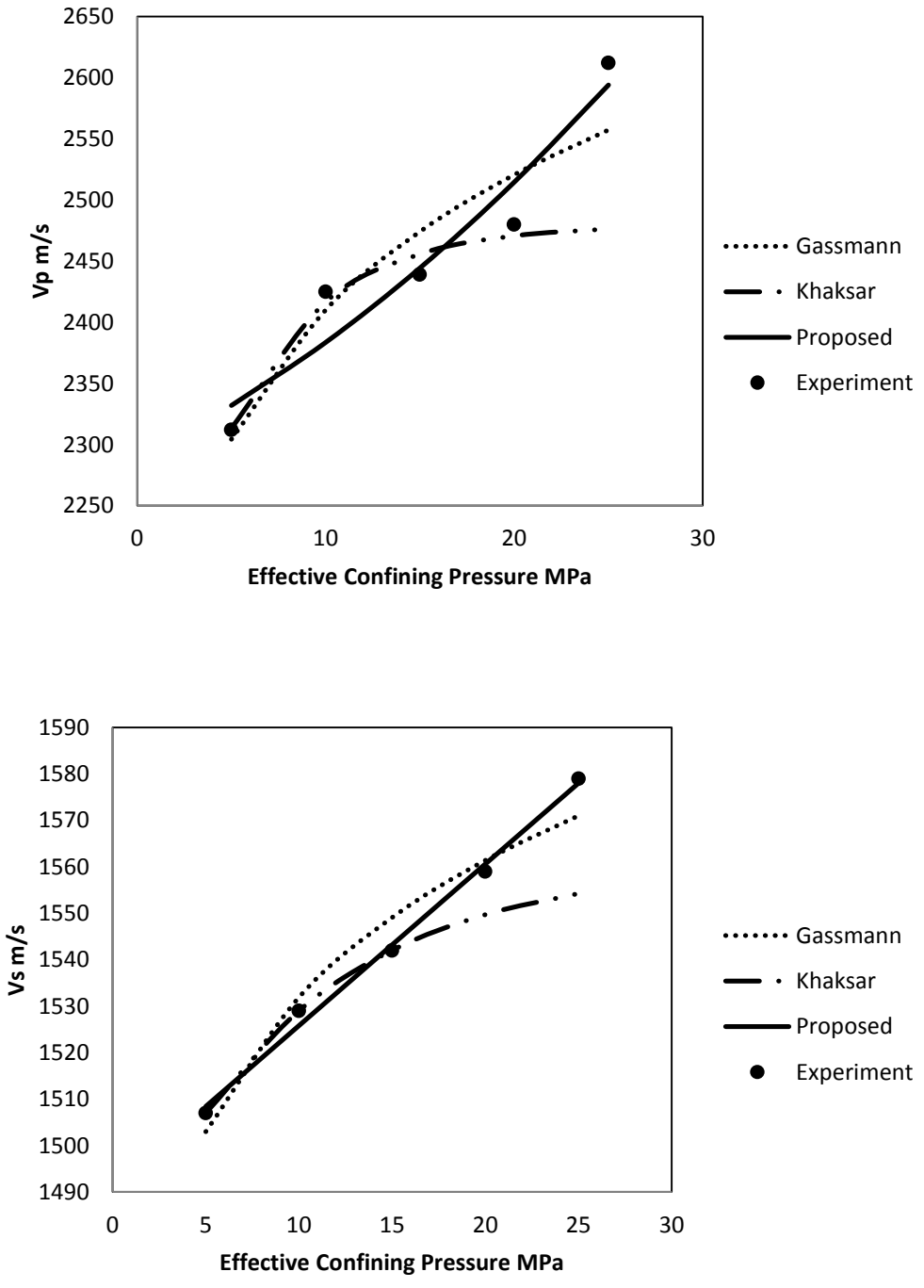

Figure 7.10 P-wave Velocity and S-wave vs. Effective Confining Pressure - Curve Fits for A Typical Dry Sample No. 15

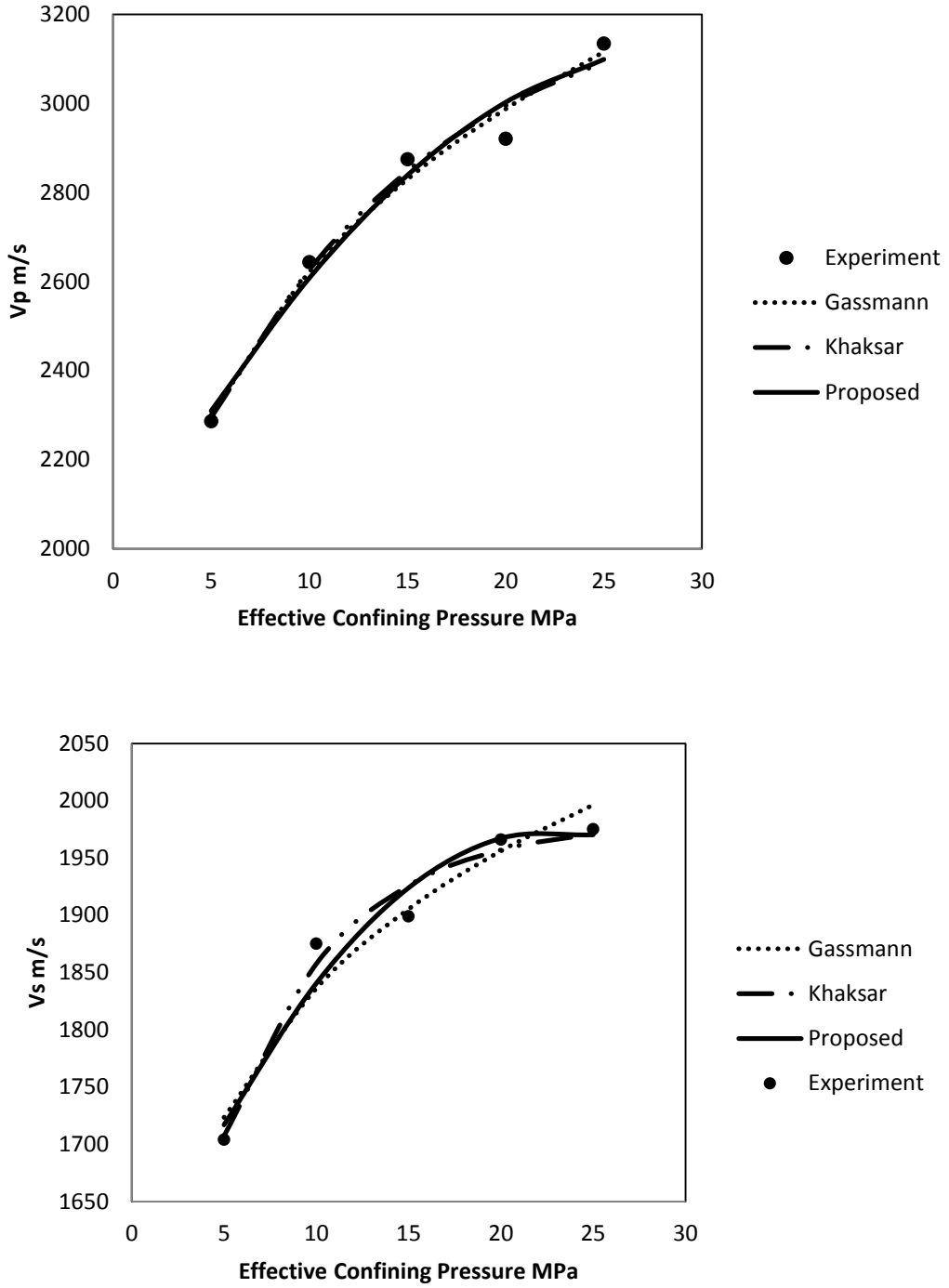

Figure 7.11 P-wave Velocity and S-wave vs. Effective Confining Pressure - Curve Fits for A Typical Saturated Sample No.22

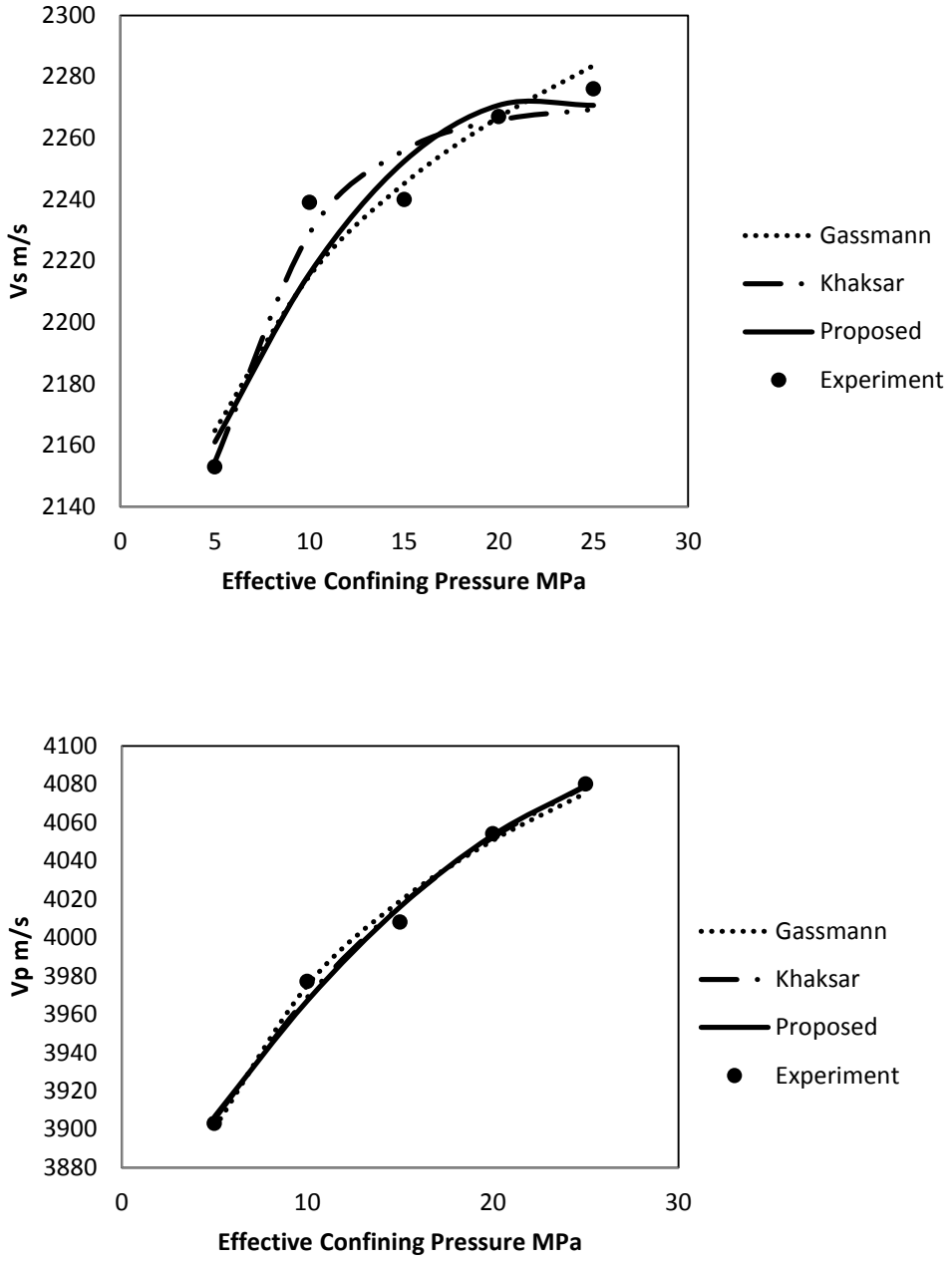

Figure 7.12 P-wave Velocity and S-wave vs. Effective Confining Pressure - Curve Fits for A Typical Saturated Sample No. 13

7.3.2 Velocity with Porosity

The general linear relationship between velocity and porosity can be expressed by an Equation proposed by Berry (1959) and [41] as shown below:

$$V_{P,S} = a * \emptyset + V_o \qquad (7.7)$$

The value of slope from P-wave velocity vs. porosity for experimental data in dry samples by using Berry (1959) relationship, a_P, is -46.305, -54.448, -55.94, -56.461, and 57.20 for 5MPa, 10MPa, 15MPa, 20MPa, and 25MPa respectively. For a_s, the values are -22.97, -23.93, -24.34, -24.79 and -25.15 for 5MPa, 10MPa, 15MPa, 20MPa, and 25MPa respectively.

Similar plots between velocity and porosity was produced for values at zero confining pressure. In order to generate velocity values at zero confining pressure, Equation 7.5 and 7.6 were reduced to:

$$V_P = C_P (7.8)$$

$$V_s = C_s (7.9)$$

Figures 7.13 and 7.14 show the crossplot between the extrapolated velocity values (Equations 7.8 and 7.9) and porosity for dry and saturated samples.

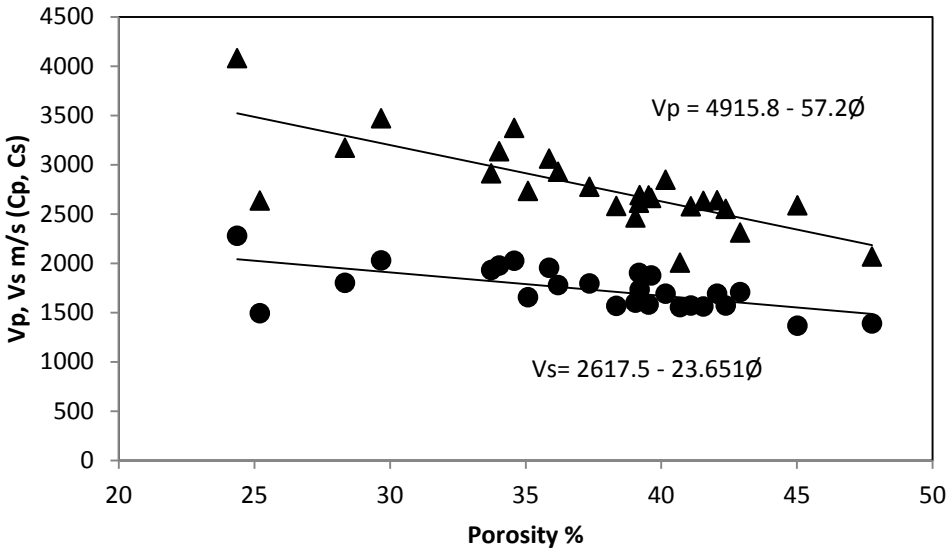

Figure 7.13 P-wave and S-wave Velocities vs. Porosity for Dry samples at Atmospheric Pressure.

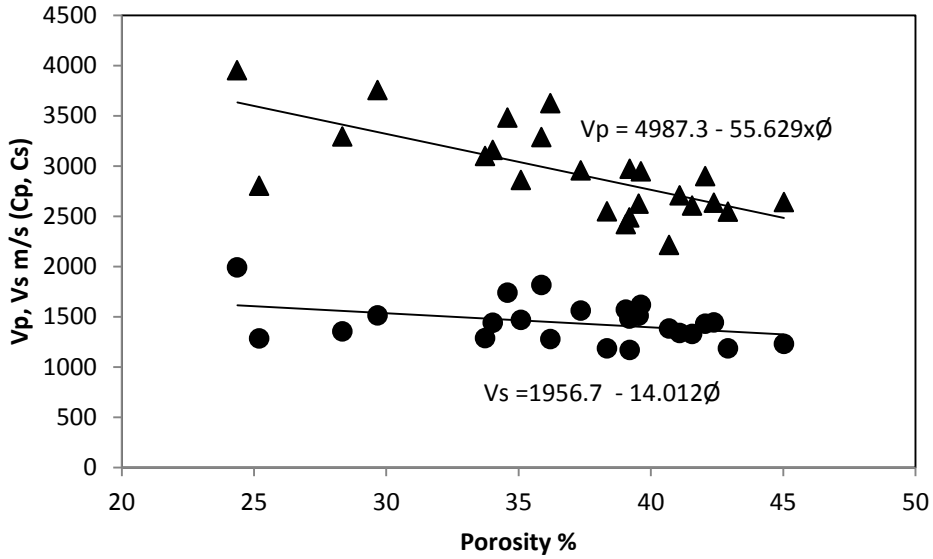

Figure 7.14 P-wave and S-wave Velocities vs. Porosity for Saturated Samples at Atmospheric Pressure

From Figures 7.13 and 7.14 following observations can be made:

1- Both P- and S- wave velocity decrease with increasing porosity. The relative decrease is more noticeable in S-wave velocities.
2- The linear decrease of velocities with porosity is described satisfactory by Equation 7.7 proposed by Berry (1959) [42].

At high effective confining pressure (20 MPa) the velocity versus porosity will give Figures 7.15 and 7.16.

Following observations can be made based on Figures 7.13 through 7.16:

1- Again, both P- and S- wave velocity decrease with increasing porosity in saturated samples.
2- Generally, the effects of porosity on the shear velocity V_s are larger than on the compressional velocity V_p.

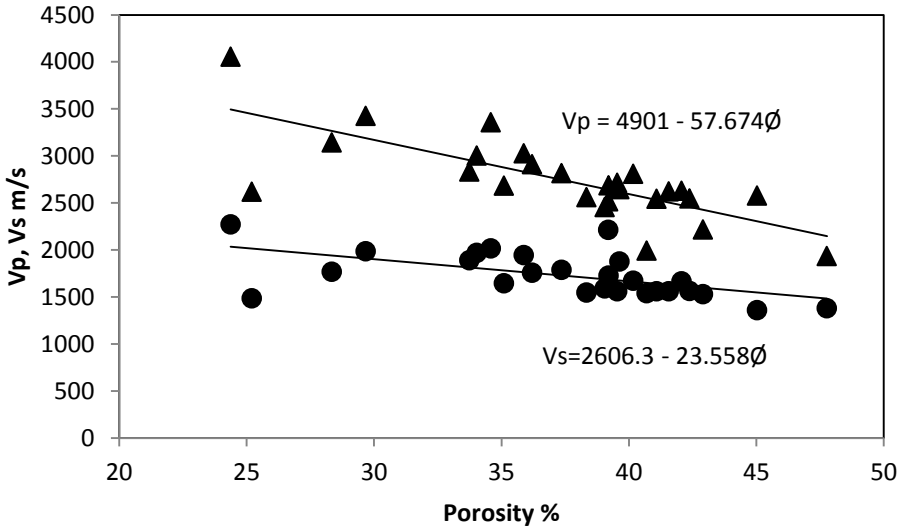

Figure 7.15 P-wave and S-wave Velocities vs. Porosity for Dry Samples t Effective Confining Pressure 20 MPa

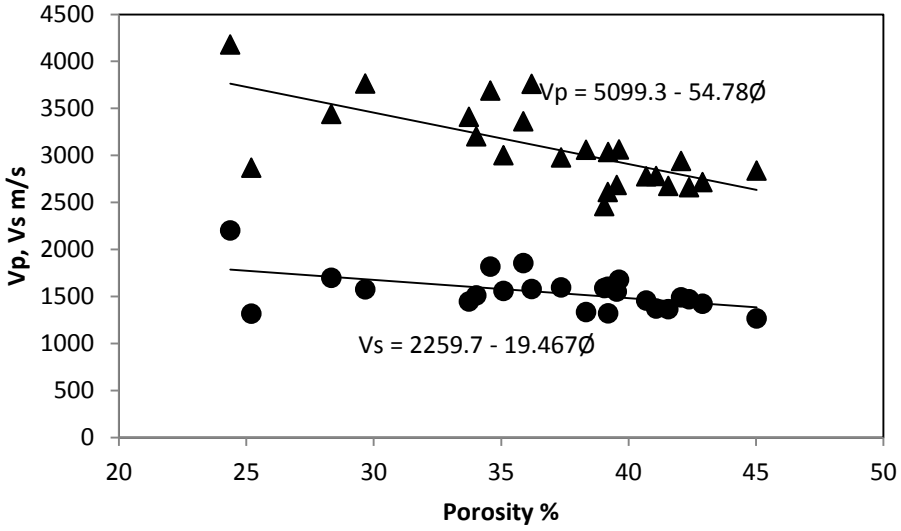

Figure 7.16 P-wave and S-wave Velocities vs. Porosity for Saturated Samples at Effective Confining Pressure 20MPa

7.3.3 Velocity Ratio Plots

The behavior of V_p/V_s ratio as a function of pressure is presented in this section. Some authors [43] use the V_p/V_s versus V_p crossplot as lithology discriminator carbonate rocks.

Figures 7.17 through 7.19 show the V_p/V_s ratio as a function of confining pressure for three samples. Rest of the data on this behaviour is printed in Appendices A and B.

Figures 7.17 through 7.19 show that the saturation causes an increase in V_p/V_s ratio at all confining pressures, which is consistent with studies separated in the literature. In addition for dry case the slope of V_p/V_s slightly increases with increase in confining pressure in most of the samples, whereas in saturated samples, the trend is just the opposite. This is consistent with Khaksar results.

7.3.4 Crossplot Velocity

Figures 7.20 – 7.23 show cross plots of compressional and shear wave velocities, at various confining pressures, for samples under dry and saturated condition, respectively. Plotted on these figures are the actual experimental data and their linear fits. As can be seen, the linear models describe the data almost adequately.

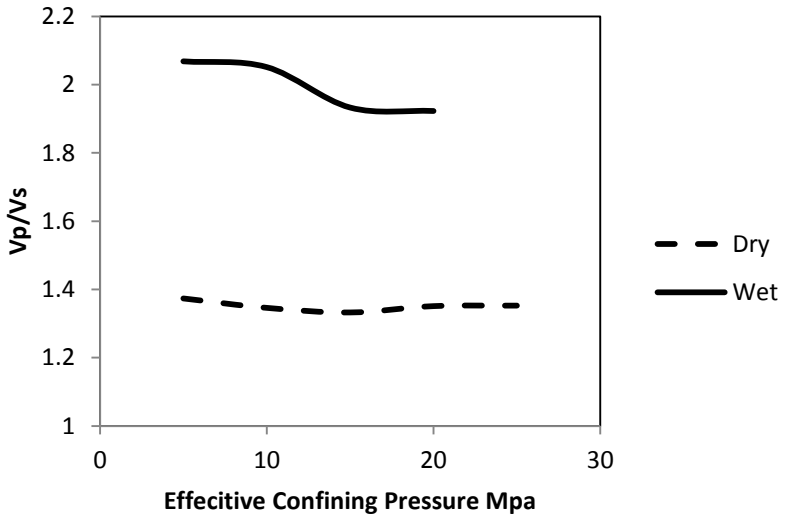

Figure 7.17 The V_p/V_s ratio vs. Confining Pressure for Sample No. 1

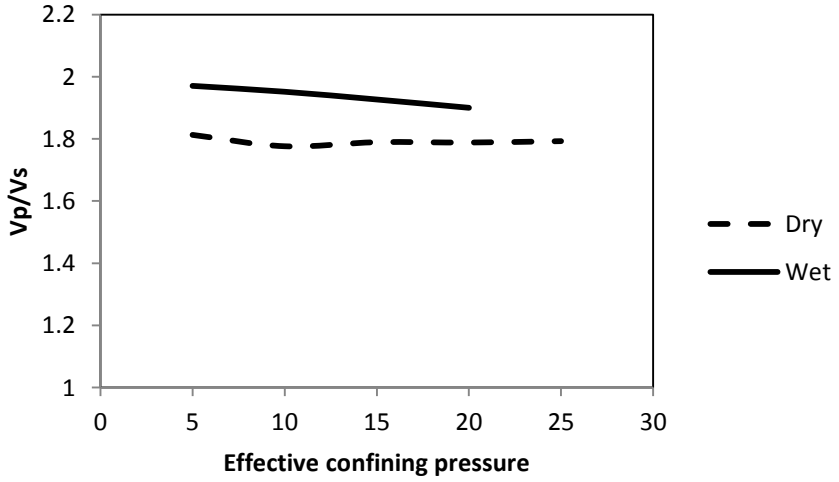

Figure 7.18 The V_p/V_s ratio vs. Confining Pressure for Sample No. 12

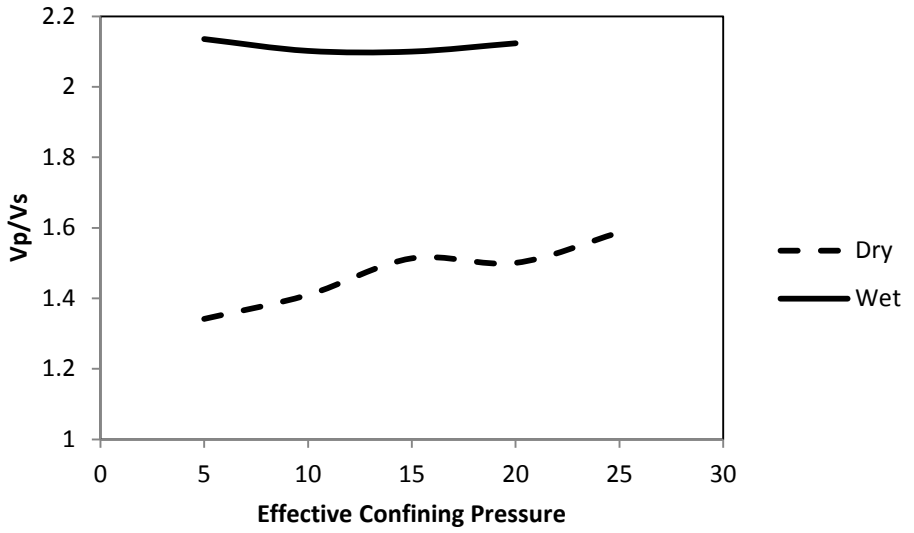

Figure 7.19 The V_p/V_s ratio vs. Confining Pressure for Sample No. 13

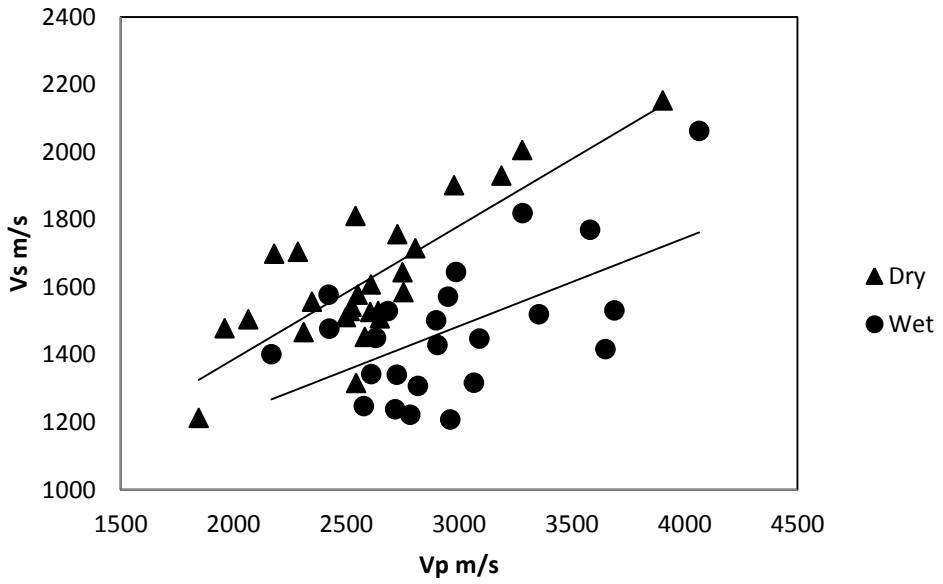

Figure 7.20 Vs vs. Vp cross plots for dry and wet samples at 5 MPa Confining Pressure

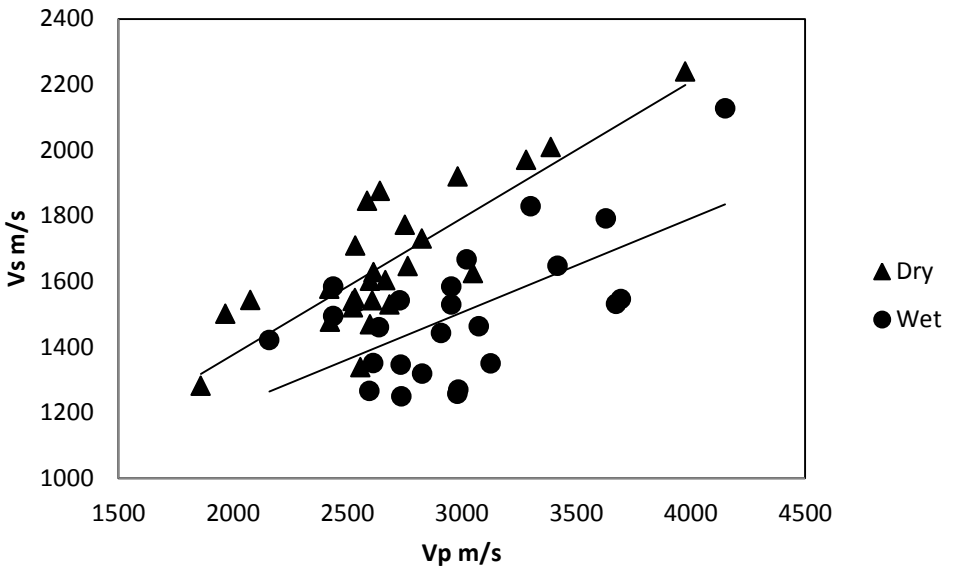

Figure 7.21 Vs vs. Vp cross plots for dry and wet samples at 10 MPa confining pressure

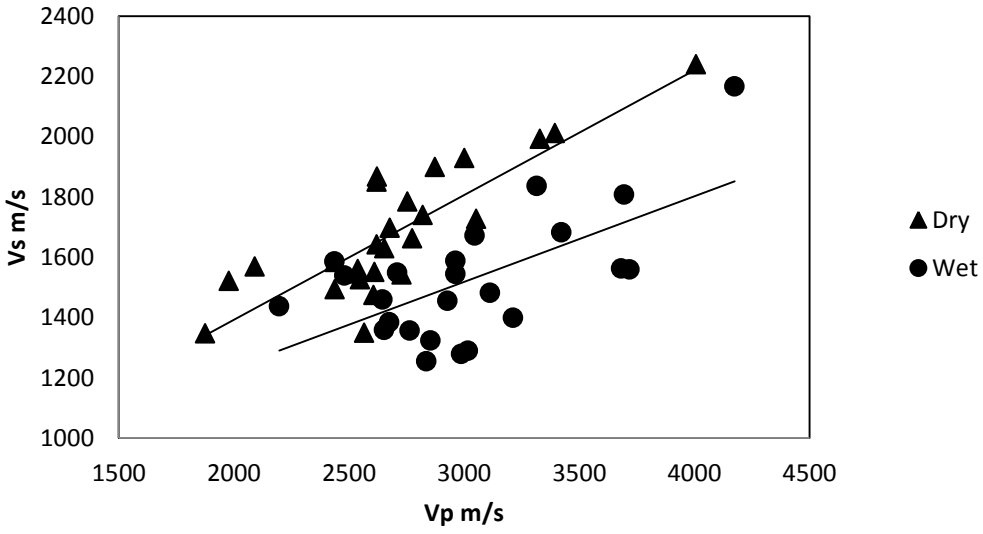

Figure 7.22 Vs vs. Vp cross plots for dry and wet samples at 15 MPa confining pressure

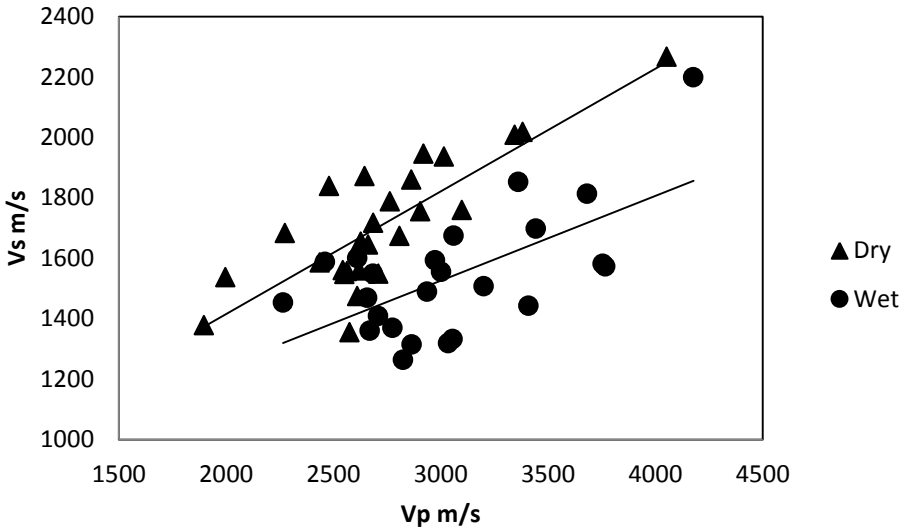

Figure 7.23 Vs vs. Vp cross plots for dry and wet samples at 20 MPa confining pressure

CHAPTER 8

CONCLUSIONS AND RECOMMENDATIONS

This research aimed to studying acoustic waves "sonic waves" in carbonate rock. The outcomes will enhance exploration efforts and reservoir characterization, and help integrating geological, geophysical, and engineering data. Investigations are therefore conducted to determine the acoustic properties of rock, especially the wave velocities as functions of variables such as saturating fluid and confining pressure, which a rock is subjected to during the producing life of a reservoir.

The overall or general objective of this research was to study the area of Lidam and develop empirical relationships between acoustics (compressional velocity V_p, shear-wave velocity V_s) at various fluid saturations (dry, brine) and core porosity for carbonate reservoir rocks.

Sixty one specimens of 1.5 inch (38 mm) and thirty two specimens of 1 inch (25 mm) diameter were drilled from cores ranging from 5 in diameter to 8 in diameter, total samples are ninety three samples used in this study.

The measurement of porosity was conducted using two devices: Helium Porosimeter and AP-608 Automated Porosimeter- Permeameter, plus porosity that have been conducted from thin Section.

8.1 Conclusions

- Preliminary classification (outcrop, hand-spacemen, and core plug) eight facies have been found but depending on thin section description and Dunham's classification, four facies have been noticed which was considered as basic classification for Dam formation.
- Four textures was found in Al-Lidam area:
    - Mudstone: porosity range from 7 to 15%,pore size 50-400 micron, calcite 90-100%, and quartz 5-10%.
    - Wackestone: porosity range from 25 to 27 %, pore size 50 – 200 microns, calcite 97 – 98%, and quartz 2 – 3%.
    - Packstone: porosities range from 25 to 34%, pore size 50 -300 microns, quartz 2 -20%, calcite 85 – 98%.
    - Grainstone: porosity range from 22 to 40 %, pore size 50 – 800 microns, quartz 1- 10%, calcite 90 – 99%.
- The majority of samples are under grainstone classification and they have the highest value of porosity.
- Dual Porosity Model was used to predict the network structure and distribution in rock and the distance between pores. According to this model, the distance between pores range from 6.8 to 431 microns and mean pore radius ranges from 2.11 to 156.11 microns. From the results obtained it was observed the distance between pores relate directly to permeability and inversely with porosity as in Korvin model.

- The measured porosity values using Helium Porosimeter range between 24.36% and 54.22% with an average value 37.87%. The corresponding values porosity for AP-608 Automated Porosimeter- Permeameteris range between 24.97% and 55.73% with an average value 38.5%. The difference between two measurements is found to be less than 4 %. Samples that have porosity higher than 47% were eliminated from this study because they were considered to be highly porous. The high values of porosity could be due to the human error in measurement, sample preparation, and/or Equipment error.
- The Dam formation outcrop samples reflected wide range of permeability values from 0.39 mD to 18748.2 mD, with an average of 3375.3 mD. Most samples range from .39mD to 1 D. A sample having permeability higher than 11D was eliminated because it was considered to be highly permeable.
- 26 rock samples having 1.5 in. diameter and 2.0 in. length were chosen for measuring P-wave and S-wave velocities. Readings were taken at confining pressures of 5MPa through 25MPa with increments of 5MPa for dry case. In case of testing under saturated condition, brine was used as saturating fluid with these properties: NaCl, 100,000 ppm, and 1.06 grams/cc density. Data was acquired at confining pressure levels from 10 MPa through 25 MPa with increments of 5 MPa. Throughout the testing, pore pressure was maintained around 5 MPa.
- Both P-wave and S-waves velocities increase with the increase in confining pressure for dry samples. The P-wave velocity increased and the two S-waves velocities decreased with confining pressure under saturated condition. The rate

of increase in P-wave velocity with confining pressure under dry condition is more than that for samples under saturated condition.

- Gassmann's and Khaksar's empirical equations were applied on these data.
- The best fit between velocity and effective confining pressure ($5 \leq P \geq 20$) for the data is represented by these empirical equations:

$$V_P = A_P * P^2 + B_P * P + C_P$$

$$V_s = A_s * P^2 + B_s * P + C_s$$

The value of A_p, B_p, C_p, and A_s, B_s, C_s were evaluated for every samples.

- The new empirical relationship has the least Relative Absolute Error (RAE) and gives better estimate for fitting the experimental data. For dry samples, the three empirical equations (Gassmann, Khaksar, and New relationship) are almost close to each other in fitting the experimental data. For saturated samples, Gassmann's equation does not fit the experimental data satisfactory and it has the highest for value of RAE.
- At confining pressure of 25 MPa and pore pressure of 5 MPa the best fit for velocity vs. porosity data are given by:

$$V_p = 5099.3 - 54.78Ø$$

$$V_s = 2259.7 - 19.467Ø$$

- From the above equations P- and S- wave velocities decrease with increase porosity. The decrease is more noticeable in S-wave velocities. The linear decrease in velocities with porosity is conformity with the velocity average

equation of Berry (1959). Generally, the effects of variation in porosity on the shear velocity are larger than on the compressional velocity.

- The saturation causes an increase in V_p/V_s ratio for all confining pressures. That consistent with trends reported in the literature. Also, for dry case the slope of V_p/V_s slightly increases with the increase in confining pressure, whereas in saturated samples, the trend is just the opposite.

8.2 Recommendations and future work

The future work may include the following aspects:

- Study the connectivity between pores and gross geometrical classification of pore size using mercury porosimetry method.
- Use XRD for more details about the petrographic description.
- Study the attenuation of compressional and shear waves versus temperature (T) for samples saturated with heavy oil at constant reservoir confining pressure.
- Study the attenuation of compressional and shear waves versus confining pressure for samples saturated with light oil at constant reservoir temperature.
- Measure velocities of compressional (V_p) and shear waves (V_s) versus temperature (T) for samples saturated with heavy oil at constant reservoir confining pressure.
- Measure velocities of compressional (V_p) and shear waves (V_s) versus confining pressure for samples saturated with light oil at constant reservoir temperature.

References

[1] A. M. Nur, J. D. Walls, K. Winkler, and J. DeVilbiss, "Effects of Fluid Saturation on Waves in Porous Rock and Relations to Hydraulic Permeability," *Society of Petroleum Engineers Journal*, vol. 20, pp. 450-458, 12/01/1980 1980.

[2] B. Z. Thierry Bourbie, "Hydraulic and acoustic properties as a function of porosity in Fontainebleau sandstone," *JOURNAL OF GEOPHYSICAL RESEARCH*, vol. 90, pp. 1,524, 1985.

[3] W. F. I. Murphy, "Effects of partial water saturation on attenuation in sandstones," *The Acoustical Society of America* vol. 71, pp. 1458-1468, 1982.

[4] T. Bourbie, Cousst, O., Zinszner, B., *Acoustics of porous media,*. Paris: IFP publications, 1987.

[5] F. Gassmann, "Elastic waves through a packing of spheres," *Society of Exploration Geophysicists*, vol. 16 pp. 673-685, 1951.

[6] A. R. G. a. L. W. G. Malcolm Robert Jesse Wyllie, "Elastic wave velocities in heterogeneous and porous media," *ociety of Exploration Geophysicists*, vol. 21, pp. 41-70, 1956.

[7] L. L. Raymer, S. G. John, and E. R. Hunt, "AN IMPROVED SONIC TRANSIT TIME-TO-POROSITY TRANSFORM," Society of Petrophysicists & Well Log Analysts, 1980.

[8] H. De-hua and A. Nur, *The Effects of Porosity And Clay Content On Wave Velocities In Sandstones*, 1986.

[9] F. S. E. Anselmetti, Gregor P., "Controls on sonic velocity in carbonates," *Pure and Applied Geophysics PAGEOPH*, vol. 141, pp. 287-323, 1993.

[10] M. J. Simon, R. A. Timothy, and M. Clive, *The Effect of Degree of Saturation On Ultrasonic Velocity And Attenuation In Sandstones*, 1997.

[11] Khaksar, Griffiths, and McCann, "Compressional- and shear-wave velocities as a function of confining stress in dry sandstones," *Geophysical Prospecting*, vol. 47, pp. 487-508, 1999.

[12] C. M. a. J. S. Solomon Assefa, "Attenuation of P- and S-waves in limestones," *Geophysical Prospecting,* vol. 47, pp. 359–392, 1999.

[13] H. Eskandari, Rezaee, M.R., Javaherian, A., and Mohammadnia, M, "Shear Wave Velocity Estimation Utilizing Wireline Logs for a Carbonate Reservoir, South-West Iran," *Iranian Int. J. Sci,* vol. 4, pp. 209-221, 2003.

[14] S. Ravi, P. Manika, S. Ganpat, and G. C. Katiyar, *On the Applicability of Gassmann Model In Carbonates,* 2006.

[15] M. B. Ludmila Adam, and Ivar Brevik, "Gassmann's fluid substitution and shear modulus variability in carbonates at laboratory seismic and ultrasonic frequencies," *Society of Exploration Geophysicists,* 2006.

[16] H. B. Klaas Verwer, and Jeroen A. M. Kenter, "Case History Acoustic properties of carbonates: Effects of rock texture and implications for fluid substitution," *Society of Exploration Geophysicists,* vol. 73, pp. B51-B65, 2008.

[17] Steineke, "Geological Reconnaissance of the Coastal Plain of Hasa Province, Northeastern Saudi Arabia," vol. (unpublished), 1935.

[18] H. W. a. R. C. H. Thralls, "Geology and oil resources of eastern Saudi Arabia," in *20th International Geology Congress*, Mexico, 1956, pp. 9–32.

[19] R. W. Powers, L.F. Ramirez, C.D. Redmon and E.L. Elber Jr, "Geology of the Arabian Peninsula: sedimentary geology of Saudi Arabia," *US Geological Survey Professional Paper,* vol. 560-D, p. 147, 1966.

[20] O. Irtem, "Miocene Tidal Flat Stromatolites of the Dam Formation, Saudi Arabia," *Arabian Journal of Science and Engineering,* vol. 12, pp. 145 -153., 1986.

[21] J. W. Tleel, "Surface geology of Dammam Dome, Eastern Province, Saudi Arabia," *Bulletin of American Association of Petroleum Geologists,* vol. 57, pp. 558-576, 1973.

[22] S. S. Al-Enezi, "Comparison of Recent and Miocene foraminifera from Eastern Saudi Arabia," in *Earth Science*. vol. Master Dhahran: KFUPM, 2006, p. 155.

[23] F. M. S. Alkhaldi, "Controls on Hierarchy of Miocene Buildups within a High Resolution Cycle Stratigraphic Framework of Dam Formation, Lidam Area, Saudi Arabia," in *Earth Science*. vol. Master Dharhan: KFUPM, 2009, p. 134.

[24] M. E. Tucker "Sedimetry Petrology: an introduction to the origin of Sedimentry rocks 3rd.," *Blackwell Science* 2005.

[25] R. J. Dunham, "Classification of Carbonate Rocks According to Depositional Texture," *American Association of Petroleum Geologists,* pp. 108-121, 1962.

[26] W. A. Pryor, "Permeability- Porosity patterns and variations in some Holocene sand bodies.," *AAPG Bulletin,* vol. 57, pp. 162-189, 1973.

[27] D. B. McWorter, and D.K. Sunada, "Groundwater Hydrology and hydraulics," *Water Resources Publications, Ft. Collins, CO.,* 1977.

[28] D. Tiab, and Donaldson, *Petrophisics: Theory and Practice of Measuring Reservoir Rock and Fluids Transport Properties.* New York: Elsevier, 2004.

[29] U. M. Y. BERNABE, and B. EVANS, "Permeability-porosity Relationships in Rocks Subjected to Various Evolution Processes," *Pure and Applied Geophysics PAGEOPH,* vol. 160, pp. 937-960, 2003.

[30] G. Korvin, "A Percolation Model for the Permeability of Kaolinite-Bearing Sandstones," Society of Petroleum Engineers, 1989.

[31] C. Perez-Rosales, "On the Relationship Between Formation Resistivity Factor and Porosity," *Society of Petroleum Engineers Journal,* vol. 22, pp. 531-536, 08/01/1982 1982.

[32] G. Korvin, "Geophysical well logging," in *Unpublished Lecture Notes* Dhahran, 1999.

[33] P. E. Doyen, "Crack geometry of igneous rocks: a maximum entropy inversion of elastic and transport properties," *J. Geoph. Res.*, vol. 92, pp. 8169-8181, 1987.

[34] P. K. Lamm, "Solution of ill-posed Volterra equations via variable smoothing Tikhonov regularization," *SIAM*, pp. 92-108, 1997.

[35] E. M. Lifshitz, and L.P. Pitaevskii,, "Statistical Physics, Pt.1, Pergamon, New York.," 1980.

[36] P. E. Doyen, "Crack geometry of igneous rocks: a maximum entropy inversion of elastic and transport properties," *J. Geoph. Res.*, vol. 92, pp. 8169-8181, 1987.

[37] J. M. Taylor, " Pore-space reduction in sandstones," *AAPG Bulletin*, vol. 34, pp. 701-716, 1950.

[38] H. D.-H. a. Z. M. D. Eberhart-Phillips D., "Empirical relationships among seismic velocity, effective pressure, porosity, and clay content in sandstone," *Geophysics* vol. 54, pp. 82–89, 1989.

[39] F. D., "Ultrasonic compressional and shear velocities in dry clastic rocks as a function of porosity, clay content, and confining pressure," *Geophysical Journal International,* vol. 108, pp. 125–135, 1992.

[40] J. S.M., "Velocities and quality factors of sedimentary rocks at low and high effective pressures," *Geophysical Journal International* vol. 123, pp. 774–780, 1995.

[41] E. B. James, *Acoustic Velocity in Porous Media*, 1959.

[42] J. E. Berry, "Acoustic velocity in porous media," *Journal of Petroleum Technoloty,* vol. 11, pp. 262-270., 1959.

[43] S. Assefa, C. McCann, J. Sothcott, T. Austin, and S. Johnstad "he effects of porosity-pore-fluid and minerology on Vp/Vs in carbonate rocks," *T. EAGE 61st Conference, Helsinki, Finland, 7-11th June, 1999*, pp. Paper 2-02, 1999.

Vitae

Name	: Murtada Abdein Ali Elhaj
Nationality	: Sudanese
Date of Birth	: 1/7/1983
Email	: muaali@kfupm.edu.sa; muaali@uofk.edu
Mobile No.	: +966-563597317; +249-912893136
Address	: King Fahd University of Petroleum & Minerals
Academic Background	: Petroleum Engineering

APPENDICES

APPENDIX A

PETROPHYSICS DATA

Table A1: Thin Section

Serial No.	Sample No.	Sample Name	Direction	Length (inch)	Diameter (inch)	Thin Section
1	1	Dam-1-A-1	V	2.8	1.5	No
2	2	Dam-1-A-2	V	2.9	1.5	No
3	3	**Dam-1-A-3**	V	3.3	1.5	**Yes**
4	4	Dam-1-B-4	V	2.5	1	No
5	5	**Dam-1-B-5**	V	2.8	1	**Yes**
6	6	**Dam-1-B-6**	V	2.5	1	**Yes**
7	7	Dam-1-B-7	V	2	1	No
8	8	**Dam-1-B-8**	V	2.2	1	**Yes**
9	9	**Dam-2-9**	H	2.5	1.5	**Yes**
10	10	**Dam-2-10**	H	1.8	1.5	**Yes**
11	11	**Dam-2-11**	H	2.6	1.5	**Yes**
12	12	Dam-2-12	H	3.2	1.5	No
13	13	**Dam-2-13**	V	3.8	1.5	**Yes**
14	14A	Dam-2-14	V	1.3	1.5	No
15	14B	Dam-2-14	V	2.7	1.5	No
16	15A	Dam-2-15	V	0.9	1.5	No
17	15B	Dam-2-15	V	2.5	1.5	No
18	16	**Dam-3-16**	H	2.8	1.5	**Yes**
19	17	**Dam-3-17**	H	2.3	1.5	**Yes**
20	18	**Dam-3-18**	V	3.1	1.5	**Yes**
21	19	Dam-3-19	V	2.9	1.5	No
22	20	**Dam-3-20**	V	3.2	1.5	**Yes**
23	21	**Dam-4-A-21**	V	2.7	1.5	**Yes**
24	22	Dam-4-A-22	V	2.7	1.5	No
25	23	Dam-4-A-23	V	2.9	1.5	No
26	24	Dam-4-A-24	V	3	1.5	No
27	25	Dam-4-A-25	V	3.1	1.5	No
28	26	**Dam-4-A-26**	H	2.2	1.5	**Yes**
29	27	**Dam-4-A-27**	H	1.9	1.5	**Yes**
30	28	Dam-4-A-28	V	3.1	1.5	No
31	29	**Dam-4-A-29**	H	2.3	1.5	**Yes**
32	30	Dam-4-B-30	V	2.6	1	No
33	31	Dam-4-B-31	V	3.2	1	No
34	32	Dam-4-B-32	V	3.5	1	No
35	33A	Dam-4-B-33	V	0.8	1	No
36	33B	Dam-4-B-33	V	2.5	1	No
37	34	Dam-4-B-34	V	2.4	1	No
38	35	Dam-4-B-35	V	2.5	1	No
39	36	Dam-4-B-36	V	2.6	1	No
40	37	Dam-4-B-37	V	2.4	1	No
41	38	Dam-4-B-38	V	2.5	1.5	No

Table A1: Thin Section (Cont.)

Serial No.	Sample No.	Sample Name	Direction	Length (inch)	Diameter (inch)	Thin Section
42	39	Dam-4-B-39	V	2.5	1	No
43	40	Dam-4-B-40	V	2.8	1	No
44	41	Dam-4-C-41	H	2.9	1	No
45	42	Dam-4-C-42	H	2.5	1.5	No
46	43	Dam-4-C-43	V	2.6	1	No
47	44	Dam-4-C-44	H	1.7	1.5	No
48	45	Dam-4-C-45	H	2.6	1	No
49	46	Dam-5-46	H	1.9	1	Yes
50	47	Dam-5-47	H	1.7	1	Yes
51	48	Dam-5-48	H	1.2	1	Yes
52	49	Dam-6-A-49	V	2.4	1.5	No
53	50	Dam-6-A-50	V	2.4	1.5	Yes
54	51	Dam-6-A-51	V	3.2	1.5	No
55	52	Dam-6-A-52	V	2.8	1.5	No
56	53	Dam-6-A-53	V	2.6	1.5	No
57	54	Dam-6-A-54	V	2.8	1.5	No
58	55	Dam-6-B-55	V	3	1.5	Yes
59	56	Dam-6-B-56	H	3.5	1.5	Yes
60	57	Dam-6-B-57	V	2.5	1.5	No
61	58	Dam-6-B-58	H	3.4	1.5	No
62	59A	Dam-6-B-59	V	0.8	1.5	No
63	59B	Dam-6-B-59	V	1.9	1.5	No
64	60	Dam-6-B-60	H	3.5	1.5	No
65	61	Dam-6-B-61	H	3.4	1.5	No
66	62	Dam-6-B-62	V	3	1.5	No
67	63	Dam-6-B-63	H	3.2	1	No
68	64	Dam-6-B-64	H	2.9	1	Yes
69	65	Dam-6-B-65	H	2.8	1	No
70	66	Dam-7-66	V	3	1.5	Yes
71	67	Dam-7-67	V	2.1	1.5	Yes
72	68	Dam-7-68	V	1.6	1.5	Yes
73	69	Dam-7-69	V	1	1.5	Yes
74	70	Dam-8-70	V	2.6	1.5	Yes
75	71	Dam-8-71	V	3.9	1.5	No
76	72A	Dam-8-72	V	1.1	1.5	No
77	72B	Dam-8-72	V	2.6	1.5	No
78	73A	Dam-8-73	V	1.5	1.5	No
79	73B	Dam-8-73	V	2.5	1.5	No
80	74	Dam-8-74	V	2.5	1.5	No

Table A1: Thin Section (Cont.)

Serial No.	Sample No.	Sample Name	Direction	Length (inch)	Diameter (inch)	Thin Section
81	75	Dam-8-75	H	2.7	1.5	No
82	76	Dam-8-76	H	3.2	1.5	No
83	77	Dam-8-77	H	3.3	1.5	No
84	78	Dam-8-78	V	1.5	1	No
85	79	Dam-8-79	V	1.6	1	Yes
86	80	Dam-8-80	V	1.6	1	Yes
87	81	Dam-8-81	V	1.9	1	No
88	82	Dam-8-82	V	1.9	1	No
89	83	Dam-8-83	V	2	1	No
90	84	Dam-8-84	V	1.7	1	No
91	85	Dam-8-85	V	1.8	1	No
92	86	Dam-8-86	V	1.8	1	No
93	87	Dam-8-87	V	0.9	1	Yes

Table A2: Porosity and Permeability Measurements

Serial No.	Sample No.	Porosity (%)		Permeability (mD)
		AP-608 Method	H.P Method	
1	1	42.913	42.089	4.4
2	2	34.072	34.134	5.4
3	3	33.382	33.964	2.4
4	4	32.567	32.941	3.8
5	5	31.07	31.916	1.7
6	6	32.357	33.348	1.8
7	7	37.188	38.376	0.4
8	8	33.812	34.468	3.1
9	9	25.576	28.128	2.6
10	10	28.947	31.053	5.2
11	11	25.07	26.241	1.4
12	12	24.369	24.973	2.3
13	13	34.028	35.133	7.4
14	14a	27.22	29.853	2.0
15	14b	28.348	29.086	1.6
16	15a	32.469	32.279	4.5
17	15b	33.739	35.172	6.4
18	16	24.794	25.192	3.2
19	17	25.681	26.577	4.1
20	18	26.655	27.929	6.2
21	19	25.204	25.339	3.1
22	20	26.581	26.174	12.9
23	21	39.543	40.949	383.0
24	22	39.189	40.701	1060.3
25	23	39.057	40.58	333.1
26	24	38.345	40.335	498.1
27	25	39.209	40.953	395.6
28	26	37.714	37.236	645.3
29	27	39.215	40.645	789.0
30	29	38.408	40.028	299.5
31	30	39.839	40.741	18748.2
32	31	35.356	35.242	7945.0
33	32	32.503	33.058	14656.3
34	33a	30.403	30.198	8648.0
35	33b	31.185	31.152	10640.3
36	34	28.131	29.406	9859.2
37	35	33.577	33.236	15589.7
38	36	31.658	32.189	7292.3
39	37	33.709	34.183	16864.5
40	38	36.208	38.428	7351.7
41	39	30.85	30.272	12371.3

Table A2: Porosity and Permeability Measurements (Cont.)

Serial No.	Sample No.	Porosity (%)		Permeability (mD)
		AP-608 Method	H.P Method	
42	40	34.603	35.712	11297.0
43	41	45.818	45.512	1666.6
44	42	44.586	44.301	4199.0
45	43	31.024	32.001	3.6
46	45	44.453	44.044	1595.2
47	47	31.489	32.473	12.1
48	49	54.223	55.728	6237.1
49	50	50.893	50.007	5351.4
50	52	50.717	50.689	5873.5
51	53	50.189	50.161	2979.4
52	54	51.77	51.27	5307.8
53	55	40.167	40.283	9180.6
54	57	40.58	41.296	3153.1
55	58	34.581	35.812	13750.7
56	59a	42.462	43.987	5178.8
57	59b	39.064	40.195	2389.2
58	60	33.891	33.751	7235.1
59	61	29.673	30.128	8412.3
60	62	35.873	35.517	12284.2
61	63	37.534	37.783	8547.8
62	64	37.329	40.074	7336.9
63	65	36.11	37.342	9108.7
64	66	40.697	40.455	14419.4
65	70	43.79	44.204	9.4
66	71	35.097	35.229	5.3
67	72a	46.93	46.959	14.2
68	72b	45.029	46.963	13.5
69	73a	41.225	41.623	8.5
70	73b	39.632	40.038	7.3
71	74	42.065	42.757	5.5
72	75	41.563	42.017	8.3
73	76	41.092	42.972	5.7
74	77	42.388	42.536	10.0
75	78	37.141	37.257	3.8
76	79	38.236	38.81	5.5
77	80	34.93	35.286	3.0
78	81	37.358	37.226	6.0
79	82	42.6	45.376	16.3
80	83	44.515	45.7	13.0

Table A2: Porosity and Permeability Measurements (Cont.)

Sample No.	Porosity (%)		Permeability (mD)
	AP-608 Method	H.P Method	
max	54.223	55.728	18748.2
min	24.369	24.973	0.4
avg.	36.779	37.475	3375.3

Table A3: Porosity and Permeability Average Measurements

Serial No.	Sample No.	Porosity (%)		Permeability (mD)
		AP-608 Method	H.P Method	
81	84	38.291	39.291	11.8
82	85	41.226	42.118	11.9
83	86	41.677	41.629	12.1

Table A4: Porosity Measurements Comparison between Thee Methods

Serial No.	Sample No.	Porosity (%)		
		AP-608 Method	H.P Method	Thin Section Method
1	3	33.382	33.964	27
2	5	31.07	31.916	25
3	8	33.812	34.468	30
4	9	25.576	28.128	22
5	10	28.947	31.053	25
6	11	25.07	26.241	22
7	13	34.028	35.133	29
8	16	24.794	25.192	10
9	17	25.681	26.577	9
10	18	26.655	27.929	7
11	20	26.581	26.174	11
12	21	39.543	40.949	35
13	26	37.714	37.236	35
14	27	39.215	40.645	34
15	47	31.489	32.473	26
16	50	50.893	50.007	35
17	55	40.167	40.283	35
18	64	37.329	40.074	40
19	66	40.697	40.455	30
20	70	43.79	44.204	34
21	79	38.236	38.81	27
22	80	34.93	35.286	15

APPENDIX B

THIN SECTION PHOTOMICROGRAPH

PETROGRAPHIC STUDY OF 30 THIN SECTIONS OF ROCK SAMPLES FROM AL LIDAM AREA

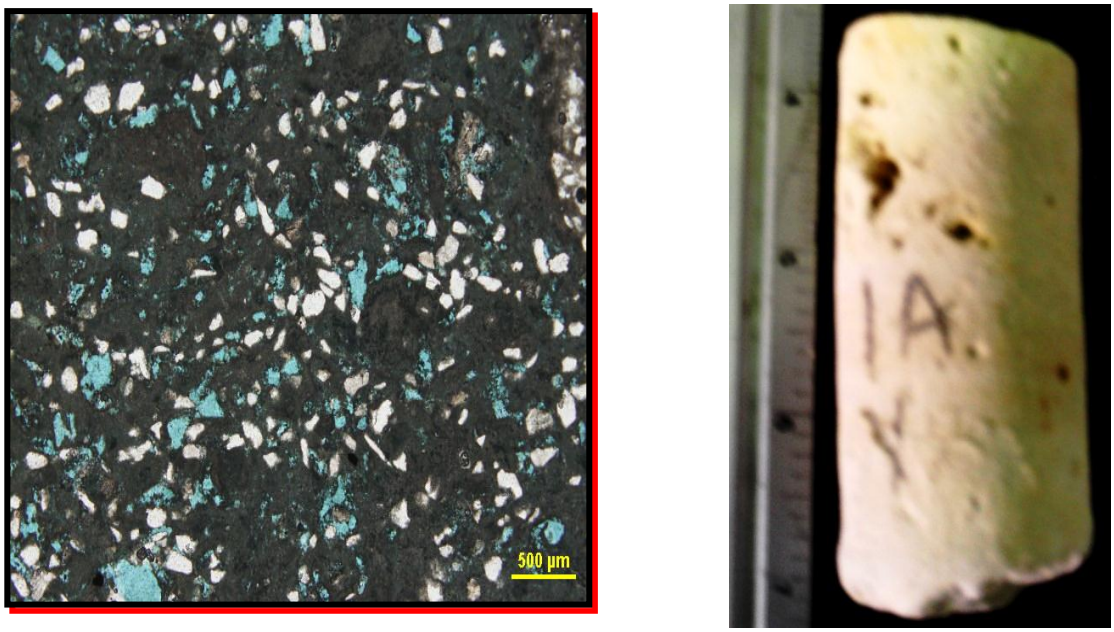

Figure B-1. Thin section photomicrograph for Dam – 1 – A – 3

Descriptions	**Sandy peloidal lime packstone:** Fine to medium-grained (125-250 micron), peloids, intraclasts, forams, unidentified fossils, mainly moldic porosities, minor amounts of intraparticle porosities.
Sample Name	Dam – 1 – A – 3
Porosity	27 %
Permeability	2.4 mD
Pore Size	50-300 micron
Quartz	20 %
Calcite	80 %
Length	3.3 in.
Diameter	1.5 in
Direction	Vertical

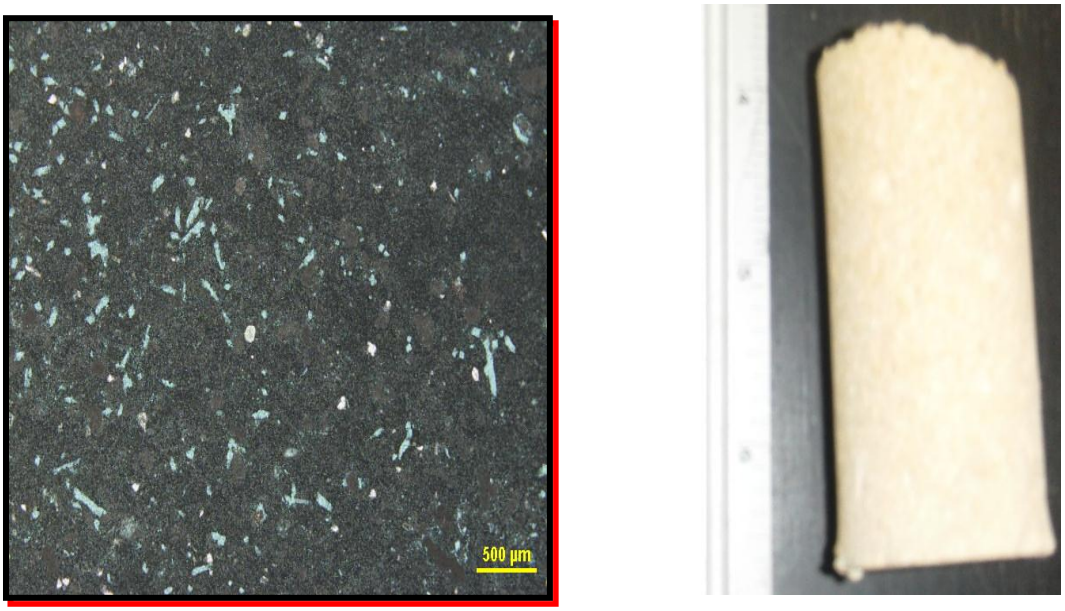

Figure B -2. Thin section photomicrograph for Dam – 1 – B – 5

Descriptions	**Peloidal Lime Wackestone:** Peloids, forams, unidentified fossils, burrowed, mainly moldic porosities, minor amounts of burrow fill and intraparticle porosities.
Sample Name	Dam – 1 – B – 5
Porosity	25%
Permeability	1.7 mD
Pore Size	50-200 micron
Quartz	quartz 2 %
Calcite	98 %
Length	2.8 in
Diameter	1 in.
Direction	Vertical

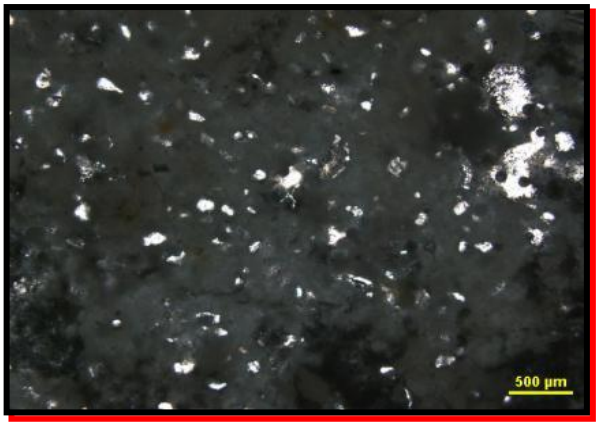

Figure B -3. Thin section photomicrograph for Dam – 1 – B – 6

Descriptions	**Clayey sandy peloidal lime wackestone. (corrupted)**
Sample Name	Dam – 1 – B – 6
Porosity	corrupted
Permeability	corrupted
Pore Size	corrupted
Quartz	corrupted
Calcite	corrupted
Length	2.5 cm
Diameter	1 in.
Direction	Vertical

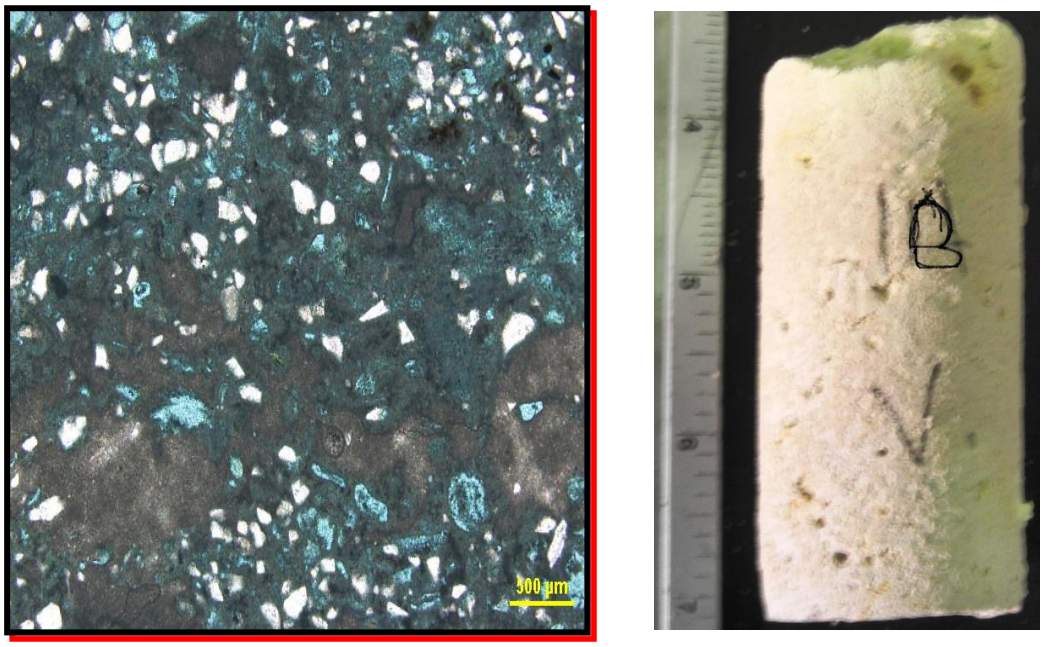

Figure B -4. Thin section photomicrograph for Dam – 2- 8

Descriptions	**Sandy peloidal intraclastic lime packstone:** Fine to medium-grained (125-250 micron), peloids, intraclasts, forams, unidentified fossils, mainly moldic porosities, minor amounts of intraparticle porosities
Sample Name	Dam – 2- 8
Porosity	30 %
Permeability	3.1 mD
Pore Size	size 50-200 micron (up to 2000 micron pore)
Quartz	15%,
Calcite	85%.
Length	3.2 in
Diameter	1 in.
Direction	Vertical

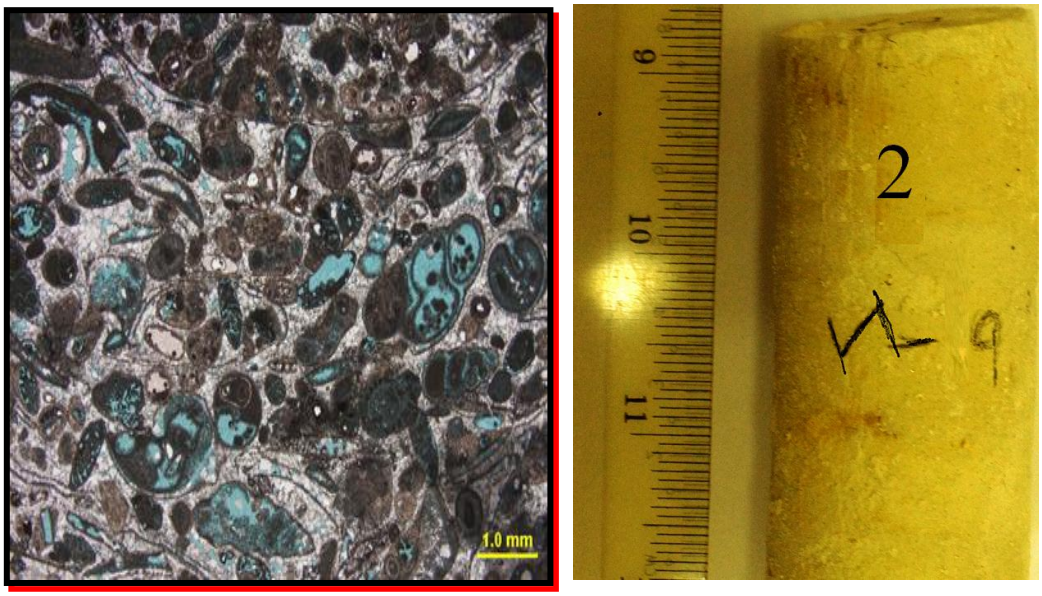

Figure B -5. Thin section photomicrograph for Dam – 2 – 9

Descriptions	**Calcite cemented peloidal oolitic bivalve gastropod lime grainstone:** Medium to coarse-grained (250-1000 micron), peloids, oolites, bivalves, gastropods, forams, well sorted, rounded, interparticle, moldic and intraparticle porosities, interparticle pores reduced by blocky calcite cement and finely bladed isopachous calcite rim cement.
Sample Name	Dam – 2 – 9
Porosity	22%
Permeability	2.6 mD
Pore Size	50-800 micron (up to 3000 micron pore)
Quartz	1%
Calcite	99%
Length	3.5 in.
Diameter	1.5 in.
Direction	Horizontal

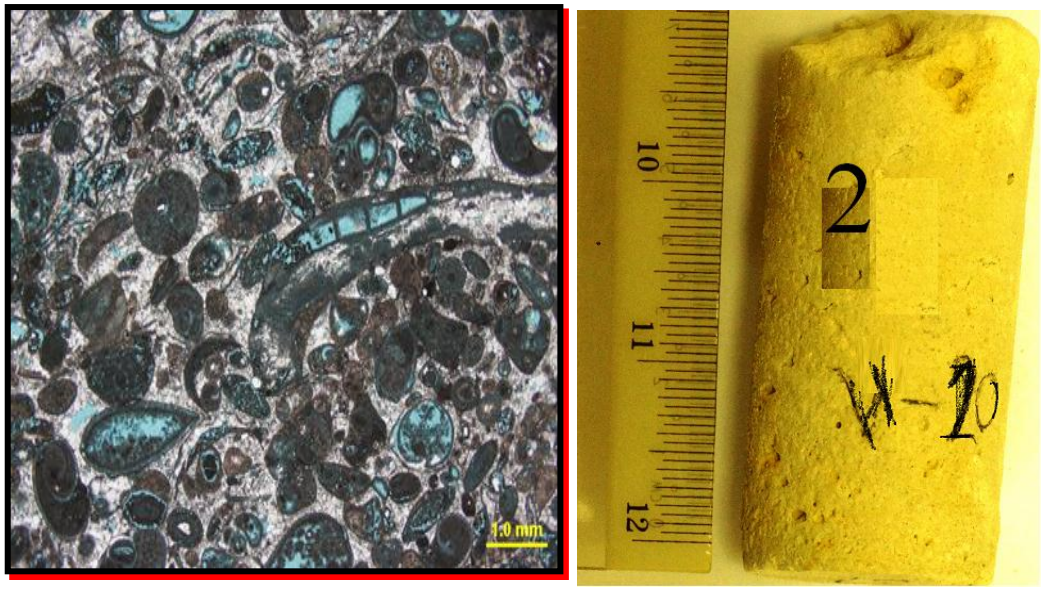

Figure B -6. Thin section photomicrograph for Dam – 2 – 10

Descriptions	**Calcite cemented peloidal oolitic skeletal lime grainstone:** Medium to coarse-grained (250-1000 micron), peloids, oolites, intraclasts, bivalves, gastropods, forams, well sorted, rounded, moldic, interparticle and intraparticle porosities, interparticle pores reduced by blocky calcite cement and finely bladed isopachous calcite rim cement.
Sample Name	Dam – 2 – 10
Porosity	25 %
Permeability	5.2 mD
Pore Size	50-800 micron (up to 1 cm pore)
Quartz	1%
Calcite	99%
Length	2.8 in.
Diameter	1.5 in.
Direction	Horizontal

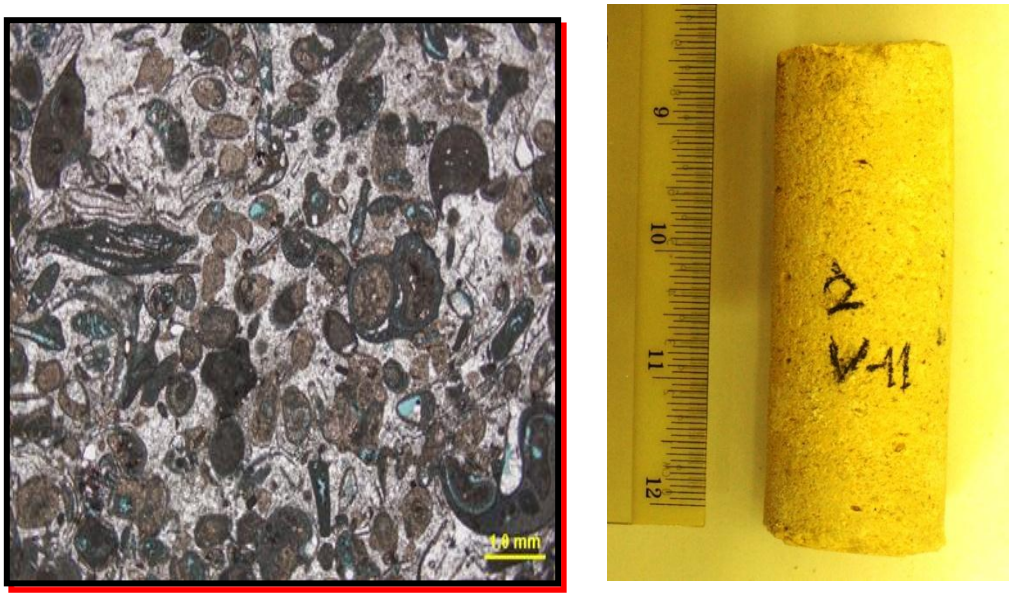

Figure B -7. Thin section photomicrograph for Dam – 2 – 11

Descriptions	**Calcite cemented peloidal oolitic bivalve gastropod lime grainstone:** Medium to coarse-grained (250-1000 micron), peloids, oolites, intraclasts, bivalves, gastropods, forams, well sorted, rounded, intraparticle, moldic, and interparticle porosities, interparticle pores reduced by blocky calcite cement and finely bladed isopachous calcite rim cement.
Sample Name	Dam – 2 – 11
Porosity	22 %
Permeability	1.4 mD
Pore Size	50-300 micron (up to 2000 micron pore)
Quartz	1%
Calcite	99%
Length	3.5 in.
Diameter	1.5 in.
Direction	Horizontal

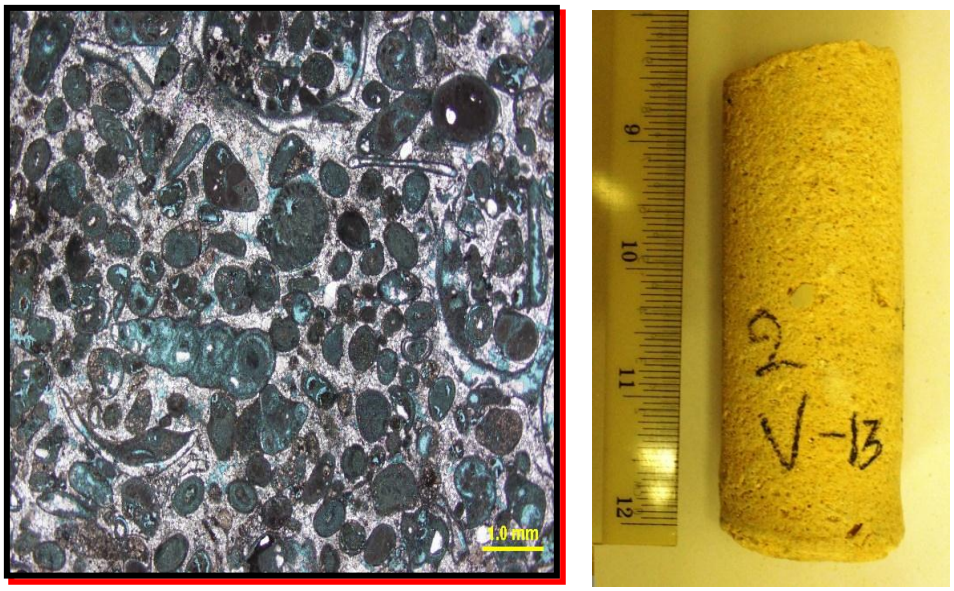

Figure B -8. Thin section photomicrograph for Dam – 2 – 13

Descriptions	**Calcite cemented peloidal oolitic bivalve gastropod lime grainstone:** Medium to coarse-grained (250-1000 micron), peloids, oolites, intraclasts, bivalves, gastropods, forams, well sorted, rounded, intraparticle, moldic, and interparticle porosities, interparticle pores reduced by blocky calcite cement and finely bladed isopachous calcite rim cement.
Sample Name	Dam – 2 – 13
Porosity	29 %
Permeability	7.4 mD
Pore Size	50-400 micron (up to 3000 micron pore)
Quartz	1%
Calcite	99%
Length	3.8 in.
Diameter	1.5 in.
Direction	Vertical

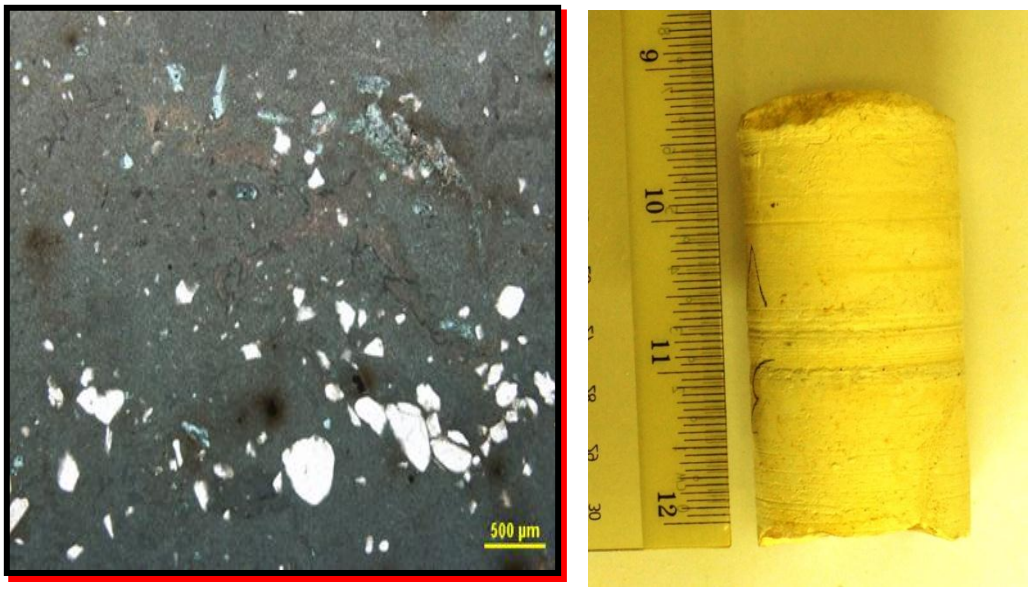

Figure B -9. Thin section photomicrograph for Dam – 3 – 16

Descriptions	**Sandy lime mudstone:** Peloids, unidentified fossils, moldic porosities.
Sample Name	Dam – 3 – 16
Porosity	10 %
Permeability	3.2 mD
Pore Size	50-200 micron
Quartz	10%
Calcite	90%
Length	2.8 in.
Diameter	1.5 in.
Direction	Horizontal

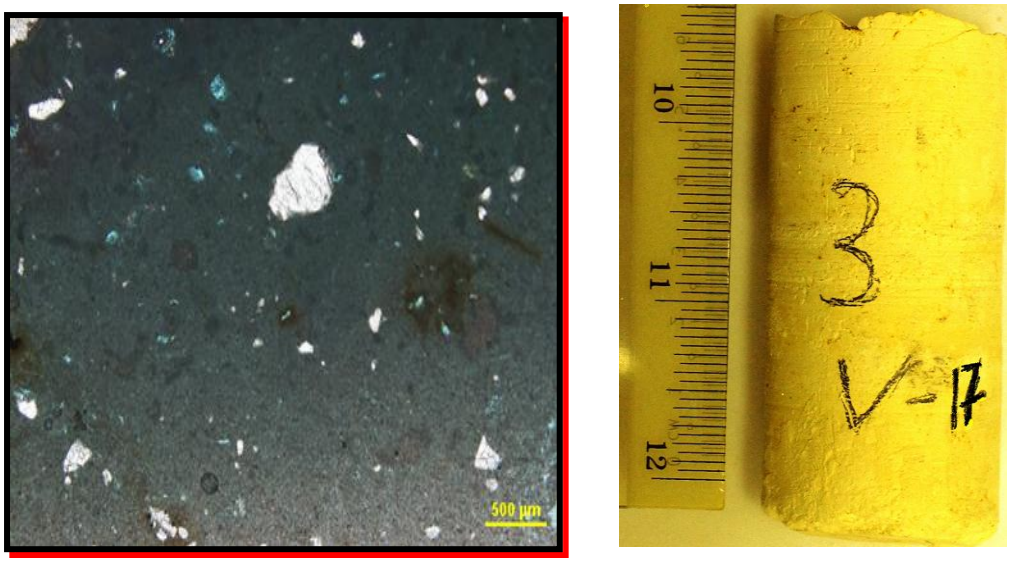

Figure B -10. Thin section photomicrograph for Dam – 3 – 17

Descriptions	**Sandy lime mudstone:** Peloids, intraclasts, moldic porosities, 3% porosity (3% moldic and unknown amount of probable micro porosity), pore size micron, quartz, calcite
Sample Name	Dam – 3 – 17
Porosity	9 %
Permeability	4.1 mD
Pore Size	50-200
Quartz	10%
Calcite	90%
Length	2.3 cm
Diameter	1.5 in.
Direction	Horizontal

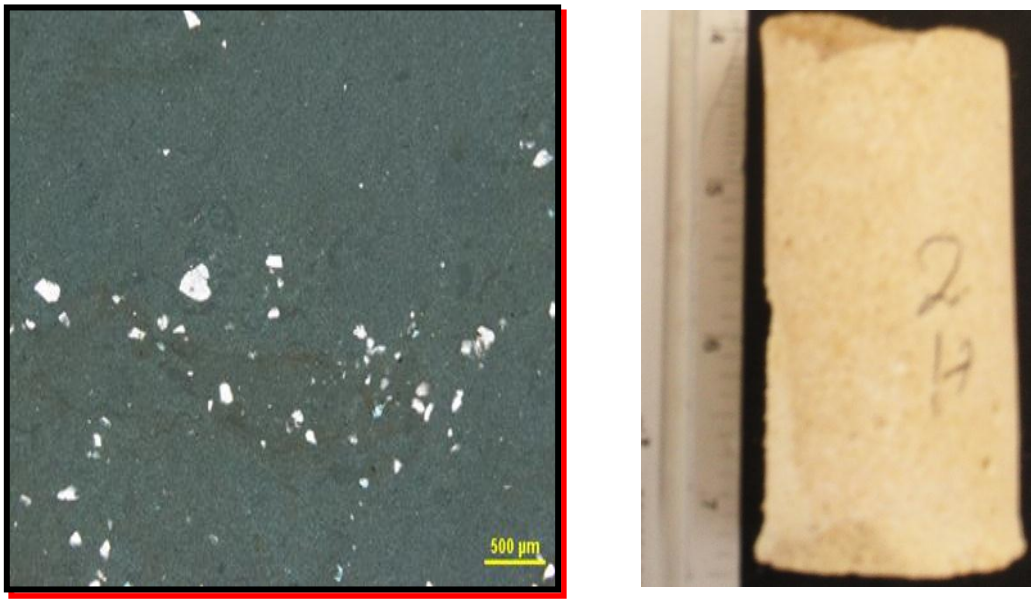

Figure B -11. Thin section photomicrograph for Dam – 3 – 18

Descriptions	**Lime mudstone:** Peloids, burrowed, mainly burrow fill and moldic porosities.
Sample Name	Dam – 3 – 18
Porosity	7 %
Permeability	6.2 mD
Pore Size	50-400 micron
Quartz	5%
Calcite	95%.
Length	3.1 in.
Diameter	1.5 in.
Direction	Horizontal

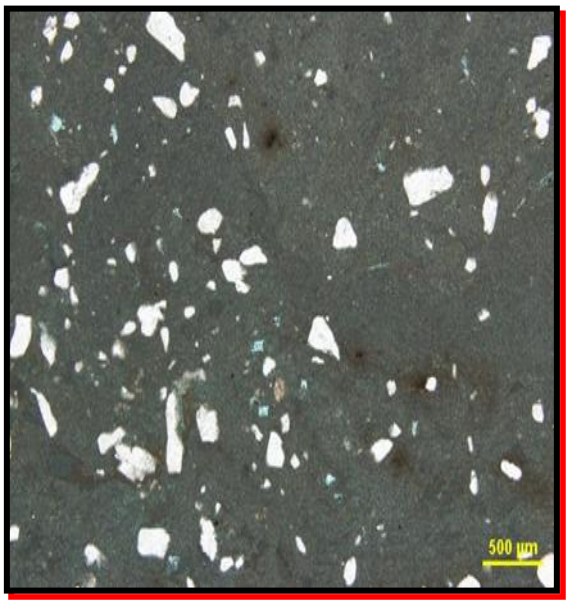

Figure B -12. Thin section photomicrograph for Dam – 3 – 20

Descriptions	**Sandy lime mudstone:** Peloids, burrowed, mainly burrow fill and moldic porosities.
Sample Name	Dam – 3 – 20
Porosity	11 %
Permeability	12.9 mD
Pore Size	50-400 micron
Quartz	10%
Calcite	90%
Length	2.7 in.
Diameter	1.5 in.
Direction	Vertical

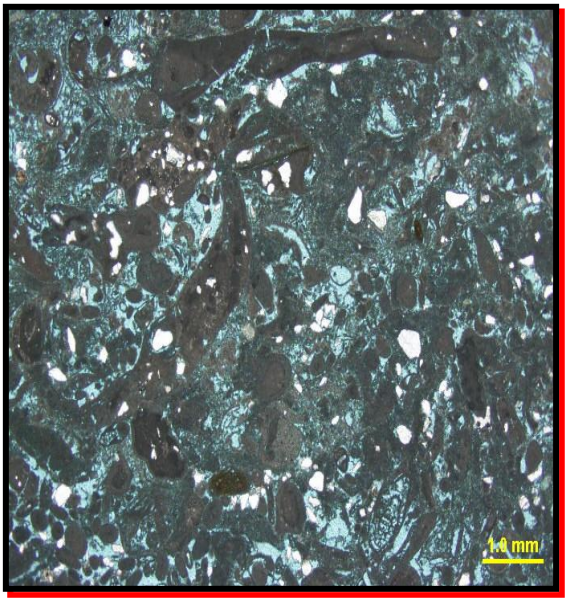

Figure B -13. Thin section photomicrograph for Dam – 4 – A - 21

Descriptions	**Peloidal intraclastic skeletal lime grainstone:** Medium to coarse-grained (250-1000 micron), peloids, intraclasts, bivalves, forams, gastropods, moderately sorted, subrounded, mainly reduced interparticle porosities, minor amounts of intraparticle and moldic porosities, interparticle pores reduced by finely bladed isopachous calcite rim cement, pore size, quartz, calcite
Sample Name	Dam – 4 – A - 21
Porosity	35 %
Permeability	383 mD
Pore Size	50-500 micron
Quartz	7%
Calcite	93%.
Length	2.9 in.
Diameter	1.5 in.
Direction	Vertical

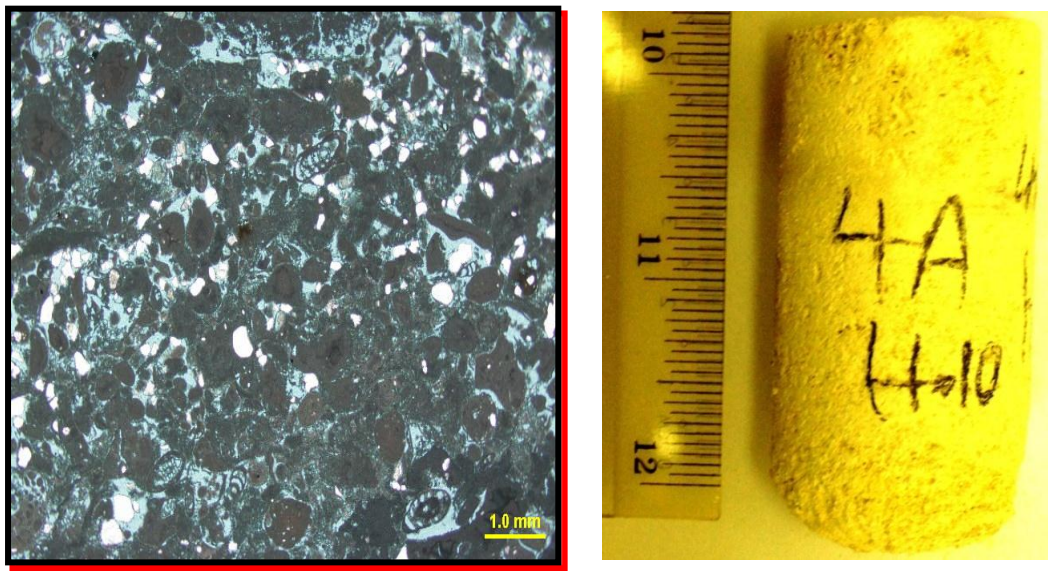

Figure B -14. Thin section photomicrograph for Dam – 4 – A - 26

Descriptions	**Sandy peloidal skeletal lime grainstone:** Medium to coarse-grained (250-1000 micron), peloids, intraclasts, forams, bivalves, gastropods, moderately sorted, subrounded, mainly reduced interparticle porosities, minor amounts of intraparticle and moldic porosities, interparticle pores reduced by finely bladed isopachous calcite rim cement.
Sample Name	Dam – 4 – A - 26
Porosity	34 %
Permeability	645.3 mD
Pore Size	50-500 micron
Quartz	10%
Calcite	90%.
Length	2.2 in.
Diameter	1.5 in.
Direction	Horizontal

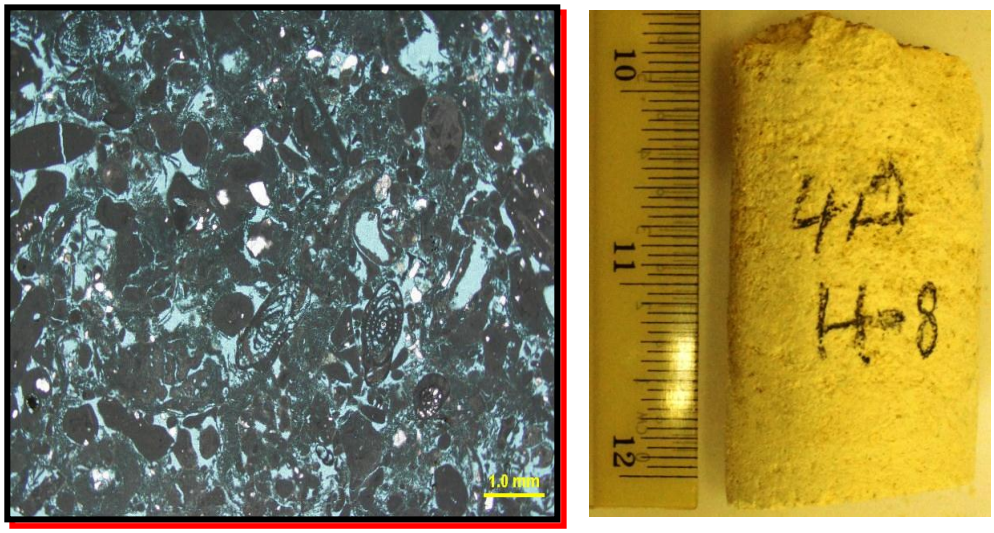

Figure B -15. Thin section photomicrograph for Dam – 4 – A - 27

Descriptions	**Peloidal skeletal lime grainstone:** Medium to coarse-grained (250-1000 micron), peloids, intraclasts, forams, bivalves, gastropods, corals, moderately sorted, subrounded, mainly reduced interparticle porosities, minor amounts of intraparticle and moldic porosities, interparticle pores reduced by finely bladed isopachous calcite rim cement. pore size, quartz, calcite
Sample Name	Dam – 4 – A - 27
Porosity	35 %
Permeability	789 mD
Pore Size	50-500 micron
Quartz	5%
Calcite	95%.
Length	1.9 cm
Diameter	1.5 in.
Direction	Horizontal

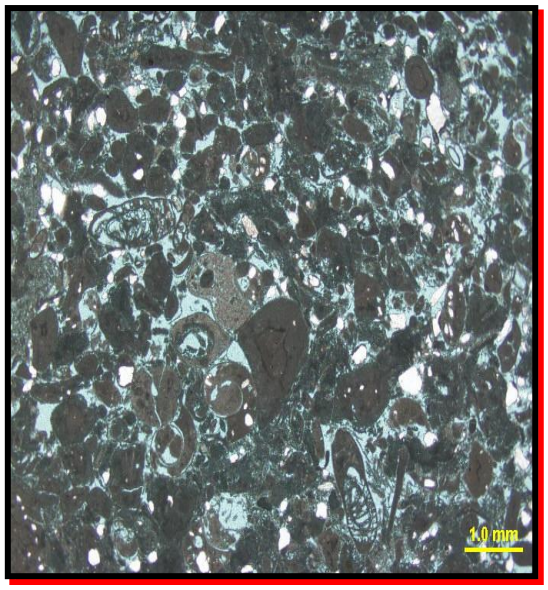

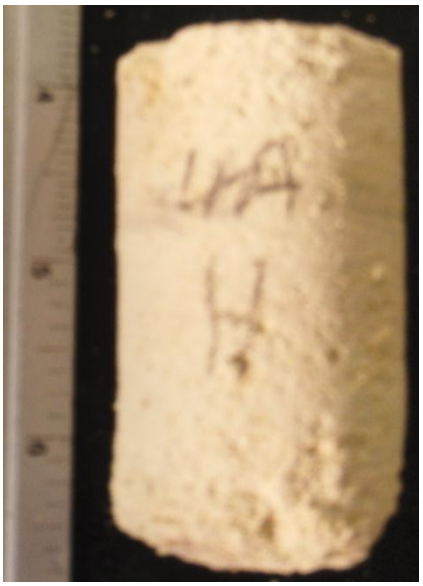

Figure B -16. Thin section photomicrograph for Dam – 4 – A - 29

Descriptions	**Peloidal skeletal lime grainstone:** Medium to coarse-grained (250-1000 micron), peloids, intraclasts, forams, bivalves, gastropods, moderately sorted, subrounded, mainly reduced interparticle porosities, minor amounts of intraparticle and moldic porosities, interparticle pores reduced by finely bladed isopachous calcite rim cement.
Sample Name	Dam – 4 – A - 29
Porosity	33 %
Permeability	299.5 mD
Pore Size	50-500 micron
Quartz	4%
Calcite	96%
Length	2.3 in.
Diameter	1.5 in.
Direction	Horizontal

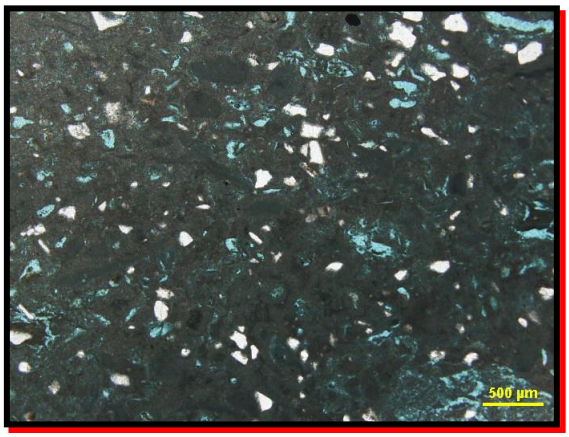

Figure B -17. Thin section photomicrograph for Dam – 5 – 46

Descriptions	**Sandy peloidal skeletal lime packstone:** Fine to medium-grained (125-250 micron), peloids, intraclasts, bivalves, forams, unidentified fossils, mainly moldic porosities, minor amounts of intraparticle porosities.
Sample Name	Dam – 5 – 46
Porosity	25 %
Permeability	Broken
Pore Size	50-200 micron
Quartz	10%,
Calcite	90%.
Length	1.9 cm
Diameter	1 in.
Direction	Horizontal

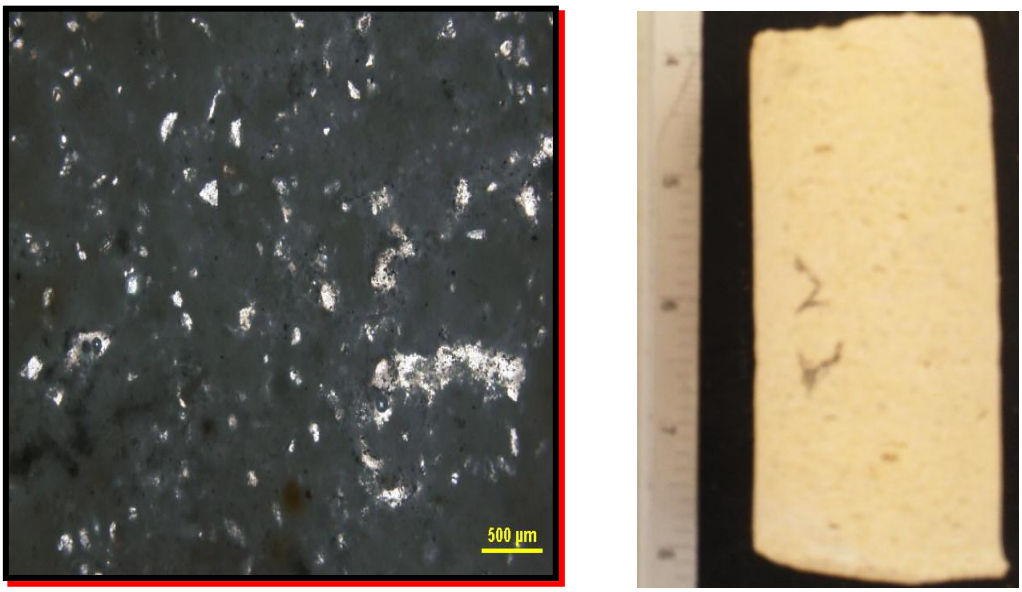

Figure B -18. Thin section photomicrograph for Dam – 5 – 47

Descriptions	**Sandy peloidal skeletal lime packstone. (corrupted)**
Sample Name	Dam – 5 – 47
Porosity	25 %
Permeability	12.2 mD
Pore Size	(corrupted)
Quartz	(corrupted)
Calcite	(corrupted)
Length	3.9 in.
Diameter	1 in.
Direction	Horizontal

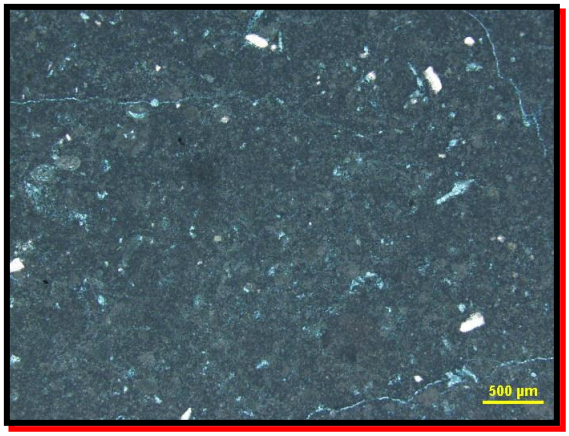

Figure B -19. Thin section photomicrograph for Dam – 5 – 48

Descriptions	**Peloidal skeletal lime packstone:** Fine to medium-grained (125-250 micron), peloids, intraclasts, unidentified fossils, fracture, leached dolomite and moldic porosities.
Sample Name	Dam – 5 – 48
Porosity	20 %
Permeability	Broken
Pore Size	50-200 micron
Quartz	2%
Calcite	98%
Length	Broken
Diameter	1.0 in.
Direction	Horizontal

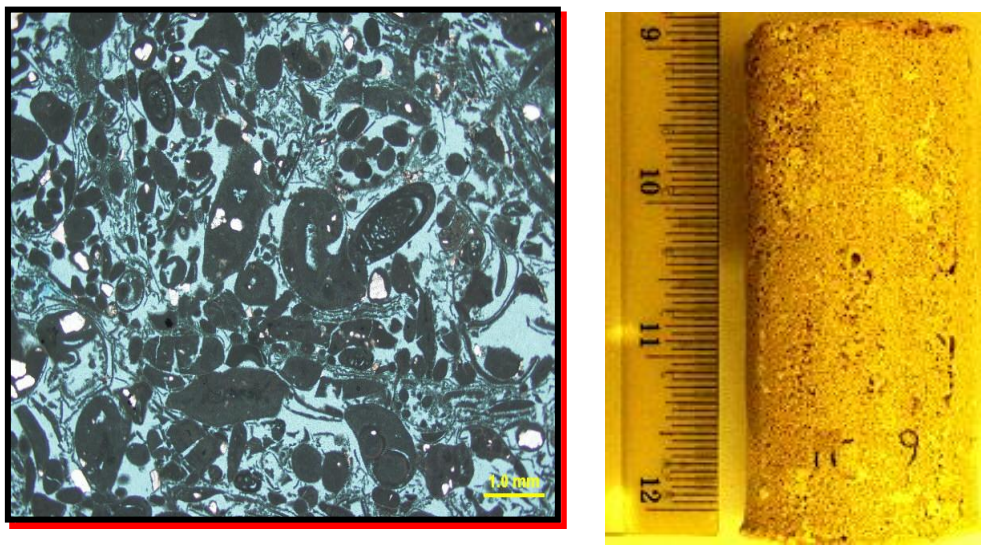

Figure B -20. Thin section photomicrograph for Dam – 6 – A – 50

Descriptions	**Peloidal skeletal lime grainstone:** Medium to coarse-grained (250-1000 micron), peloids, coated grains, intraclasts, forams, bivalves, gastropods, well sorted, rounded, mainly reduced interparticle porosities, minor amounts of moldic and intraparticle porosities, interparticle pores reduced by finely bladed isopachous calcite rim cement.
Sample Name	Dam – 6 – A – 50
Porosity	35 %
Permeability	5351.4 mD
Pore Size	50-600 micron
Quartz	3%
Calcite	97%.
Length	3.0 in.
Diameter	1.5 in.
Direction	Vertical

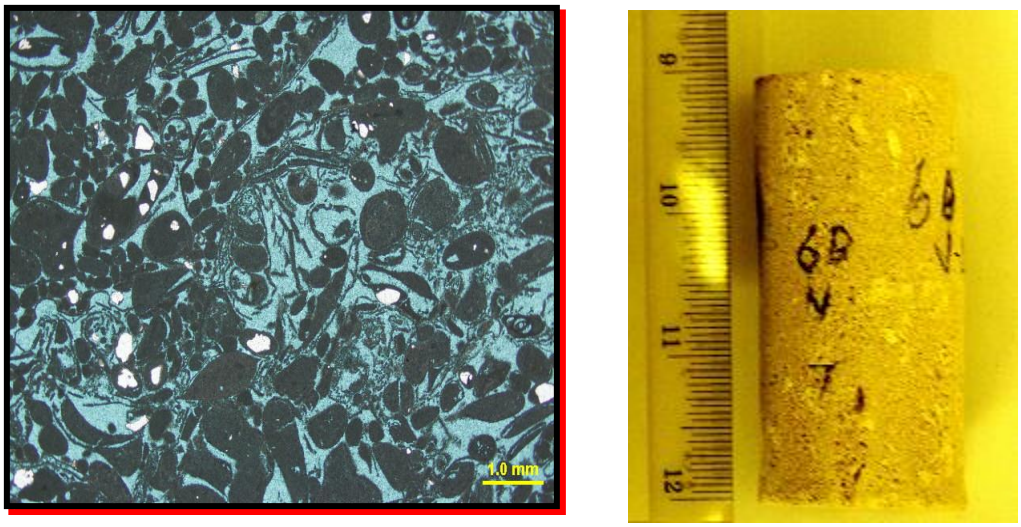

Figure B -21. Thin section photomicrograph for Dam – 6 – B – 55

Descriptions	**Peloidal skeletal lime grainstone:** Medium to coarse-grained (250-1000 micron), peloids, coated grains, intraclasts, forams, bivalves, gastropods, well sorted, rounded, mainly reduced interparticle porosities, minor amounts of moldic and intraparticle porosities, interparticle pores reduced by finely bladed isopachous calcite rim cement.
Sample Name	Dam – 6 – B – 55
Porosity	35 %
Permeability	9180.6 mD
Pore Size	50-700 micron
Quartz	3%
Calcite	97%.
Length	3.0 in.
Diameter	1.5 in.
Direction	Vertical

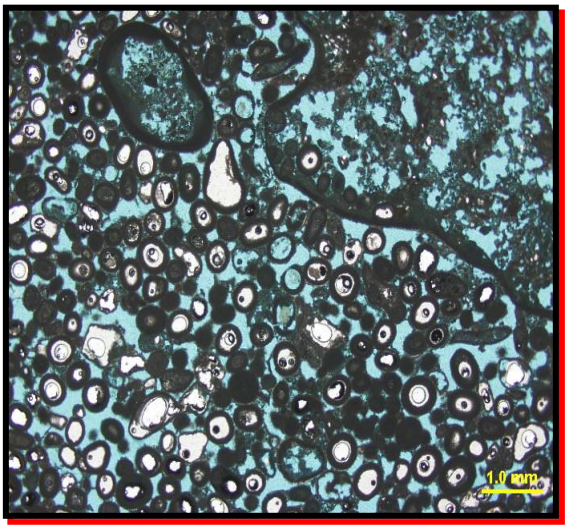

Figure B -22. Thin section photomicrograph for Dam – 6 – B – 56

Descriptions	**Oolitic intraclastic peloidal lime grainstone:** Medium-grained (250-500 micron), oolites, intraclasts, peloids, and well sorted, well rounded, mainly interparticle porosities, moderate amounts of moldic and intraparticle porosities, interparticle pores reduced by finely bladed isopachous calcite rim cement.
Sample Name	Dam – 6 – B – 56
Porosity	40 %
Permeability	3165.8 mD
Pore Size	50-500
Quartz	1%
Calcite	99%
Length	3.1 in.
Diameter	1.5 in.
Direction	Horizontal

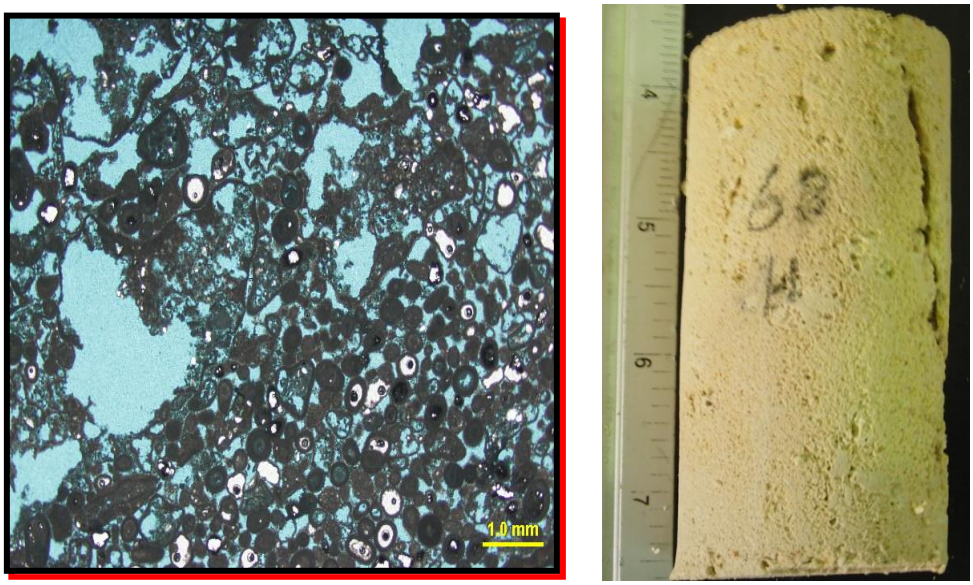

Figure B -23. Thin section photomicrograph for Dam – 6 – B – 64

Descriptions	**Oolitic intraclastic peloidal lime grainstone:** Medium-grained (250-500 micron), oolites, intraclasts, peloids, well sorted, well rounded, mainly moldic porosities, moderate amounts of interparticle and intraparticle porosities, interparticle pores reduced by finely bladed isopachous calcite rim cement.
Sample Name	Dam – 6 – B – 64
Porosity	40 %
Permeability	7336.9 mD
Pore Size	50-400 micron (up to 0.8 cm. pore)
Quartz	1%
Calcite	99%
Length	3.9 in
Diameter	1.0 in.
Direction	Horizontal

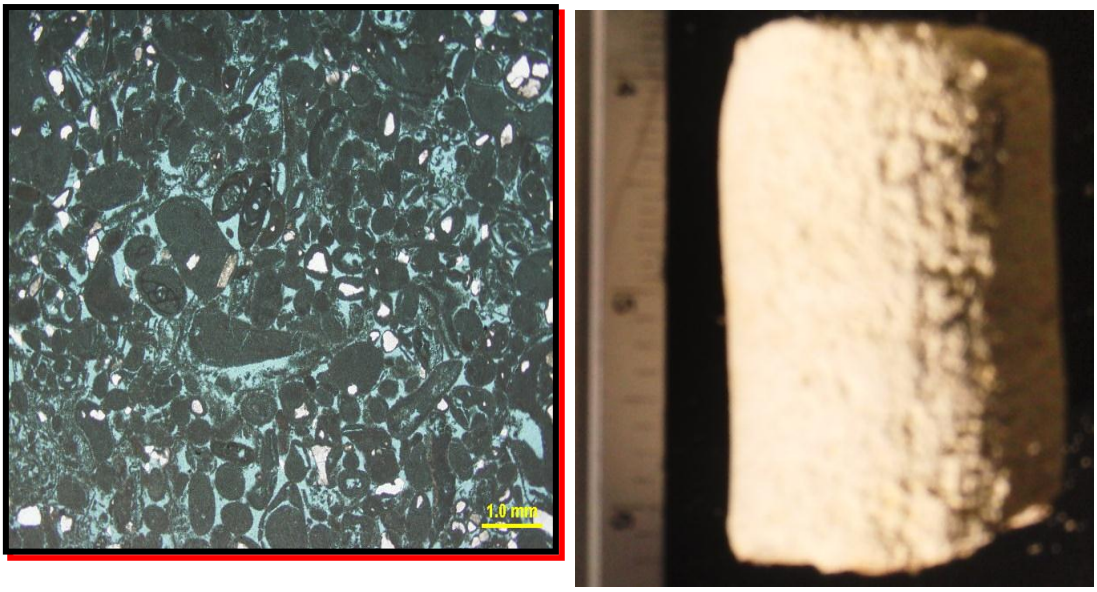

Figure B-24. Thin section photomicrograph for Dam – 7 – 66

Descriptions	**Peloidal skeletal lime grainstone:** Medium to coarse-grained (250-1000 micron), peloids, coated grains, intraclasts, forams, bivalves, gastropods, well sorted, well rounded, mainly reduced interparticle porosities, minor amounts of moldic porosities and intraparticle porosities, interparticle pores reduced by finely bladed isopachous calcite rim cement, pore size, quartz, calcite
Sample Name	Dam – 7 – 66
Porosity	30 %
Permeability	14419.4 mD
Pore Size	50-400 micron
Quartz	5%
Calcite	95%.
Length	2.0 in.
Diameter	1.5 in.
Direction	Vertical

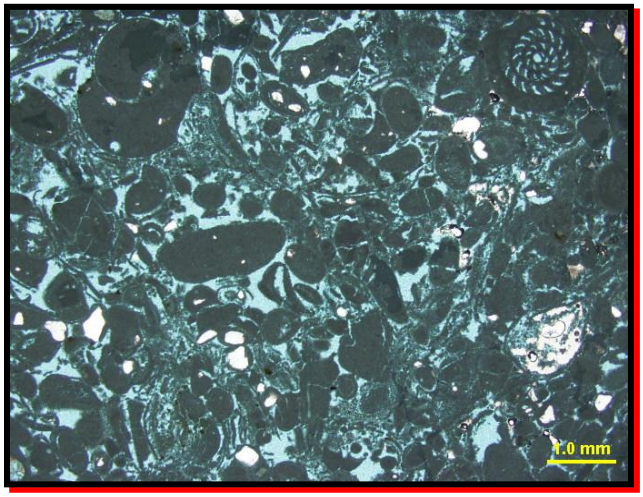

Figure B-25. Thin section photomicrograph for Dam – 7 – 67

Descriptions	**Peloidal skeletal lime grainstone:** Medium to coarse-grained (250-1000 micron), peloids, coated grains, intraclasts, forams, bivalves, gastropods, well sorted, well rounded, mainly reduced interparticle porosities, minor amounts of moldic porosities and intraparticle porosities, interparticle pores reduced by finely bladed isopachous calcite rim cement, pore size, quartz, calcite
Sample Name	Dam – 7 – 67
Porosity	35 %
Permeability	Broken
Pore Size	50-400 micron
Quartz	5%
Calcite	95%.
Length	Broken
Diameter	1.5 in.
Direction	Vertical

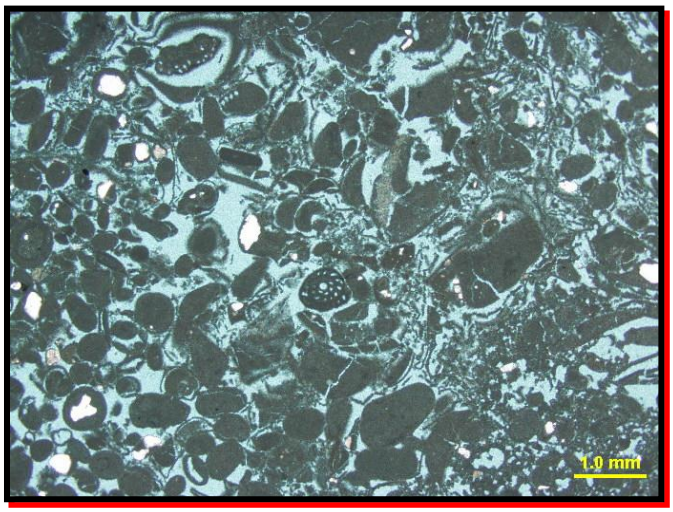

Figure B-26. Thin section photomicrograph for Dam – 7 – 68

Descriptions	**Peloidal skeletal lime grainstone:** Medium to coarse-grained (250-1000 micron), peloids, coated grains, intraclasts, forams, bivalves, gastropods, well sorted, well rounded, mainly reduced interparticle porosities, minor amounts of moldic porosities and intraparticle porosities, interparticle pores reduced by finely bladed isopachous calcite rim cement.
Sample Name	Dam – 7 – 68
Porosity	35 %
Permeability	Broken
Pore Size	50-800 micron (few up to 1000 micron pores)
Quartz	5%
Calcite	95%
Length	Broken
Diameter	1.5 in.
Direction	Vertical

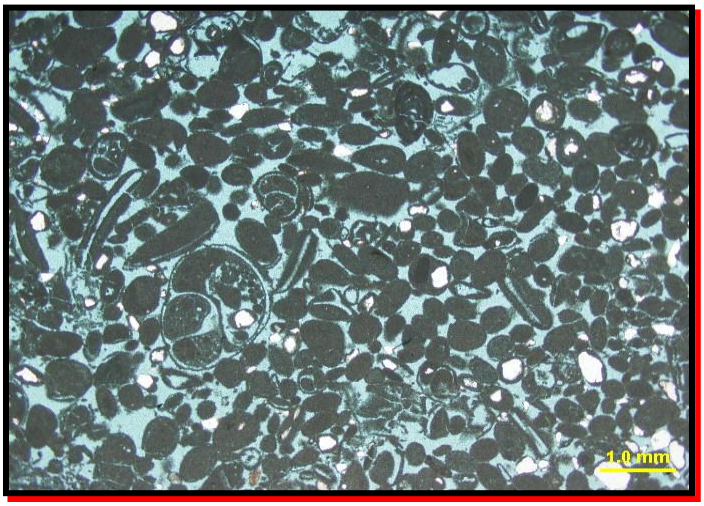

Figure B-27. Thin section photomicrograph for Dam – 7 – 69

Descriptions	**Peloidal skeletal lime grainstone:** Medium to coarse-grained (250-1000 micron), peloids, coated grains, intraclasts, forams, bivalves, gastropods, well sorted, well rounded, mainly reduced interparticle porosities, minor amounts of moldic porosities and intraparticle porosities, interparticle pores reduced by finely bladed isopachous calcite rim cement.
Sample Name	Dam – 7 – 69
Porosity	35 %
Permeability	Broken
Pore Size	50-500 micron (few up to 3000 micron pores)
Quartz	3%
Calcite	97%.
Length	Broken
Diameter	1.5 in.
Direction	Vertical

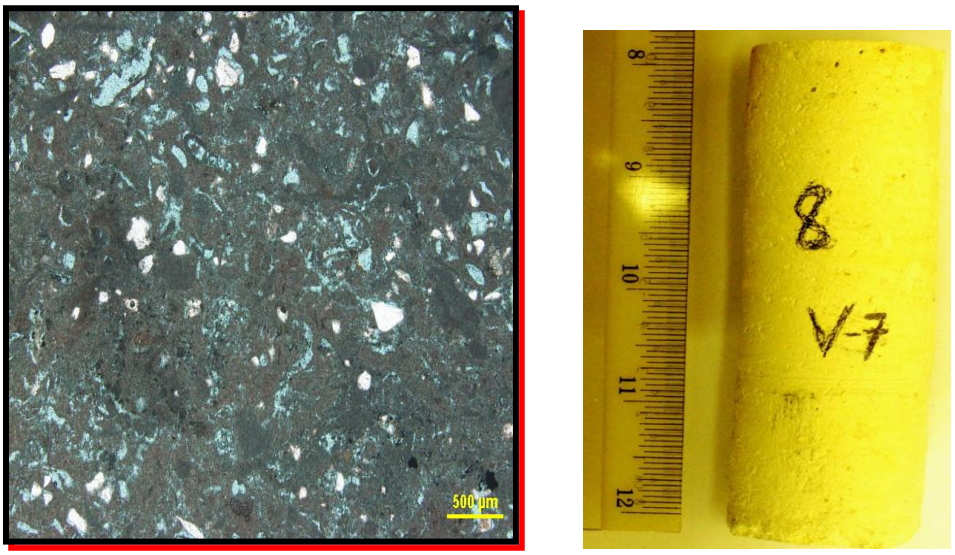

Figure B-28. Thin section photomicrograph for Dam – 8 – 70

Descriptions	**Peloidal skeletal lime packstone/grain dominaned lime packstone:** Fine to medium-grained (125-250 micron), peloids, pellets, intraclasts, bivalves, forams, unidentified fossils, mainly moldic porosities, minor amounts of interparticle and intraparticle porosities.
Sample Name	Dam – 8 – 70
Porosity	34 %
Permeability	0.4 mD
Pore Size	50-300 micron (few up to 2000 micron pores)
Quartz	5%
Calcite	95%
Length	4.0 in.
Diameter	1.5 in.
Direction	Vertical

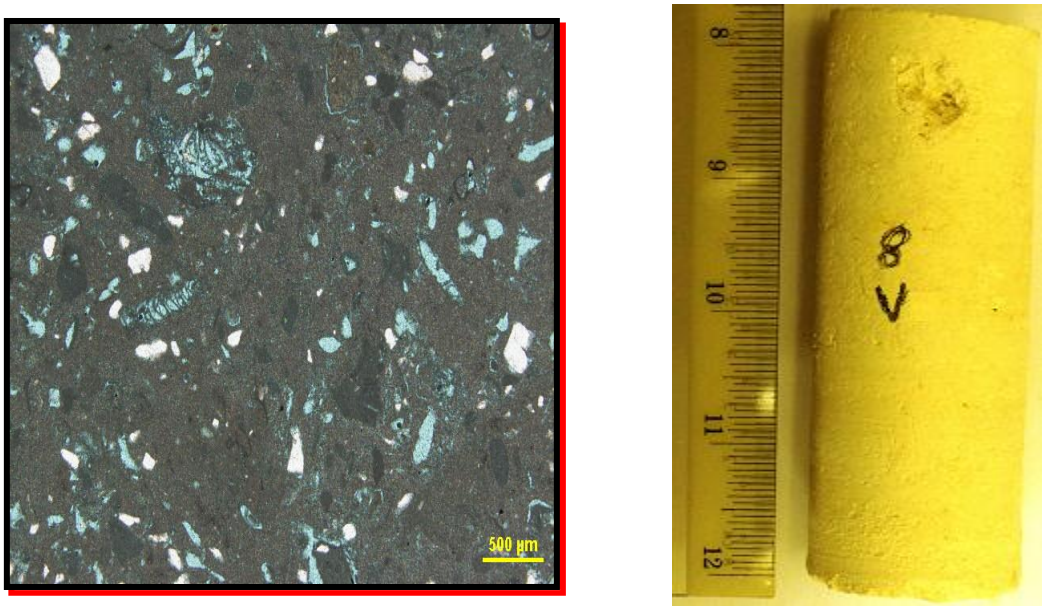

Figure B-29. Thin section photomicrograph for Dam – 8 – 79

Descriptions	**Peloidal skeletal lime wackestone:** Fine to medium-grained (125-250 micron), peloids, pellets, bivalves, forams, echinoids, unidentified fossils, mainly moldic porosities, minor amounts of intraparticle porosities, 15% porosity (12% moldic and 3% intraparticle), pore size, quartz, calcite.
Sample Name	Dam – 8 – 79
Porosity	27 %
Permeability	1.8 mD
Pore Size	50-200 micron (few up to 1000 micron pores)
Quartz	3%
Calcite	97%
Length	4.4 in.
Diameter	1.0 in.
Direction	Vertical

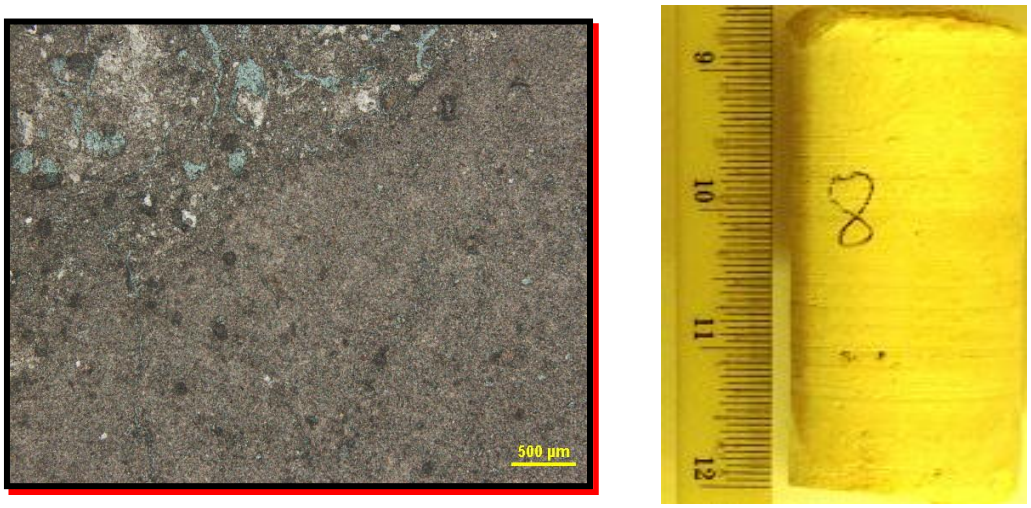

Figure B -30. Thin section photomicrograph for Dam – 8 – 80

Descriptions	**Peloidal lime mudstone:** Peloids**,** forams, unidentified fossils, burrowed, mainly burrow fill porosities, minor amounts of fracture and moldic porosities. pore size, calcite
Sample Name	Dam – 8 – 80
Porosity	15 %
Permeability	3.0 mD
Pore Size	50-400 micron
Quartz	---
Calcite	100%.
Length	3.2 in.
Diameter	1.0 in.
Direction	Vertical

APPENDIX C

ACOUSTIC DATA (DRY)

Table C: P-Wave and S-Waves Velocity and their ratio as a Function of the Confining Pressure.

Serial No.	Sample Name.	Confining Pressure (MPa)	P (m/s)	S1 (m/s)	S2 (m/s)	P/S1
1	Dam-1-A-1	5	2066	1504	1508	1.37367
		10	2077	1543	1550	1.346079
		15	2091	1569	1579	1.332696
		20	2274	1693	1688	1.343178
		25	2309	1707	1698	1.352665
2	Dam-2-12	5	3903	2153	2211	1.812819
		10	3977	2239	2239	1.776239
		15	4008	2240	2235	1.789286
		20	4054	2267	2261	1.788266
		25	4080	2276	2266	1.792619
3	Dam-2-13	5	2286	1704	1715	1.341549
		10	2643	1875	1887	1.4096
		15	2874	1899	1899	1.513428
		20	2920	1966	1967	1.485249
		25	3134	1975	1692	1.586835
4	Dam-2-14	5	2755	1585	1514	1.73817
		10	3050	1625	1629	1.876923
		15	3053	1727	1707	1.767805
		20	3099	1779	1767	1.74199
		25	3169	1799	1682	1.761534
5	Dam-2-15	5	2182	1699	1605	1.284285
		10	2535	1709	1699	1.483324
		15	2620	1850	1850	1.416216
		20	2863	1910	1913	1.498953
		25	2910	1930	1920	1.507772
6	Dam-3-19	5	2583	1452	1423	1.778926
		10	2600	1469	1435	1.769912
		15	2606	1474	1436	1.767978
		20	2612	1484	1478	1.760108
		25	2635	1491	1489	1.76727
7	Dam-4-A-21	5	2649	1507	1491	1.757797
		10	2685	1529	1517	1.75605
		15	2729	1542	1530	1.76978
		20	2710	1559	1540	1.738294
		25	2685	1579	1544	1.700443
8	Dam-4-A-22	5	2312	1466	1471	1.57708
		10	2425	1477	1484	1.641842
		15	2439	1494	1453	1.63253
		20	2480	1839	1828	1.348559
		25	2612	1900	1915	1.374737

Table C: P-Wave and S-Waves Velocity and their ratio as a Function of the Confining Pressure.

9	Dam-4-A-23	5	2349	1556	1506	1.50964
		10	2422	1577	1567	1.535828
		15	2439	1584	1570	1.539773
		20	2437	1586	1575	1.53657
		25	2461	1598	1579	1.54005
10	Dam-4-A-24	5	2499	1511	1513	1.653872
		10	2525	1520	1526	1.661184
		15	2548	1526	1527	1.669725
		20	2552	1548	1534	1.648579
		25	2578	1568	1544	1.644133
11	Dam-4-A-25	5	2643	1529	1514	1.728581
		10	2667	1603	1589	1.663755
		15	2677	1697	1687	1.57749
		20	2686	1727	1725	1.555298
		25	2689	1732	1738	1.55254
12	Dam-4-B-38	5	2807	1715	1710	1.636735
		10	2826	1730	1721	1.633526
		15	2821	1740	1739	1.621264
		20	2905	1755	1740	1.655271
		25	2926	1777	1752	1.646595
13	Dam-6-A-54	5	1846	1212	1194	1.523102
		10	1860	1282	1248	1.450858
		15	1876	1347	1348	1.392725
		20	1897	1378	1369	1.376633
		25	2065	1388	1399	1.487752
14	Dam-6-B-55	5	2750	1644	1630	1.672749
		10	2764	1646	1635	1.679222
		15	2775	1662	1639	1.669675
		20	2808	1674	1665	1.677419
		25	2846	1689	1673	1.685021
15	Dam-6-B-58	5	3188	1930	1920	1.651813
		10	3281	1970	1950	1.665482
		15	3330	1992	1975	1.671687
		20	3345	2018	1992	1.657582
		25	3370	2023	2003	1.665843
16	Dam-6-B-61	5	3281	2006	2007	1.635593
		10	3389	2009	2011	1.686909
		15	3395	2012	20015	1.687376
		20	3382	2018	2017	1.675917
		25	3468	2027	2033	1.710903

Table C: P-Wave and S-Waves Velocity and their ratio as a Function of the Confining Pressure.

17	Dam-6-B-62	5	2978	1901	1880	1.566544
		10	2982	1919	1903	1.553934
		15	3001	1929	1925	1.555728
		20	3016	1946	1947	1.549846
		25	3061	1952	1951	1.568135
18	Dam-7-66	5	1961	1478	1469	1.326793
		10	1968	1501	1492	1.311126
		15	1979	1521	1518	1.301118
		20	1997	1537	1532	1.299284
		25	2005	1553	1554	1.29105
19	Dam-8-71	5	2551	1577	1592	1.617628
		10	2599	1601	1618	1.62336
		15	2654	1629	1642	1.62922
		20	2662	1645	1658	1.618237
		25	2733	1655	1670	1.65136
20	Dam-8-72	5	2544	1316	1318	1.933131
		10	2558	1338	1322	1.911809
		15	2566	1349	1337	1.90215
		20	2576	1355	1345	1.901107
		25	2585	1364	1352	1.895161
21	Dam-8-73	5	2542	1810	1779	1.40442
		10	2587	1845	1803	1.402168
		15	2622	1867	1817	1.404392
		20	2646	1872	1829	1.413462
		25	2661	1875	1832	1.4192
22	Dam-8-74	5	2610	1608	1634	1.623134
		10	2615	1628	1637	1.606265
		15	2620	1642	1643	1.595615
		20	2628	1665	1654	1.578378
		25	2636	1689	1647	1.560687
23	Dam-8-75	5	2607	1526	1491	1.708388
		10	2609	1542	1510	1.691958
		15	2611	1551	1524	1.68343
		20	2620	1559	1529	1.680564
		25	2630	1560	1529	1.685897
24	Dam-8-76	5	2516	1529	1474	1.64552
		10	2524	1540	1516	1.638961
		15	2534	1546	1544	1.639069
		20	2564	1557	1561	1.646757
		25	2576	1570	1579	1.640764

Table C: P-Wave and S-Waves Velocity and their ratio as a Function of the Confining Pressure.

25	Dam-8-77	5	2525	1541	1505	1.638546
		10	2533	1549	1522	1.635249
		15	2539	1560	1534	1.627564
		20	2545	1560	1544	1.63141
		25	2550	1569	1547	1.625239
26	Dam-8-81	5	2727	1756	1796	1.552961
		10	2752	1772	1801	1.553047
		15	2754	1784	1815	1.543722
		20	2763	1788	1817	1.545302
		25	2774	1793	1825	1.547128

APPENDIX D

ACOUSTIC DATA (WET)

Table D: P-Wave and S-Waves Velocity and their ratio as a Function of the Confining Pressure.

Serial No.	Sample No.	E.C.P (MPa)	Vp (m/s)	Vs1 (m/s)	Vs2 (m/s)	Vp/Vs1
1	Dam-1-A-1	5	2579	1247	1257	2.0681
		10	2597	1266	1276	2.0513
		15	2675	1384	1379	1.9328
		20	2709	1409	1392	1.9226
2	Dam-2-12	5	4065	2063	2016	1.9704
		10	4151	2127	2075	1.9515
		15	4175	2167	2111	1.9266
		20	4178	2199	2140	1.8999
3	Dam-2-13	5	3090	1447	1435	2.1354
		10	3075	1463	1463	2.1018
		15	3112	1482	1488	2.0998
		20	3200	1507	1501	2.1234
4	Dam-2-14	5	3355	1519	1521	2.2086
		10	3418	1647	1652	2.0752
		15	3422	1683	1683	2.0332
		20	3444	1698	1703	2.0282
5	Dam-2-15	5	3067	1317	1167	2.3277
		10	3126	1350	1346	2.3155
		15	3213	1399	1381	2.2966
		20	3410	1443	1438	2.3631
6	Dam-3-19	5	2818	1307	1349	2.1560
		10	2827	1319	1365	2.1432
		15	2854	1324	1371	2.1555
		20	2865	1315	1372	2.1787
7	Dam-4-A-21	5	2685	1529	1517	1.7560
		10	2729	1542	1530	1.7697
		15	2710	1549	1540	1.7495
		20	2685	1549	1544	1.7333
8	Dam-4-A-22	5	2425	1477	1484	1.6418
		10	2439	1494	1453	1.6325
		15	2480	1539	1528	1.6114
		20	2612	1600	1615	1.6325
9	Dam-4-A-23	5	2422	1577	1567	1.5358
		10	2439	1584	1570	1.5397
		15	2437	1586	1575	1.5365
		20	2461	1588	1579	1.5497
10	Dam-4-A-24	5	2784	1222	1141	2.2782
		10	2985	1270	1255	2.3503
		15	3017	1290	1290	2.3387
		20	3056	1333	1327	2.2925

Table D: P-Wave and S-Waves Velocity and their ratio as a Function of the Confining Pressure.

11	Dam-4-A-25	5	2961	1208	1211	2.451159
		10	2981	1257	1239	2.371519
		15	2987	1279	1280	2.335418
		20	3035	1319	1315	2.300986
12	Dam-4-B-38	5	3649	1416	1416	2.576977
		10	3675	1531	1539	2.400392
		15	3719	1559	1550	2.385504
		20	3756	1581	1565	2.375712
13	Dam-6-B-58	5	3581	1770	1750	2.023164
		10	3630	1792	1775	2.02567
		15	3695	1808	1782	2.043695
		20	3682	1813	1803	2.030888
14	Dam-6-B-61	5	3689	1531	1500	2.409536
		10	3695	1546	1515	2.390039
		15	3682	1563	1556	2.355726
		20	3768	1573	1571	2.395423
15	Dam-6-B-62	5	3282	1819	1803	1.804288
		10	3301	1829	1825	1.804811
		15	3316	1836	1837	1.8061
		20	3361	1852	1851	1.814795
16	Dam-7-66	5	2168	1401	1392	1.547466
		10	2159	1421	1418	1.519353
		15	2197	1437	1432	1.52888
		20	2265	1453	1454	1.558844
17	Dam-8-71	5	2899	1501	1518	1.931379
		10	2954	1529	1542	1.931982
		15	2962	1545	1558	1.917152
		20	3003	1555	1570	1.93119
18	Dam-8-72	5	2718	1238	1222	2.195477
		10	2736	1249	1237	2.190552
		15	2836	1255	1245	2.259761
		20	2825	1264	1252	2.234968
19	Dam-8-73	5	2987	1645	1603	1.815805
		10	3022	1667	1617	1.812837
		15	3046	1672	1629	1.82177
		20	3061	1675	1632	1.827463
20	Dam-8-74	5	2905	1428	1437	2.034314
		10	2910	1442	1443	2.018031
		15	2928	1455	1444	2.012371
		20	2936	1489	1447	1.971793

Table D: P-Wave and S-Waves Velocity and their ratio as a Function of the Confining Pressure.

21	Dam-8-75	5	2611	1342	1310	1.945604
		10	2613	1351	1324	1.934123
		15	2653	1359	1329	1.952171
		20	2670	1360	1329	1.963235
22	Dam-8-76	5	2724	1340	1316	2.032836
		10	2734	1346	1344	2.031204
		15	2764	1357	1361	2.036846
		20	2776	1370	1379	2.026277
23	Dam-8-77	5	2633	1449	1422	1.817115
		10	2639	1460	1434	1.807534
		15	2645	1460	1444	1.811644
		20	2658	1469	1447	1.809394
24	Dam-8-81	5	2952	1572	1401	1.877863
		10	2954	1584	1415	1.864899
		15	2963	1588	1417	1.865869
		20	2974	1593	1425	1.866918

APPENDIX E

VELOCITIES vs. CONFINING PRESSURE PLOTS

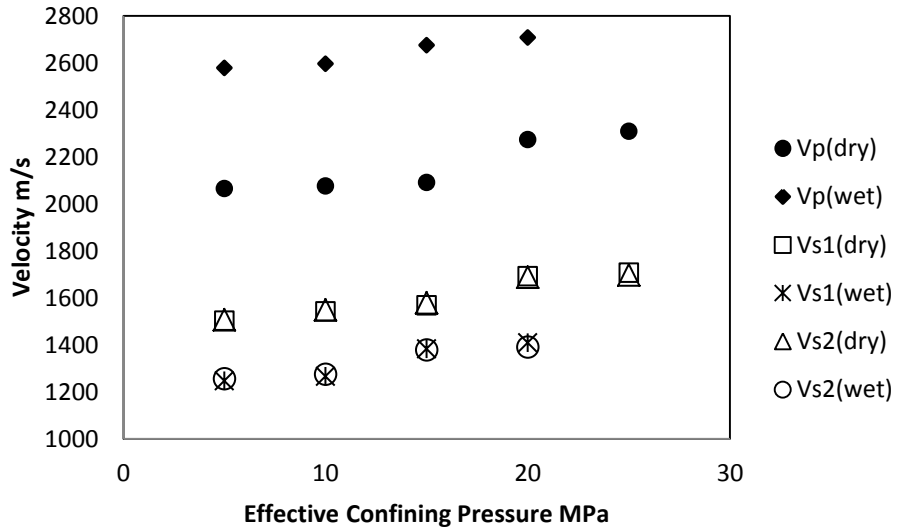

Figure E-1 Velocities vs. Confining Pressure for dry and saturated Sample No. 1

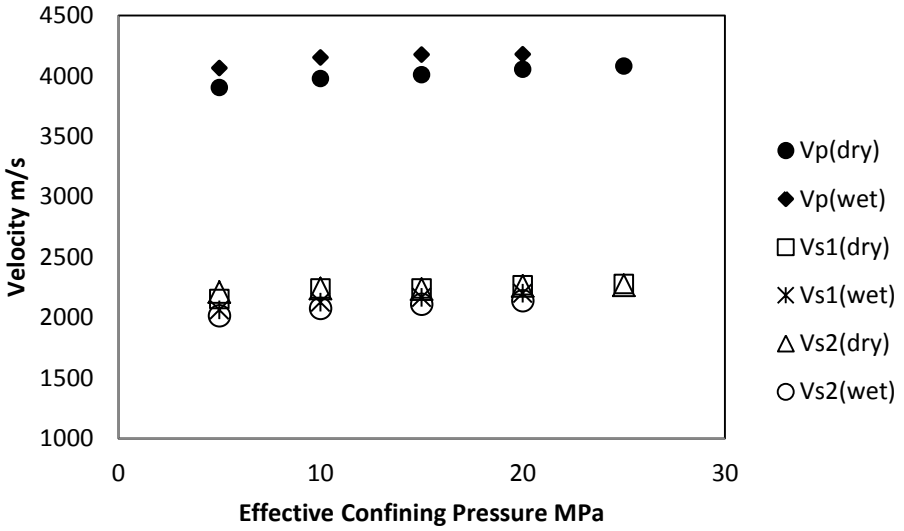

Figure E-2 Velocities vs. Confining Pressure for dry and saturated Sample No. 12

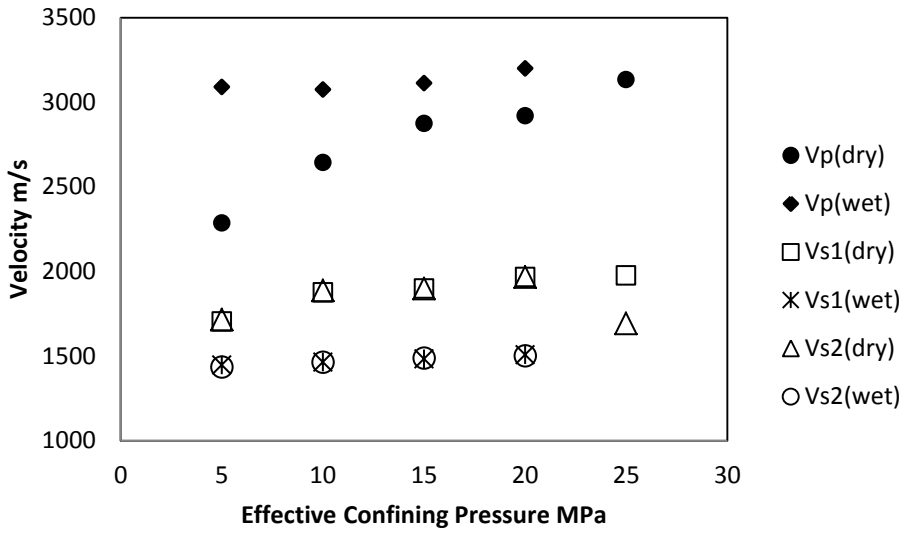

Figure E-3 Velocities vs. Confining Pressure for dry and saturated Sample No. 13

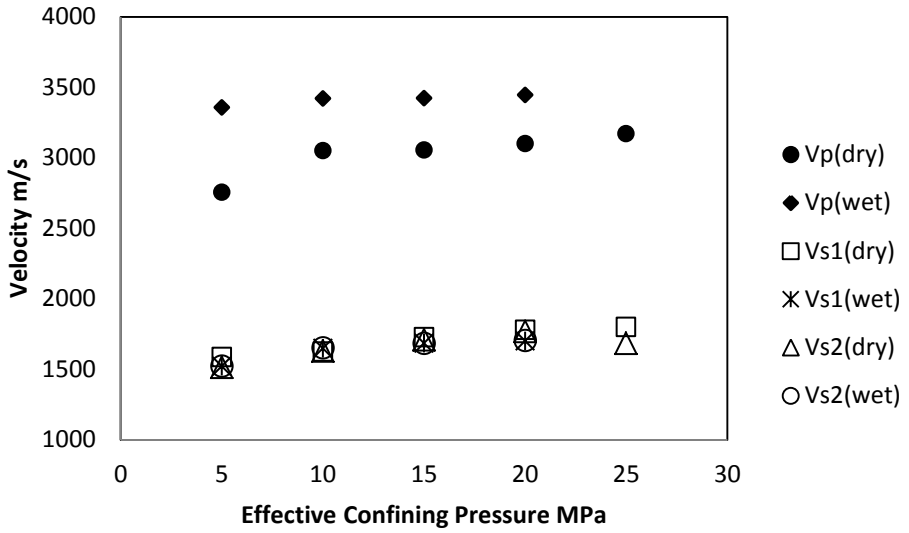

Figure E-4 Velocities vs. Confining Pressure for dry and saturated Sample No. 14

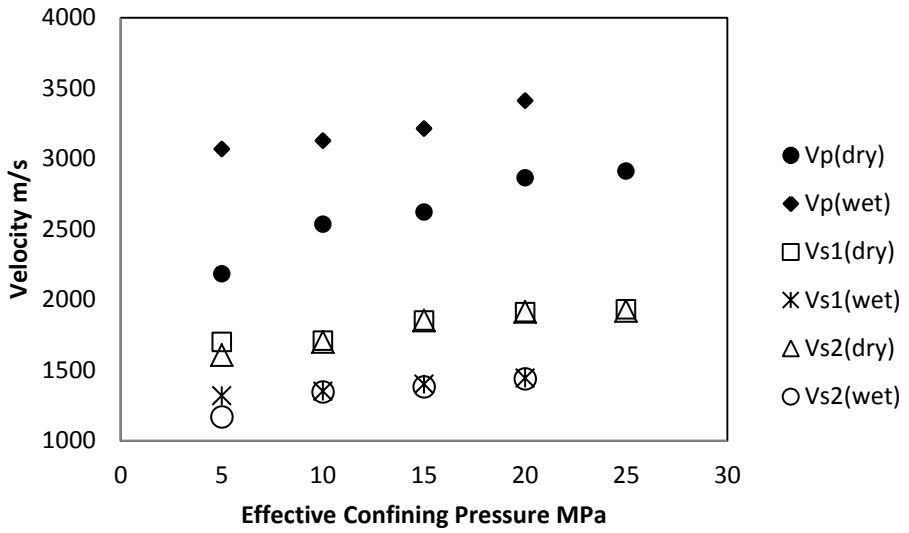

Figure E-5 Velocities vs. Confining Pressure for dry and saturated Sample No. 15

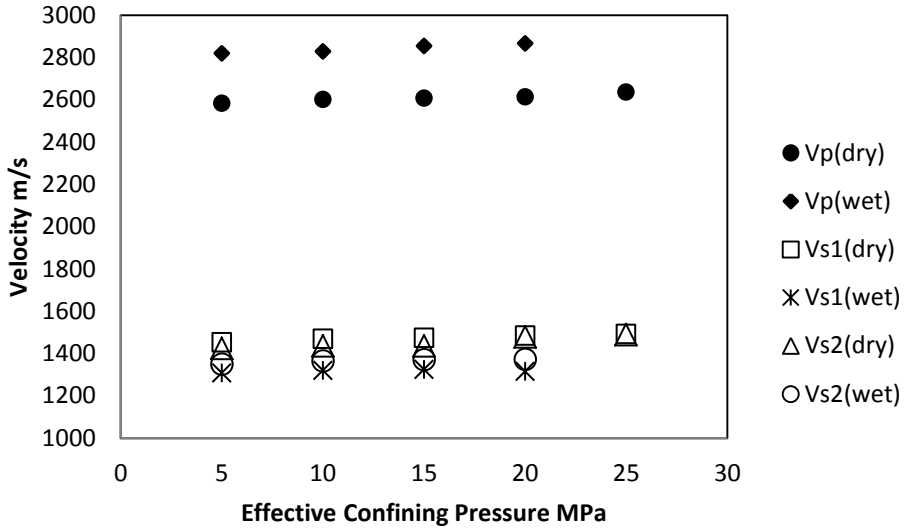

Figure E-6 Velocities vs. Confining Pressure for dry and saturated Sample No. 19

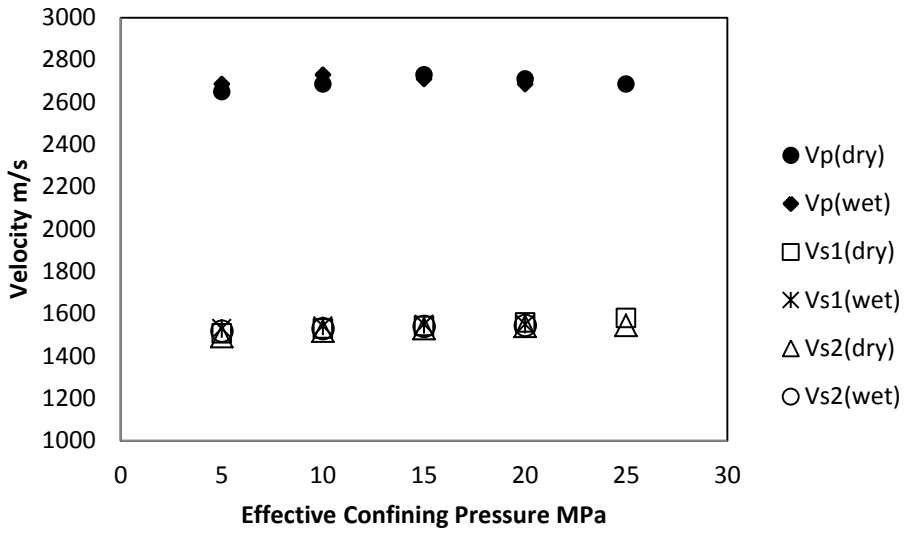

Figure E-7 Velocities vs. Confining Pressure for dry and saturated Sample No.21

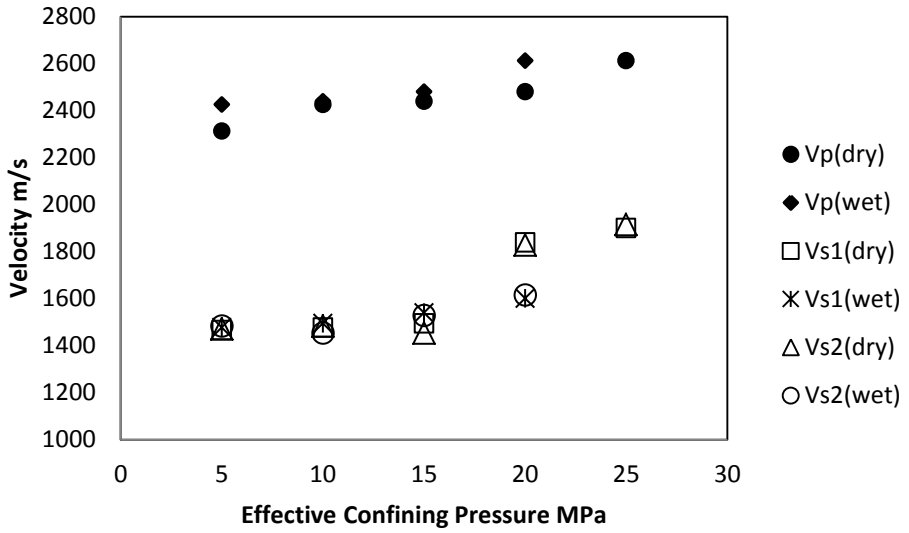

Figure E-8 Velocities vs. Confining Pressure for dry and saturated Sample No.22

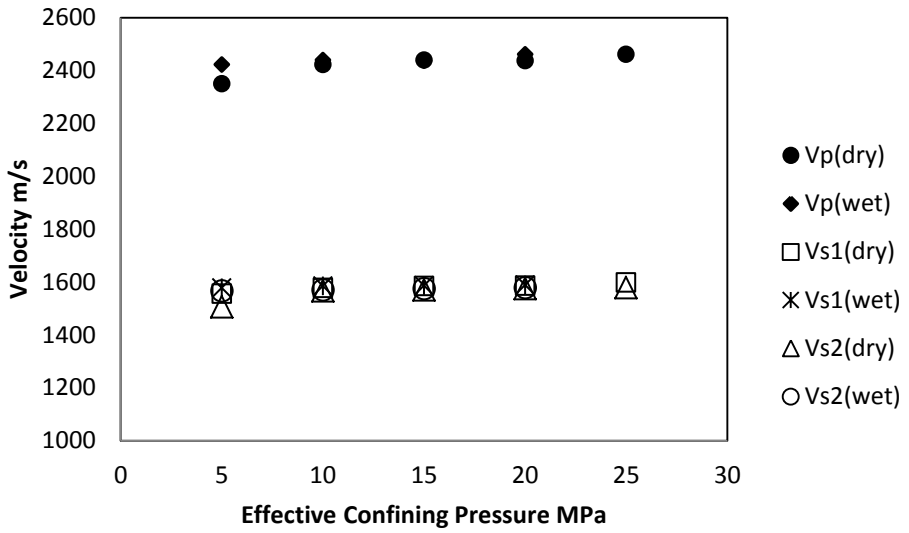

Figure E-9 Velocities vs. Confining Pressure for dry and saturated Sample No.23

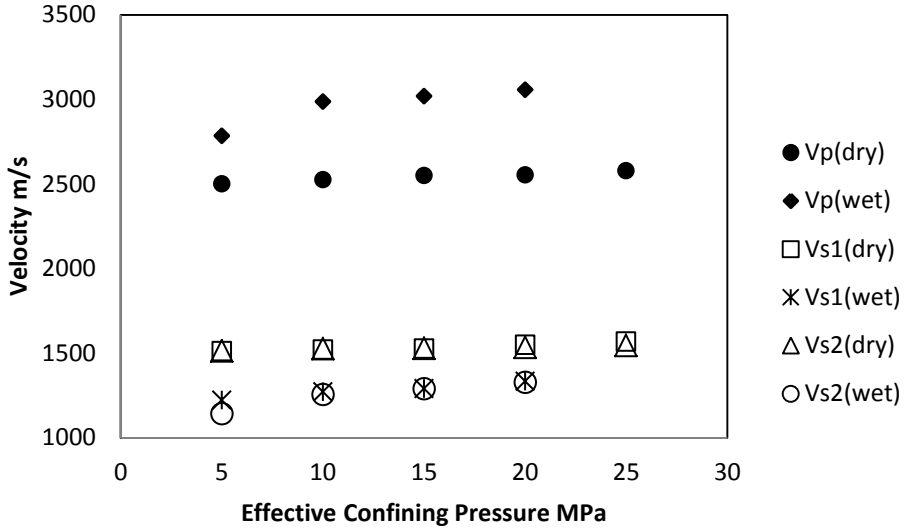

Figure E-10 Velocities vs. Confining Pressure for dry and saturated Sample No.24

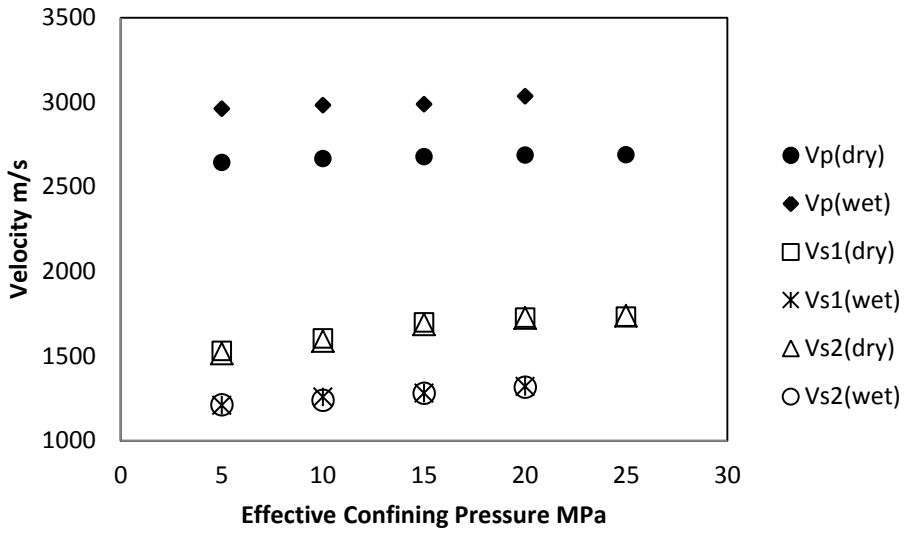

Figure E-11 Velocities vs. Confining Pressure for dry and saturated Sample No. 25

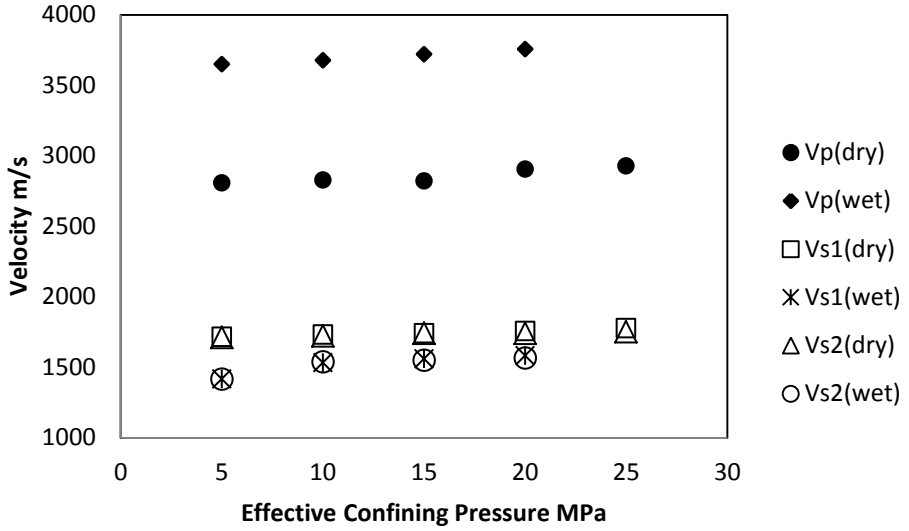

Figure E-12 Velocities vs. Confining Pressure for dry and saturated Sample No. 38

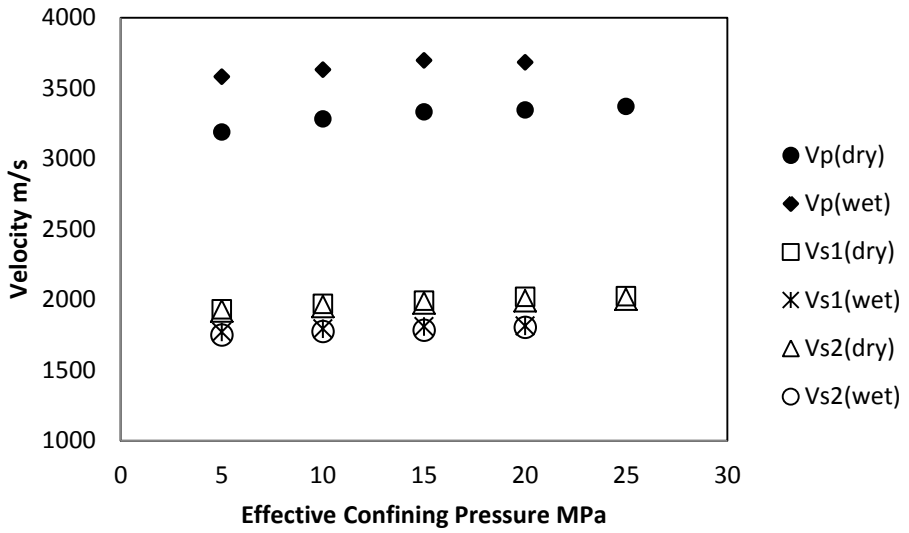

Figure E-13 Velocities vs. Confining Pressure for dry and saturated Sample No. 58

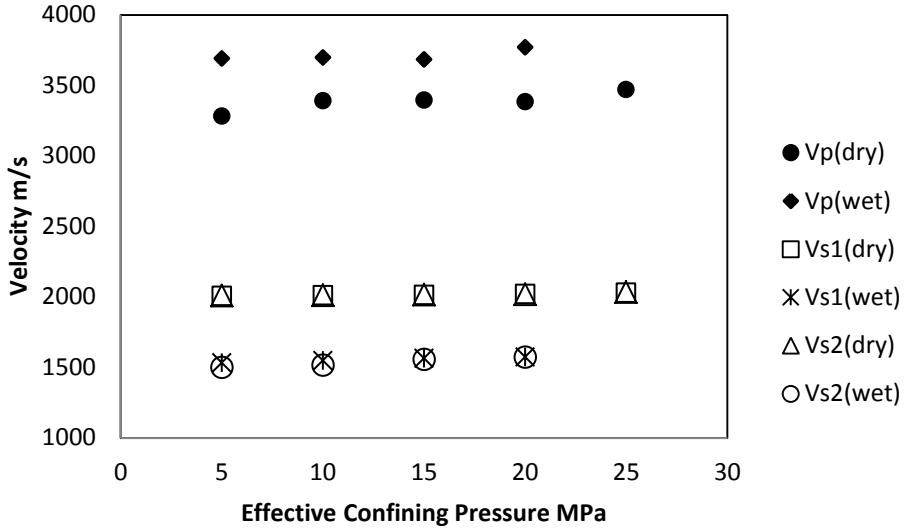

Figure E-14 Velocities vs. Confining Pressure for dry and saturated Sample No. 61

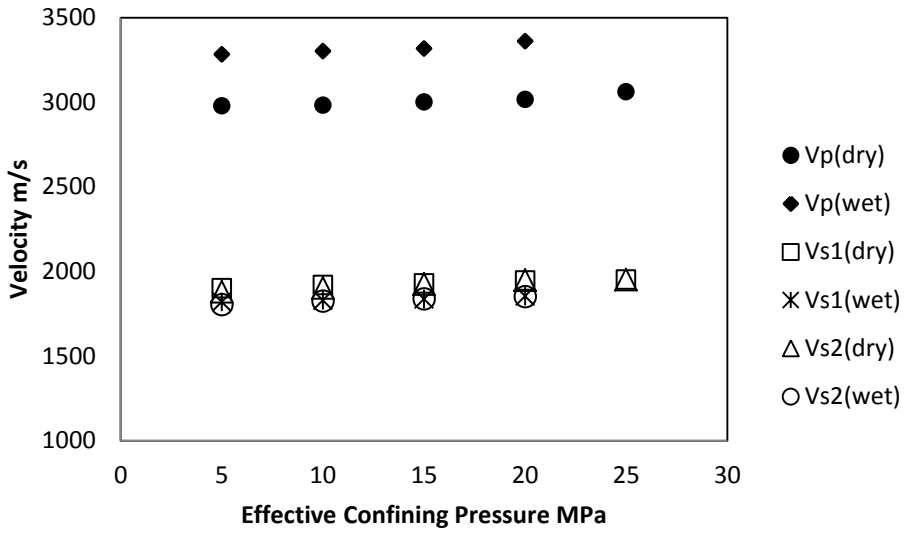

Figure E-15 Velocities vs. Confining Pressure for dry and saturated Sample No. 62

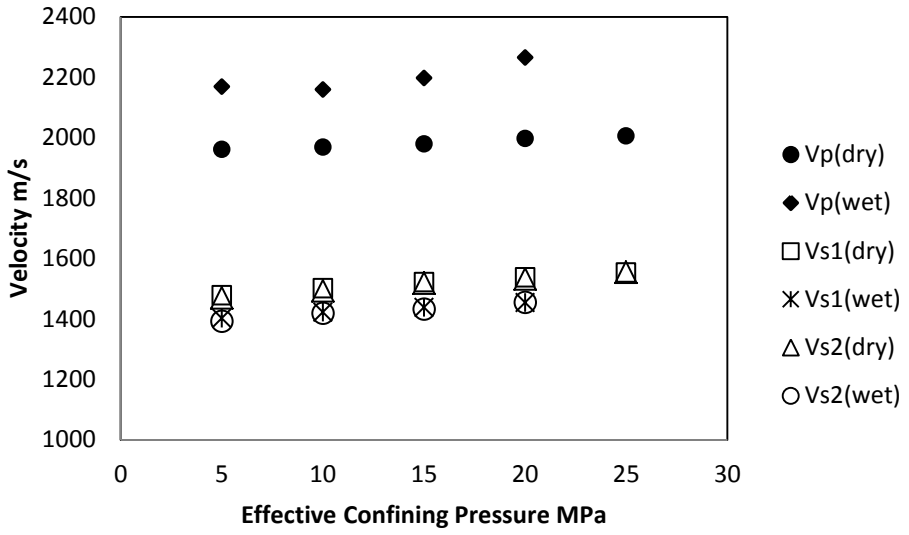

Figure E-16 Velocities vs. Confining Pressure for dry and saturated Sample No. 66

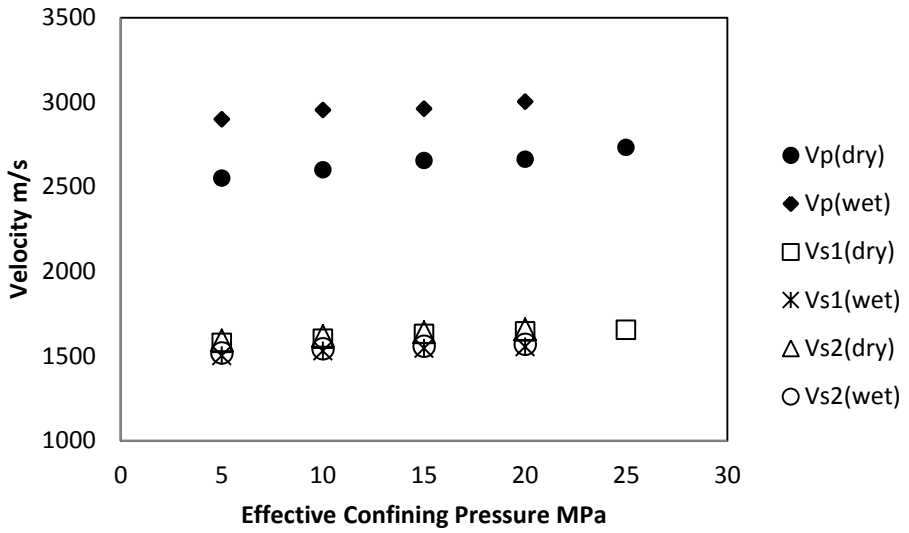

Figure E-17 Velocities vs. Confining Pressure for dry and saturated Sample No. 71

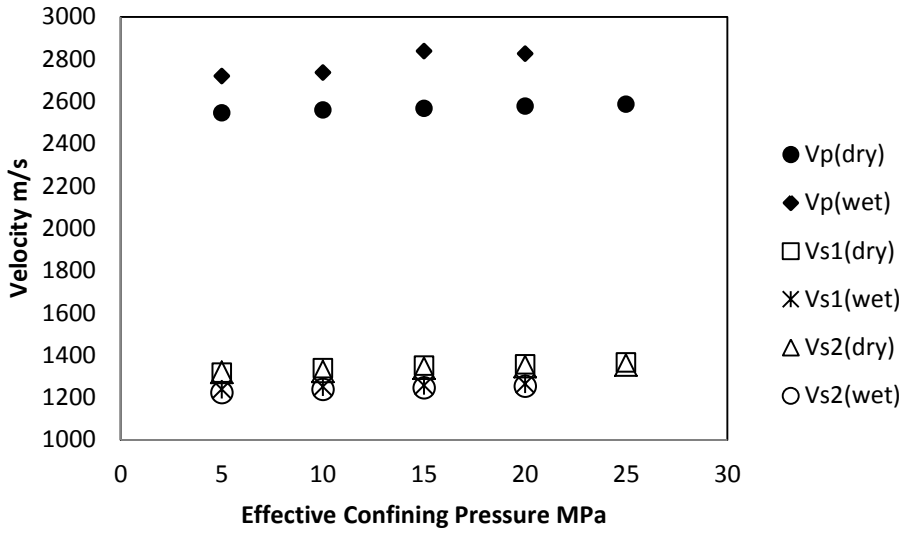

Figure E-18 Velocities vs. Confining Pressure for dry and saturated Sample No. 72

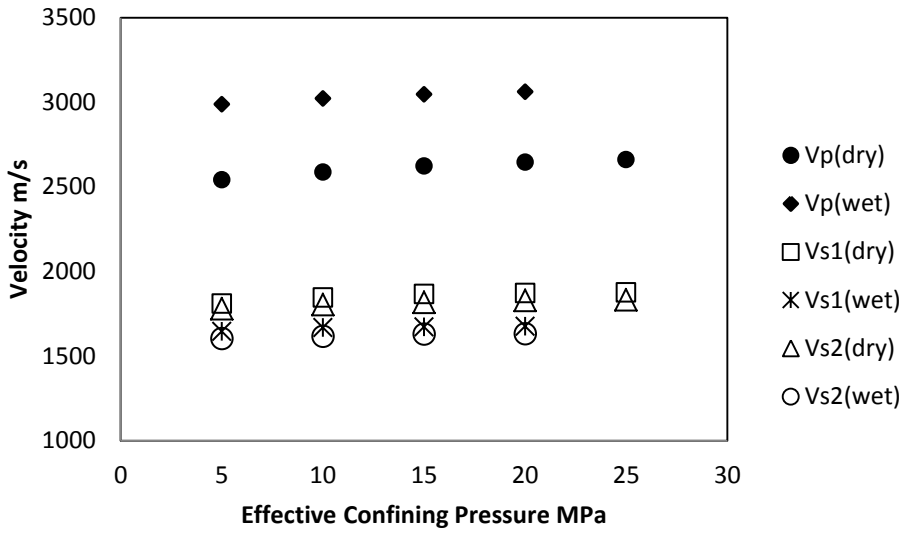

Figure E-19 Velocities vs. Confining Pressure for dry and saturated Sample No. 73

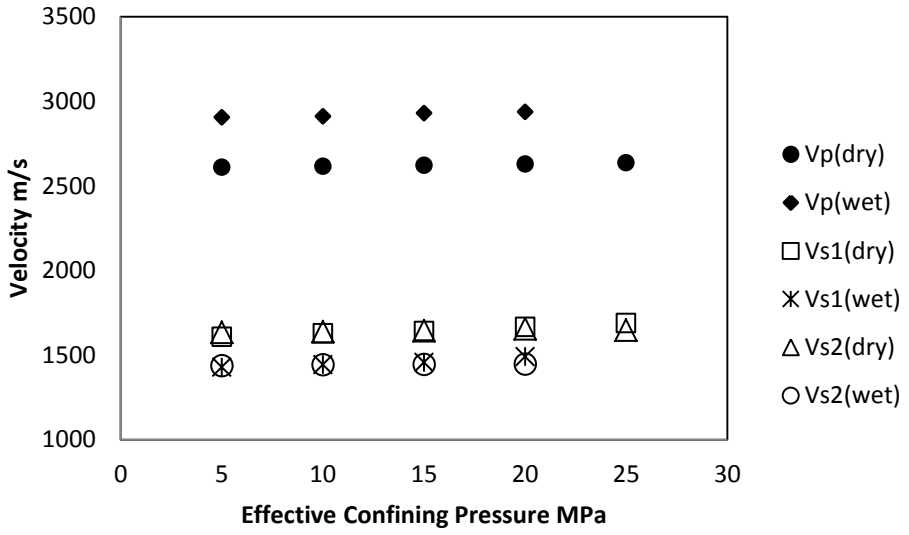

Figure E-20 Velocities vs. Confining Pressure for dry and saturated Sample No. 74

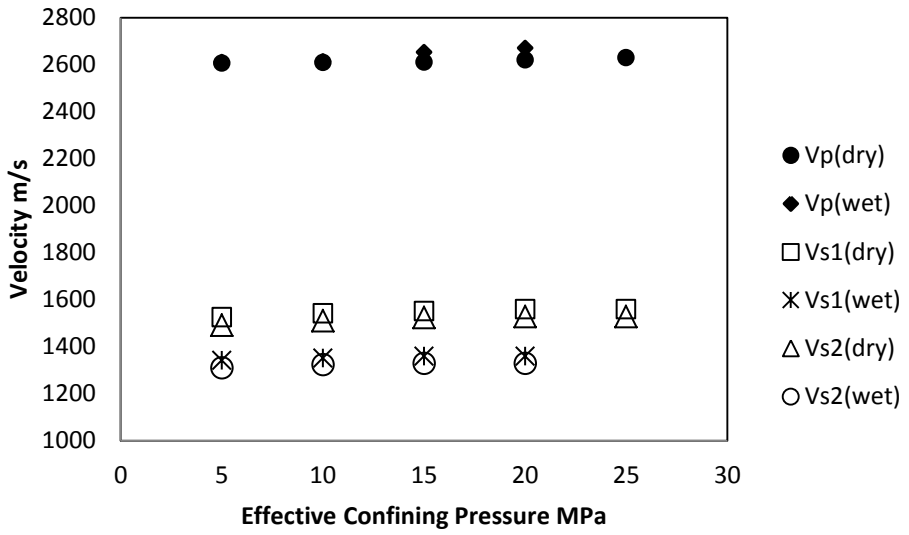

Figure E-21 Velocities vs. Confining Pressure for dry and saturated Sample No. 75

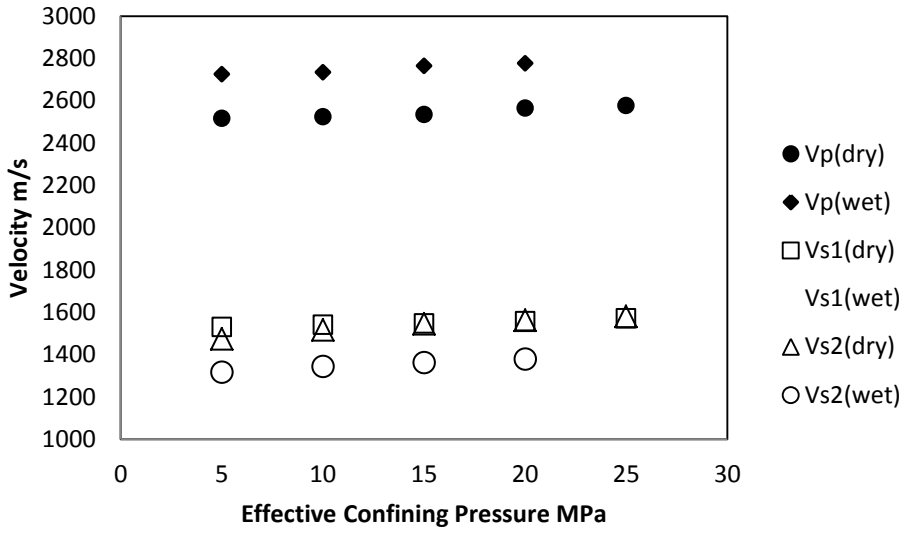

Figure E-22 Velocities vs. Confining Pressure for dry and saturated Sample No. 76

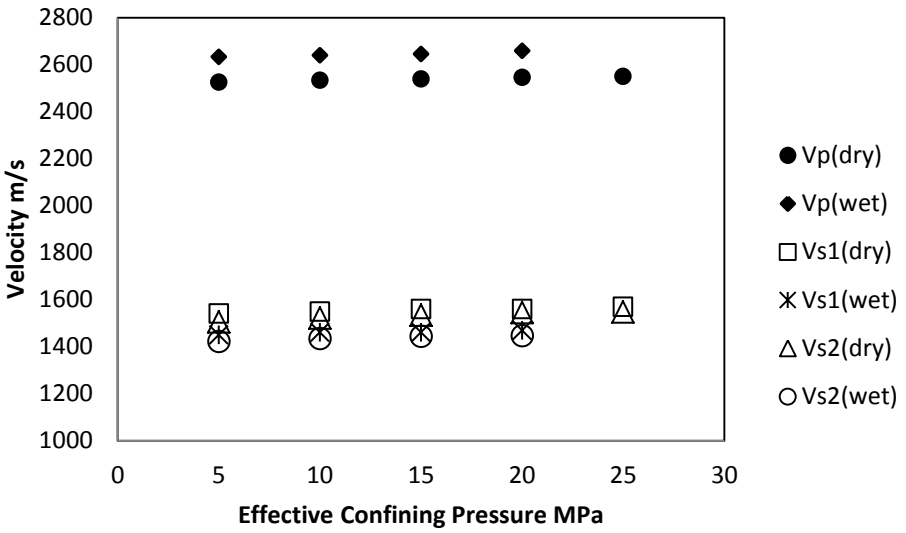

Figure E-23 Velocities vs. Confining Pressure for dry and saturated Sample No. 77

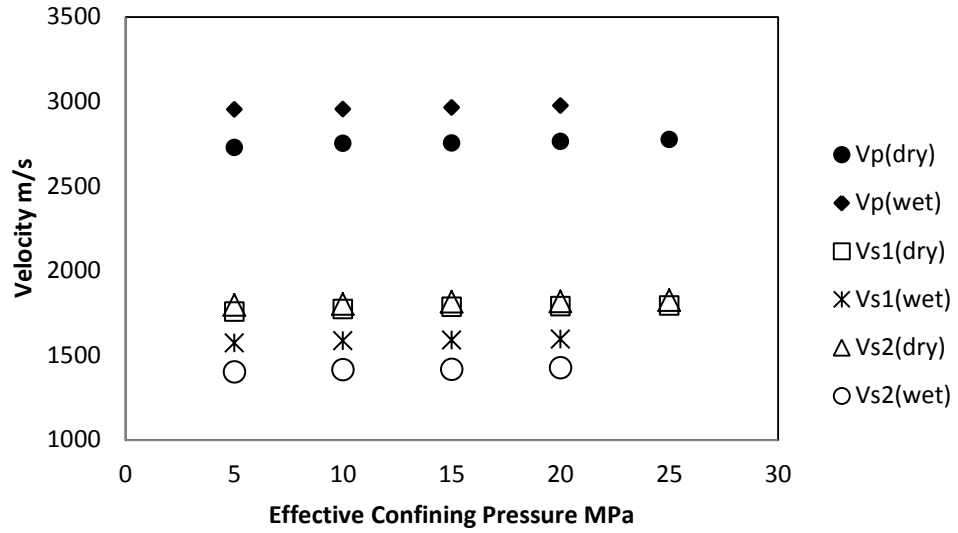

Figure E-24 Velocities vs. Confining Pressure for dry and saturated Sample No. 81

APPENDIX F

CURVES FITTING FOR TYPICAL DRY SAMPLES

PART A - P-WAVE VELOCITY CURVE FIT FOR ALL THE SAMPLES

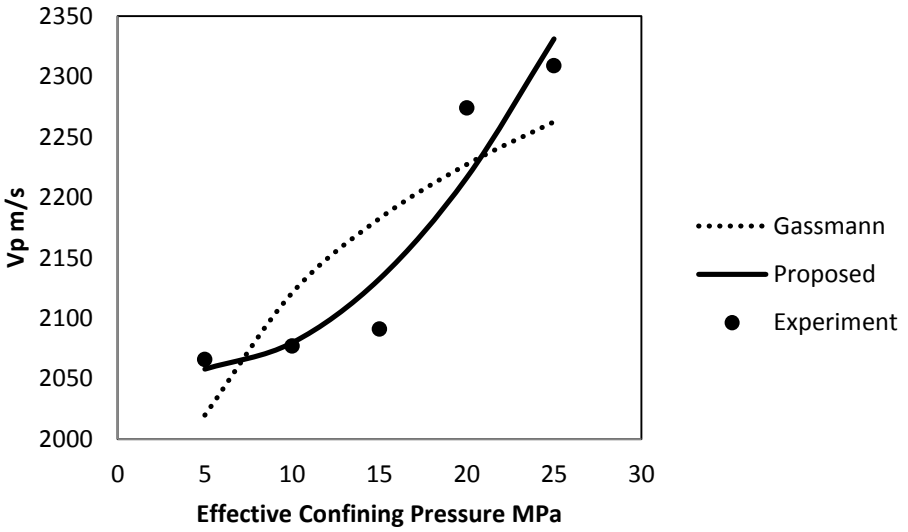

Figure F-1 Fit for P-wave velocity vs. Effective Confining Pressure Curves for Sample No. 1

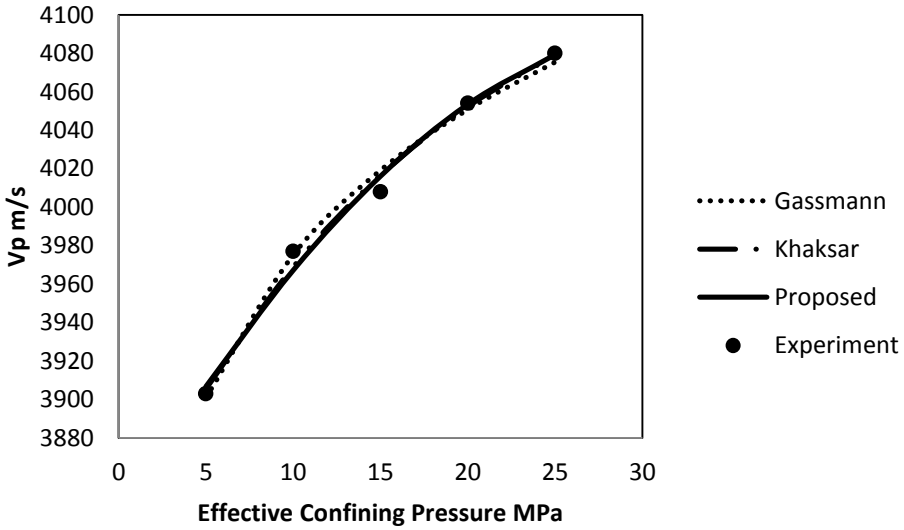

Figure F-2 Fit for P-wave velocity vs. Effective Confining Pressure Curves for Sample No. 12

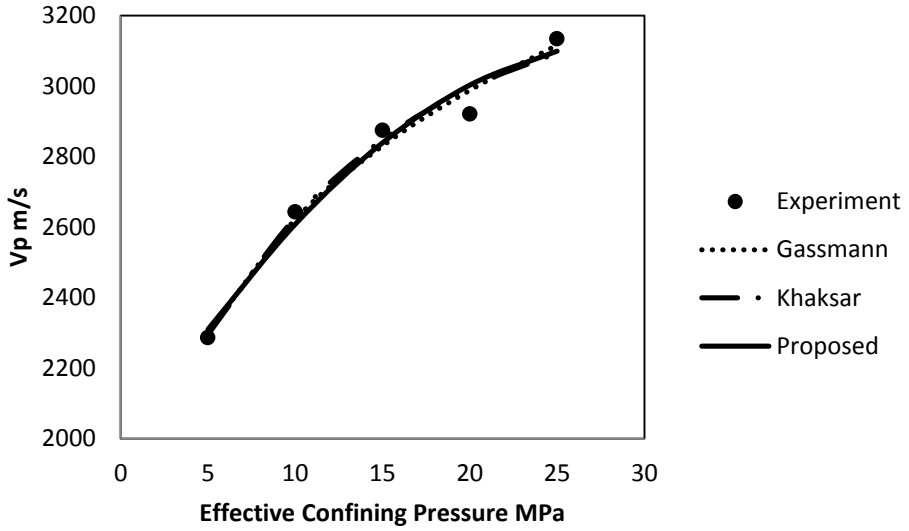

Figure F-3 Fit for P-wave velocity vs. Effective Confining Pressure Curves for Sample No. 13

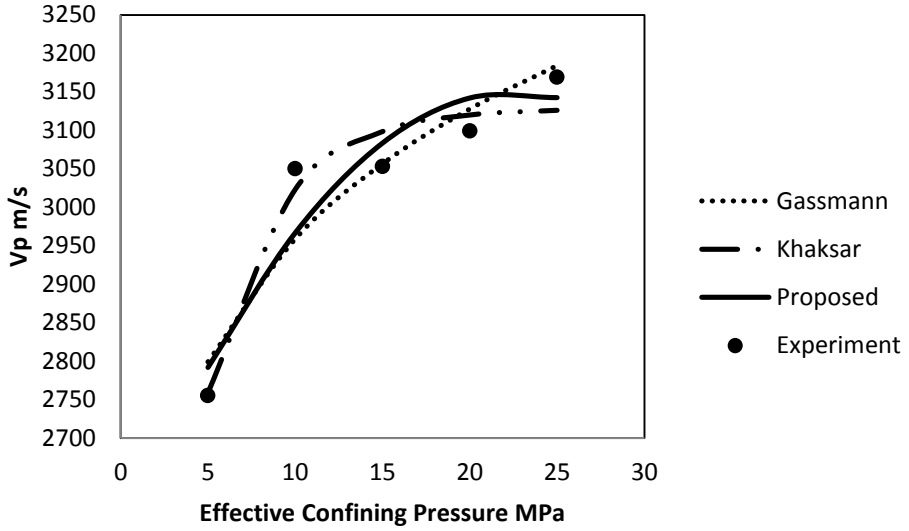

Figure F-4 Fit for P-wave velocity vs. Effective Confining Pressure Curves for Sample No. 14

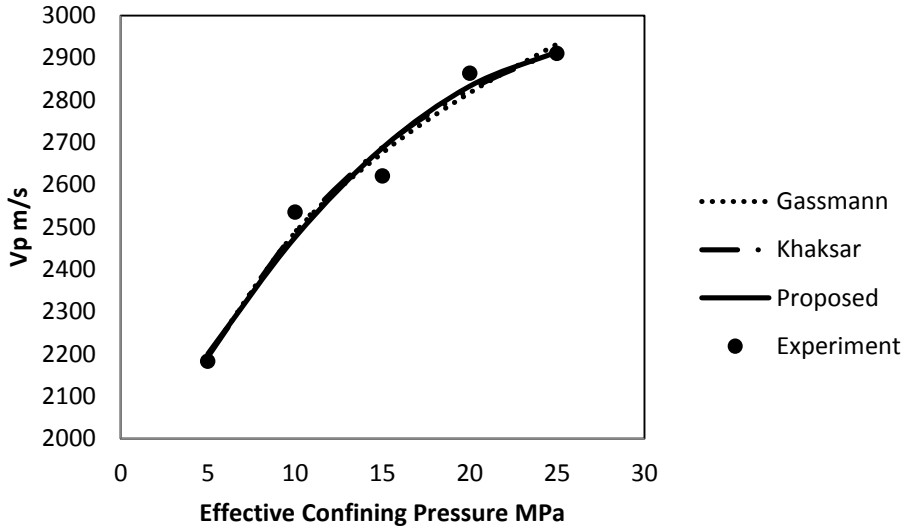

Figure F-5 Fit for P-wave velocity vs. Effective Confining Pressure Curves for Sample No. 15

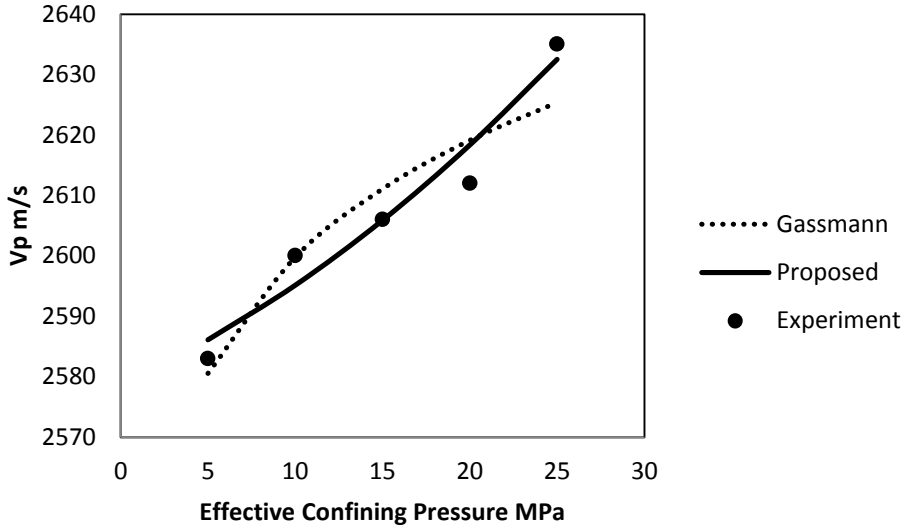

Figure F-6 Fit for P-wave velocity vs. Effective Confining Pressure Curves for Sample No. 19

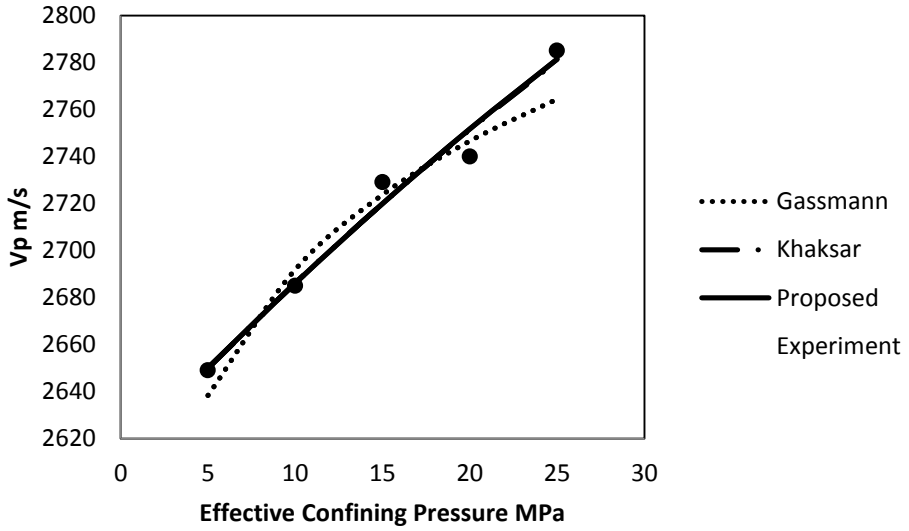

Figure F-7 Fit for P-wave velocity vs. Effective Confining Pressure Curves for Sample No. 21

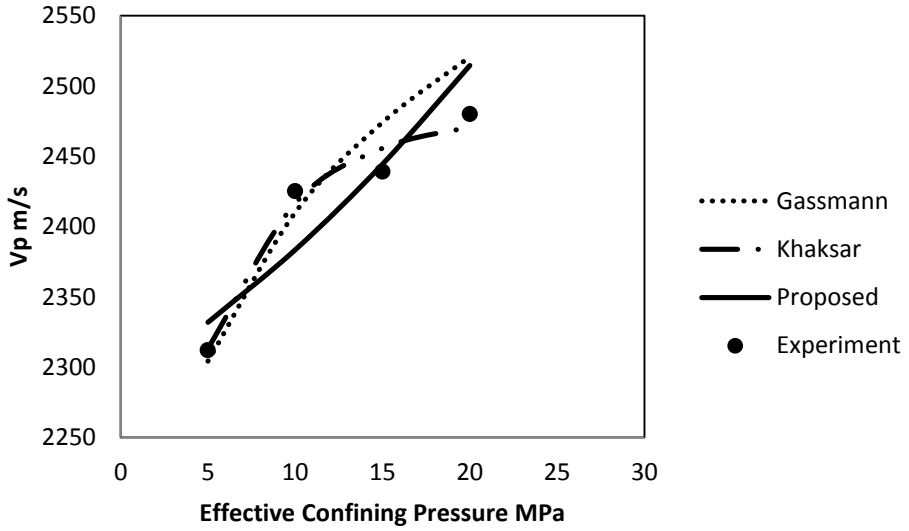

Figure F-8 Fit for P-wave velocity vs. Effective Confining Pressure Curves for Sample No. 22

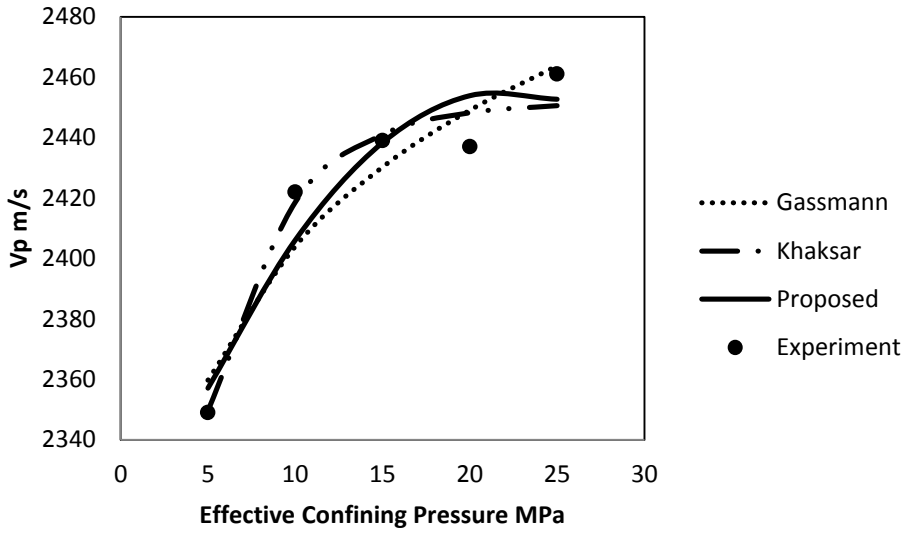

Figure F-9 Fit for P-wave velocity vs. Effective Confining Pressure Curves for Sample No. 23

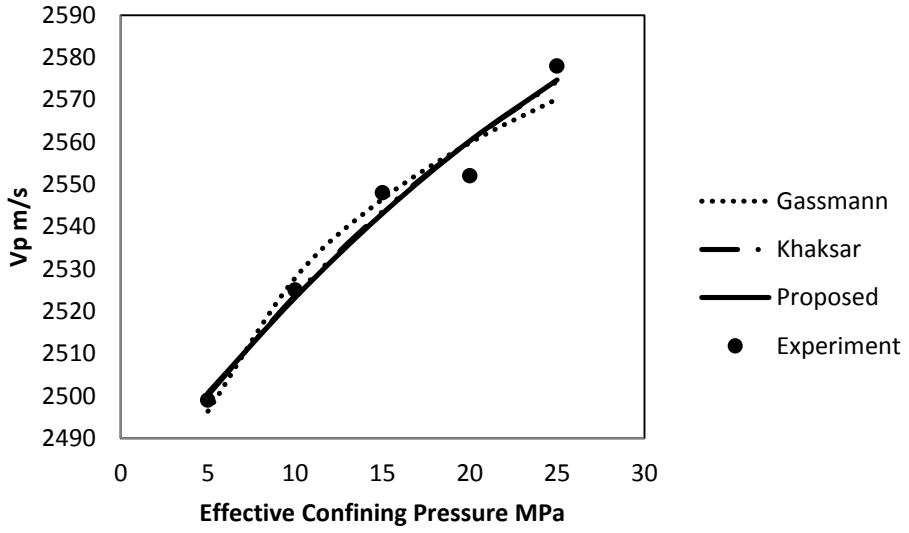

Figure F-1 Fit for P-wave velocity vs. Effective Confining Pressure Curves for Sample No. 24

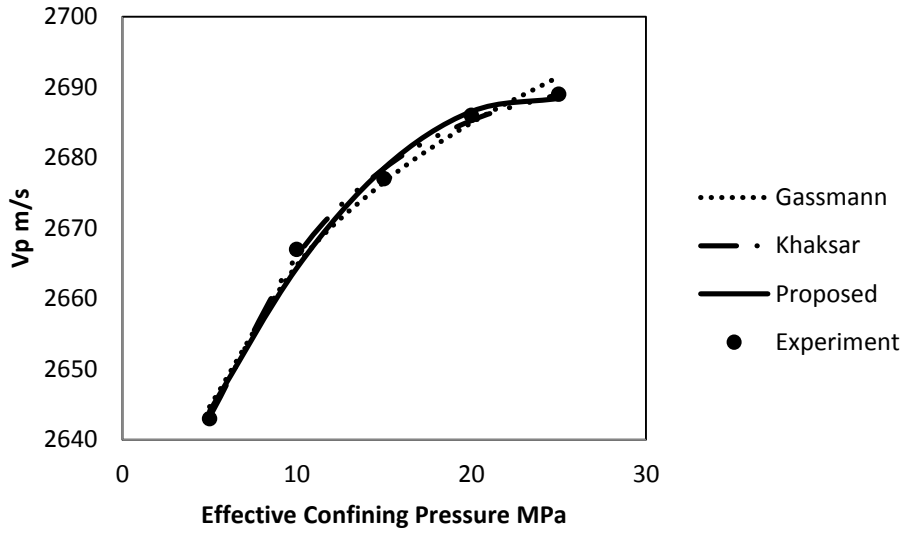

Figure F-11 Fit for P-wave velocity vs. Effective Confining Pressure Curves for Sample No. 25

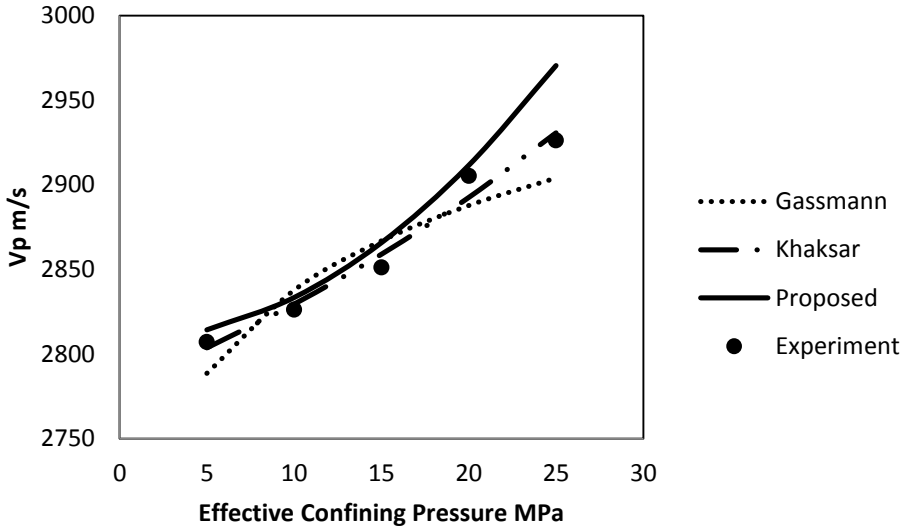

Figure F-12 Fit for P-wave velocity vs. Effective Confining Pressure Curves for Sample No. 38

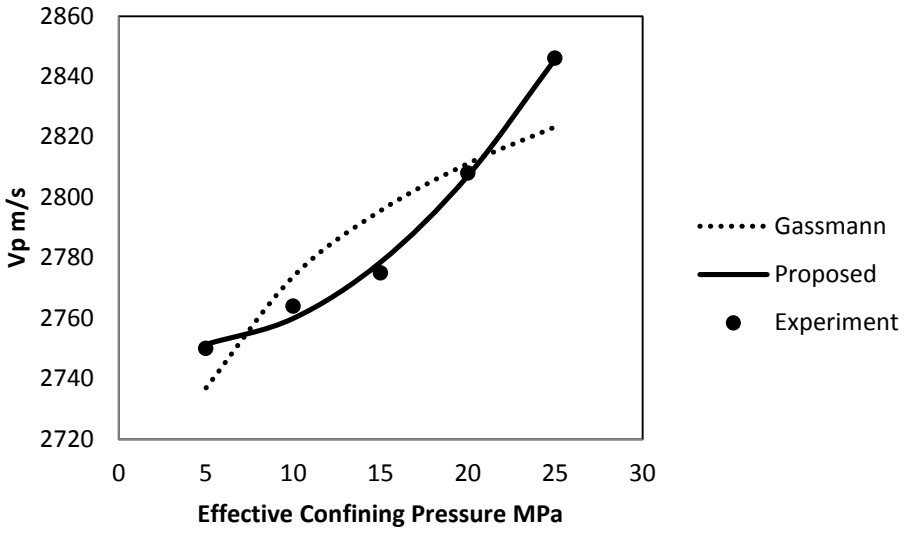

Figure F-13 Fit for P-wave velocity vs. Effective Confining Pressure Curves for Sample No. 54

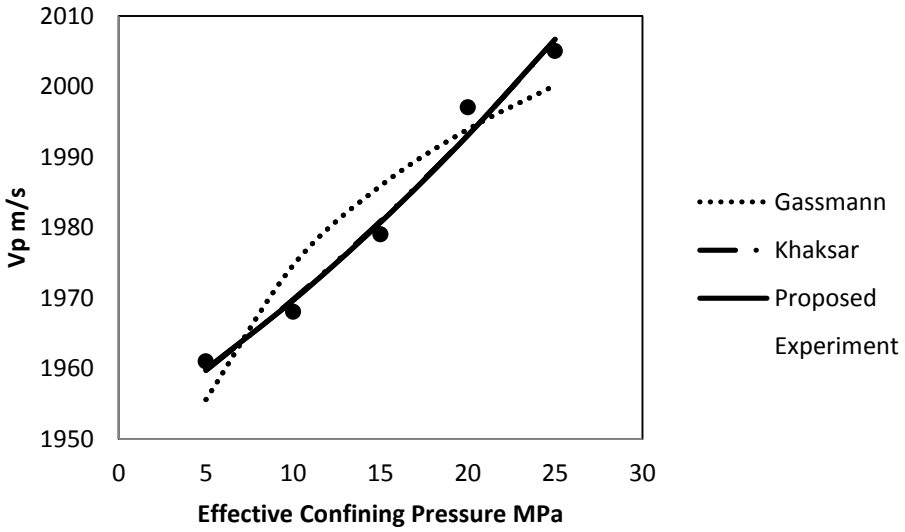

Figure F-14 Fit for P-wave velocity vs. Effective Confining Pressure Curves for Sample No. 55

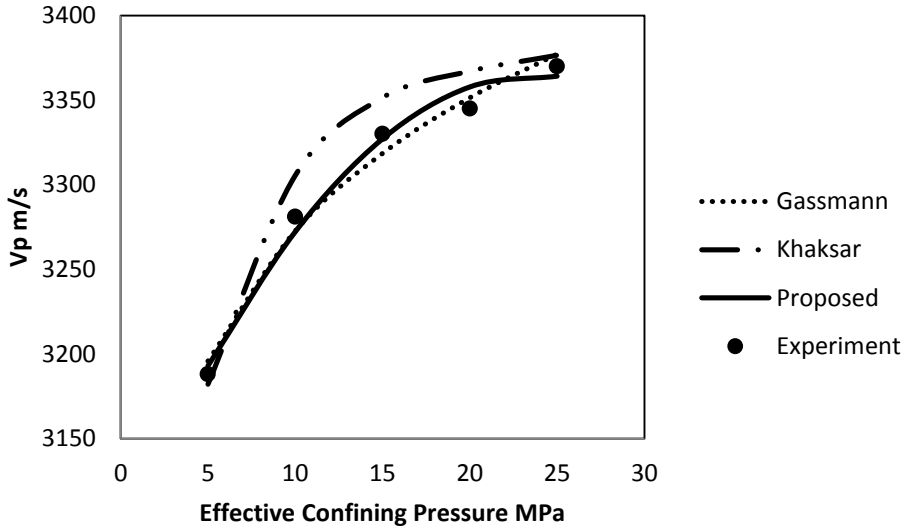

Figure F-15 Fit for P-wave velocity vs. Effective Confining Pressure Curves for Sample No. 58

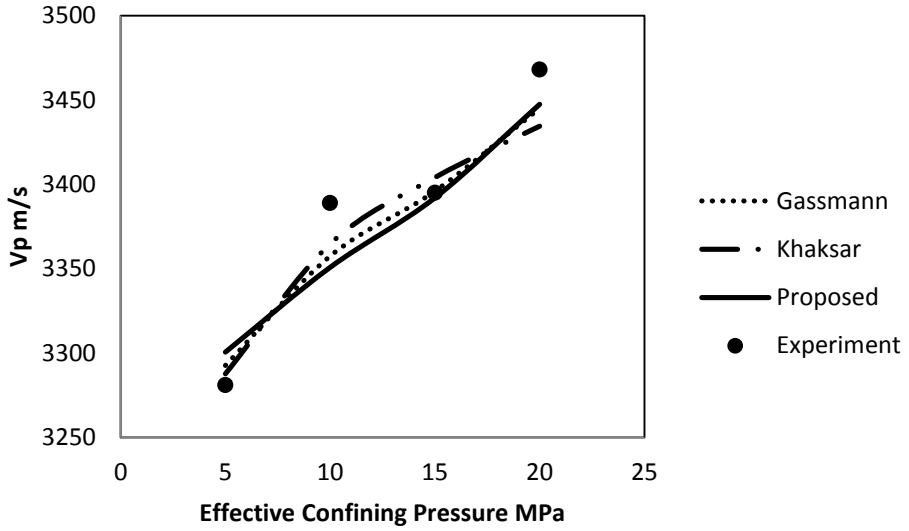

Figure F-16 Fit for P-wave velocity vs. Effective Confining Pressure Curves for Sample No. 61

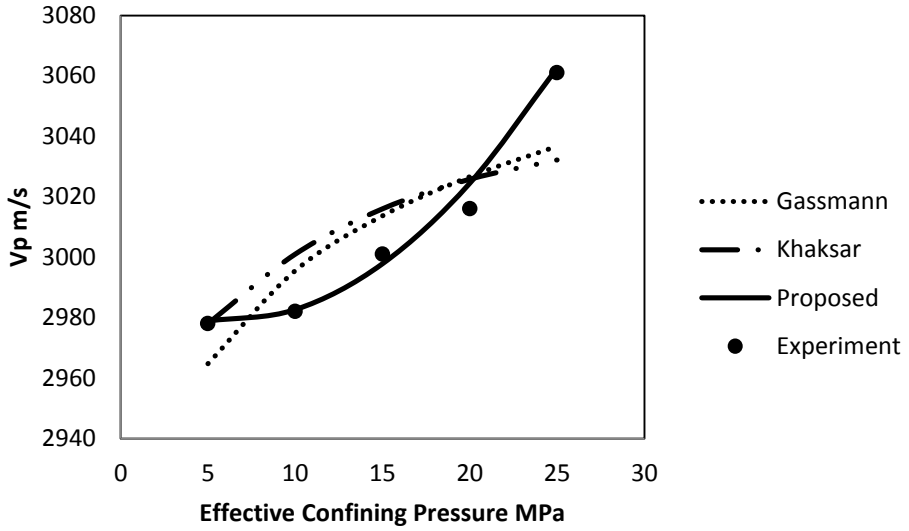

Figure F-17 Fit for P-wave velocity vs. Effective Confining Pressure Curves for Sample No. 62

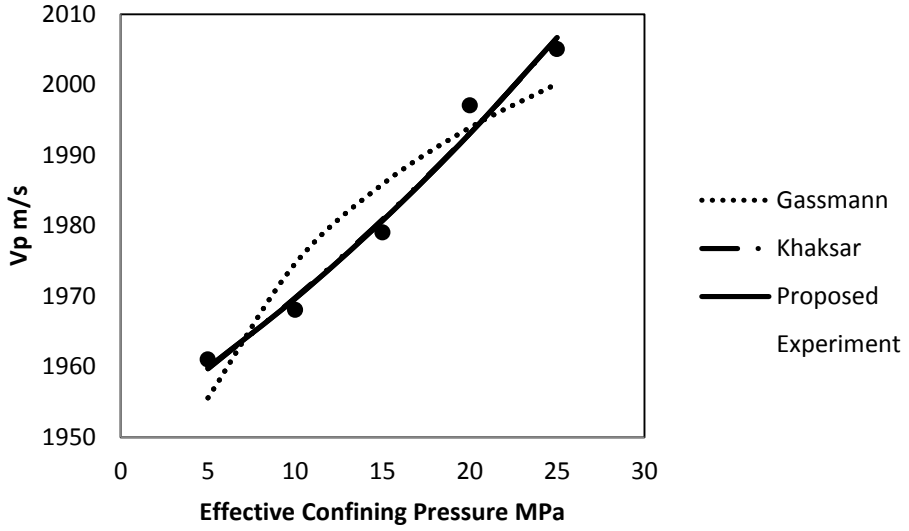

Figure F-18 Fit for P-wave velocity vs. Effective Confining Pressure Curves for Sample No. 66

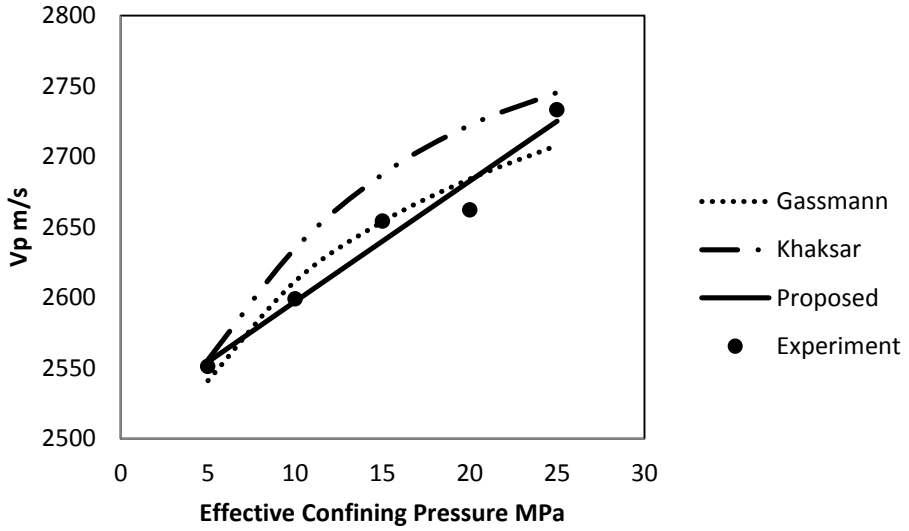

Figure F-4 Fit for P-wave velocity vs. Effective Confining Pressure Curves for Sample No. 71

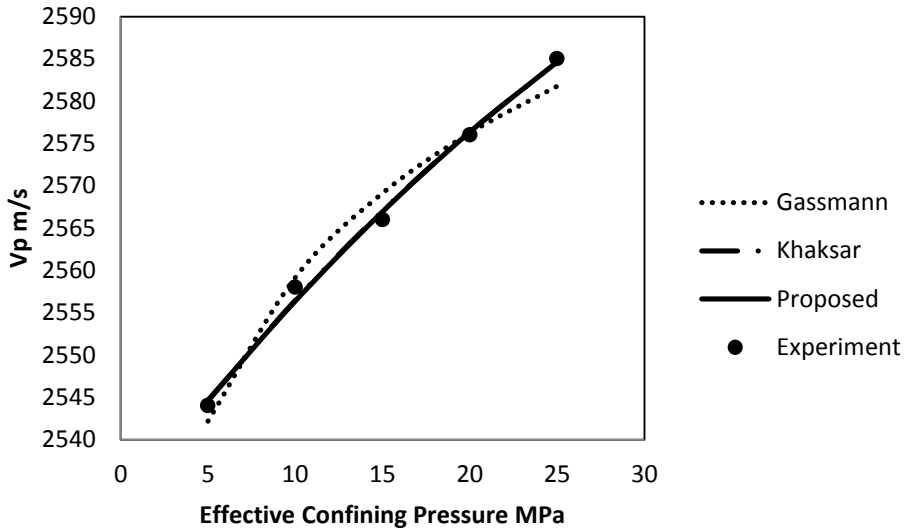

Figure F-19 Fit for P-wave velocity vs. Effective Confining Pressure Curves for Sample No. 72

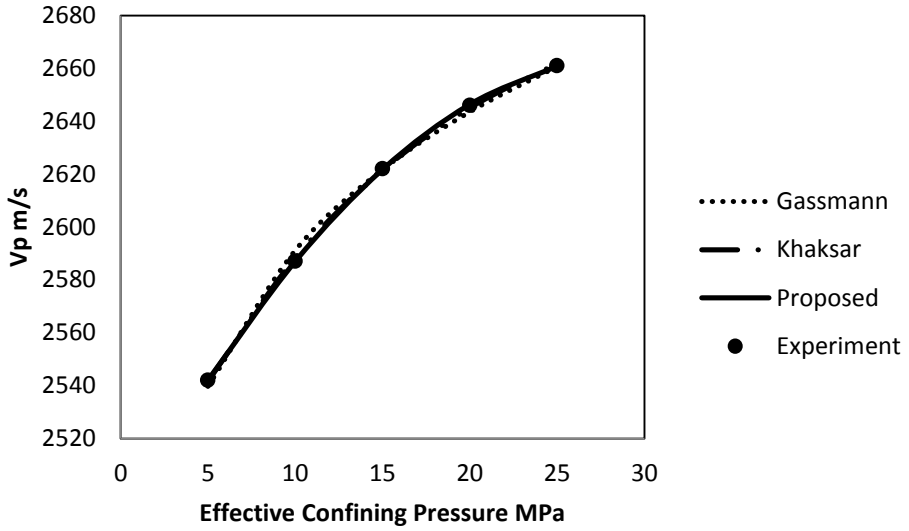

Figure F-20 Fit for P-wave velocity vs. Effective Confining Pressure Curves for Sample No. 73

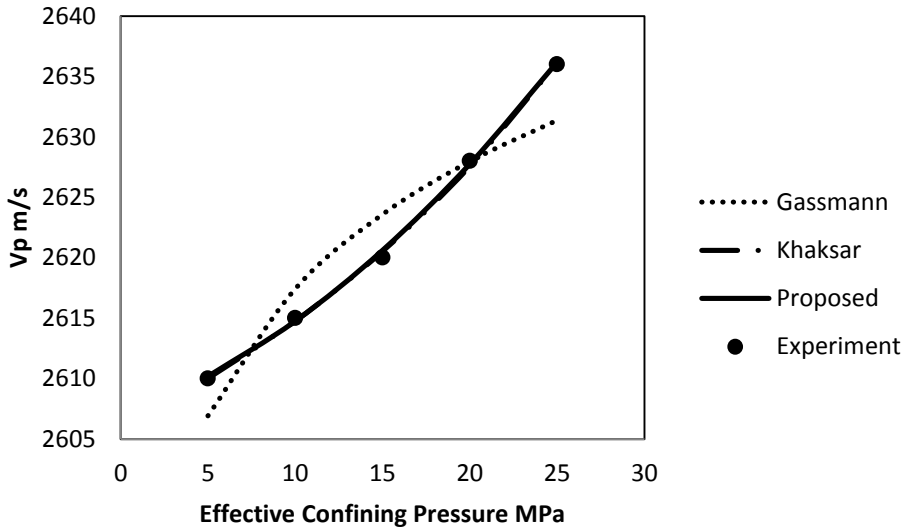

Figure F-21 Fit for P-wave velocity vs. Effective Confining Pressure Curves for Sample No. 74

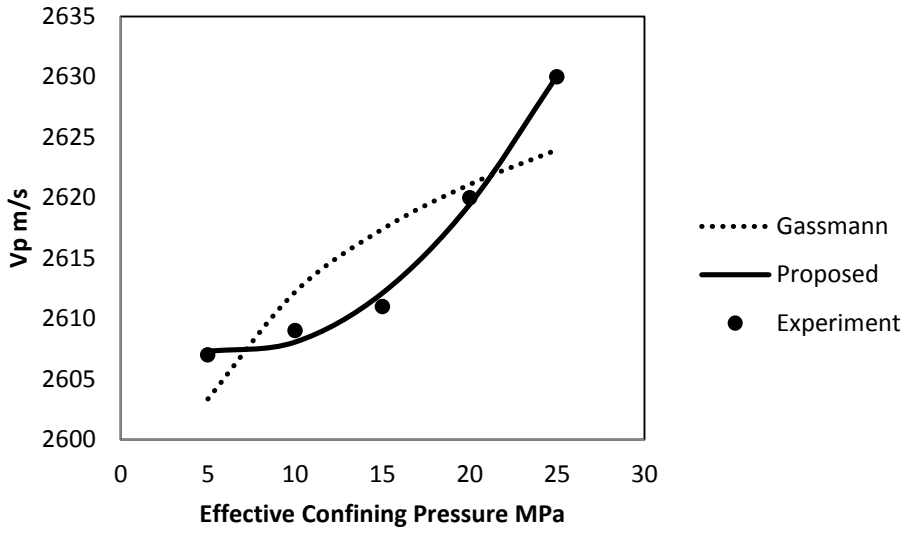

Figure F-22 Fit for P-wave velocity vs. Effective Confining Pressure Curves for Sample No. 75

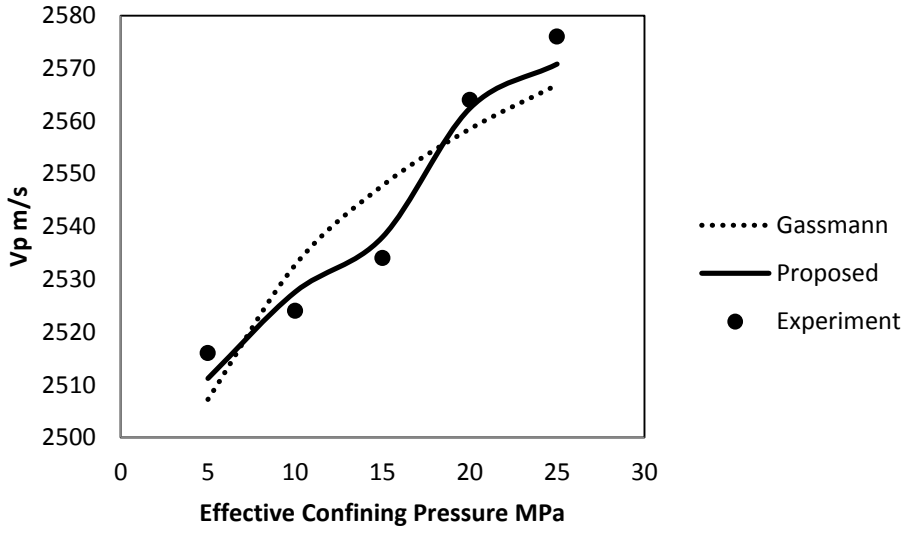

Figure F-23 Fit for P-wave velocity vs. Effective Confining Pressure Curves for Sample No. 76

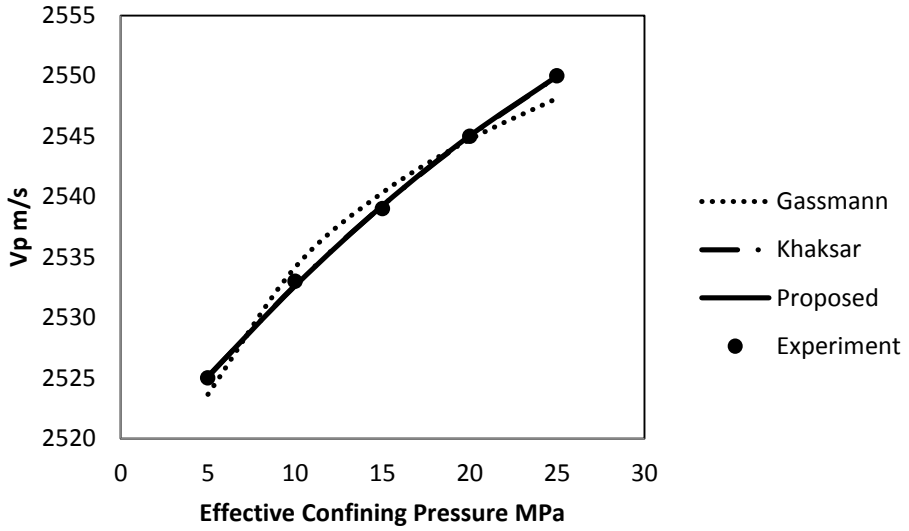

Figure F-24 Fit for P-wave velocity vs. Effective Confining Pressure Curves for Sample No. 77

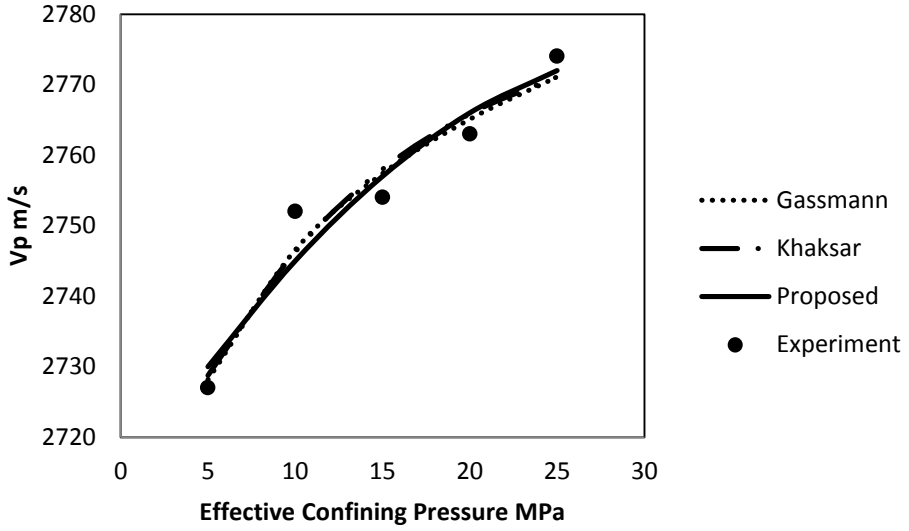

Figure F-25 Fit for P-wave velocity vs. Effective Confining Pressure Curves for Sample No. 81

PART B –S-WAVE VELOCITY CURVE FIT FOR TYPICAL SATURATED SAMPLES

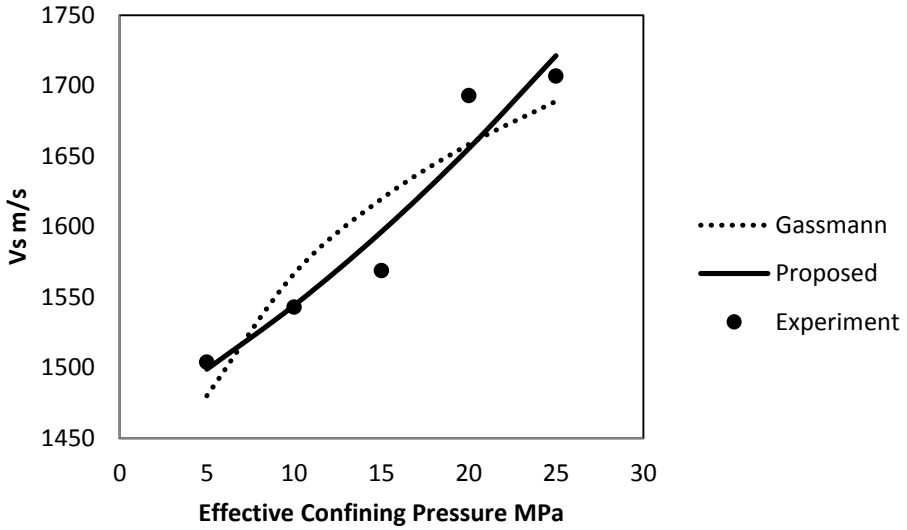

Figure F-1 S-wave velocity vs. Effective Confining Pressure Curves Fit for Sample No. 1

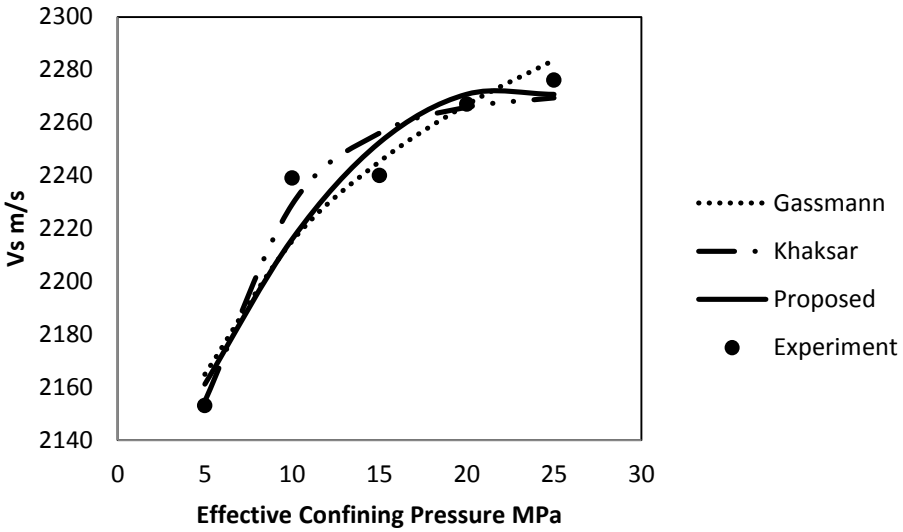

Figure F-2 S-wave velocity vs. Effective Confining Pressure Curves Fit for Sample No. 12

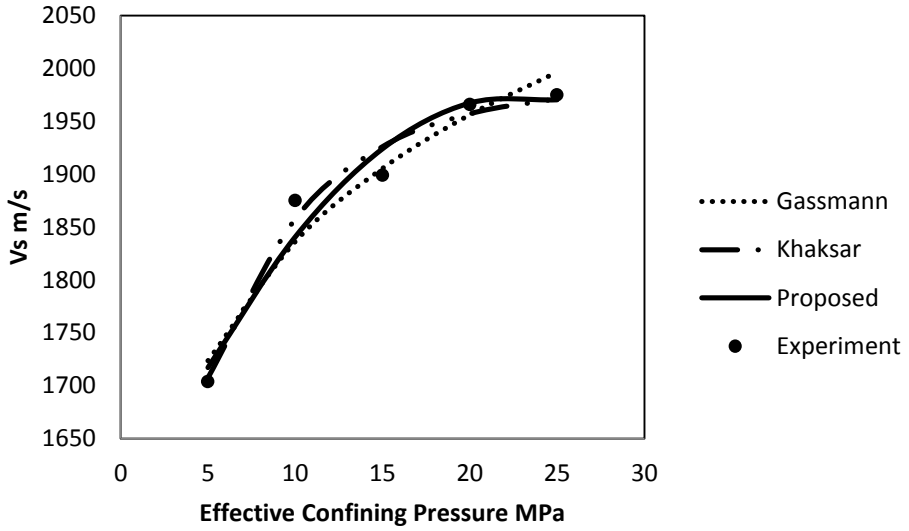

Figure F-3 S-wave velocity vs. Effective Confining Pressure Curves Fit for Sample No. 13

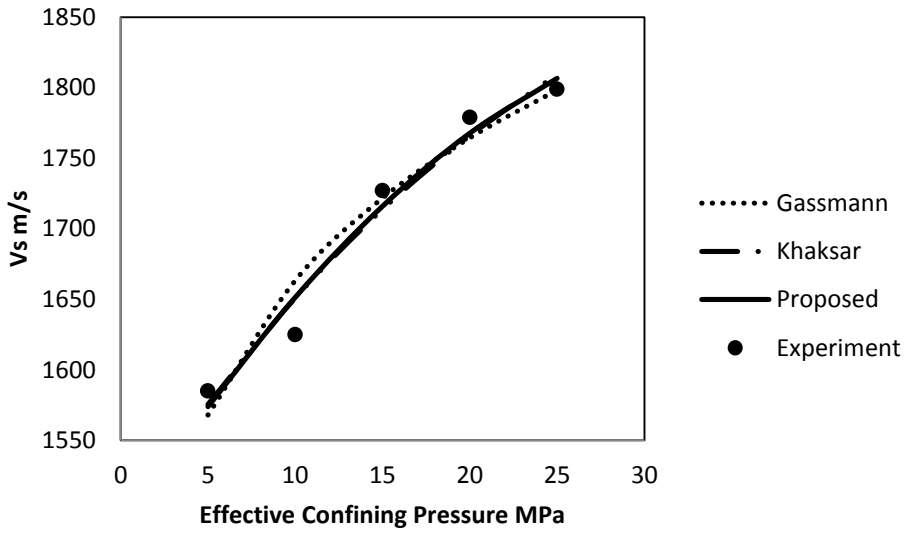

Figure F-4 S-wave velocity vs. Effective Confining Pressure Curves Fit for Sample No. 14

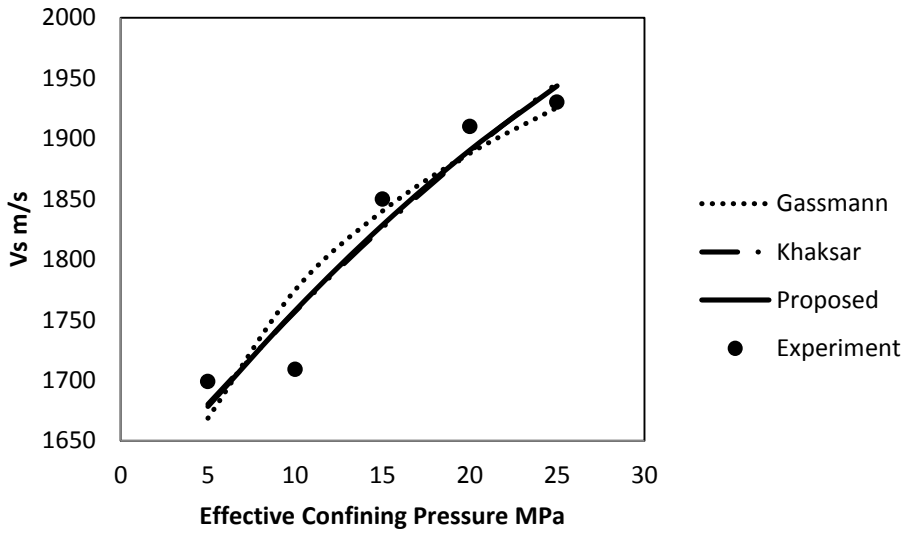

Figure F-1 S-wave velocity vs. Effective Confining Pressure Curves Fit for Sample No. 15

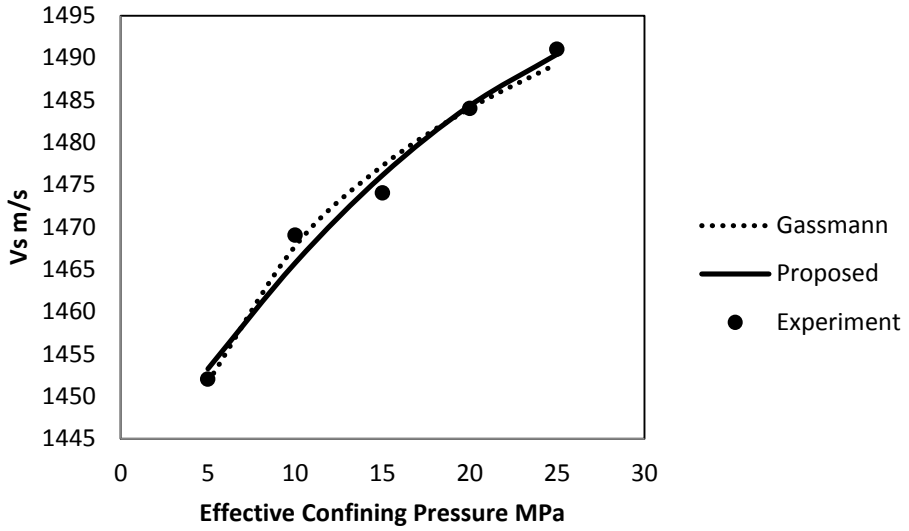

Figure F-5 S-wave velocity vs. Effective Confining Pressure Curves Fit for Sample No. 19

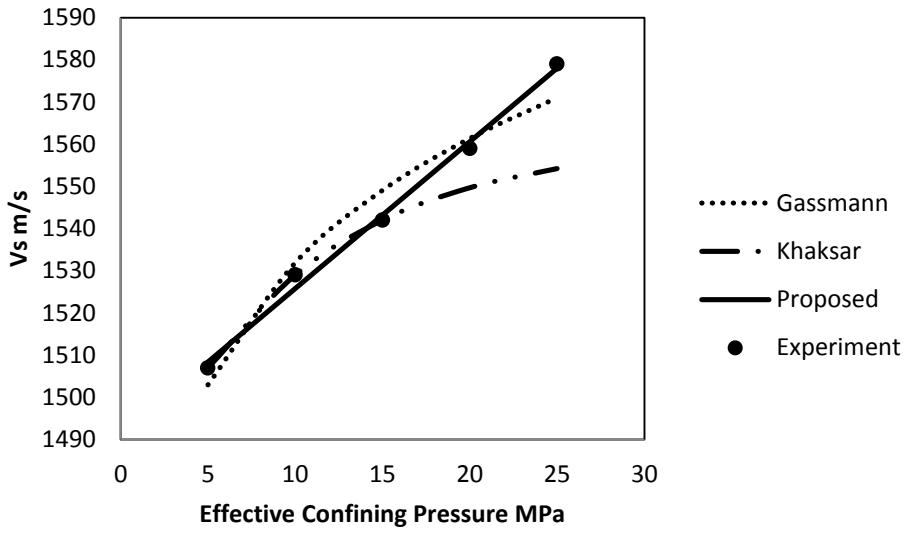

Figure F-6 S-wave velocity vs. Effective Confining Pressure Curves Fit for Sample No. 21

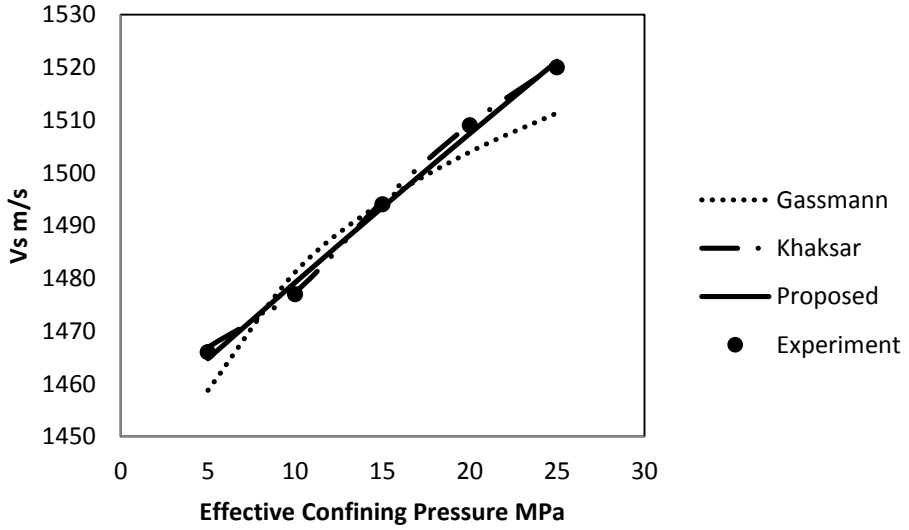

Figure F-7 S-wave velocity vs. Effective Confining Pressure Curves Fit for Sample No. 22

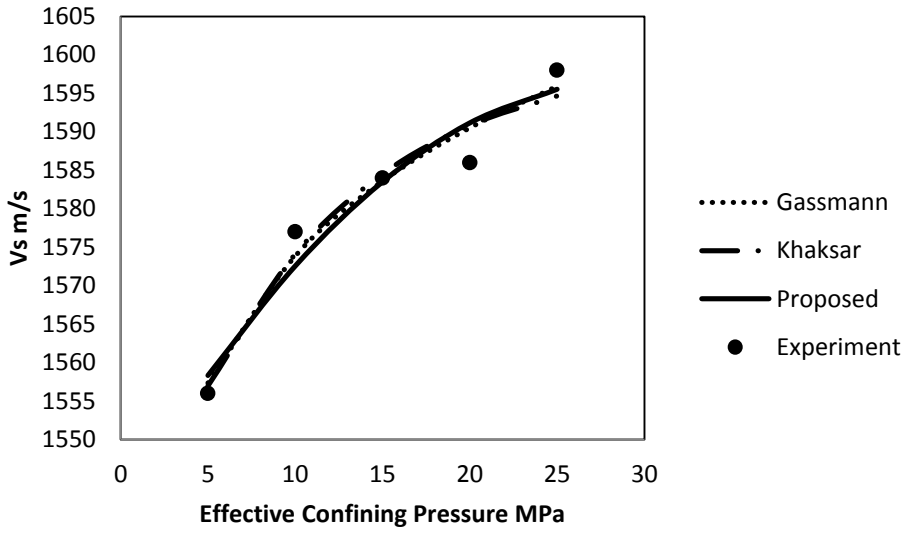

Figure F-8 S-wave velocity vs. Effective Confining Pressure Curves Fit for Sample No. 23

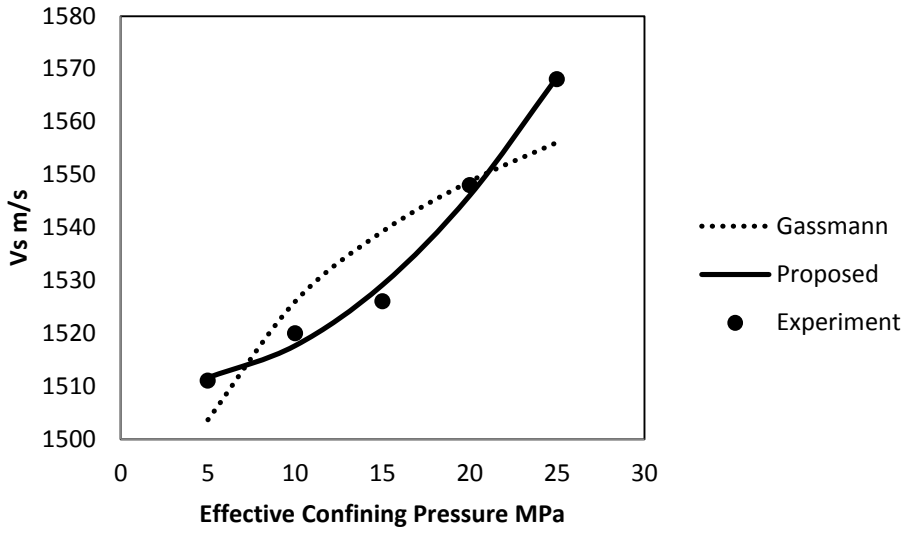

Figure F-9 S-wave velocity vs. Effective Confining Pressure Curves Fit for Sample No. 24

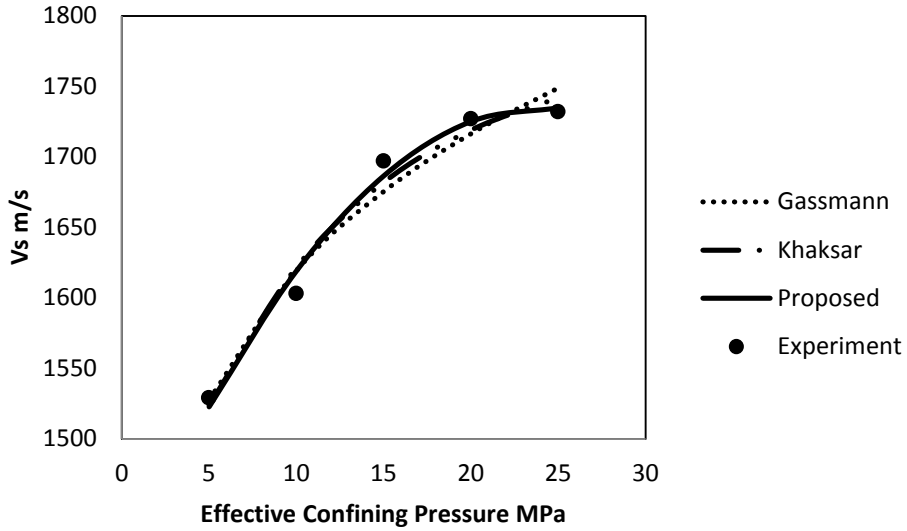

Figure F-10 S-wave velocity vs. Effective Confining Pressure Curves Fit for Sample No. 25

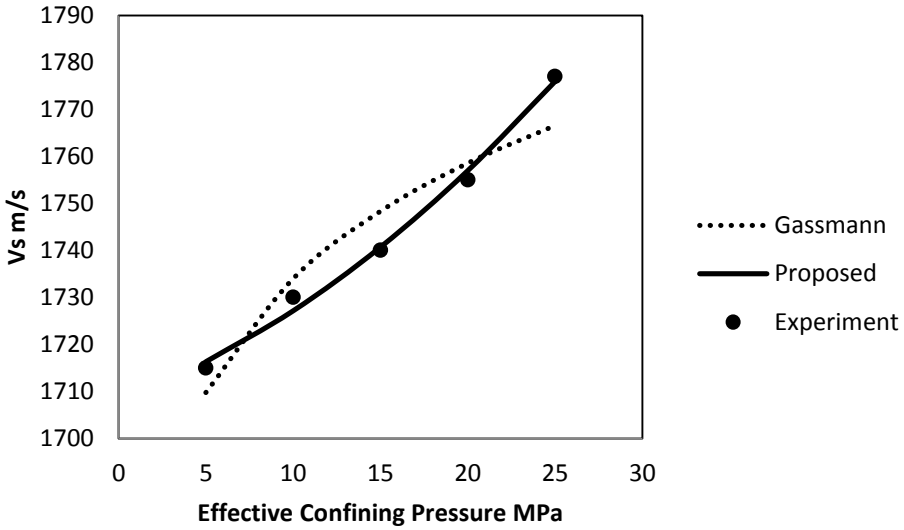

Figure F-11 S-wave velocity vs. Effective Confining Pressure Curves Fit for Sample No. 38

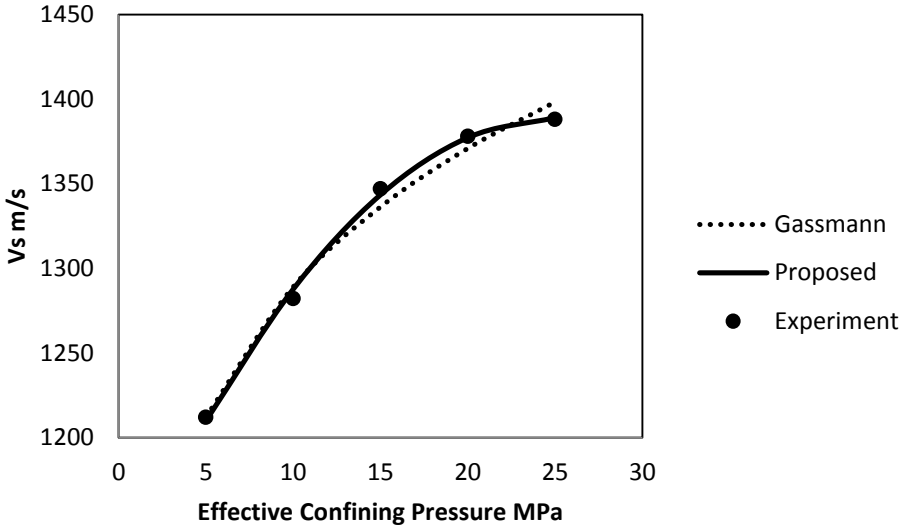

Figure F-12 S-wave velocity vs. Effective Confining Pressure Curves Fit for Sample No. 54

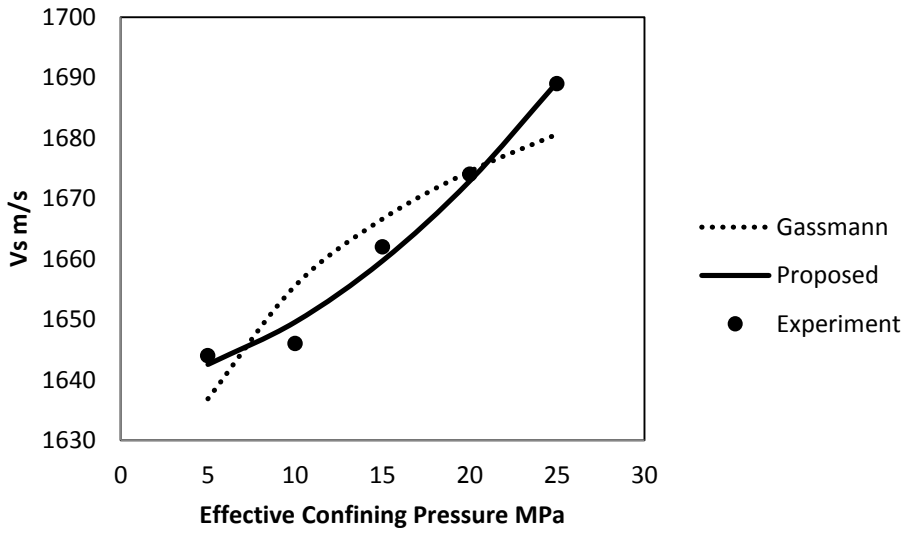

Figure F-13 S-wave velocity vs. Effective Confining Pressure Curves Fit for Sample No. 55

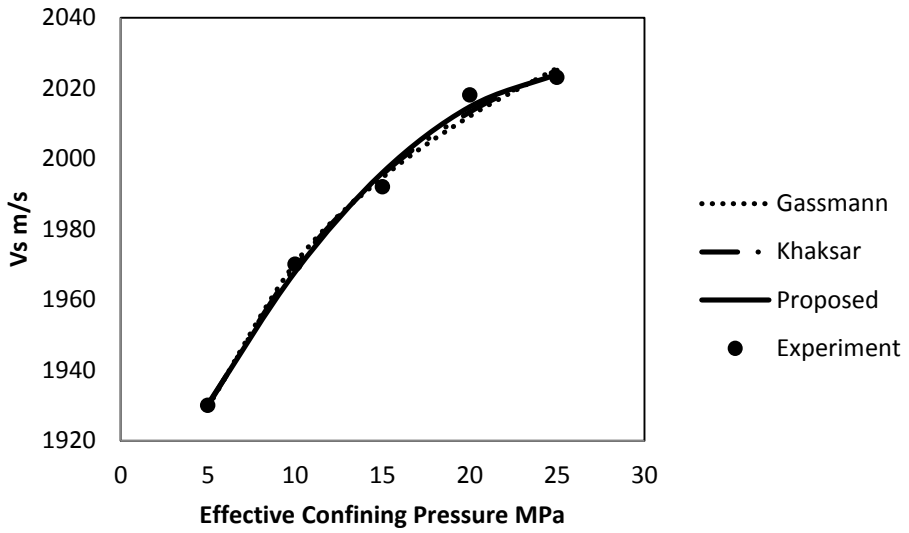

Figure F-14 S-wave velocity vs. Effective Confining Pressure Curves Fit for Sample No. 58

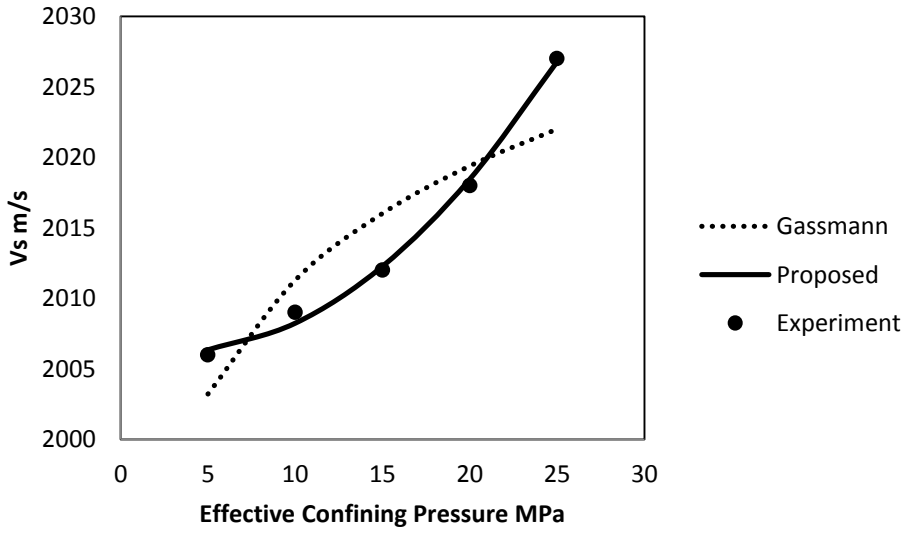

Figure F-15 S-wave velocity vs. Effective Confining Pressure Curves Fit for Sample No. 61

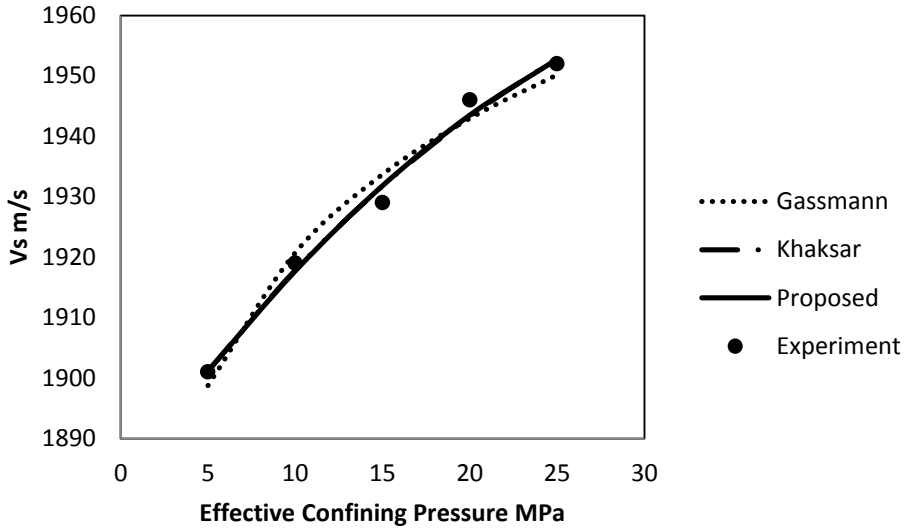

Figure F-16 S-wave velocity vs. Effective Confining Pressure Curves Fit for Sample No. 62

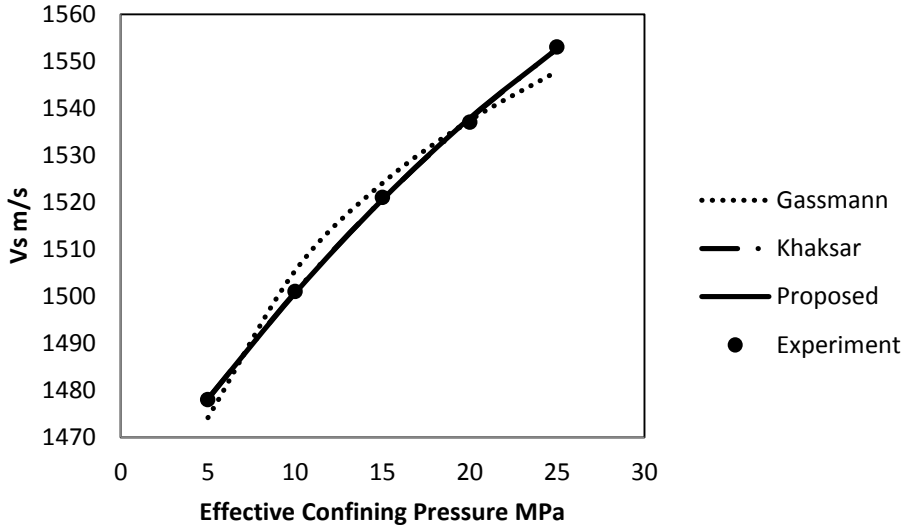

Figure F-17 S-wave velocity vs. Effective Confining Pressure Curves Fit for Sample No. 66

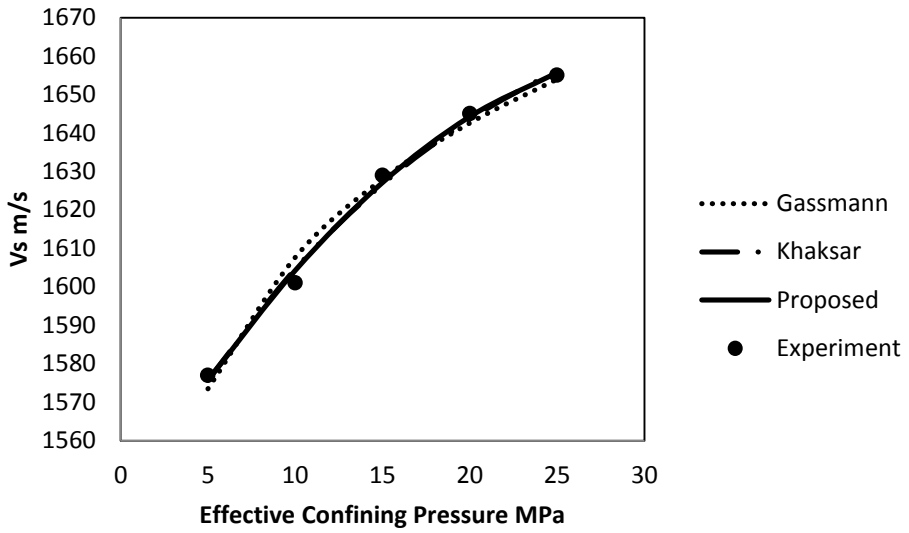

Figure F-18 S-wave velocity vs. Effective Confining Pressure Curves Fit for Sample No. 71

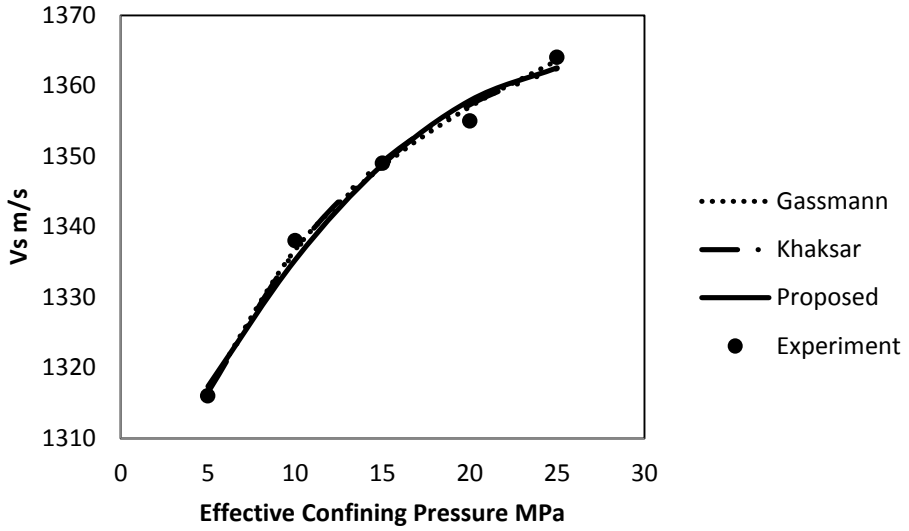

Figure F-19 S-wave velocity vs. Effective Confining Pressure Curves Fit for Sample No. 72

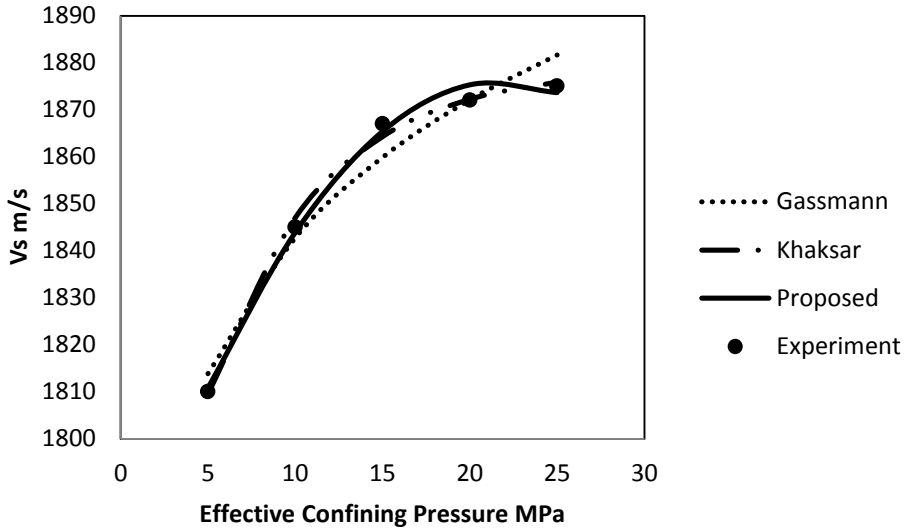

Figure F-20 S-wave velocity vs. Effective Confining Pressure Curves Fit for Sample No. 73

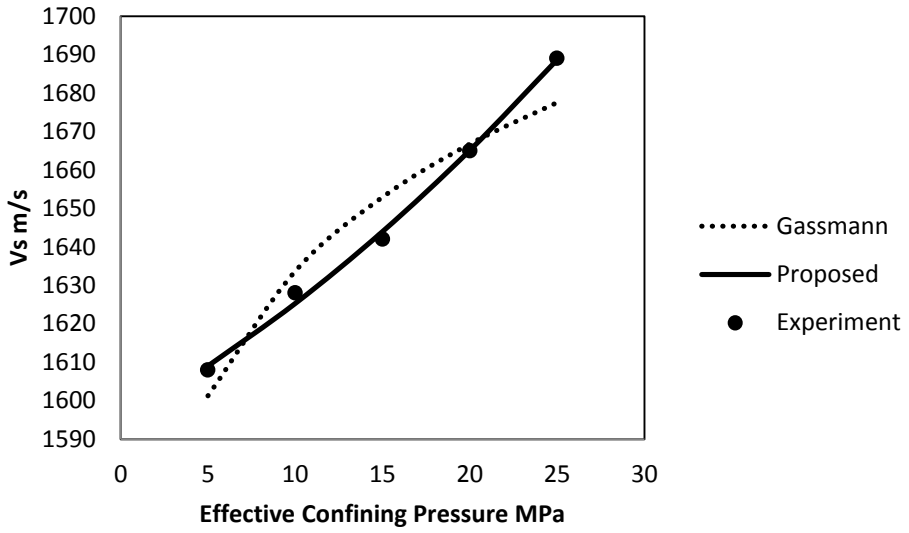

Figure F-21 S-wave velocity vs. Effective Confining Pressure Curves Fit for Sample No. 74

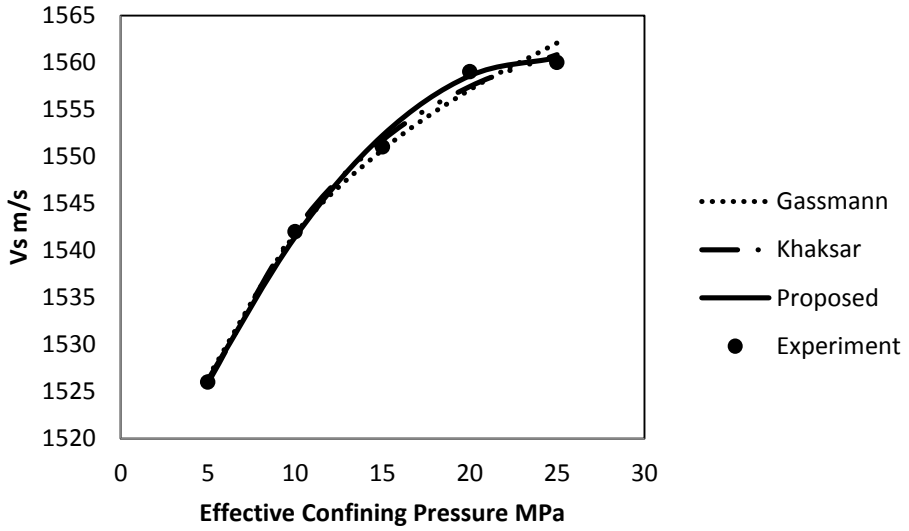

Figure F-22 S-wave velocity vs. Effective Confining Pressure Curves Fit for Sample No. 75

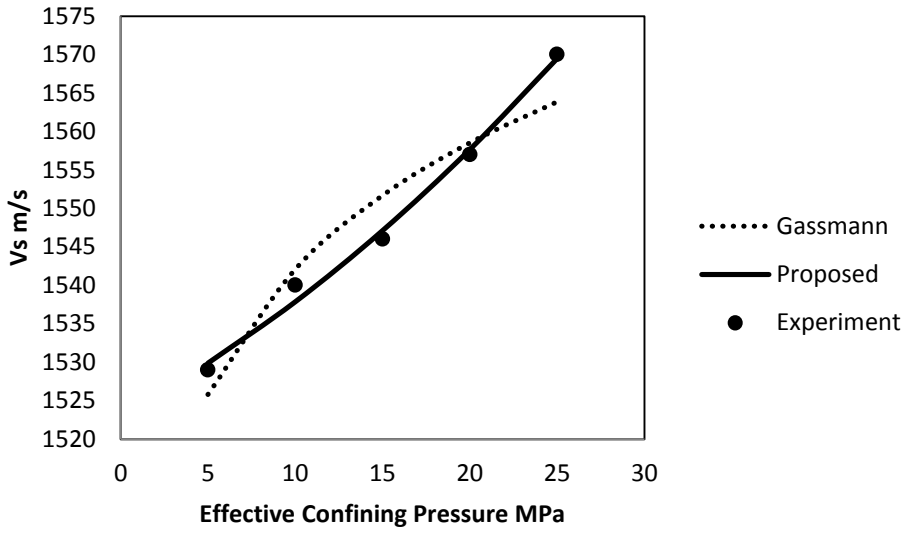

Figure F-23 S-wave velocity vs. Effective Confining Pressure Curves Fit for Sample No. 76

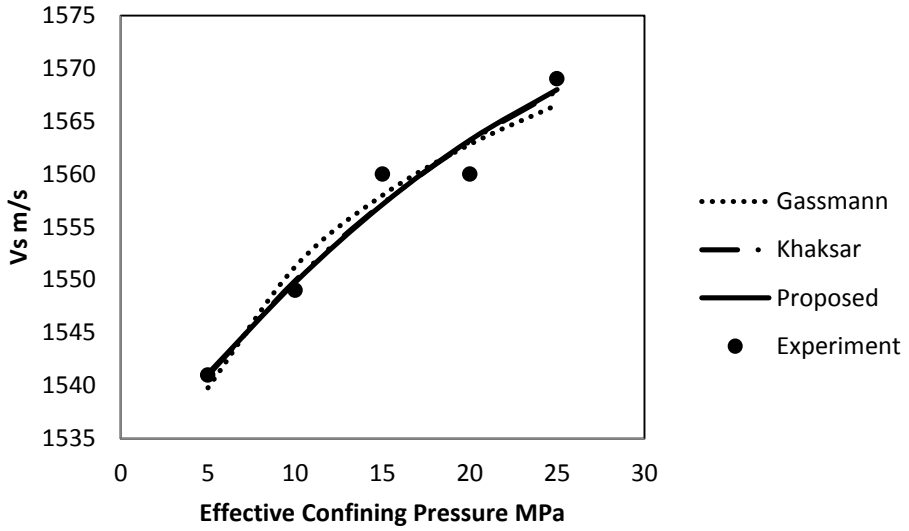

Figure F-24 S-wave velocity vs. Effective Confining Pressure Curves Fit for Sample No. 77

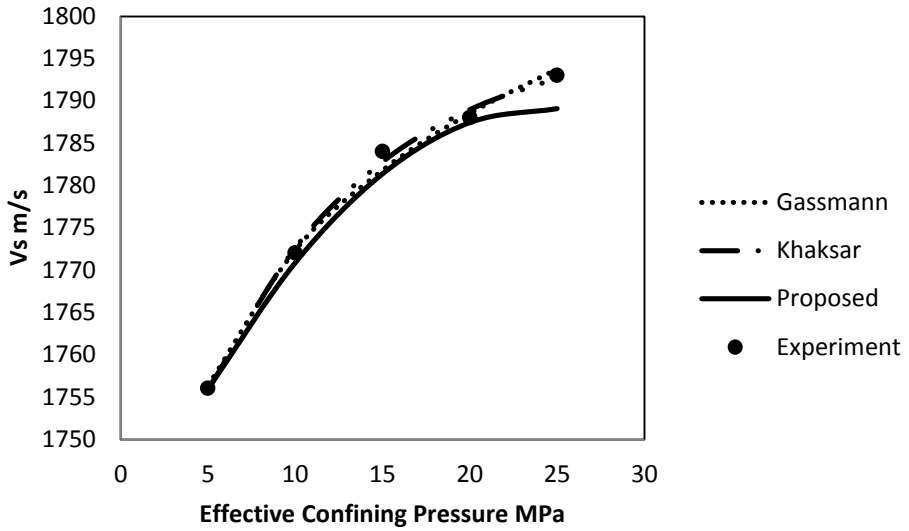

Figure F-25 S-wave velocity vs. Effective Confining Pressure Curves Fit for Sample No. 81

APPENDIX G

CURVES FITTING FOR TYPICAL SATURATED SAMPLES

PART A - P-WAVE VELOCITY CURVE FIT FOR ALL THE SAMPLES

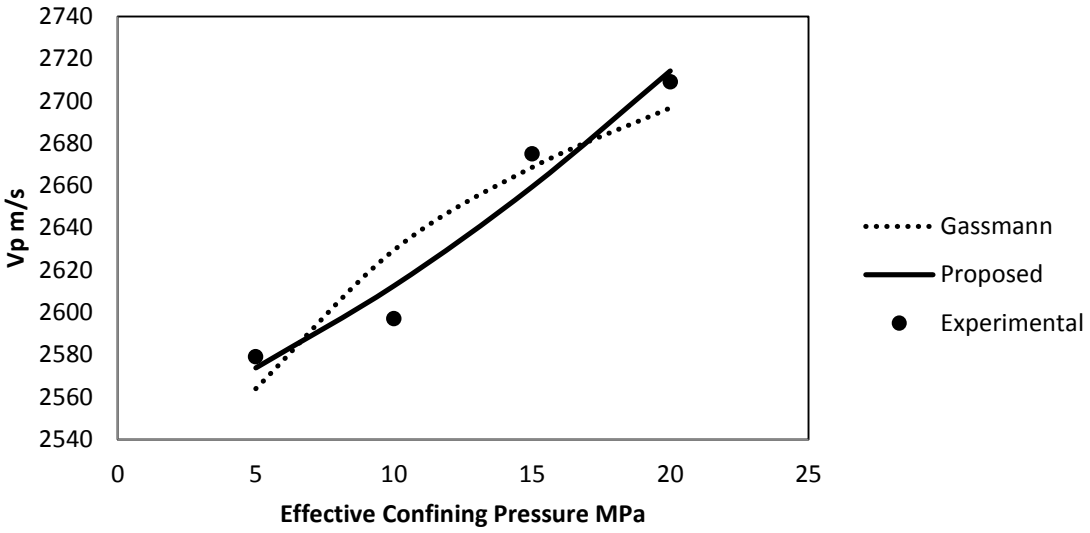

Figure G-1 P-wave velocity vs. Effective Confining Pressure Curves Fit for Sample No. 1

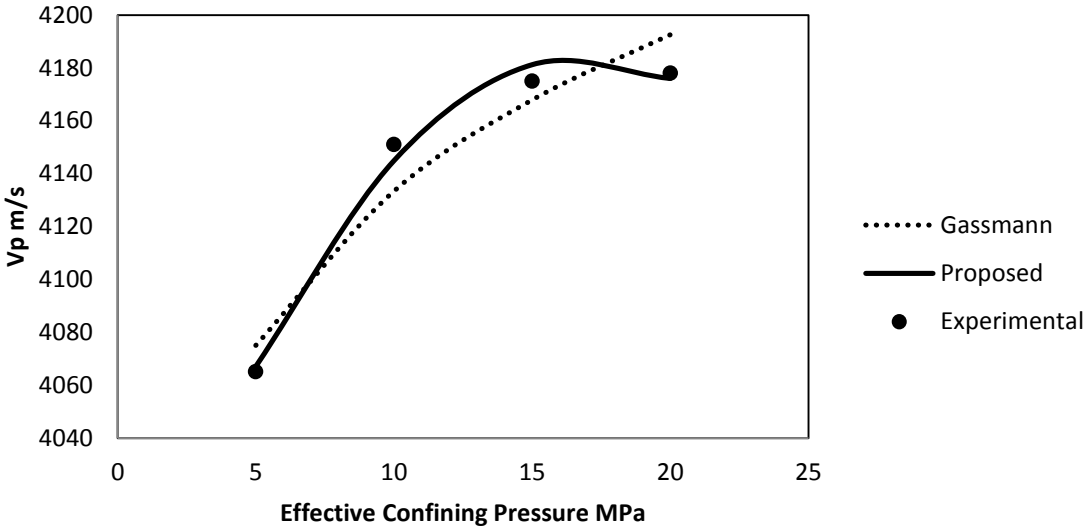

Figure G-2 P-wave velocity vs. Effective Confining Pressure Curves Fit for Sample No. 12

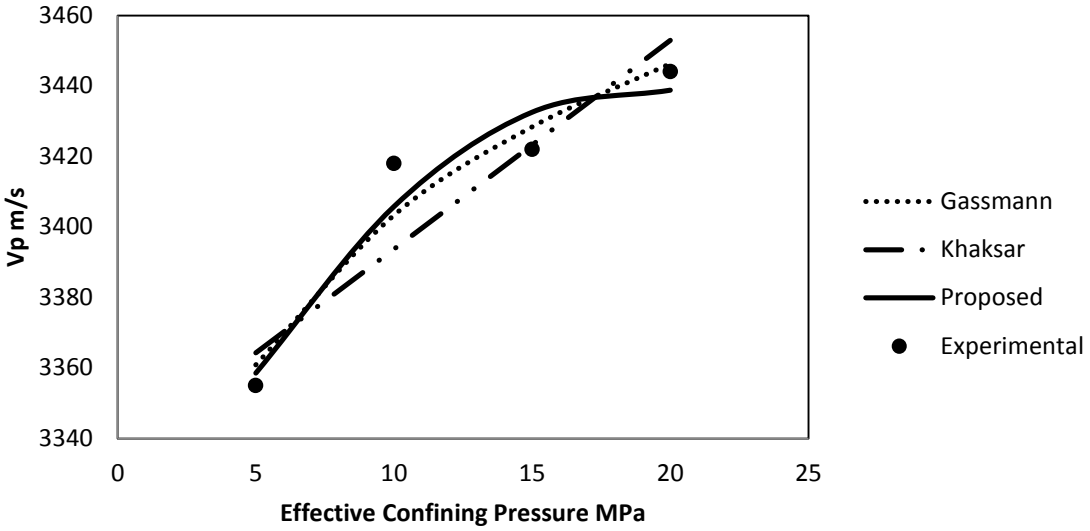

Figure G-4 P-wave velocity vs. Effective Confining Pressure Curves Fit for Sample No. 14

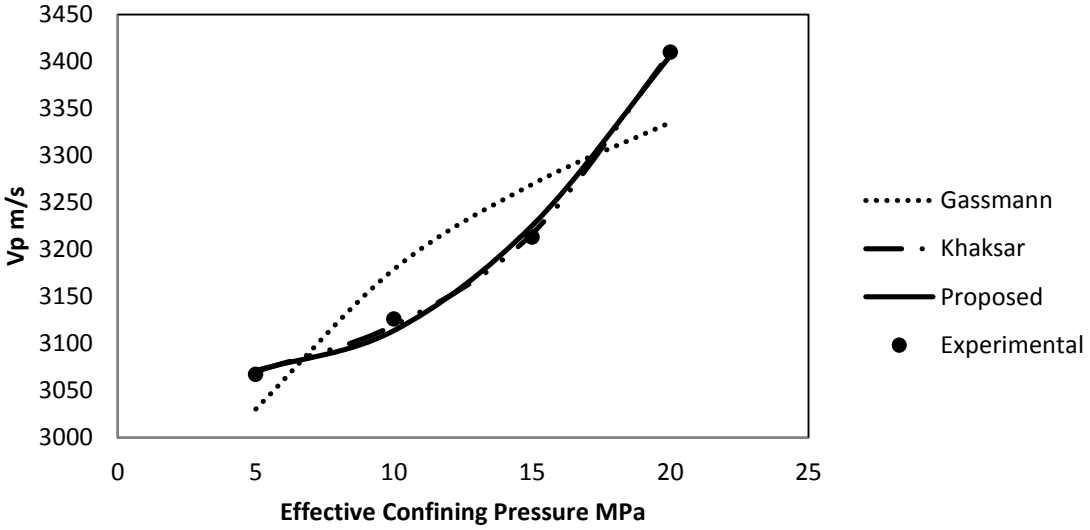

Figure G-5 P-wave velocity vs. Effective Confining Pressure Curves Fit for Sample No. 15

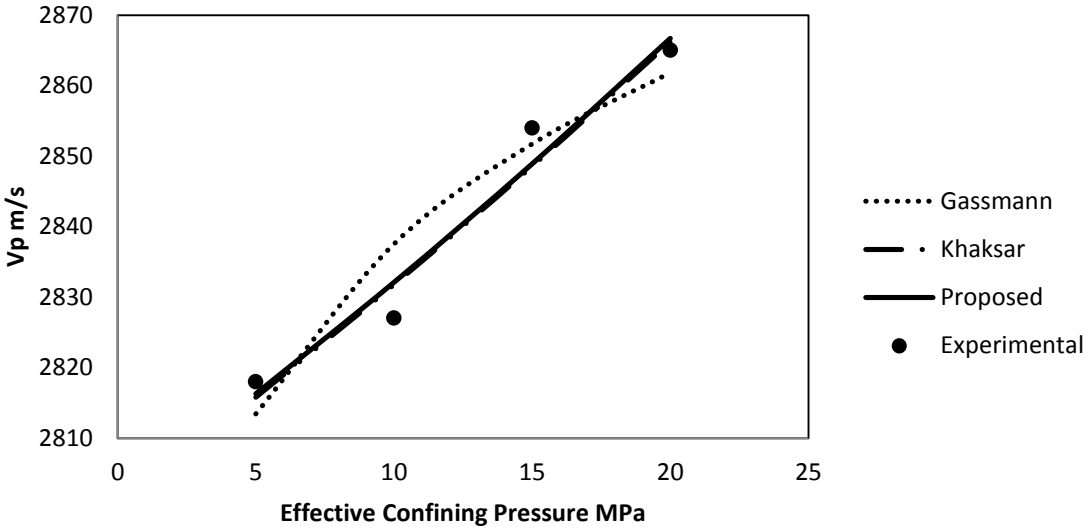

Figure G-6 P-wave velocity vs. Effective Confining Pressure Curves Fit for Sample No. 19

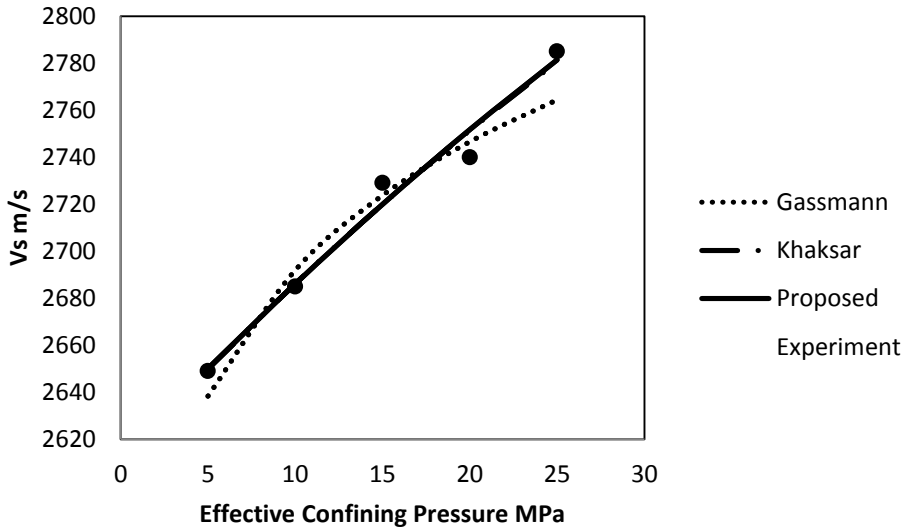

Figure G-7 P-wave velocity vs. Effective Confining Pressure Curves Fit for Sample No. 21

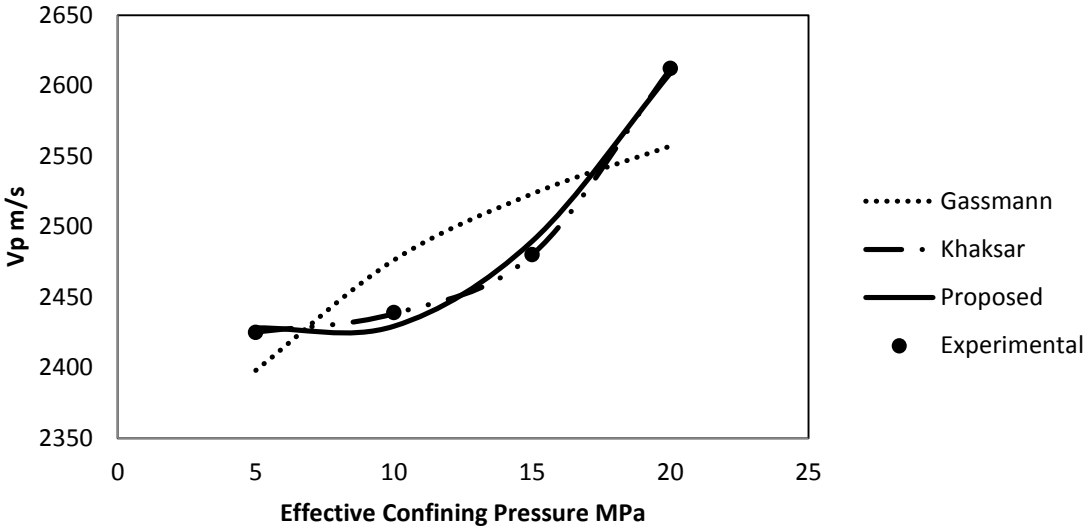

Figure G-8 P-wave velocity vs. Effective Confining Pressure Curves Fit for Sample No. 22

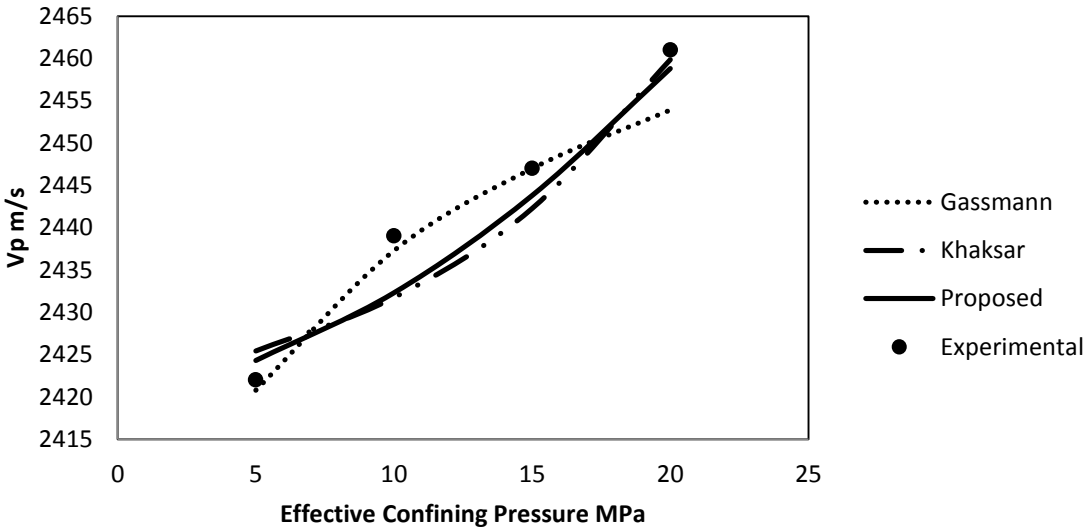

Figure F-9 P-wave velocity vs. Effective Confining Pressure Curves Fit for Sample No. 23

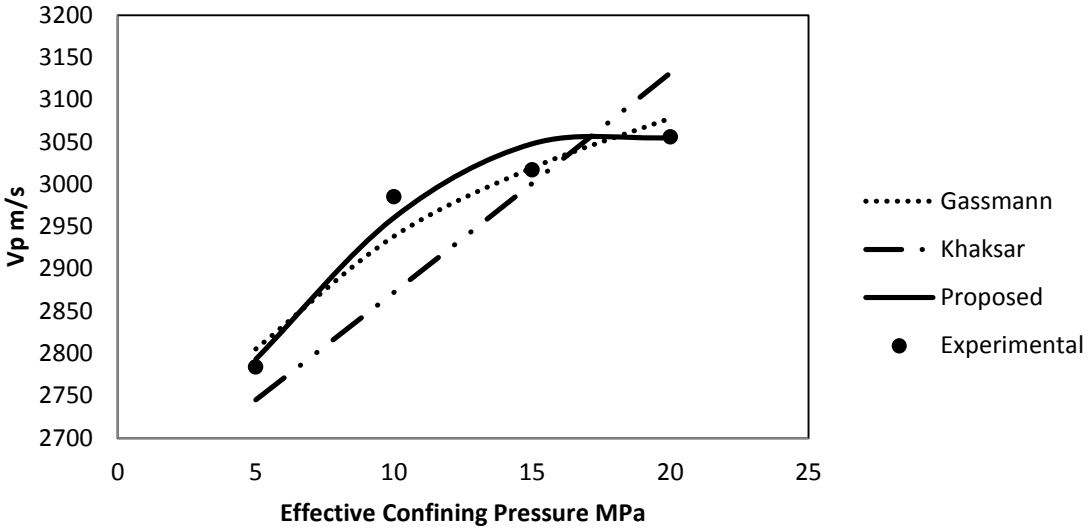

Figure F-10 P-wave velocity vs. Effective Confining Pressure Curves Fit for Sample No. 24

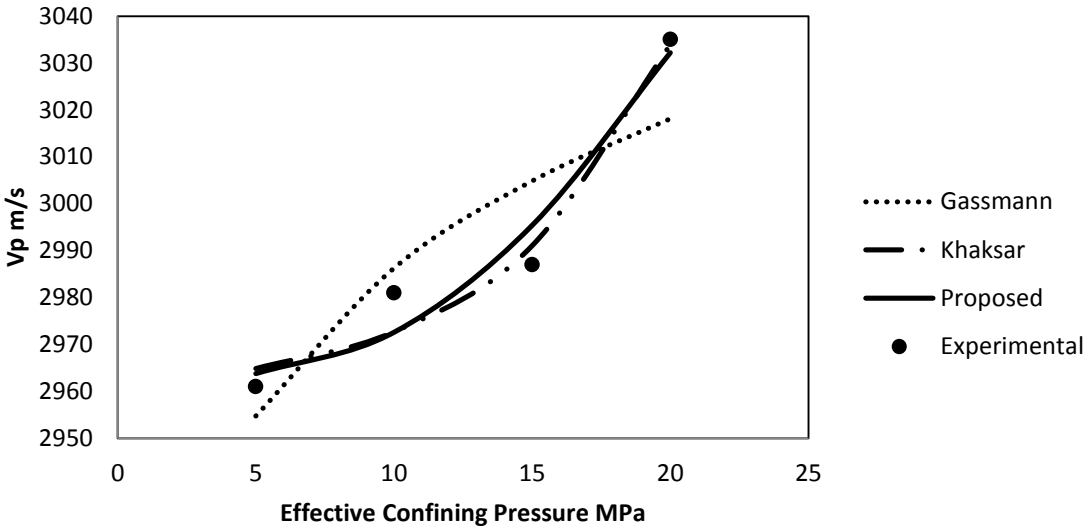

Figure G-11 P-wave velocity vs. Effective Confining Pressure Curves Fit for Sample No. 25

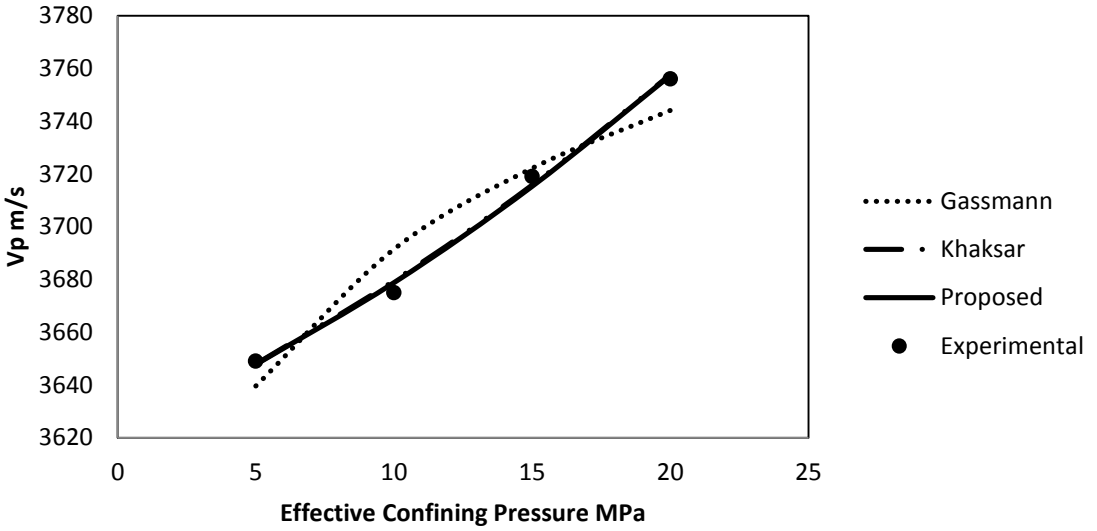

Figure F-12 P-wave velocity vs. Effective Confining Pressure Curves Fit for Sample No. 38

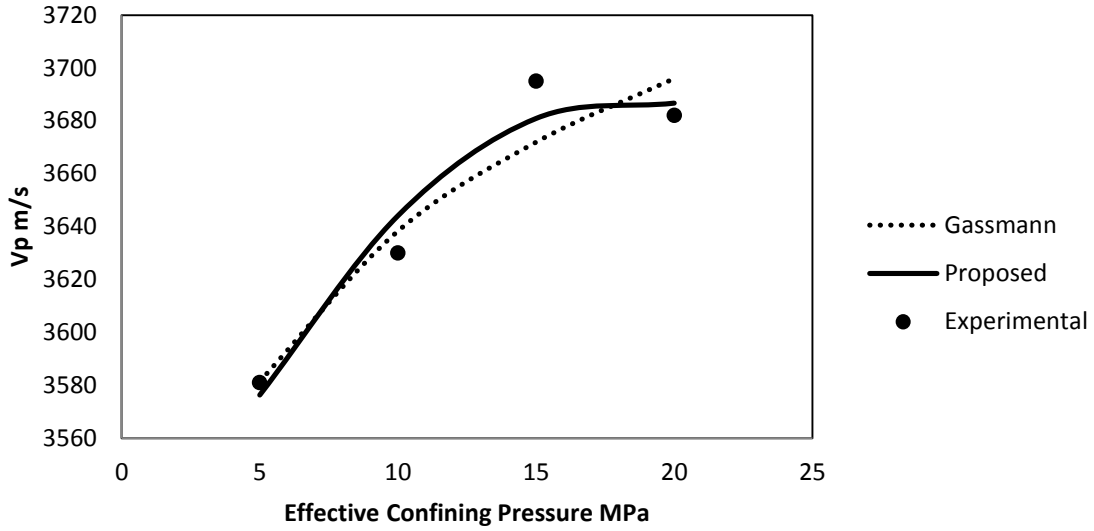

Figure G-13 P-wave velocity vs. Effective Confining Pressure Curves Fit for Sample No. 58

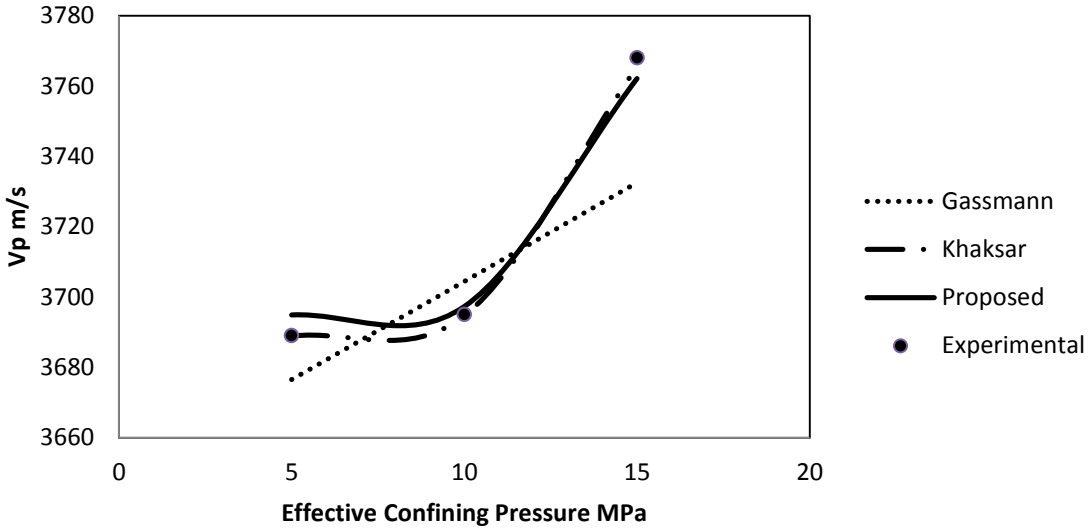

Figure G-14 P-wave velocity vs. Effective Confining Pressure Curves Fit for Sample No. 61

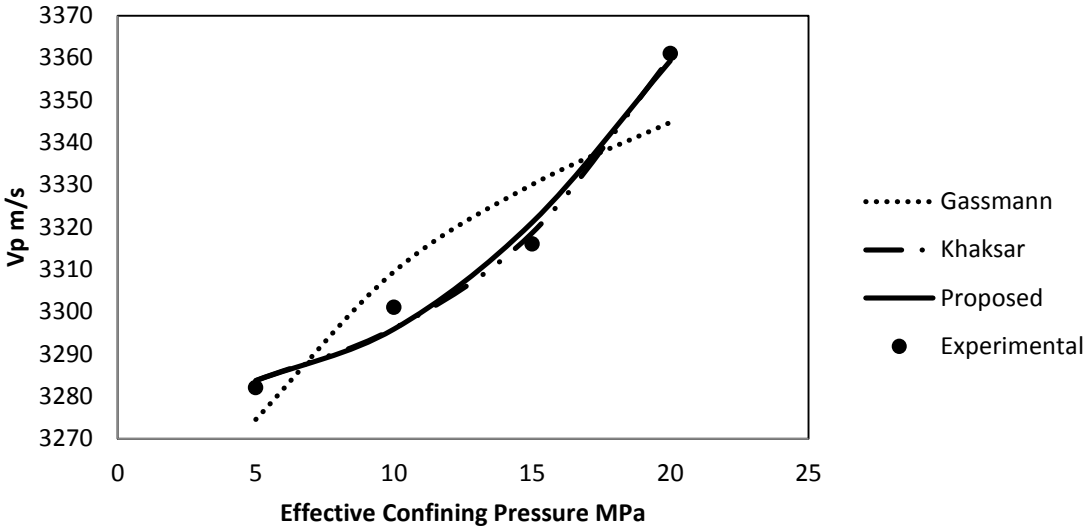

Figure G-15 P-wave velocity vs. Effective Confining Pressure Curves Fit for Sample No. 62

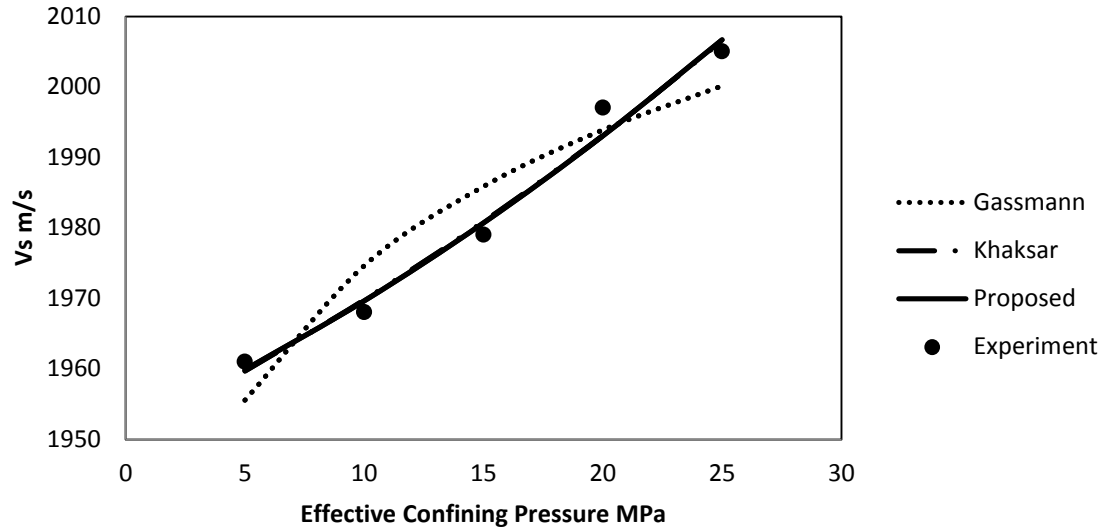

Figure G-16 P-wave velocity vs. Effective Confining Pressure Curves Fit for Sample No. 66

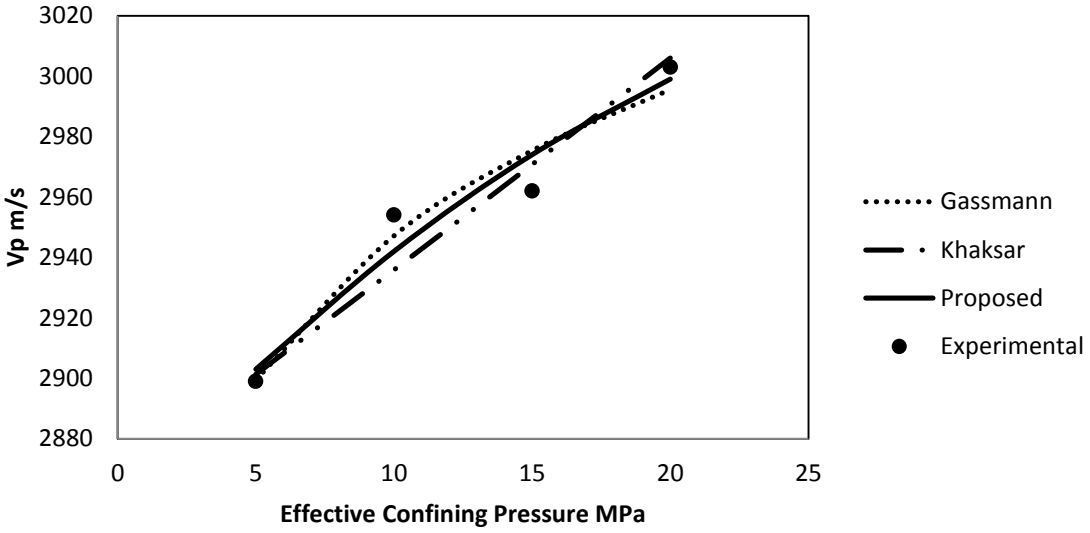

Figure G-17 P-wave velocity vs. Effective Confining Pressure Curves Fit for Sample No. 71

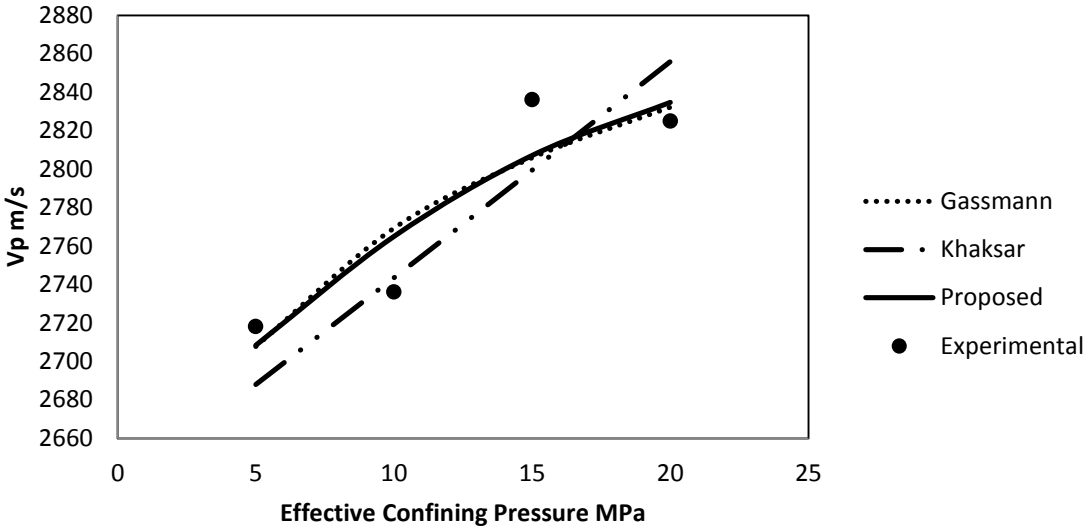

Figure G-18 P-wave velocity vs. Effective Confining Pressure Curves Fit for Sample No. 72

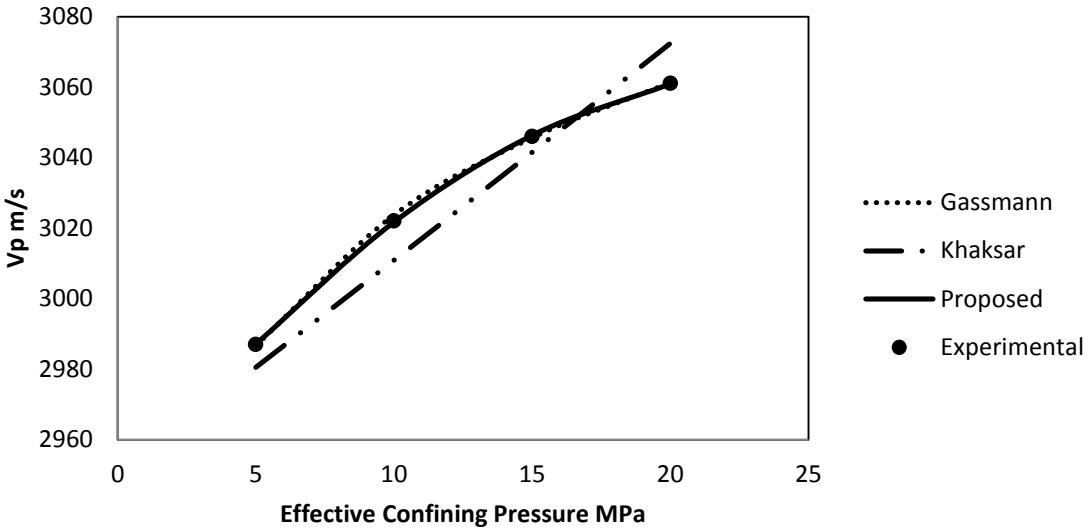

Figure G-19 P-wave velocity vs. Effective Confining Pressure Curves Fit for Sample No. 73

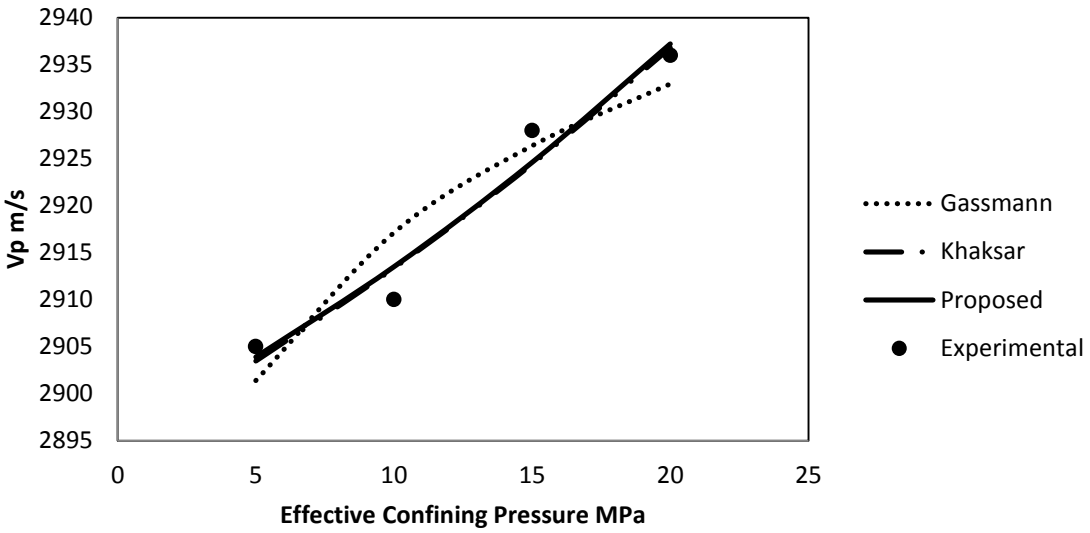

Figure G-20 P-wave velocity vs. Effective Confining Pressure Curves Fit for Sample No. 74

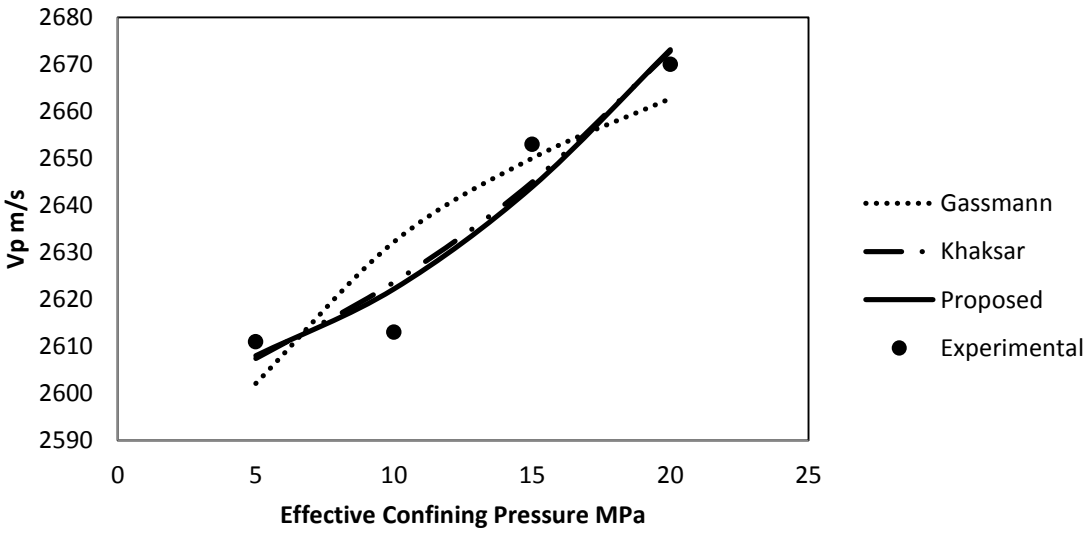

Figure G-21 P-wave velocity vs. Effective Confining Pressure Curves Fit for Sample No. 75

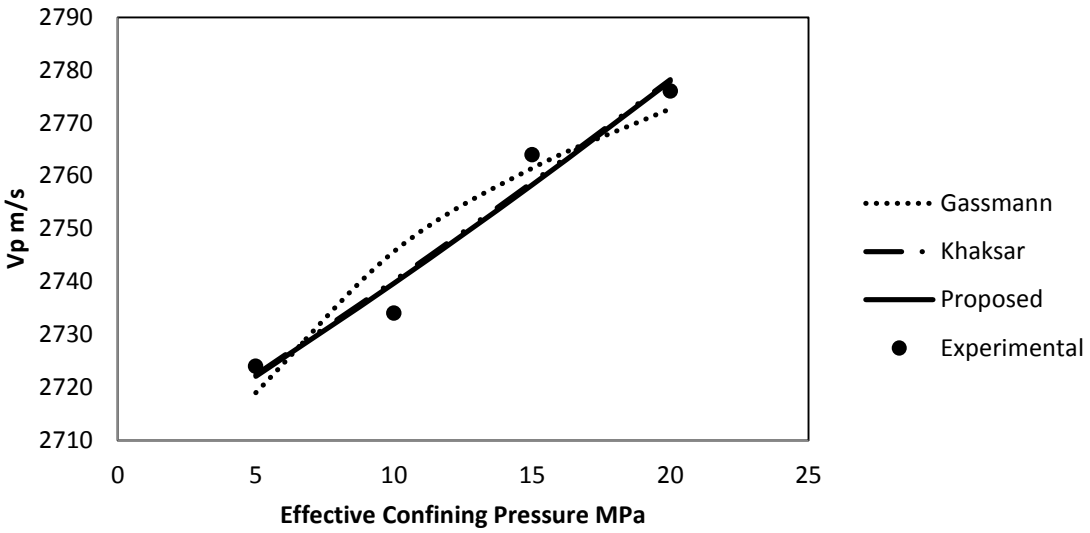

Figure G-22 P-wave velocity vs. Effective Confining Pressure Curves Fit for Sample No. 76

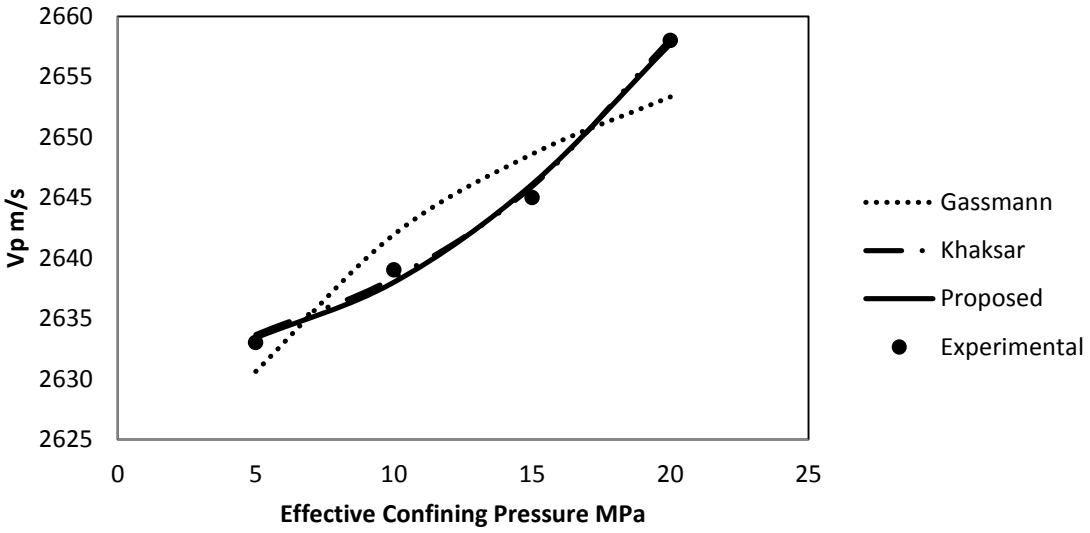

Figure G-23 P-wave velocity vs. Effective Confining Pressure Curves Fit for Sample No. 77

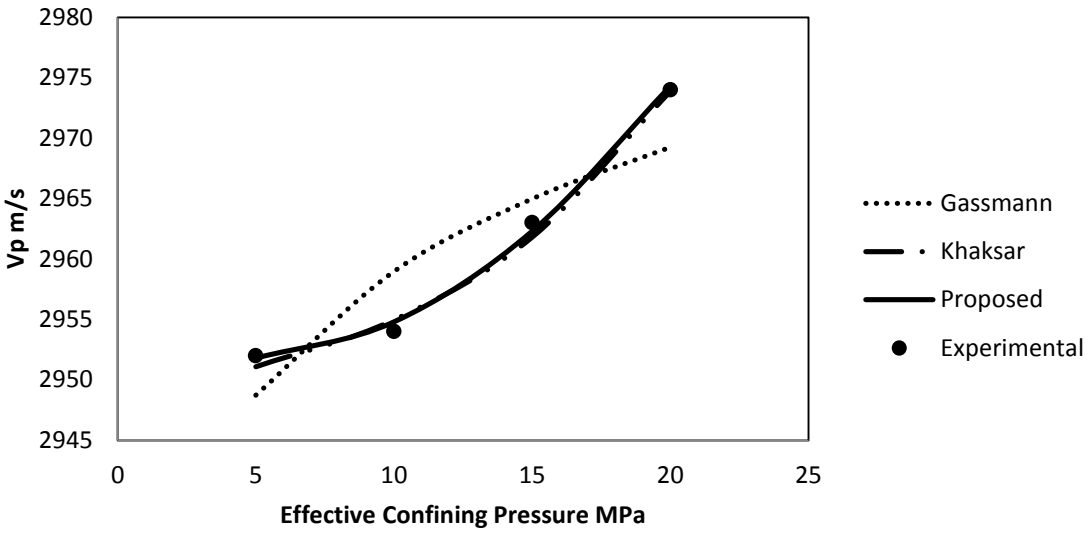

Figure G-24 P-wave velocity vs. Effective Confining Pressure Curves Fit for Sample No. 81

PART B –S-WAVE VELOCITY CURVE FIT FOR TYPICAL SATURATED SAMPLES

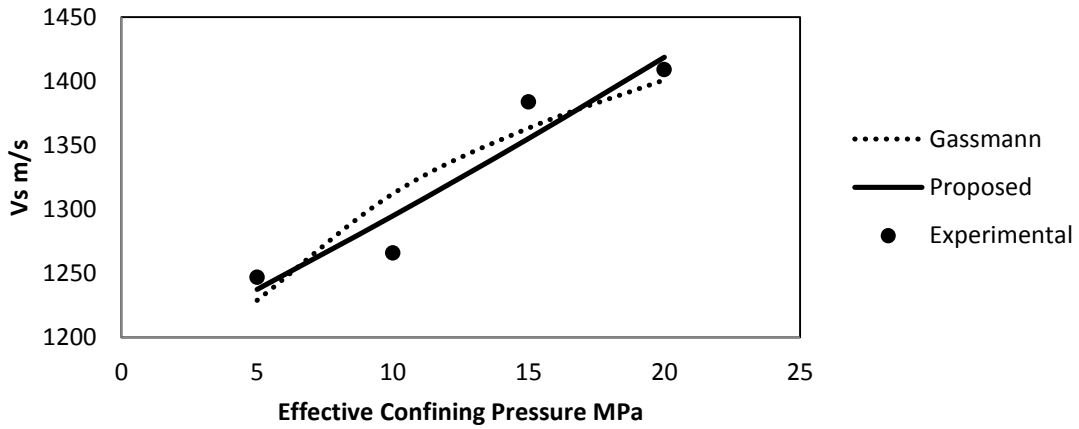

Figure G-1 S-wave velocity vs. Effective Confining Pressure Curves Fit for Sample No. 1

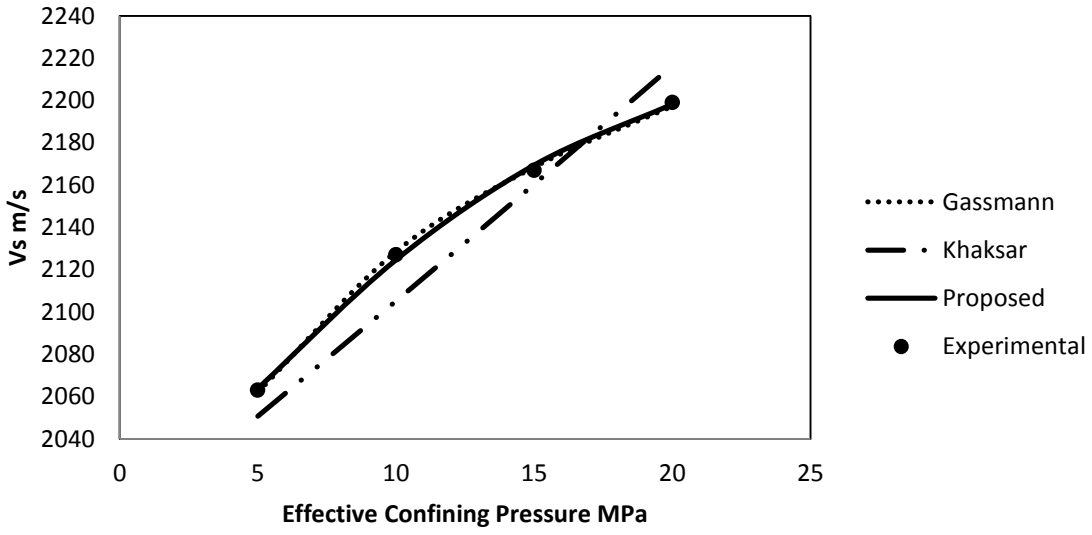

Figure G-2 S-wave velocity vs. Effective Confining Pressure Curves Fit for Sample No. 12

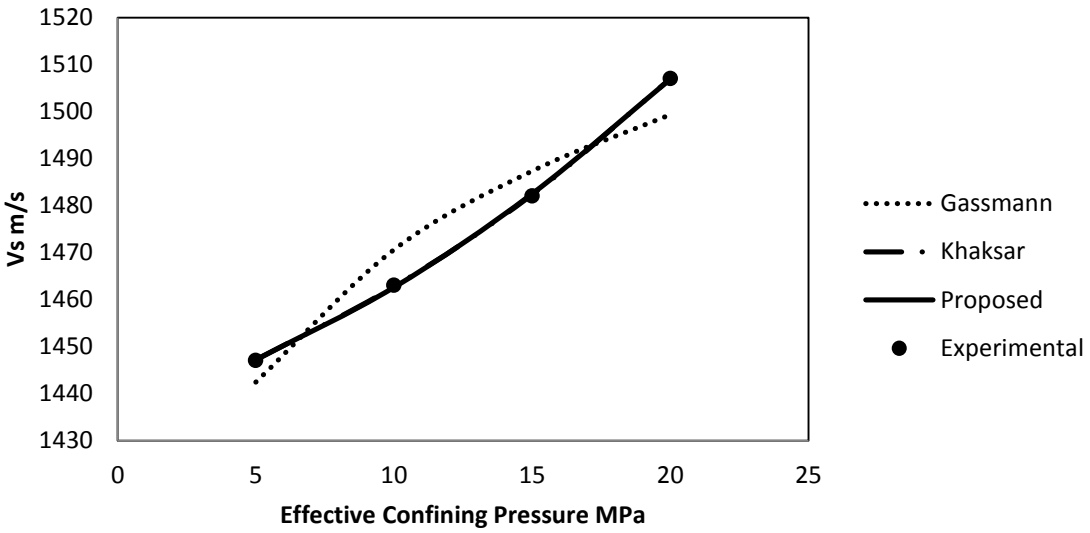

Figure G-3 S-wave velocity vs. Effective Confining Pressure Curves Fit for Sample No. 13

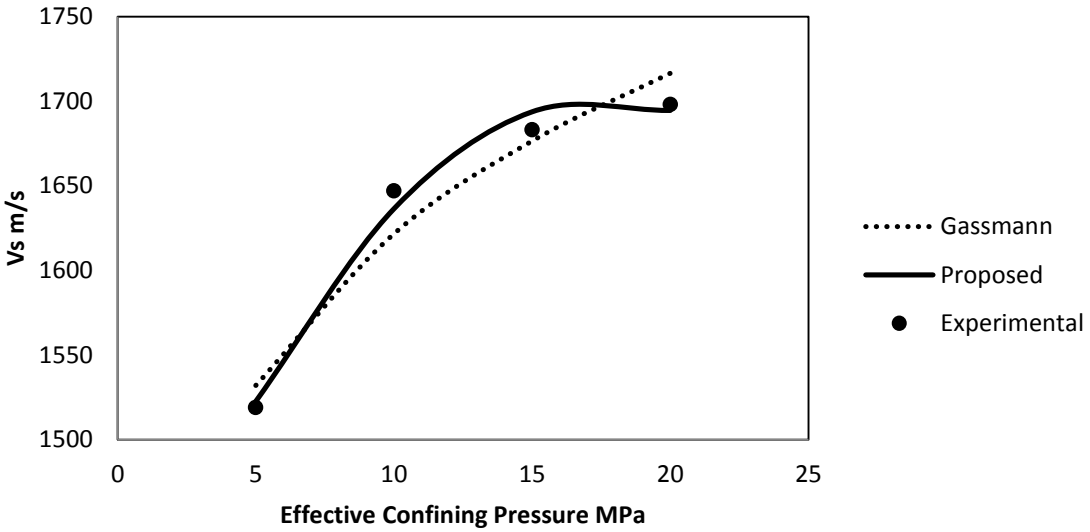

Figure G-4 S-wave velocity vs. Effective Confining Pressure Curves Fit for Sample No. 14

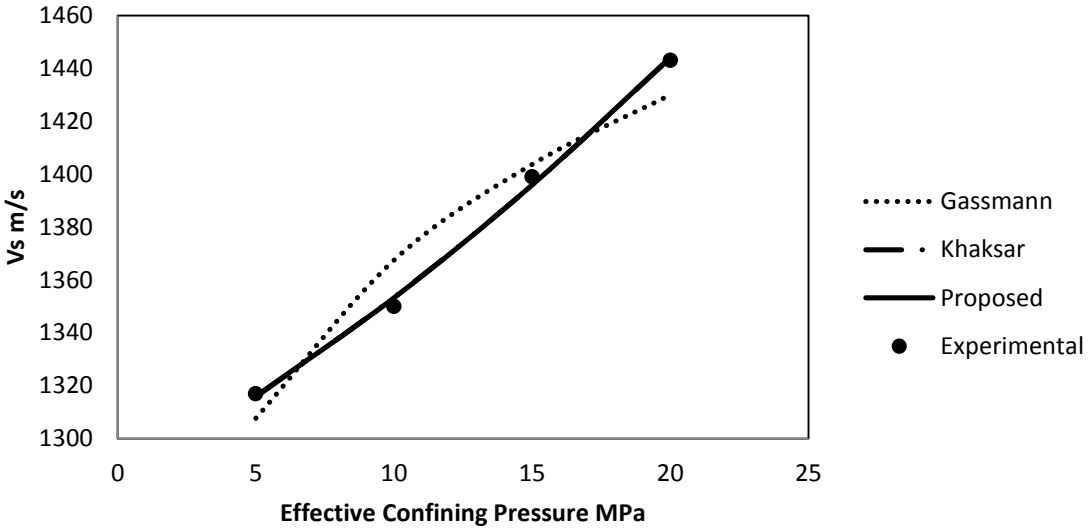

Figure G-5 S-wave velocity vs. Effective Confining Pressure Curves Fit for Sample No. 15

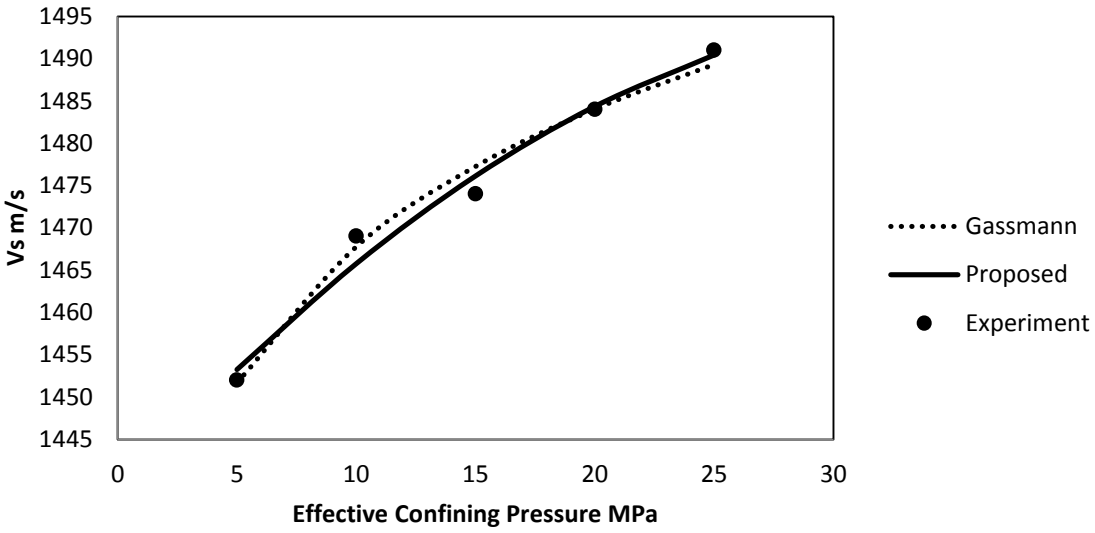

Figure G-6 S-wave velocity vs. Effective Confining Pressure Curves Fit for Sample No. 19

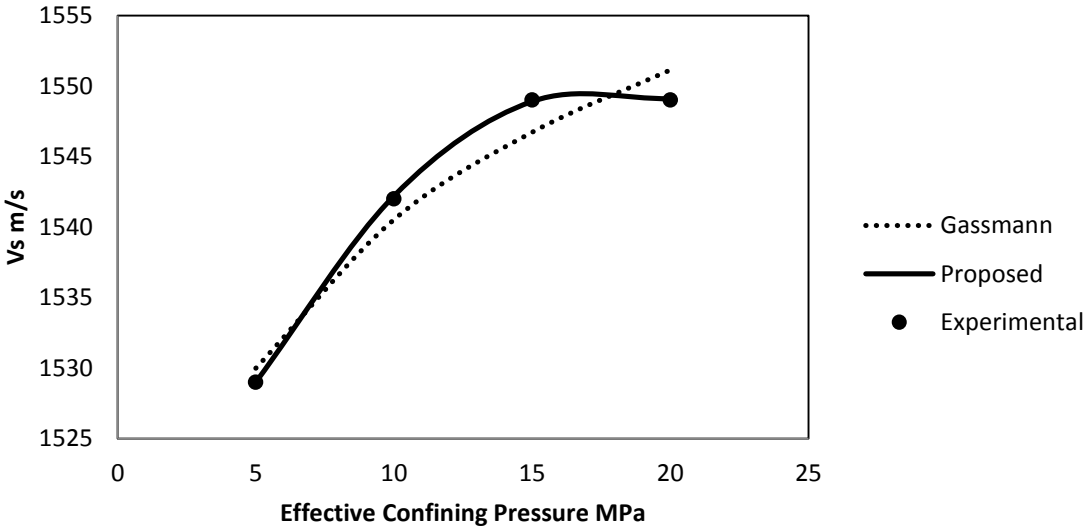

Figure G-7 S-wave velocity vs. Effective Confining Pressure Curves Fit for Sample No. 21

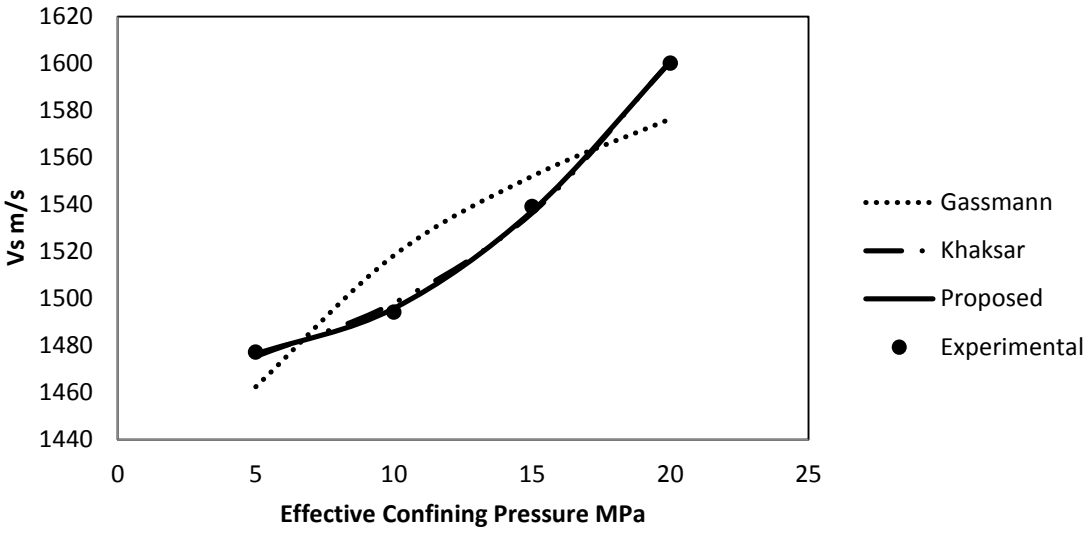

Figure G-8 S-wave velocity vs. Effective Confining Pressure Curves Fit for Sample No. 22

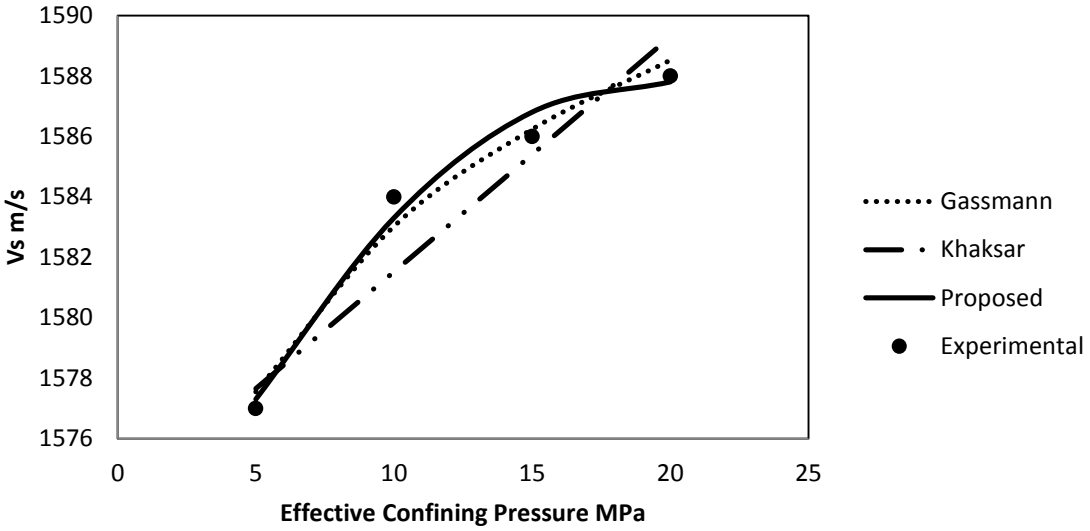

Figure G-9 S-wave velocity vs. Effective Confining Pressure Curves Fit for Sample No. 23

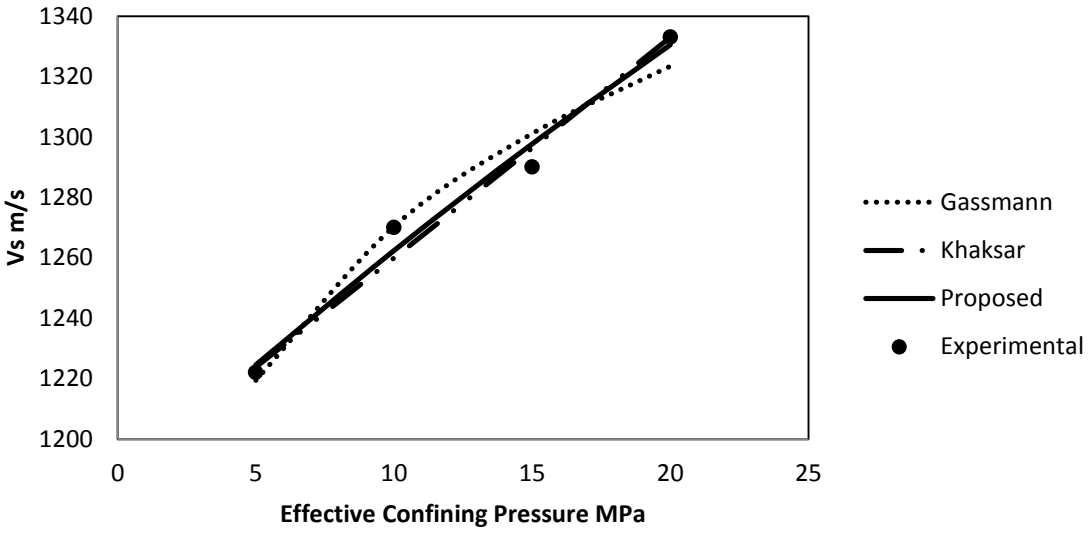

Figure G-10 S-wave velocity vs. Effective Confining Pressure Curves Fit for Sample No. 24

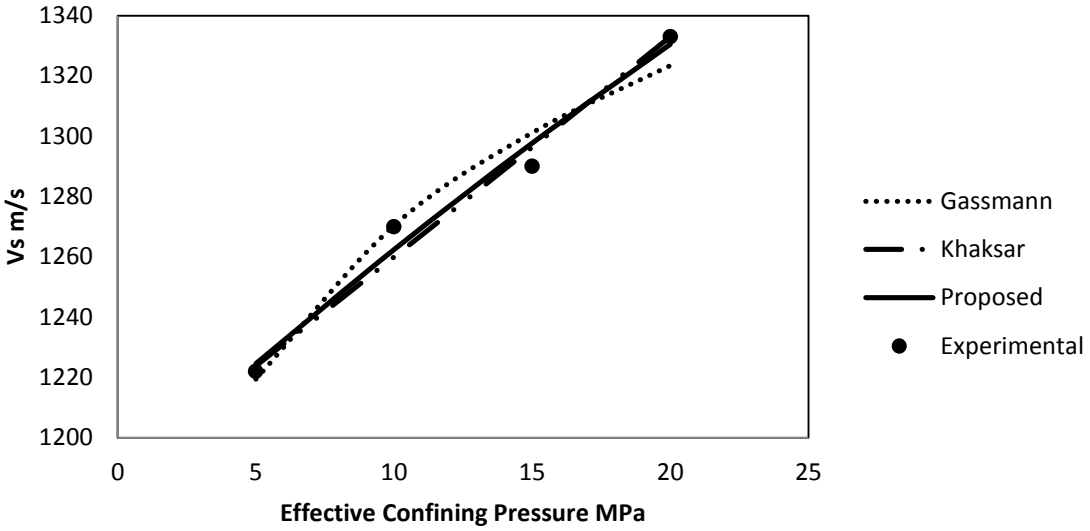

Figure G-11 S-wave velocity vs. Effective Confining Pressure Curves Fit for Sample No. 25

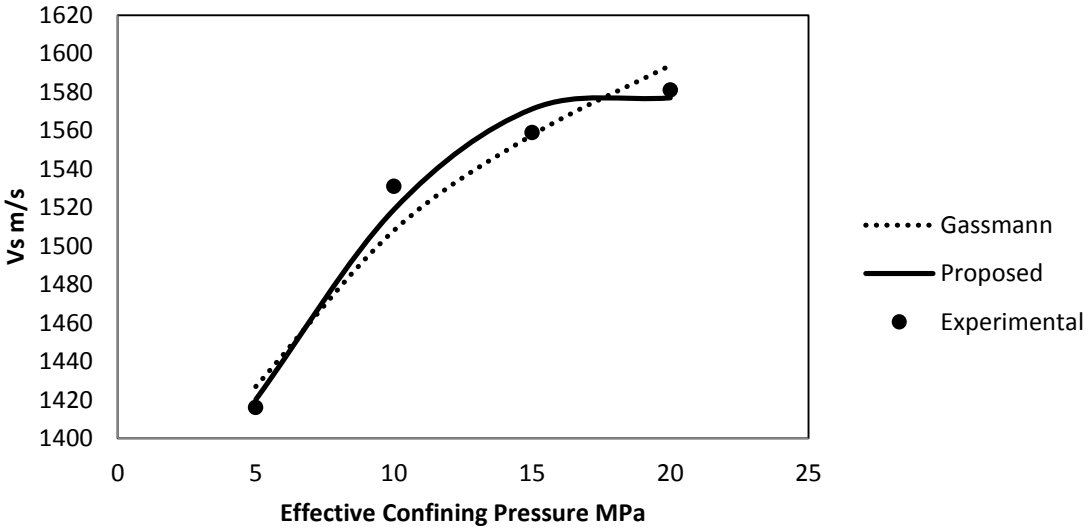

Figure G-12 S-wave velocity vs. Effective Confining Pressure Curves Fit for Sample No. 38

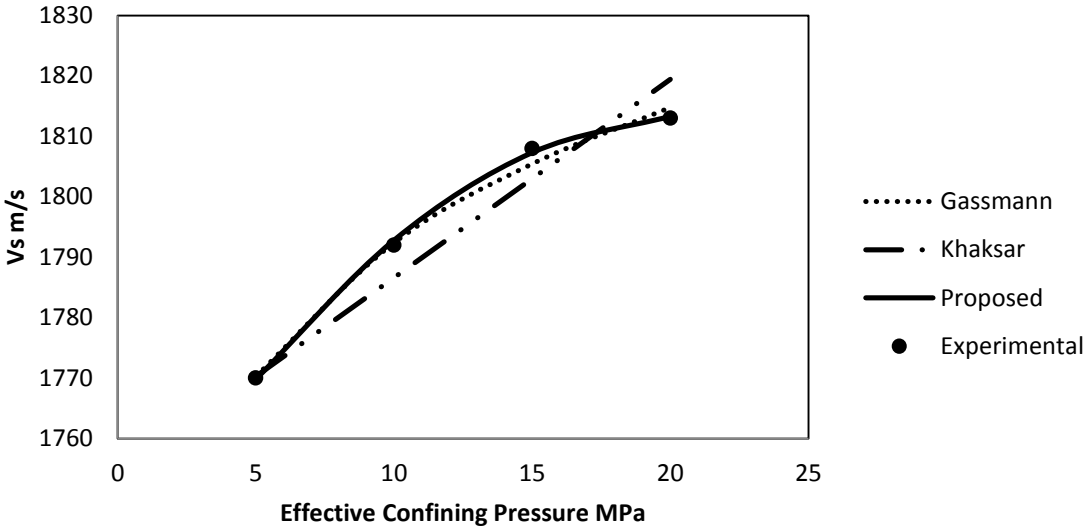

Figure G-13 S-wave velocity vs. Effective Confining Pressure Curves Fit for Sample No. 58

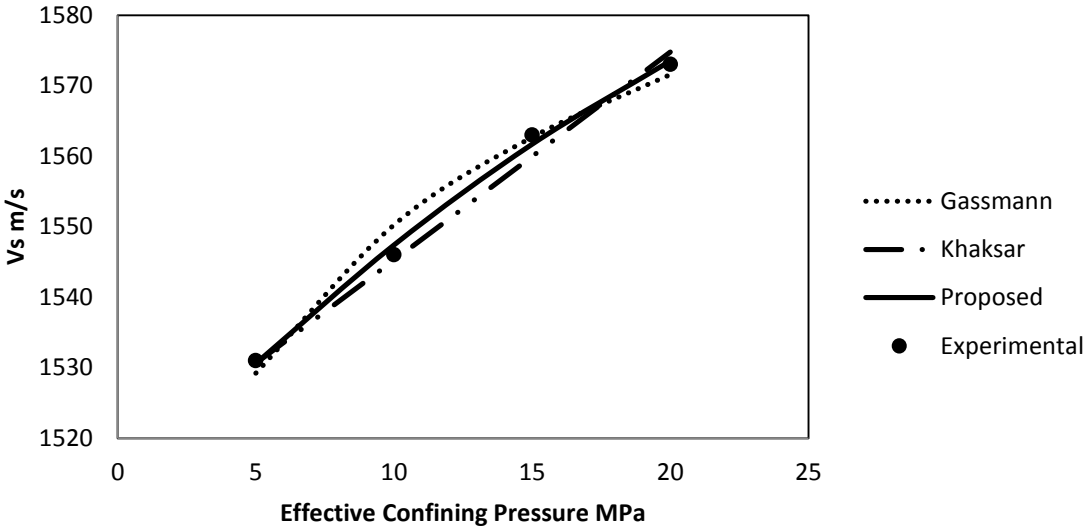

Figure G-14 S-wave velocity vs. Effective Confining Pressure Curves Fit for Sample No. 61

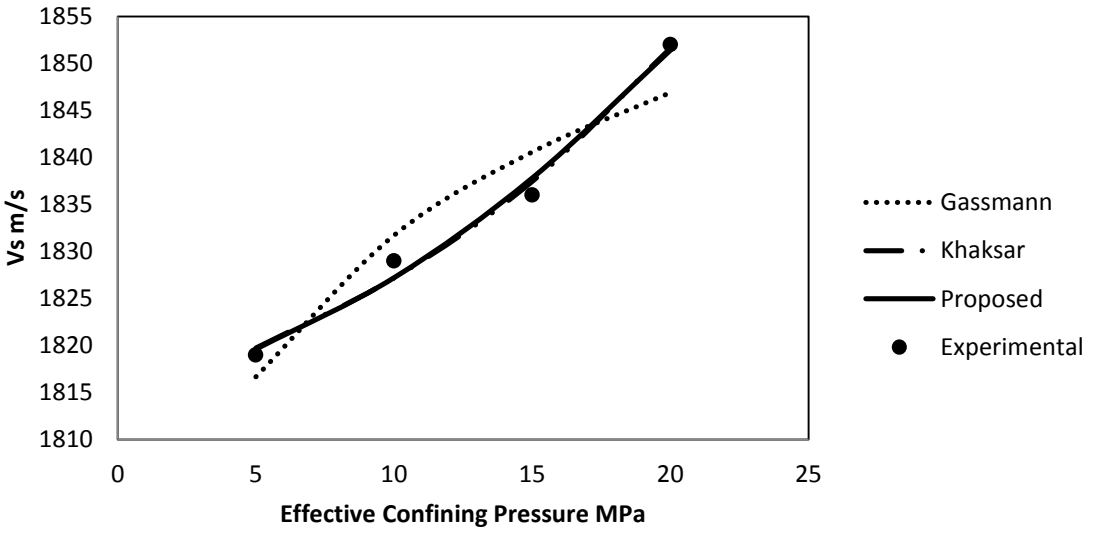

Figure G-15 S-wave velocity vs. Effective Confining Pressure Curves Fit for Sample No. 62

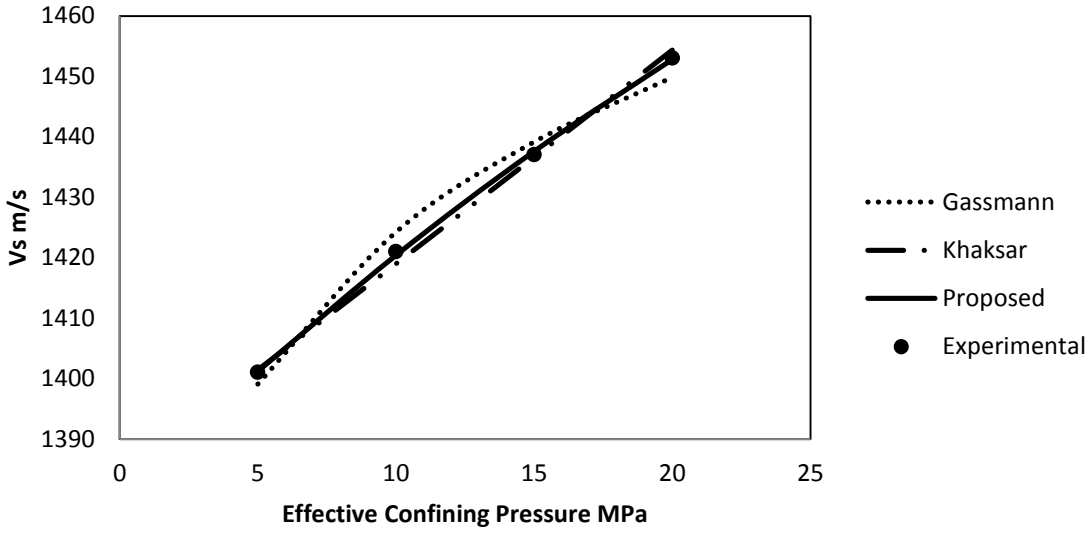

Figure G-16 S-wave velocity vs. Effective Confining Pressure Curves Fit for Sample No. 66

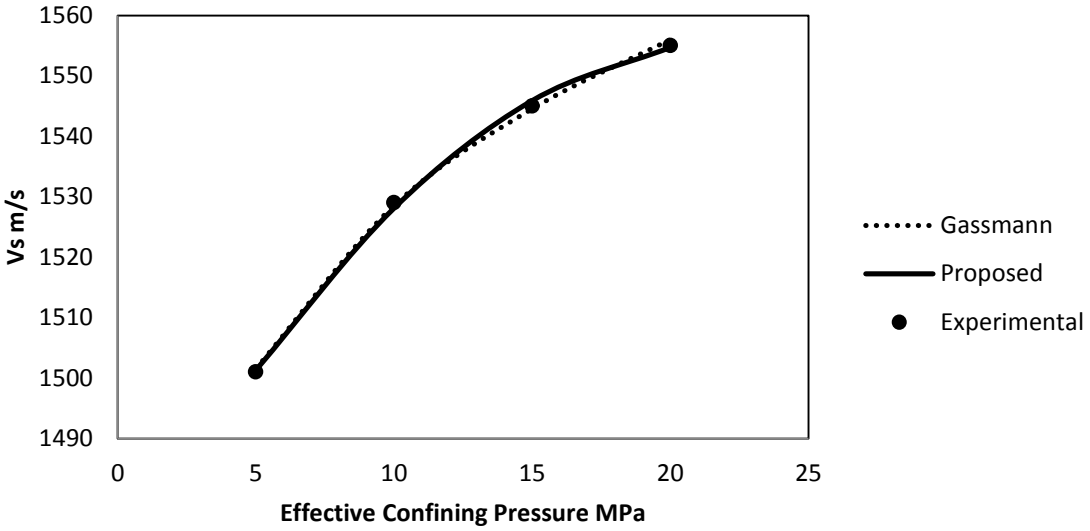

Figure G-17 S-wave velocity vs. Effective Confining Pressure Curves Fit for Sample No. 71

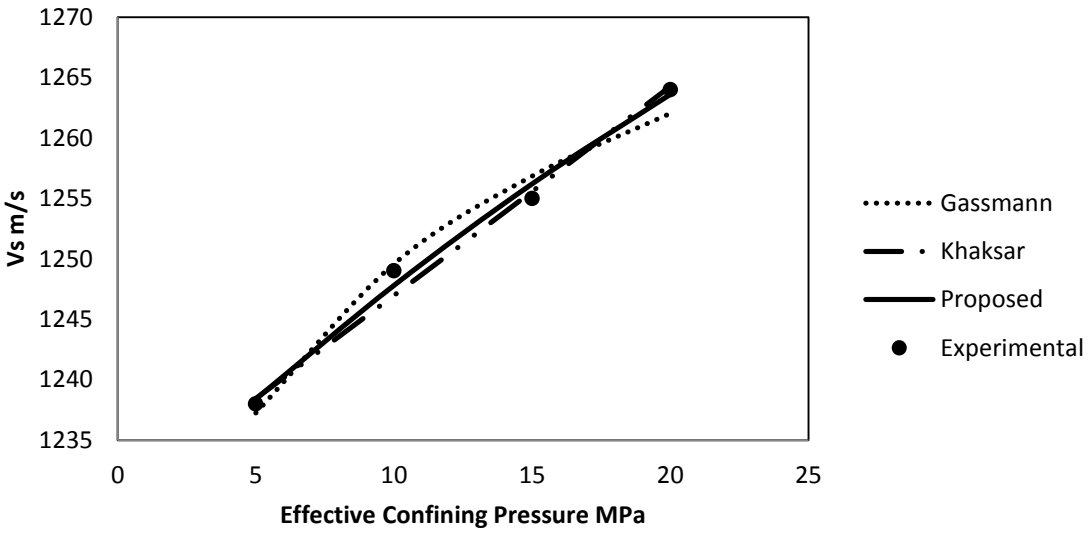

Figure G-18 S-wave velocity vs. Effective Confining Pressure Curves Fit for Sample No. 72

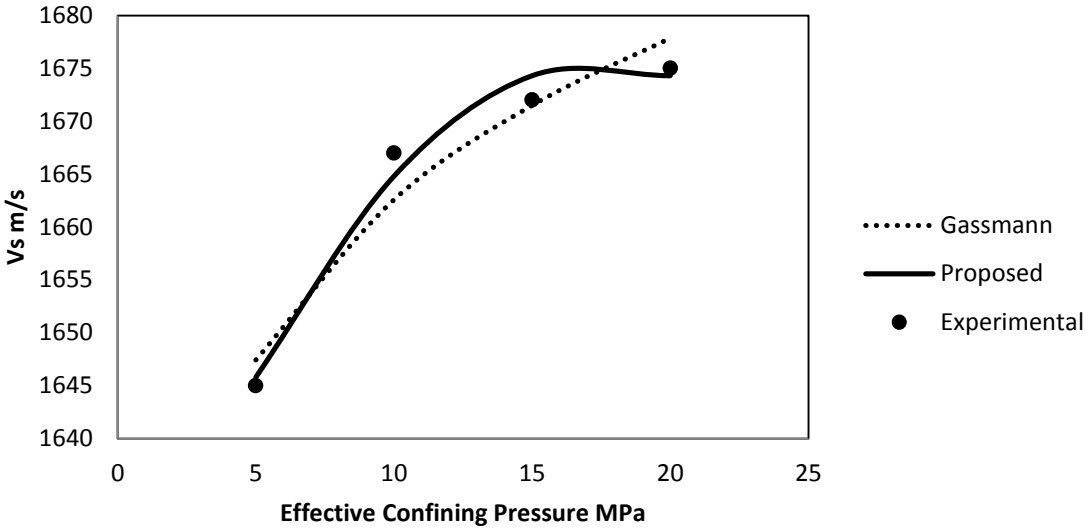

Figure G-19 S-wave velocity vs. Effective Confining Pressure Curves Fit for Sample No. 73

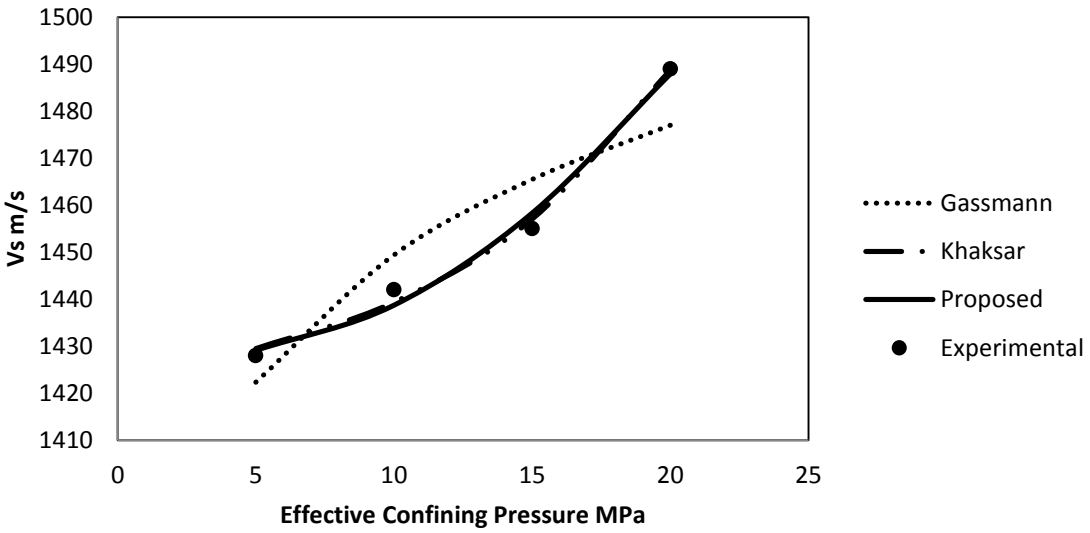

Figure G-20 S-wave velocity vs. Effective Confining Pressure Curves Fit for Sample No. 74

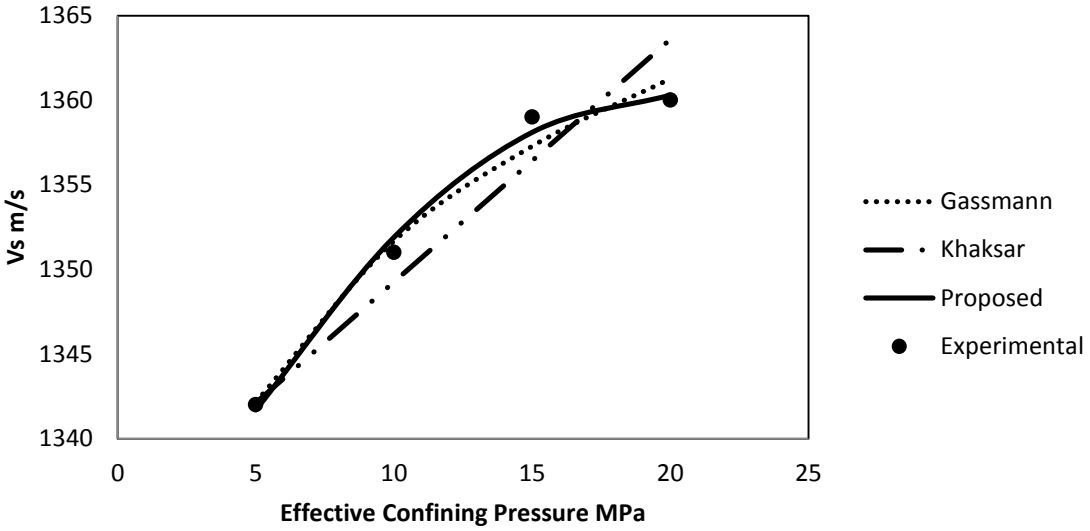

Figure G-21 S-wave velocity vs. Effective Confining Pressure Curves Fit for Sample No. 75

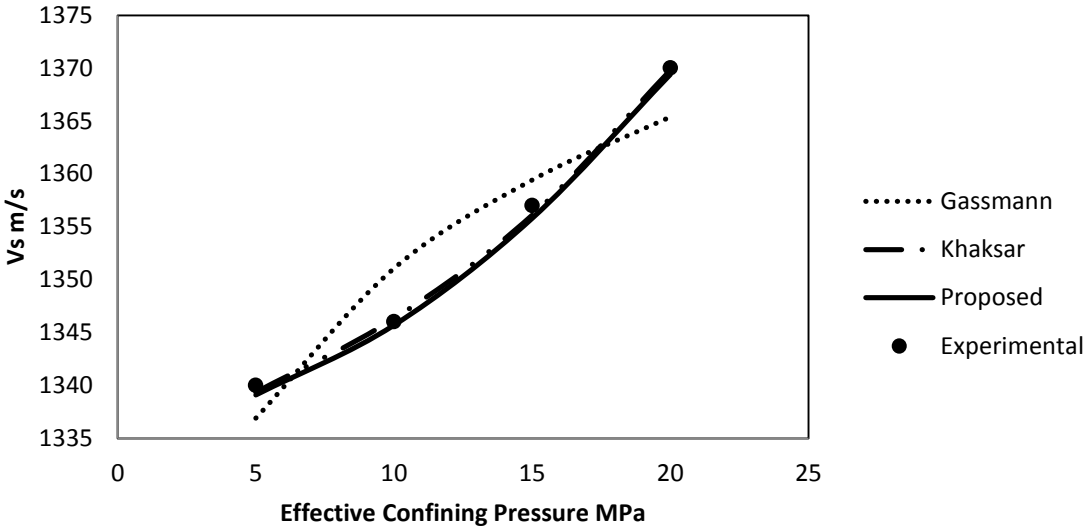

Figure G-22 S-wave velocity vs. Effective Confining Pressure Curves Fit for Sample No. 76

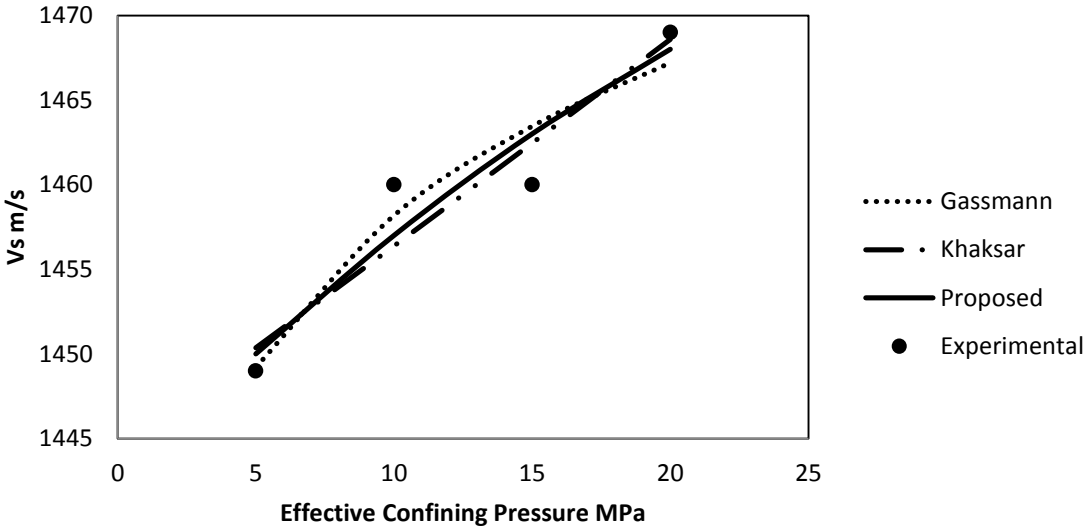

Figure G-23 S-wave velocity vs. Effective Confining Pressure Curves Fit for Sample No. 77

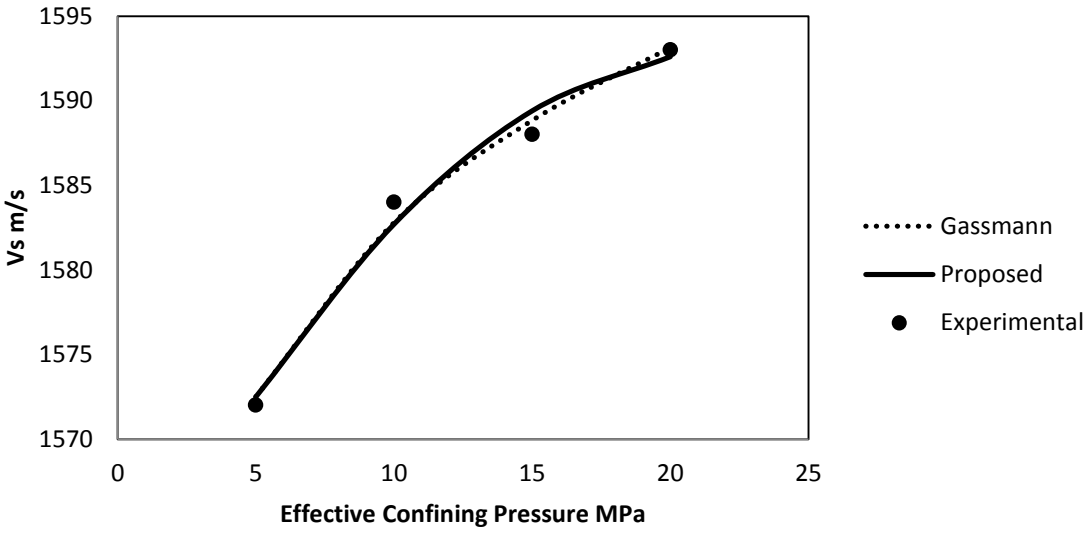

Figure G-24 S-wave velocity vs. Effective Confining Pressure Curves Fit for Sample No. 81